Analysis of the Performance of Cable-Stayed Bridges under Extreme Events

Thesis by

Yukari Aoki

In University of Technology, Sydney

Faculty of Engineering and Information Technology

The Centre for Built Infrastructure Research (*CBIR*)

For the degree of Doctoral of Philosophy

April 2014

CERTIFICATE OF ORIGINAL AUTHORSHIP

I certify that the work in this thesis has not previously been submitted for a degree nor has it been submitted as part of requirements for a degree except as fully acknowledged within the text.

I also certify that the thesis has been written by me. Any help that I have received in my research work and the preparation of the thesis itself has been acknowledged. In addition, I certify that all information sources and literature used are indicated in the thesis.

Student name: Yukari Aoki

Signature of Student: Production Note: Signature removed prior to publication.

Date: April 2014

Acknowledgement

I would like to express my special appreciation and thanks to my supervisors Professor Bijan Samali, Dr Ali Saleh and Dr Hamid Valipour. I would like to thank you for encouraging my research and for allowing me to grow as a researcher. Your advice on both research as well as on my career have been priceless. It would not have been possible to write this doctoral thesis without the help and support of you.

I would also like to thank ARC linkage research committee members from UNSW and UWS, as well as RMS (Road and Maritime Service,NSW) to support this project. I also want to thank to the UTS structural lab member (Mr Rami Haddad, Mr Peter Brown, Mr, David Hooper and Mr David Dicker) to help my experimental project. All of you have been there to support me when I recruited patients and collected data for my Ph.D. thesis.

A special thanks to my parents. Words cannot express how grateful I am to my father (Mr Takayuki Aoki) and my mother (Ms Yoshiko Aoki) for all of the sacrifices that you've made on my behalf. Your prayer for me was what sustained me thus far. Finally, I thank all my friends in Australia, Japan and elsewhere for their support and encouragement.

List of Publications

AOKI, Y., SAMALI, B., SALEH, A. and VALIPOUR, H. 2011. Impact of sudden failure of cables on the dynamic performance of a cable-stayed bridge. *In:* PONNAMPALAM, V., ANCICH, E. & MADRIO, H. (eds.) *AUSTROADS 8th BRIDGE CONFERENCE.* Sydney, Australia.

AOKI, Y., SAMALI, B., SALEH, A. and VALIPOUR, H. 2012a. Assement of Key Response Quantities for Design of a Cable-Stayed Bridge Subjected to Sudden Loss of Cable(s). *In:* SAMALI, B., ATTARD, M. M. & SONG, C. (eds.) *Australasian Conference on The Mechanics of Structures and Matreials, ASMCM 22.* Sydney, Australia: Taylor&Francis Group.

AOKI, Y., VALIPOUR, H. R., SAMALI, B. and SALEH, A. 2012b. A Study on Potential Progressive Collapse Response of Cable-Stayed Bridges. *Advances in Structural Engineering,* 16**,** 18.

SAMALI, B., AOKI, Y., SALEH, A. & VALIPOUR, H. 2014. Effect of loading pattern and deck configuration on the progressive collapse response of cable-stayed bridges. *Australian Journal of Structural Engineering,* In Progress.

ABSTRUCT

In bridge structures, loss of critical members (e.g. cables or piers) and associated collapse may occur due to several reasons, such as wind (e.g. Tacoma narrow bridge), earthquakes (e.g. Hanshin highway) traffic loads (e.g. I-35W Mississippi River Bridge) and potentially some blast loadings. One of the most infamous bridge collapses is the Tacoma Narrow Bridge in United States. This suspension bridge collapsed into the Tacoma Narrow due to excessive vibration of the deck induced by the wind. The collapse mechanism of this bridge is called "zipper-type collapse", in which the first stay snapped due excessive wind-induced distortional vibration of the deck and subsequently the entire girder peeled off from the stays and suspension cables. The zipper-type collapse initiated by rupture of cable(s) also may occur in cable-stayed bridges and accordingly guideline, such as PTI, recommends considering the probable cable loss scenarios during design phase. Moreover, the possible extreme scenario which can trigger the progressive collapse of a cable-stayed bridge should be studied. Thus, there are three main objectives for this research, which are the effect of sudden loss of critical cable(s), cable loss due to blast loadings and progressive collapse triggered by the earthquake. A finite element (FE) model for a cable-stayed bridge designed according to Australian standards is developed and analysed statically and dynamically for this research purpose. It is noted that an existing bridge drawing in Australia cannot be used due to a confidential reason. The bridge model has steel deck which is supported by total of 120 stays. Total length of this bridge is 1070m with 600m mid-span.

This thesis contains 8 chapters starting with the introduction as chapter 1.

In chapter 2, comprehensive literature review is presented regarding three main objectives.

In chapter 3 to 5, results of the cable loss analyses are presented. In chapter 3, the dynamic amplification factor (*DAF*) for sudden loss of cable and demand-to-capacity ratio (*DCR*), which indicate the potential progressive collapse, in different structural components including cables, towers and the deck are calculated corresponding with the most critical cable. The 2D linear-elastic FE model with/without geometrical

nonlinearity is used for this analysis. It is shown that *DCR* usually remains below one (no material nonlinearity occurs) in the scenarios studied for the bridge under investigation, however, *DAF* can take values larger than 2 which is higher than the values recommended in several standards. Moreover, effects of location, duration and number of cable(s) loss as well as effect of damping level on the progressive collapse resistance of the bridge are studied and importance of each factor on the potential progressive collapse response of the bridges investigated.

As it was shown in chapter 3, a 2D linear-elastic model is used commonly to determine the loss of cable. However, there is a need to study the accuracy and reliability of commonly-used linear elastic models compared with detailed nonlinear finite element (FE) models, since cable loss scenarios are associated with material as well as geometrical nonlinearities which may trigger progressive collapse of the entire bridge. In chapter 4, 2D and 3D finite element models of a cable-stayed bridge with and without considering material and geometrical nonlinearities are developed and analysed. The progressive collapse response of the bridge subjected to two different cable loss scenarios at global and local levels are investigated. It is shown that the linear elastic 2D FE models can adequately predict the dynamic response (i.e. deflections and main stresses within the deck, tower and cables) of the bridge subject to cable loss. Material nonlinearities, which occurred at different locations, were found to be localized and did not trigger progressive collapse of the entire bridge.

In chapter 5, using a detailed 3D model developed in the previous chapter, a parametric study is undertaken and effect of cable loss scenarios (symmetric and un-symmetric) and two different deck configurations, i.e. steel box girder and open orthotropic deck on the progressive collapse response of the bridge at global and local level is investigated. With regard to the results of FE analysis, it is concluded that deck configuration can affect the potential progressive collapse response of cable-stayed bridges and the stress levels in orthotropic open decks are higher than box girders. Material nonlinearities occurred at different locations were found to be localized and therefore cannot trigger progressive collapse of the entire bridge. Furthermore, effect of geometrical nonlinearities within cables (partly reflected in Ernst's modulus) is demonstrated to have some effect on the progressive collapse response of the cable-stayed bridges and accordingly should be considered.

In chapter 6, the blast loads are applied on the bridge model and determined the bridge responses, since the blast load is one of the most concerned situations after 911 terrorist attacks. The effect of blast loadings with different amount of explosive materials and locations along the deck is investigated to determine the local deck damage corresponding to the number of cable loss. Moreover, the results obtained from the cable loss due to blast loadings are compared with simple cable loss scenarios (which are shown in chapter 3 to 5). In addition, the potential of the progressive collapse response of the bridge at global and local level is investigated. With regard to the results of FE analysis, it is concluded that the maximum 3 cables would be lost by the large amount of TNT equivalent material due to damage of the anchorage zone. Simple cable loss analysis can capture the results of loss of cable due to blast loadings including with local damages adequately. Short cables near the tower are affected by blast loadings, while they are not sensitive for the loss of cables. Furthermore, loss of three cables with damaged area did not lead progressive collapses.

Finally, in chapter 7, dynamic behaviour of cable-stayed bridges subjected to seismic loadings is researched using 3D finite element models, because large earthquakes can lead to significant damages or even fully collapse of the bridge structures. Effects of the type (far- or near-field) and directions of seismic loadings are studied in several scenarios on the potential progressive collapse response of the bridge at global and local level. According to the case studies in this chapter, it is shown that near filed earthquakes applied along the bridge affected to deck and cables significantly. Moreover, the mechanism of bridge collapsed due to longitudinal excitation is analysed by an explicit analysis, which showed the high plastic strain occurring around the pin support created the permanent damage.

The summary and suggestions for this research are shown in final chapter 8.

Table of Contents

List of Figures

List of Tables

List of Symbols

A	Cross-sectional area
b	Width of the deck
$CLDF$	Cable loss dynamic forces
DC	Dead load of structural components and non-structural attachments
DW	Dead load of wearing surfaces and utilities
E	Modulus of elasticity
$\overline{E}$	Equivalent modulus of elasticity
E_{sh}	Hardening modulus of steel
EV	Extreme event load
I	Moment of inertia of the section
IM	Vehicular dynamic load allowance taken
l	Horizontal span
LL	Full vehicular live load placed in actual stripped lanes
M	Bending moment
M_y	Yield moment
N	Axial force
N_y	Yield Force
R	Distance between contact surface and the denote centre
t	Thickness of the steel plate
W	Equivalent TNT amount
y	Distance from the neutral axis moment of inertia of the section
Z	Scaled distance (in $m/kg^{1/3}$),
$\varepsilon_{i\text{-}PT}$	Initial post-tensioning strain in cables
γ	Density
σ	Existing stress from dynamic analysis
σ_u	Ultimate stress
σ_y	Yield stress
λ_{ey}	Yield limit slenderness ratio

Chapter 1 : Introduction

1.1 Introduction

Bridge structures are often subjected to severe conditions, such as wild weather, earthquakes, impact of traffic accidents and even explosions. As a result of such extreme external loads, bridge structures could suffer loss of some of their critical structural members (e.g. cables or piers) and subsequent collapse may occur, since a progressive collapse is typically triggered by a sudden loss of one or more critical structural components.

In 2011, the state of Queensland in Australia experienced severe floods. A significant economic damage (a total of 4.5 billion Australian dollars) was sustained as a result of roadway and railway damages and closure, including bridge structures (Lee et al., 2013, Roads, 2012, Pritchard, 2013). In Japan, a magnitude 9.0 earthquake followed by large Tsunami created enormous damage to a large area of a coastal region. The estimated cost of damage was in tens of billions of US dollar (Nakanishi et al., 2013). About 30 of Japanese railway bridges, viaducts (101 girders lost) and hundreds of kilometres of highway were damaged (Kawashima et al., 2011; Koseki et al., 2012, Unjoh, 2012).

Figure 1-1 Timber bridge damaged by floodwaters (Pritchard, 2013).

Figure 1-2 Bridges damaged by tsunami (Unjoh, 2012).

Figure 1-3 I-35W Mississippi River bridge collapse.

Some of the bridges collapsed due to various loading conditions are shown in Figures 1-1 to 1-3. During the evening rush hour on 1st of August 2007, I-35W Mississippi River Bridge suddenly crashed into the river. 13 people were killed and many people suffered serious injuries. Design failure was identified as one of the most significant causes of this collapse, although heavy traffic load was a contributing factor as well (Hao, 2010). Moreover, after the 911 terrorist attacks, structural collapses due to malicious actions have become a critical factor in bridge design. According to a Canadian transportation report, about 199 bridges were attacked or considered to be attacked by terrorists between 2002 and 2008 (Canada, 2009). Also, Jenkins and Gersten (2001) reported in the FTA report that about 58% of terrorist attacks targeted the transportation sector including bridge structures.

Collapses or critical damages to bridges can significantly affect the economy as well as human lives, thus bridges should be designed to withstand these severe conditions.

1.2 Objectives

In this research, cable-stayed bridges are the main subject, since Road and Maritime Service (RMS) of NSW government in Australia is interested in dynamic behaviour of this type of bridge under severe loading conditions. Considering the high cost of experimental work for testing large scale bridges, the best and perhaps the only available option for such studies would be advanced numerical models which can properly capture local and global behaviour of the structure including material and geometrical nonlinearities. In this research, ANSYS and LS-DYNA software are employed to conduct finite element (FE) analyses and simulate the behaviour of cable stayed bridges subjected to extreme loading scenarios such as cable loss, blast and earthquake. The developed FE models can take account of material as well as geometrical non-linearity. Also, the effect of inertia and dynamic loads are considered in the FE models.

Cable-stayed bridges as well as suspension bridges can be exposed to severe loading conditions and might be damaged as a result. One of the most notable bridge collapses has been the spectacular collapse of the Tacoma Narrows Bridge in the United States due to aerodynamic instability caused by wind loads. The bridge's main span collapsed into the Tacoma Narrow on 7th November 1940, four months after it was opened. The main reason for the collapse of Tacoma Narrows Bridge was wind-induced resonance and the ratio between the span and the deck depth as well as very low torsional stiffness of the deck (Kwon and Qian, 2012, Miyachi et al., 2012). In Tacoma bridge case, the first stay snapped by excessive wind-induced distortion of the bridge deck, the entire girder peeled off from the stays and suspension cable(s) as seen in Figure 1-4. Such cable loss scenarios can/may lead to high impulsive dynamic loads in the structure that can potentially trigger a "zipper-type" progressive collapse of the entire bridge (Starossek, 2011).

Accordingly, in cable-stayed bridges, the likelihood of occurrence of progressive collapse triggered by cable loss scenarios must be thoroughly investigated. PTI (2007) recommends considering the probable cable loss scenarios during the design phase. Static analysis and application of a Dynamic Amplification Factor (*DAF*) of 2 is recommended to determine the effect of loss of cable(s). However, some researchers

have questioned the validity of static analyses in conjunction with a single value *DAF* (Mozos and Aparicio, 2010a, Mozos and Aparicio, 2010b, Starossek, 2011).

The initial objectives of this thesis are,

1) accurately determine the *DAF* corresponding to the location/number of cable loss(s) as well as the effect of damping ratio
2) determine the relation between *DAF* and potential progressive collapse which is identified by the Demand-Capacity Ratio (*DCR*)
3) in the context of alternate load path method (ALP), identify the most critical cable(s) which their loss can potentially trigger the progressive collapse of the entire bridge
4) evaluate the influence of loading patterns (i.e. unsymmetrical and symmetrical) in conjunction with different cable loss scenarios on the potential progressive collapse response of the bridge

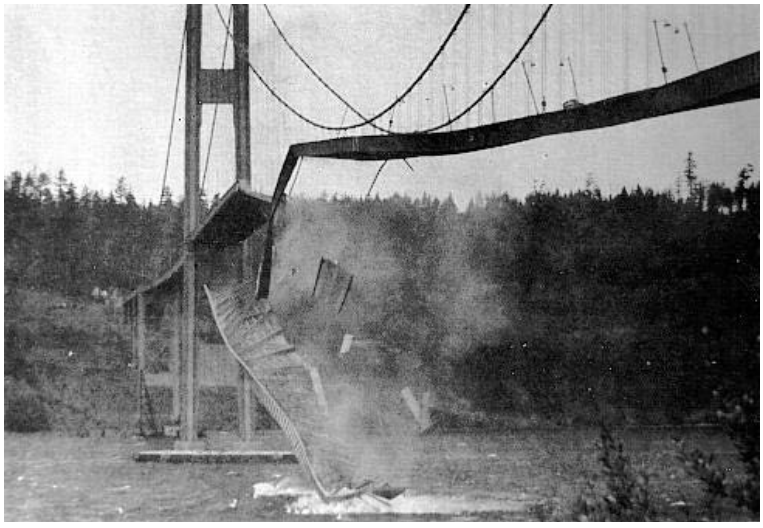

Figure 1-4 Zipper-type collapse of the Tacoma Narrows Bridge (Starossek, 2011).

For cable-stayed bridges, the cables and their anchorage zones have relatively small cross sectional areas and are exposed to severe loading conditions (e.g. corrosion, impact of vehicles and blast). These extreme loads can cause damage to the anchorage zones as a result of high stress concentration, and can lead to loss of cables (Yang et al., 2011, Tang and Hao, 2010, Hao and Tang, 2010, Tang, 2009, Åkesson, 2008, Hao,

2010, Starossek, 2011, Kiger et al., 2010, Mitchell et al., 2006). In this thesis, malicious actions in the form of blast loadings are chosen since the blast loadings analysis is one of the most important topics for iconic structures like bridges after 911 terrorist attacks. With regard to the research reported in the literature that specifically relates to bridges subjected to blast loadings, in the second part of this thesis finite element models of a cable stayed bridge are developed and analysed using LS-DYNA software. Also, the explosive charge and process of air blast propagation are directly modelled in the LS-DYNA software. The main focus of this second part is to

5) identify the type and extent of the damages caused by air blast in the vicinity of anchorage zone of cable
6) determine the number of lost cables following blast scenarios in which the size and location of explosives vary
7) evaluate the dynamic response of the cable-stayed bridges following loss of cable(s) caused by direct blast loadings.
8) evaluate the accuracy of alternate load path (ALP) for capturing the behaviour of cable stayed bridges subjected to blast loading

Finally, the detailed continuum-based finite element models developed in ANSYS and LS-DYNA software are employed to capture the dynamic behaviour of a cable-stayed bridge under earthquake loadings and

9) determine the most critical direction and type of seismic loadings
10) identify the critical structural components that suffer the most damage under the earthquake loadings
11) identify the damage mechanism and mode of failure in cable stayed bridges subject to seismic action

Initially the ANZAC bridge was supposed to be considered in this research project, however, due to security and confidentiality reasons the analysis of an existing bridge in Australia was ruled out by RMS as the main sponsor of this research project. Accordingly, for this project a cable stayed bridge was analysed and designed according to minimum requirements of Australian standards.

1.3 Thesis Organization

The thesis consists of 8 chapters as follows:

1) Chapter 1 presents a brief background and introduction of the thesis and the main objectives of the research.

2) Chapter 2 reviews the relevant literature on the three main topics including cable loss analysis and the magnitude of dynamic amplification factor (*DAF*) for bridges subjected to blast loadings and the dynamic behaviour of bridges under seismic loadings.

3) Chapter 3 aims to determine the *DAF*s associated with different sudden cable loss scenarios. The effects of location, duration and number of lost cable as well as the effect of damping level on the progressive collapse response of the bridge are studied. The importance of each factor on the potential progressive collapse response of the bridges is identified and the demand-to-capacity ratio (*DCR*) in cables, towers and the deck are calculated for most critical cable loss scenarios. A 2D linear-elastic FE model with and without geometrical nonlinearity is used for this analysis.

4) In Chapter 4 a non-linear 3D continuum-based finite element model of the bridge is developed with full details and analysed. The accuracy of the linear elastic 2D model and *DCRs* calculated in Chapter 3 in comparison with the detailed nonlinear 3D FE model is verified in this chapter.

5) Chapter 5 investigates the effects of different symmetric and unsymmetric loading patterns and cable loss scenarios. The unsymmetric loading patterns and cable loss scenarios can induce torsional mode of vibration in the deck and subsequently trigger the progressive collapse of the entire bridge. Also, the effect of deck configuration (i.e. steel box girder and an open orthotropic deck) on the progressive collapse response of the cable stayed bridge is investigated in conjunction with loading and cable loss patterns.

6) In Chapter 6, dynamic repose of the bridge subjected to blast loading is investigated. The explosive and air blast are directly modelled to determine the number of lost cables and extent of the damage around the anchorage zone

during such loading scenarios. Different amounts of TNT equivalent explosives at different locations are considered in the analyses. In addition, the global response due to the loss of cable caused by blast loading is compared with the simple cable loss analysis (obtained in Chapters 3 and 4) in order to verify the accuracy of ALP method based on simple cable loss scenarios.

7) Chapter 7 focuses on the dynamic response of the cable-stayed bridge subjected to two different types of earthquake accelerations (i.e. horizontal and vertical). Also, the seismic accelerations are applied in four different directions (different angle of attack with respect to longitudinal axis of the bridge) to determine the most critical type of earthquake as well as the critical angle of attack. Moreover, using LS-DYNA FE model, the damage mechanism and failure mode of the bridge is determined under the most critical earthquake loadings.

8) Chapter 8 concludes the research work and highlights some recommendations for future studies regarding behaviour of cable stayed bridges subjected to extreme loading scenarios.

Chapter 2 : Literature review

2.1 Introduction

In cable-stayed bridges, damage or failure of primary structural components such as tower, piers or cables, caused by extreme loadings can lead to the collapse of the entire bridge. For this type of bridge, zipper-type collapse (defined as a horizontal progressive collapse) is one of the most concerning failure modes that can be caused by the sudden loss of cables. Analysis of sudden loss of cables in cable stayed and suspension bridges is extremely critical and it has drawn the attention of researchers in recent years and it is one of the main objectives of this research. This section presents a review of past research on the effects of sudden loss of cable, the collapse mechanism of the bridge and different analysis methods (i.e. dynamic analysis and static analysis with dynamic amplification factor) available for progressive collapse assessment of cable bridges.

Progressive collapse initiated by the loss of critical structural components occurs over a short period of time due to high strain rate loadings such as blast or impact. Since the collapse of Ronan Point apartment building in 1968, progressive collapse has been an important issue in structural design and a significant amount of research has been conducted on progressive collapse response of building structures subjected to extreme loading scenarios (Vlassis et al., 2009, Nethercot et al., 2007, Choi and Kim, 2011, Lange et al., 2012, Stoddart et al., 2013). Apart from building structures, the dynamic behaviour of the bridge structures subject to extreme loading scenarios (e.g. blast loadings) and critical member loss are currently of high interest to structural engineers and researchers. Accordingly, a comprehensive literature review regarding the effect of the explosions on bridge structures, particularly cable-stayed bridges, is presented in this chapter.

Seismic actions have caused severe damage, including progressive collapse of the bridge structures in the past, and are considered as one of the most important extreme cases in bridge design. Accordingly, a comprehensive literature review on earthquake analysis of bridge structures is also reported in this chapter.

2.2 Progressive collapse due to sudden loss of cable(s)

2.2.1 Background

Stays of cable-stayed bridges are critical structural elements which are subjected to corrosion, abrasion, wind, vehicle impact and malicious actions and these extreme loading scenarios may lead to severe damage and loss of cable(s) (Åkesson, 2008, Walther, 1999, Yang et al., 2011, Ghali and Krishnadev, 2006, Jo et al., 2002). Such cable loss scenarios can/may lead to high impulsive dynamic loads on the structure that can potentially trigger a "zipper-type" progressive collapse of the entire bridge, like Tacoma Narrows Bridge, although it was a suspension bridge (Starossek, 2011, Plaut, 2008). Accordingly, cable-stayed bridges should be designed for potential cable loss scenarios as recommended by the guidelines such as PTI (2007). This standard requires that the cable-stayed bridges should be able to withstand the loss of any cable without the occurrence of structural instability or progressive collapse.

2.2.2 The effect of the critical cable loss

Kao and Kou (2010) analysed a symmetrical, fan-shaped cable-stayed bridge under sudden breakage of cable. They determined the dynamic response of the entire bridge including bending moment along the deck, the deflection along the deck and at top of the tower, deviation of axial forces in each cable and stresses in the girders and tower. Also, the ultimate load-bearing capacity of different structural components were determined and compared with maximum tractions induced in each component to determine whether any failure occurs. The cable connected to the pin supports was identified as the most critical cable which its loss leads to a high increase of sagging deformation of the deck and tower stress. In addition, the cable connected to the mid-span was found out to be the second most critical cable which its loss can lead to a dramatic increase in the girder stresses.

Wolff and Starossek (2008) studied the collapse behaviour of a 3D cable-stayed bridge model and found out that the initial failure (loss) of the three cables around the pylon can trigger a zipper-type collapse associated with a large vertical deformation within the bridge deck. In the failure mechanism identified by Wolff and Starossek (2008), the loss of cables lead to high stress concentration in the cables adjacent to the lost ones and

subsequently these adjacent cables snap. Also, it was concluded that the extent of collapse triggered by the cable loss strongly depends on the location of the lost cable.

2.2.3 Dynamic amplification factor (*DAF*) due to sudden loss of cable(s)

The progressive collapse of the structures triggered by extreme events typically has a dynamic nature. However, in practice and for progressive collapse assessment of the structures, a static analysis is considered to be adequate, providing a proper dynamic amplification factor (*DAF*) is applied on the static analysis results (Kokot et al., 2012). The value of *DAF* adopted by different standards and guidelines varies between 1.5 and 2 (DoD, 2005, GSA, 2003, PTI, 2007). For example, the Stonecutters Bridge in Hong Kong was designed using a *DAF* of 1.5 (ARUP, 2010, Hussain et al., 2010).

Apart from the magnitude of *DAF*, the definition of *DAF* in the context of cable structures is slightly different than the *DAF* specified in the building codes. *DAF* for a cable-stayed bridge with cable loss is generally specified as follows (Zoli and Woodward, 2005):

$$DAF = \frac{\gamma - \alpha}{\beta - \alpha} \qquad 2\text{-}1$$

where α is value of response obtained from the current state prior to cable loss (static analysis without cable loss), β is the response obtained from a static analysis after the cables are lost and γ is the value of response captured by a dynamic cable loss analysis.

Zoli and Woodward (2005) carried out some cable loss analysis in an arch bridge (see in Figure 2-1) and found out that for loss of cable in an arch bridge, the *DAF* is within the range of 0.5 and 0.8 for the peak force in the tie girder and arch rib. Accordingly, it was concluded that for equivalent static analysis of arch bridges subject to cable loss, using a constant *DAF*=2 is conservative.

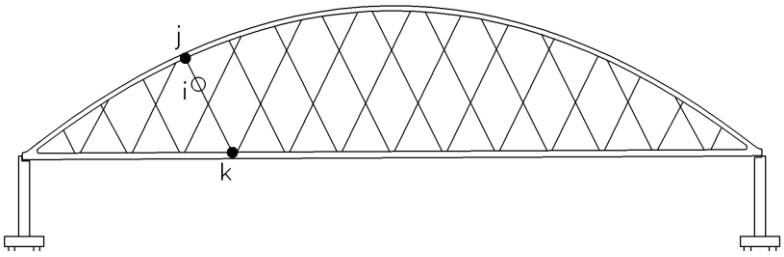

Figure 2-1 A tied arch bridge.

In a different study, Ruiz-Teran and Aparicio (2007) have argued that the application of *DAF*=2 (obtained for a system with single degree of freedom) for cable-stayed bridges with multi-degrees-of-freedom is not always conservative. Accordingly, Ruiz-Teran and Aparicio (2007) determined the *DAF* values for the case of sudden loss of cable(s) in a cable-stayed bridge. Ruiz-Teran and Aparicio (2007) found out that a load due to sudden cable loss causes the structure to deform and to oscillate around the new deformed position, thus *DAF*s should be determined considering the dynamic response of the real structure with multiple degrees of freedom. Also, it was concluded that *DAF* for each parameter of interest (i.e. deflection, bending moment and shear force) should be determined separately. The value of *DAF*s for bending moments along a bridge with under-deck stay cables is shown in Figure 2-2. It is observed that at several locations along the deck, *DAF* has taken values larger than 2. For example, the *DAF* is about 4 at a section 4 m away from the support at the far left side of the bridge deck.

Wolff and Starossek calculated the *DAF*s for bending moments along the bridge deck of a conventional cable-stayed bridge as shown in Figure 2-3 (Wolff and Starossek, 2008, Wolff and Starossek, 2009, Wolff and Starossek, 2010).

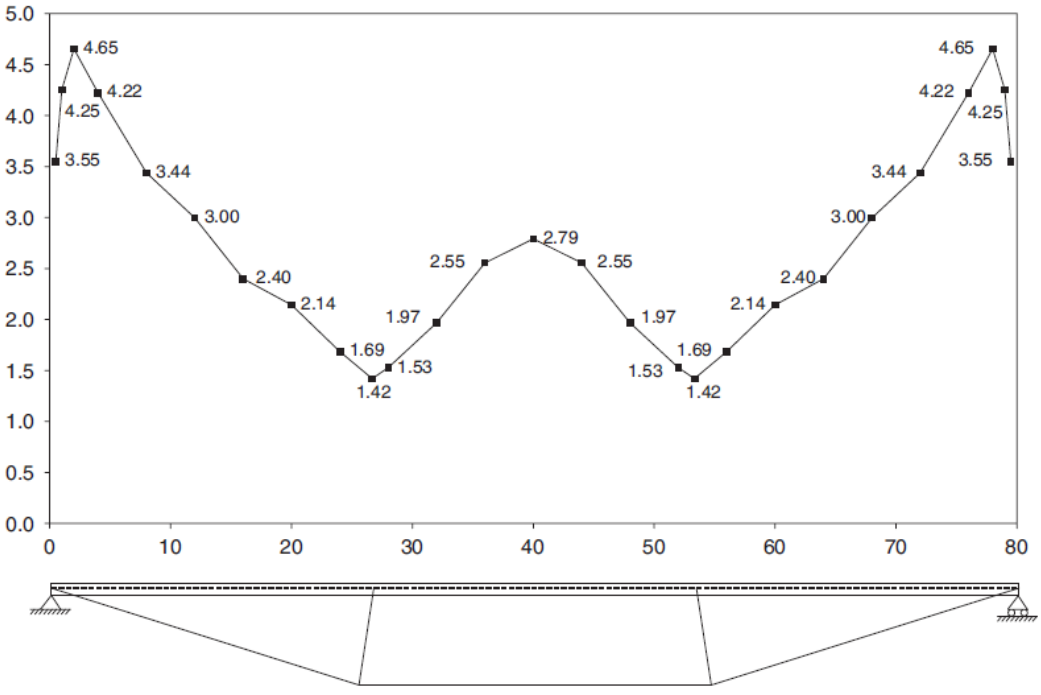

Figure 2-2 Bridge with under deck stay cable (Ruiz-Teran and Aparicio, 2007).

With regard to Figure 2-3, it is observable that *DAF*s exceed 2 at several locations along the deck. They found that applying a single *DAF* for different structural components in a cable-stayed structure cannot adequately capture the dynamic effects, because the value of *DAF* for each structural component depends on the location of the lost cable as well as type of the state variable (i.e. deflection, shear force, bending moment) under consideration.

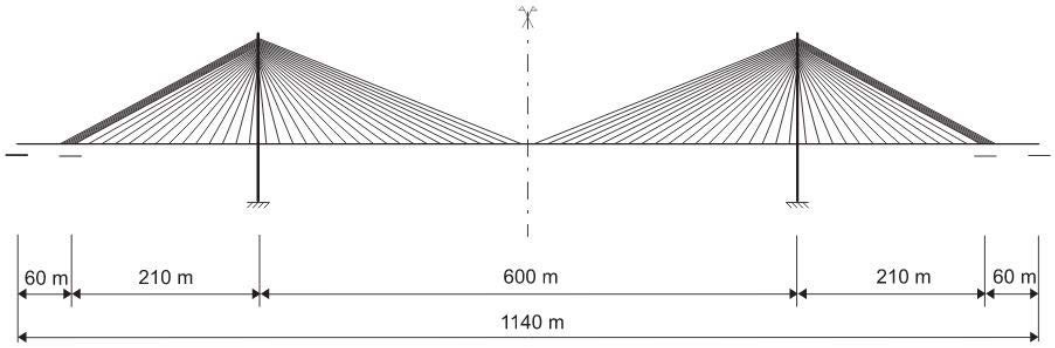

(a) Bridge configuration

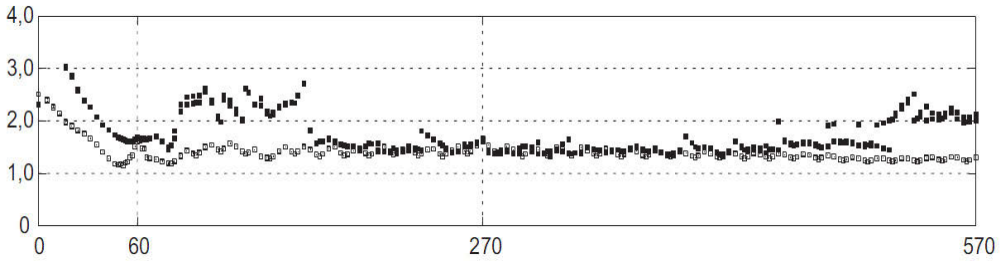

(b) DAFs for bending moment along the deck

Figure 2-3 DAFs for cable-stayed bridge with sudden loss of cable (Wolff and Starossek, 2010).

Moreover, a parametric study on the dynamic response of a series of hypothetical cable stayed bridges subjected to sudden failure of a stay have been conducted to determine the importance of the accidental ultimate state of failure of a cable in design and also investigate the adequacy of a simplified equivalent static analysis in which a *DAF*=2 is adopted (Mozos and Aparicio, 2010a, Mozos and Aparicio, 2010b).

Mozos and Aparicio (2010a&b) studied the characteristics of different bridge models and the factors that can influence the dynamic collapse response of the cable-stayed

bridges subjected to loss of one stay. The parameters considered in Mozos and Aparicio (2010a&b) includes two different damping ratios (i.e. ξ=0% & 2%), two different types of cable configuration (i.e. fan and harp patterns), three different deck dimensions and two types of pylons (I and H shape) as shown in Figure 2-4.

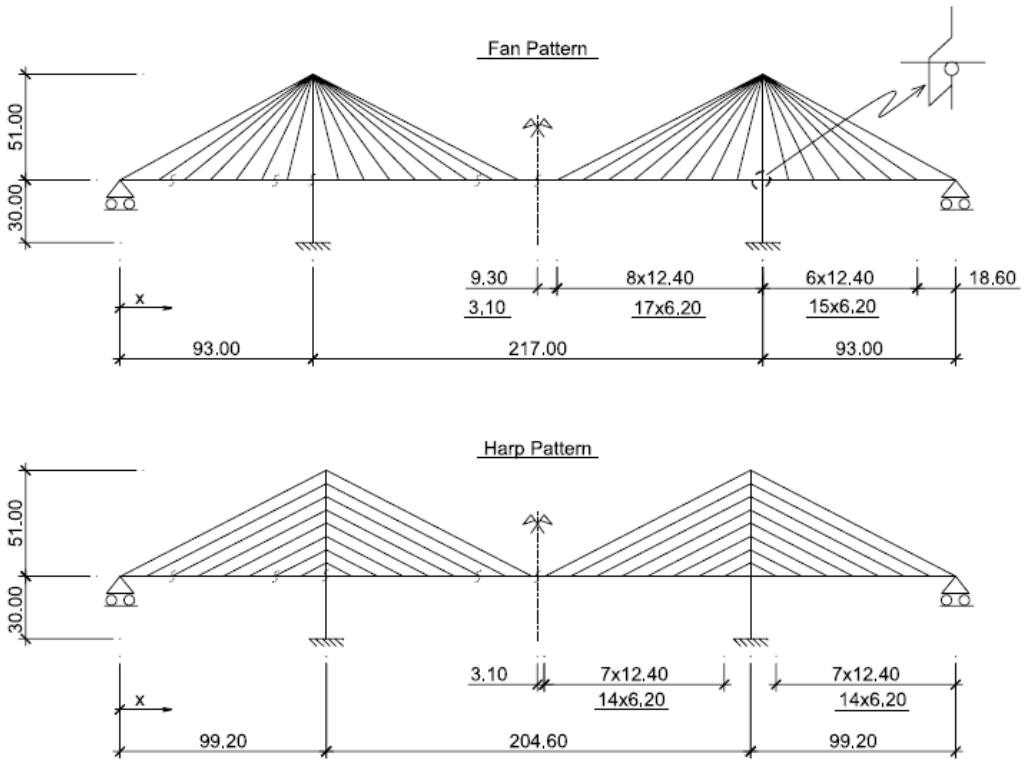

(a) Bridge configuration – longitudinal layout of the fan and harp pattern

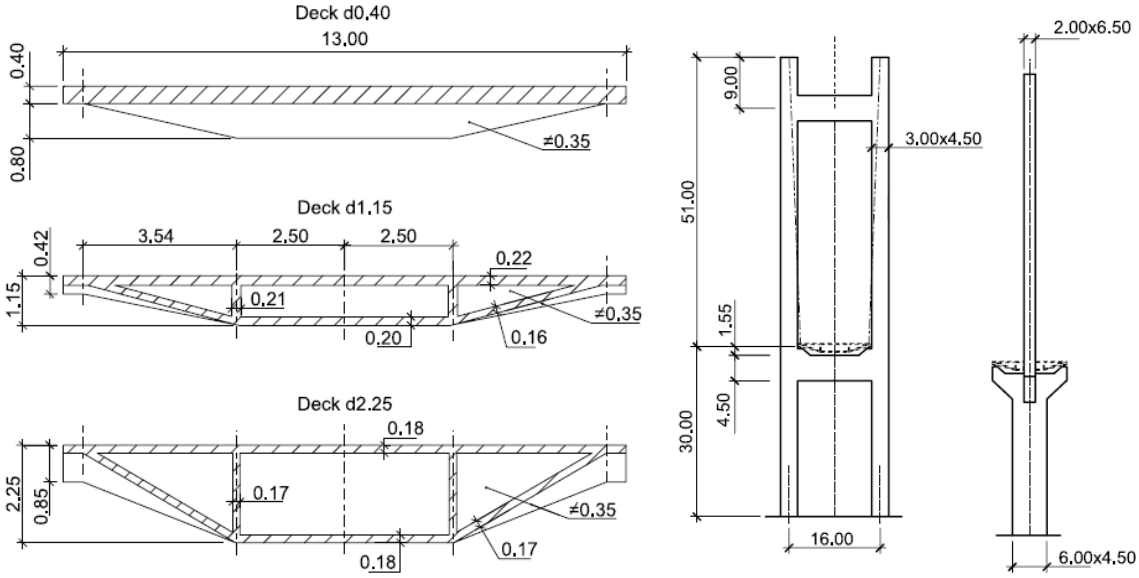

(b) Dimensions of the deck (c) Pylon design

Figure 2-4 Bridge configurations - parameters considered in Mozos and Aparicio (2010a).

To determine the *DAF*, finite element models were developed and analysed using both equivalent static approach and dynamic time integration (Newmark's time marching scheme). The value of *DAF*s for negative bending moment during a cable loss scenario for different bridge configurations and damping ratios are shown in Figure 2-5. It is observed that the *DAF* obtained for negative bending moment exceeds the value of 2 as predicted in previous studies by Ruiz-Teran and Aparicio (2007). The maximum *DAF* values are 8.0 and 5.6 in the un-damped and damped systems, respectively, and the average values are 3.35 and 2.52, respectively. Also it is seen that the layout of the stays (i.e. fan (F) or harp (H) types) as well as the dimension and configuration of the deck can significantly influence the *DAF* values.

Moreover, a small-scale test was conducted to evaluate the *DAF*s for the structures subjected to sudden loss of support and it was observed that the experimental *DAF*s are typically larger than the *DAF*=2 adopted by design standards and guidelines (Mozos and Aparicio, 2011, Tsai and You, 2012).

With regard to the existing literature on the *DAF* values, it can be concluded that a single value *DAF* cannot adequately take account of dynamic effects in the equivalent static analysis. Also, a *DAF*=2 is not always conservative according to the existing research in the literature.

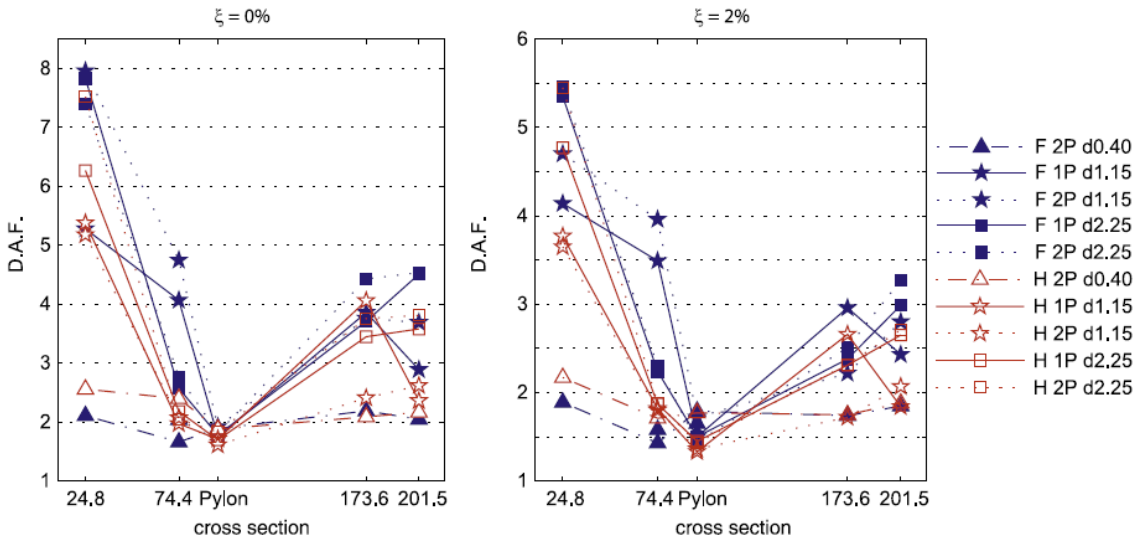

Figure 2-5 *DAF*s along the deck obtained from negative bending moment in all scenarios with undamped and damped system.

2.3 Bridges subjected to blast loadings

2.3.1 History of terrorist attacks

Due to the increase in terrorist attacks in recent years, blast loads have been recognized as one of the extreme events that must be considered in the design of important structures.

Well-known examples of terrorist attacks are the Alfred P. Murrah Federal Building in Oklahoma City (1995) and the World Trade Center in New York City (2001). The most well-known terrorist event for the Australians is the 'Bali bombing' on 12th October 2002 (Southwick et al., 2002, Mendis and Ngo, 2003). It occurred in a popular nightclub in Bali. A total of 88 Australians were killed. The most recent terrorist attack related to Australia was in Jakarta in 2009. Three Australian business men were killed in this attack (Smith, 2013). Moreover, London terrorist attacks on 7 July 2005 were unforgettable events in UK (Emergency Management Australia, 2007). After the London terrorist attacks, the Australian government held a workshop to prepare for such terrifying events (Emergency Management Australia, 2007).

2.3.2 Bridges subjected to terrorist attacks

Terrorists have targeted iconic structures such as the World Trade Center, the London metro, famous night clubs and luxury hotels. Accordingly, iconic bridges are not immune from such terrorist attacks.

According to a Canadian transportation report, about 199 bridges were attacked or considered to be attacked by terrorists between 2002 and 2008 (Canada, 2009). Also, Jenkins and Gersten (2001) reported in an FTA report that about 58% of terrorist attacks targeted the transportation sector including bridge structures.

Mahoney (2007) analysed typical highway bridges under blast loads, while Bensi et al. (2005) investigated the risk of terrorist attacks on a cable-stayed bridge and both authors calculated the economic consequences of such attacks that would be quite significant and in some cases the cost would be over $100 million. Although it is a rare case, if a bridge is subjected to a full scale terrorist attack, the structure might fully collapse. Even some minor damage may require the bridge to be closed for repairs, that may have significant economic implications.

2.3.3 Buildings subjected to blast loading

Responses of the structures or the structural components subjected to blast loadings have been studied experimentally and numerically (Jacinto et al., 2001, Li and Meng, 2002, Lawver et al., 2003, Lam et al., 2004, Ngo and Mendis, 2005, Ngo et al., 2005b, Gram et al., 2006). Also, the characteristics of the materials (such as different strength concrete or steel) subjected to impact loads were determined (Ngo et al., 2005a, Zhang et al., 2005, Ngo et al., 2007b, Zhang et al., 2007, Wright and French, 2008).

After the 911 World Trade Center terrorist attacks, it was recognised that damage by initial blast loads could lead to the progressive collapse of the entire building.

Ngo et al. (2007a) reviewed the blast load effects on the structures. They analysed the local damage of columns and the progressive collapse of an entire building which is a 52 storey building modified from a typical tall building in Australia (AS/NZS1170.2, 2002). It was found that two columns, slabs and beams above the lost columns were destroyed by the blast loadings directly. Also, it was found that if more than two floors are destroyed by blast, the progressive collapse of the entire building may be triggered.

Also, Kwasniewski (2010) studied a potential progressive collapse of a 8-storey building subjected to loss of a column at the first floor by using the LS-DYNA software. They analysed three different locations of column loss, and concluded that there was a low possibility for a progressive collapse of this particular building.

2.3.4 Bridges subjected to blast loadings

Damage of individual bridge components (such as piers and towers, cable and deck) due to blast loadings has been studied for several types of bridge structures.

Piers and towers

A 2-span 2-lane bridge with typical type III AASHTO girders was developed and analysed under blast loads by using STAAD.Pro and AT Blast software (Anwarul Islam and Yazdani, 2008). This bridge model was assumed to be made of concrete (compressive strength range between 31 MPa to 45 MPa) and subjected to the equivalent TNT value of 226.8kg (regular truck). It was concluded that this type of bridge will fail when the blast load is applied above or underneath the deck. Therefore,

Anwarul Islam and Yazdani (2008) recommended that design for blast resistance and retrofit techniques for bridges should be developed and adopted in design guidelines.

Fujikura et al. (2008) proposed a new concrete-filled steel tube column system which was investigated experimentally under blast loading. This system was shown to be effective for blast resistance since breaching and spalling of concrete are effectively prevented from occurring in this column.

Bridge Deck

Winget et al. (2005) reported a simulation of a concrete beam bridge subjected to blast loads. They considered various locations of detonation to gain a better perspective of the bridge performance against explosion. They concluded that the bridge used in their research showed high vulnerability to failure under the impact of a conventional vehicular bomb. They also argued that the response of bridges against blast load depends significantly on the bridge geometry.

Design criteria for post-tensioned box girder bridges subjected to blast loadings were presented by Kiger et al. (2010). The design criterion was derived with respect to the numerical results captured by LS-DYNA software. In their report, the main design criteria predict the relation between the equivalent explosive material size and the type of damage (e.g. no damage, spall and breach of concrete).

2.3.5 Cable-stayed bridges subjected to blast loadings

The damage criteria and dynamic response of the cable-stayed bridges subjected to blast loadings are discussed in this section. The results of the research in this field is limited to the full scale cable-stayed bridges modelled and analysed by different researchers (Hao and Tang, 2010; Tang and Hao, 2010) such as the one shown in Figure 2-6.

Bridge Pier and towers

A cable-stayed bridge with two different types of pylon (i.e. hollow steel box and concrete-filled composite pylon) subject oblast load was studied by Son and Lee (2011). Car bomb detonation was the scenario considered and simulated by dynamic-nonlinear analysis using a combined Lagrangian and Eulerian model. The explicit numerical software used in this study was MD Nastran SOL 700 (2011) to simulate the spatial and time variation of the blast load and shock wave.

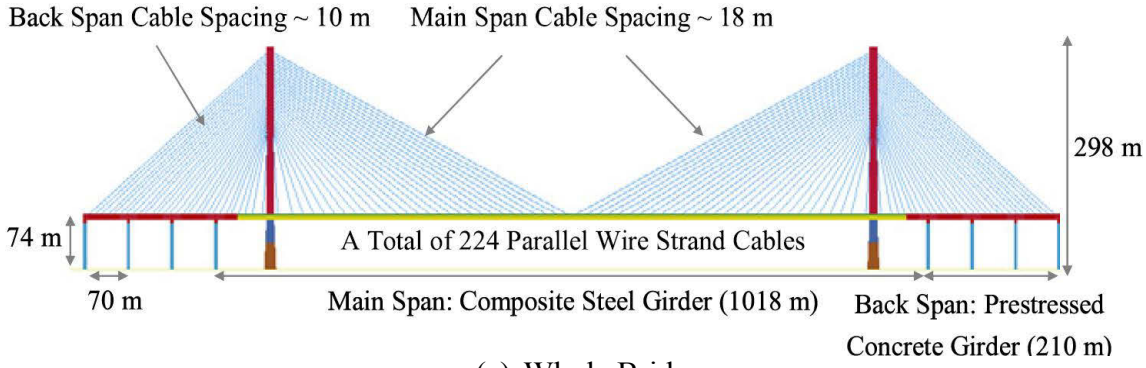

(a) Whole Bridge

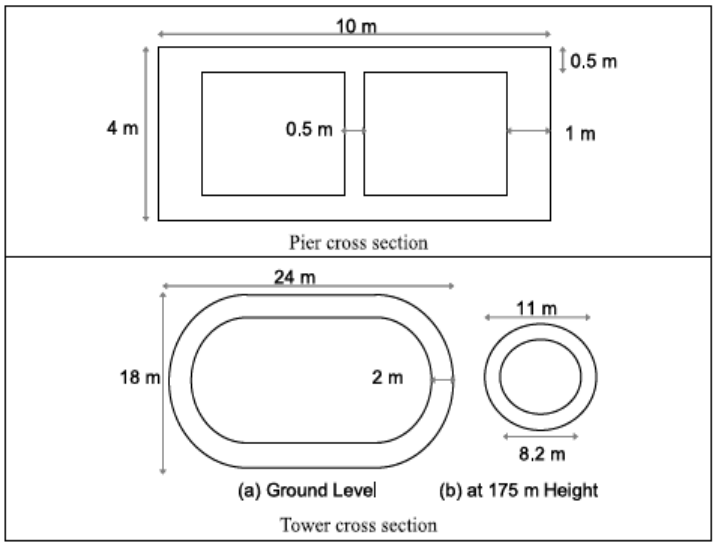

(b) Pier and Tower cross section

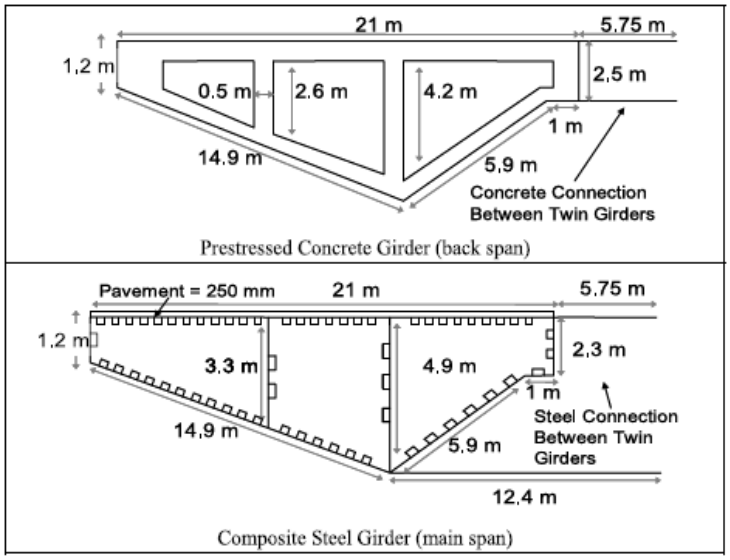

(c) Deck cross section

Figure 2-6 A cable-stayed bridge model and cross sectional area of tower and deck used in Hao and Tang, Tang and Hao (2010).

From the results of numerical model, Son and Lee (2011) concluded that a concrete-filled pylon could survive while the hollow steel box section would collapse due to a significant P-Δ effect under the same amount of explosive materials.

The concrete pier shown in Figure 2-6(b) was subjected to 1,000kg TNT explosion at 0.5m distance to determine the local damage cause by the air blast (Hao and Tang, 2010, Tang and Hao, 2010). According to Tang and Hao (2010), the surface of the pier facing the blast load showed significant damage. The web and back of the pier wall had more significant damage than the front wall. Accordingly, the damage in the pier led to significant bridge deck deformation, for instance the maximum vertical downward deflection at mid-span was 11.52 m. Moreover, a part of the deck connected to this pier fell down though the progressive collapse of the entire bridge was concluded to be unlikely.

The tower, shown in Figure 2-6b, was also studied under the same amount of TNT (Hao and Tang, 2010; Tang and Hao, 2010). However, due to the large wall thickness (2m) and the absence of web segments inside the tower, the local damage of the tower was only seen on the front surface (blast applied) of the tower. Furthermore, this local damage on the front surface did not trigger a progressive collapse. However, when the amount of explosives was increased to 10,000 kg of TNT (applied at 6.5m distance from the tower), the entire bridge did collapse due to shear failure and flexural failure on the side and rear walls of the tower. According to the parametric study conducted, if complete damage of the entire tower cross section does not occur, progressive collapse of the bridge structure is unlikely. Also, it was concluded that the progressive collapse of the entire bridge can be prevented, provided a minimum 12 m stand-off distance is required.

Deck

Deng and Jin (2009) analysed the effect of blast loads numerically. The actual bridge, named Minpu II Bridge in Shanghai was used as the benchmark bridge. The blast charge assumed was an 800 kg TNT placed on top of the bridge deck. The ANSYS AUTODYN computer program (2007) was used for blast load simulation. It was shown that the stress concentration due to blast load is limited to the blast region and cracks are distributed in small areas.

In Hao and Tang's (2010) study, the bridge had two different types of deck, the back span is a concrete deck and the mid span is a steel composite deck (see Figure 2-6(c)). Due to the differences in material properties, the steel deck showed less damage than the concrete deck. The damaged area of concrete deck is 30 m in length and 20 m in width whereas the damaged zone in the steel deck is 11.5 m wide and 10 m long.

Son and Astaneh-Asl (2011) focused on the response and failure mode of a bridge deck subjected to blast loadings. A typical orthotropic deck for cable-stayed bridges was created using nonlinear finite-element model in order to simulate the blast loadings. Son and Astaneh-Asl (2011) also adopted a new blast-resistant technology (called "fuse system") which can be used in design and construction of bridges vulnerable against progressive collapse. The major collapse mode in this typical orthotropic deck is associated with the vertical buckling failure due to significant P-Δ effects (similar to the hollow steel box pylon), however, this failure did not lead to the progressive collapse of the entire bridge.

Cables and anchorage zone

As mentioned in Williamson and Winget (2005) paper, the cable anchorage zone of a cable-stayed bridge is one of the most critical areas under blast impact. The cable itself is rarely damaged by the direct blast load impact, however, the damage around the anchorage zone will lead to loss of cable support and subsequently loss of the stay. For example, in the concrete decks, due to the damage of the anchorage region, a few cables lost their support in the bridge model shown in Figure 2-6 (Hao and Tang, 2010, Tang and Hao, 2010). In this concrete deck, 300 kg of TNT placed at 1m above the deck may cause concrete spalling damage on the bottom side as well as damage to the anchorage zone. In the case of 1,000 kg of TNT, three cables were ruptured and the maximum displacement of the bridge span was 4.54 m with 2.14 m lateral displacement of the tower. Even though, the concrete deck damage leads to the loss of some cables, the influence on the entire bridge is not significant. It is noted that the damage of the steel deck for the same bridge models was not considerable, due to resilience of structural components made of steel.

2.4 Earthquake analysis

2.4.1 Background

Significant damage and collapse of several bridges have occurred as the result of severe past earthquake events. Therefore, it is highly recommended by different guidelines that the response to seismic actions is considered in the design of bridges. For example, Xiaoyudong bridge in China was damaged during the May 12th 2008 Wenchuan earthquake with the magnitude of 8.0 (Huang et al., 2011). Due to the great Hanshin (Kobe) earthquake in 1995, the Hanshin express highway bridges suffered damage and even some parts collapsed due to buckling of steel columns, brittle failure of piers and failure of bearings (Hayashi et al., 2000, JSCE, 2010, Bruneau, 1998). The most recent strong earthquake in Japan in Fukushima also created significant damage in several bridges caused by strong ground motion as well as tsunami inundation and soil liquefaction (Kawashima et al., 2011, Hoshikuma, 2011).

These bridge damages were investigated by field surveys as well as numerical models to determine the dynamic behaviour and collapse mechanisms. During the post-earthquake inspection of the Xuaiyudong bridge, which was a 4-span frame arch bridge, it was found that the arch legs on the end pins were the weakest components, and suffered damage by strong ground motion (Huang et al., 2011). For Hanshin Highway, bending failure at the bottom of several piers occurred during the strong shakes (SEO et al., 2004, Mylonakis et al., 2006).

Recent studies focused on evaluating the seismic vulnerability and retrofitting strategies of existing bridges. A multi-span-simply-supported bridge in New Jersey was analysed numerically (Saadeghvaziri and Yazdani-Motlagh, 2008). Moreover, Konstantakopoulos et al. (2012) analysed a generic suspension bridge subjected to a combination of earthquake and moving loads. Memisoglu Apaydın (2010) investigated two existing suspension bridges in Istanbul, Turkey, and determined that although these two bridges were designed for lower earthquake loads, they can perform satisfactorily under severe seismic loadings. Regarding cable-stayed bridges, a comprehensive analysis of the seismic performance of the Minpu Double-deck cable stayed bridge was done in China (Weiab et al., 2011). Megawati et al. (2001), on the other hand, analysed

the Akashi-Kaikyo bridge to derive the ground motion at the tower base from the seismic response of the top of the tower recorded during the Kobe earthquake.

2.4.2 Cable-stayed bridge design in Japan

Cable-stayed bridges, such as Higashi Kobe bridge and Rokko bridge had suffered severe damages to various components, such as support of the tower, pin-support, deck and some dampers during the Kobe earthquake in Japan in 1995 (JSCE, 2010, Ganev et al., 1998). The Japanese Society of Civil Engineers (JSCE) revised the standard to enhance the seismic response of cable-stayed bridges after the Kobe earthquake, thus existing bridges have to be reanalysed and retrofitted if required (JSCE, 2010, Fujino and Siringoringo, 2011, Siringoringo and Fujino, 2008, Otsuka et al., 2007, Shirato, 2009). Yokohama-Bay Bridge, as an example, is a three-span cable-stayed bridge (a total span of 860 m with a mid-span of 460 m) in Yokohama Japan (see Figure 2-7). This bridge was numerically modelled to determine whether it can meet the new Japanese standard for seismic design of bridges (Fujino et al., 2005, Siringoringo et al., 2013). It was found that this bridge required retrofitting in some components to avoid major damage in certain level of seismic loadings. The list of required elements to be repaired is follows;

1) Providing adequate seating on the approach span
2) Extra cable connection between girder and end-piers, since significant damage would occur by longitudinal excitation
3) Extra stiffeners in the towers and piers
4) Providing a cable inside the lateral upper-beam near the top of the tower to prevent the beam falling down
5) Installing additional seats on the lateral beams under the girders.

Apparently, the Yokohama-Bay Bridge has been modified before the Great East Japan (Tohoku) earthquake on 11th March, 2011 (Fujino et al., 2005). It is noteworthy that the intensity of Great East Japan (Tohoku) earthquake around Yokohama Bay bridge was level 5+ (PGA 1.4-2.5 m/s^2) out of 7 (level 7 is the highest), however, due to the abovementioned structural enhancements the bridge did not experience any structural damage.

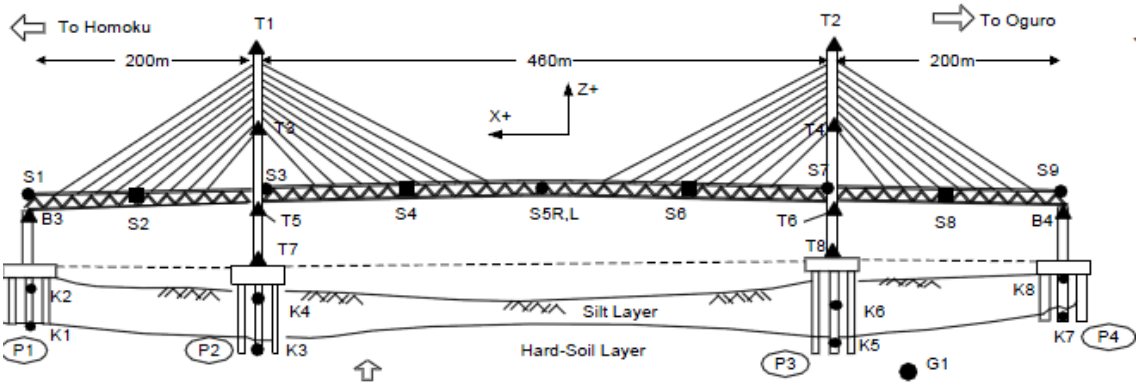

Figure 2-7 Yokohama Bay Bridge.

2.4.3 General seismic design for cable-stayed bridges

Generally, cable-stayed bridges respond well to the vertical seismic loads, because the bridges are designed to carry heavy vertical live loads. Also, the vertical components of seismic acceleration are often smaller than the horizontal (i.e. transversal and longitudinal) components. Accordingly, the seismic loadings in the directions across and along the deck have the primary significance in bridge design.

Unlike ordinary structures, cable-stayed bridges are considered important structures and are, therefore, required to survive earthquakes of high intensity without collapsing and must also remain operational after the earthquakes as they are required to serve as vital transportation links. Recommended performance-based design earthquake intensities are summarised in Table 2-1. Corresponding to these intensities, the acceptable damage levels are as follows;

- For small earthquakes, bridge should not be damaged
- For moderate earthquakes, the damage level would be small, easy to repair without closure of the bridge, and
- For large earthquakes, significant damages would occur but without bridge collapse or closure for emergency occasions.

Table 2-1 Earthquake intensity

	Earthquake intensity (probability of exceedence in 50 years)		
Bridge significance	Small	Moderate	Large
Normal	20%	4%	1%
Vital	10%	2%	1%

Tower/Pylon design

With regard to the direction of earthquake load and optimal performance of the pier, there is a significant contradiction in proper design of pylons. Parallel vertical pylon legs are preferred to transfer loads from the deck to the ground. However, for seismic loadings, this design is not optimal, as the lateral accelerations in the deck will create moments about the vertical axis. Furthermore, the lateral forces created by seismic loads are considered in a similar manner as for wind forces, except the vertical force component that must be considered in the seismic design. These factors together make the economic design of pylons by only using a portal frame or a braced frame a challenging task (Gimsing and Georgakis, 2011b). Hayashikawa et al. (2000) studied the nonlinear dynamic response of a cable-stayed bridge under three-dimensional earthquake ground motion and examined the effect of tower shapes, such as A-shape, H-shape and gate-type shapes which are shown in Figure 2-8. The steel bridge was modelled as a frame structure and the elasto-plastic finite displacement analyses using 3D beam elements were carried out. According to the analyses, the A-shaped tower is the most suitable shape among the three shapes in terms of the bending moment and curvature. However, the A-shaped tower may create large axial forces at the base of the tower. This could cause the anchor bolts at the base of the tower to fail in up-lift. Thus, the safety of the tower base must be considered in seismic design.

Also, the pyramid pylon is considered to perform well under seismic loadings (Gimsing and Georgakis, 2011b). Therefore, new bridges, such as the Stonecutters Bridge, Sutong Bridge and Rion-Antirion have employed one of these pylon geometries (ARUP, 2010, Gimsing and Georgakis, 2011a, Teyssandier et al., 2000).

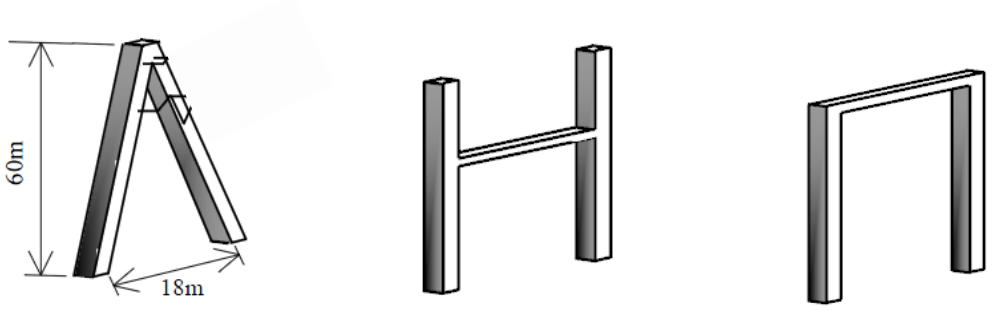

(a) A-Shape (b) H-Shape (c) Gate-Shape

Figure 2-8 The effect of tower shapes (Hayashikawa et al. (2000).

Deck design

To reduce the effects of lateral and longitudinal displacement, the mass and stiffness of the deck should be properly accounted for in the design (Gimsing and Georgakis, 2011a). Large longitudinal displacement could cause damage around the support area and up-lift of the deck as in the case of the Higashi-Kobe bridge during Kobe earthquake (JSCE, 2010). Furthermore, to avoid deck up-lift, some retrofit techniques (such as applying extra cable support or damping system) are suggested in JSCE standard (2010). Also, to minimise lateral/longitudinal displacements, seismic devices (such as dampers) are used in recent bridge designs. For example, in the Rion-Antirion bridge, located in a seismically active zone in Greece, a combined metallic fuse and damper system for the lateral connection between deck and pylons has been employed to mitigate the earthquake damage (Gimsing and Georgakis, 2011a, Infanti et al., 2004).

Other factors

Khan et al. (2006) presented the conceptual damage probability matrix for fan type cable-stayed bridges. By using a 2D bridge model, the sensitivity of annual probability of failure was determined for degree of correlation, angle of earthquakes, ratio of the ground motion components and soil condition. It was found out that the longitudinal ground acceleration is the most critical seismic load for cable stayed bridges. Also, in a different study, McCallen (2009) states that although low frequencies of ground motion waveforms (frequencies below 0.2 Hz which are normally considered as negligible for normal structure) should be included in analyses of long span bridges.

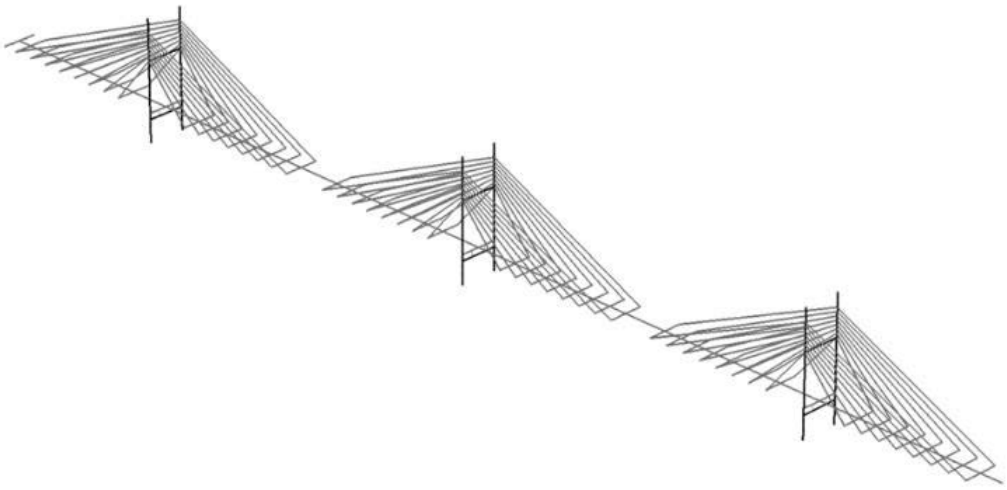

Figure 2-9 Frame finite element model of a multi-span cable stayed bridge (Okamoto and Nakamura, 2011).

New cable-stayed bridge system

The cable-stayed bridges typically have multi-spans and are, therefore, complicated systems. Their dynamic behaviour for seismic loadings is investigated individually (Okamoto and Nakamura, 2011, Ni et al., 2005, Mu et al., 2009). For example, Okamoto and Nakamura (2011) analysed the multi-span cable-stayed bridge (shown in Figure 2-9) which has a new type of hybrid tower system consisting of steel box filled with concrete. This new hybrid towers have shown high resistance under the medium and strong seismic actions.

2.4.4 Design criteria and standards

As shown in the previous sections, there are several researchers who are taking seismic behaviour of cable stayed bridges into account. However, more research is still necessary in order to identify both conceptual and optimal seismic design for cable stayed bridges (Calvi et al., 2010). In addition, several standards have limited provisions for bridges with spans in the range less than 250 m (AASHTO, 2010, AS1170.4, 2007).

2.5 Summary

This chapter presented the three main research areas pertaining to cable-stayed bridges subjected to extreme loading scenarios including sudden loss of cable(s), blast loadings as well as the seismic actions.

Sudden loss of cables

One of the most critical loading scenarios for a cable-stayed bridge is the sudden loss of cable that might lead to a "zipper-type" progressive collapse. With regard to the several research works related to sudden loss of cables summarised in Section 2-3, the following conclusions can be drawn;

- The dynamic responses of the bridge following sudden loss of cables strongly depend on the location of the lost cable.
- Dynamic amplification factors (DAFs) can be larger than 2 when abrupt loads are applied on the structures with multi degree-of-freedoms (DOFs) such as cable-stayed bridges. Therefore, design of this type of bridge based on DAF=2 is

not always conservative and it can underestimate the load factors in the critical sections.

- Different *DAF*s should be specified for each section as well as each component of the response (i.e. deflection, internal forces etc.), also the influence of action and structure type should be reflected in a properly determined *DAF*.
- In cable stayed bridges, the *DAF*s are affected by the layout of the stays, load combinations, deck stiffness as well as damping ratio.
- Given the calculation tools available for assessing structures, it is believed and strongly recommended that a dynamic analysis should be carried out for large structures subjected to sudden breakage of a component; because the simplistic equivalent static analysis approach based on *DAF*=2 could be unconservative.

Issues and suggestion

The methodology to calculate the *DAF*s for cable-stayed bridges has been quite well described in the literature. However, only limited investigations have been conducted regarding the effect of location, duration and number of lost cable(s) on the magnitude of *DAF*s. In addition, the relation between *DAF*s and the potential of progressive collapse should be determined.

Blast loads analysis

Since the 911 terrorist attacks on World Trade Centre towers 1 and 2, the terrorist attacks have become a major concern for public as well as structural engineers. Accordingly, research on the blast loading and progressive collapse of buildings subject to terrorist attacks has dramatically increased over the last decade. Targets of the blast loads are often iconic and important structures including bridges. The summary of research on the blast load analyses presented in Section 2-4 is as follows;

- Blast load analysis has a significant role in design of modern bridges
- Blast load analyses of bridge structures should be done on individual components such as piers, towers and deck, because the damage level and its implications on the entire bridge vary from one component to another. For example, a large cable-stayed bridge model may collapse due to significant

damage in one of the main tower; however, loss of one cable will not necessarily trigger the progressive collapse of the entire structure.

- It is well-established through different studies that some of the existing bridges should be retrofitted against impact of blast.
- For cable-stayed bridges, an individual cable would not be damaged by the direct air blast pressure, however, the anchorage zone of the cables are prone to severe air blast damage and subsequent loss of cable support may occur to the damage in the anchorage zone.

Issues and suggestion

The experimental and numerical studies on the local response of steel cable stayed bridges subjected to blast loading are scare. Accordingly, in this thesis a cable stayed bridge with steel multi-cell box girder deck and tower is analysed under different amount of explosives. The relationship between the number of lost cables and the amount of explosive is numerically investigated. Also, to investigate the adequacy of alternate load path (ALP), the results obtained from simple cable loss analyses will be compared with the results of the loss of cables due to blast loadings that included the local damage.

Seismic analysis

Several bridges have suffered damage during past earthquakes. Damages have been reported on the columns, piers and deck of the bridges and even some of the bridges have fully collapsed. Accordingly, seismic loadings must be considered in the design of bridge structures including cable-stayed bridges. The summary of the literature review presented in Section 2.5 are as follows;

- Cable-stayed bridges in Japan were damaged during Kobe earthquake in 1995. Examples of the reported damage are related to support of the tower, pin-support of the deck, deck itself and dampers.
- Post-earthquake analysis is important to determine the damage mechanism and to evaluate the required retrofitting techniques.
- Similar to blast load analysis, each component has design criteria against seismic loadings.

- Recently, seismic devices such as dampers or wires are required to be installed externally to reduce the impact of large seismic forces.
- Large-scale bridges such as cable-stayed bridges should be analysed and designed in a case-by-case basis, because the responses would be quite different due to lack of common design criteria.

Issues and suggestion

In this thesis, a detailed 3D nonlinear continuum-based finite element (FE) model is developed and analysed dynamically under different earthquake acceleration records in both longitudinal and transverse direction. With regard to the results of dynamic analysis, the critical direction of the earthquake loads that would lead to maximum internal forces and deflections are determined. Also, the most critical structural components, the dominant failure mode and location of plastic hinges within different structural components of a cable stayed bridge subjected to seismic action are determined.

Chapter 3 : Determining Critical Cable Loss Scenarios, *DAF* and *DCR* by 2D FE modelling

Summary of chapter

In this chapter, a linear-elastic finite element (FE) model for a cable-stayed bridge designed according to Australian standards is developed and analysed to determine the effect of sudden loss of cable(s) statically and dynamically with and without geometrical nonlinearities included. The dynamic amplification factor (*DAF*) and demand-to-capacity ratio (*DCR*) in different structural components including cables, towers and the deck are calculated and it is shown that *DCR* usually remains below 1 (irrespective of the nonlinearity occurring) in the scenarios studied for the bridge under investigation, however, *DAF* can take values larger than two. Moreover, the effects of location, duration and number of cable(s) lost as well as effect of damping level on the progressive collapse resistance of the bridge are studied and the importance of each factor on the potential progressive collapse response of the bridge is investigated.

3.1 Introduction

In cable-stayed bridges, zipper-type collapse triggered by sudden loss of cable is a catastrophic failure mode that should be prevented. Accordingly, the PTI (2007) guideline recommends that the implications of different cable loss scenarios are thoroughly investigated by equivalent static analyses in conjunction with dynamic amplification factor (*DAF*). The typical *DAF* value for building and bridge structures adopted by existing standards and guidelines is *DAF*= 2.0 (DoD, 2005, GSA, 2003, PTI, 2007), however, for cable-stayed bridges with high degrees of redundancy, application of a constant *DAF*= 2.0 in conjunction with equivalent static analysis has been questioned by several researchers (Mozos and Aparicio, 2010a, Mozos and Aparicio, 2010b, Ruiz-Teran and Aparicio, 2007, Starossek, 2011). In particular, Mozos and Aparicio (2010 a & b) compared the results of equivalent static with dynamic analysis

and concluded that the equivalent static analysis with a *DAF*= 2.0 is not always conservative for evaluating the bending moments within the pylon following loss of a single stay. Accordingly, application of a full dynamic analysis for progressive collapse assessment of bridges subjected to cable loss is highly recommended (Ruiz-Teran and Aparicio, 2009).

To determine the dynamic amplification factor (*DAF*) and the potential of progressive collapse under several parameter variation, the global responses of the entire bridge model are required. In this chapter, a 2D linear-elastic finite element model of a cable stayed bridge is developed and analysed statically and dynamically by using ANSYS software. A parametric study is undertaken and parameters influencing *DAF* and *DCR* such as the time over which the cable is removed, damping ratio and geometrical nonlinearities (large displacements) are studied. Moreover, different cable loss scenarios are examined and the most critical scenarios that lead to the maximum *DAF* and *DCR* are identified.

3.2 Dynamic amplification factor (*DAF*) and demand-to-capacity ratio (*DCR*)

The focus of this paper is on *DAF* and *DCR* values calculated for the most critical sections in the deck, pylons and cables.

The dynamic amplification factor (*DAF*) adopted by Wolff and Starossek (2009) is

$$DAF = \left| \frac{S_{dyn\,(t)} - S_{healthy}}{S_{F\,0} - S_{healthy}} \right| \tag{3-1}$$

Apart from *DAF* defined in Equation (3-1), in this research the equivalent *DAF* (reference) due to sudden loss of cable(s) is also defined as

$$\text{Equivalent } DAF = \left| \frac{S_{dyn\,(t)} - S_{healthy}}{S_{F\,1} - S_{healthy}} \right| \tag{3-2}$$

where $S_{dyn\,(t)}$ is the maximum/minimum value of the response at instant time t of the dynamic response, $S_{healthy}$ is the response obtained from the static analysis of the healthy bridge (Figure 3-1a) and S_{F0} and S_{F1} are the responses obtained from the static analyses of cases $F0$ and $F1$ as shown in Figures 3-1b and 3-1c, respectively.

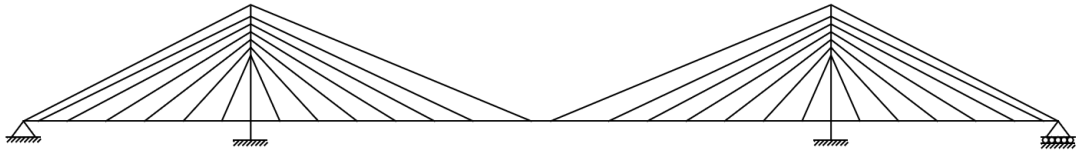

(a) Healthy Structure

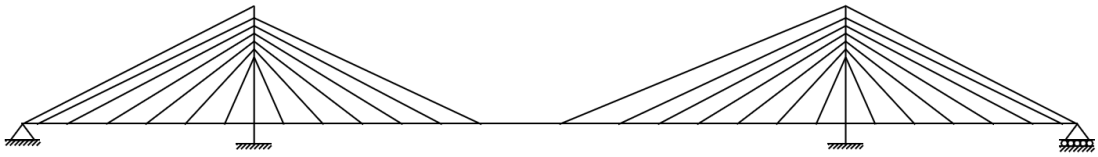

(b) Case *F0*

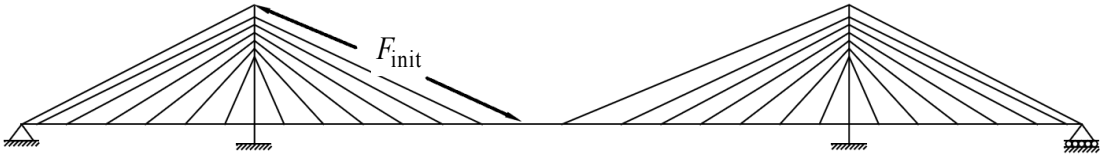

(c) Case *F1*

Figure 3-1 Different types of static analyses.

Before removing the cable(s), the healthy bridge is analysed statically and the internal forces of the members, $S_{healthy}$ are obtained from this analysis (Figure 3-1a).

At the next stage, one cable is removed (Figure 3-1b) and then the internal force of the removed cable with opposite sign, F_{init}, is applied on the deck and tower (Figure 3-1c) as recommended by Zoli and Woodward (2005) and PTI (2007). The S_{F1} values are taken from the results of this recent analysis (Figure 3-1c).

In this study, demand-to-capacity ratio (*DCR*) is defined as

$$DCR = \left| \frac{\sigma}{\sigma_y} \right| \times 100 \tag{3-3}$$

where σ is the existing stress from dynamic analysis and σ_y is the yield stress or the breaking stress of the material.

The model used in this chapter is a linear-elastic model, accordingly the *DCR* value is employed to determine whether the members have yielded. The *DCR* values greater than 100% are indicative of material yielding (material nonlinearity)

The existing stress σ at the most critical section can be calculated from

$$\sigma = \pm \frac{N}{A} + \frac{M\,y}{I} \tag{3-4}$$

where N and M are the axial force and bending moment, respectively, and y is the distance from the neutral axis. A is the cross-sectional area and I is the moment of inertia of the section as shown in Table 3-1.

The location of critical sections, where maximum σ occurs, is determined from the envelop of the dynamic analysis and *DCR* values are always calculated for combination of axial force and bending moment (obtained from the envelop of dynamic analysis) and typically the maximum *DCR* values are calculated at the most critical sections where either maximum bending moment or maximum axial force has occurred. The material is assumed to be elasto-plastic (see Figure 3-2).

Table 3-1 Material and geometrical properties of the deck, towers and cables.

		E **(GPa)**	***A*** **(m^2)**	***I*** **(m^4)**	σ_y **(MPa)**	**Yield Moment** M_y*** (MN.m)**	**Yield Force** N_y*** (MN)**
Girder		200	1.43	1.21	450	470	363.9
Tower		200	4.75	45.7	450	1,457	
Cable No.	**1-5, 26-35, 56-60**	200	0.0327		1,860		60.8
	6-10,21-25, 36-40, 51-55	200	0.0183		1,860		34.0
	11-20, 41-50	200	0.0165		1,860		30.7

* M_y and N_y are the values corresponding to the first yield of the material in absence of interaction between axial force and moment.

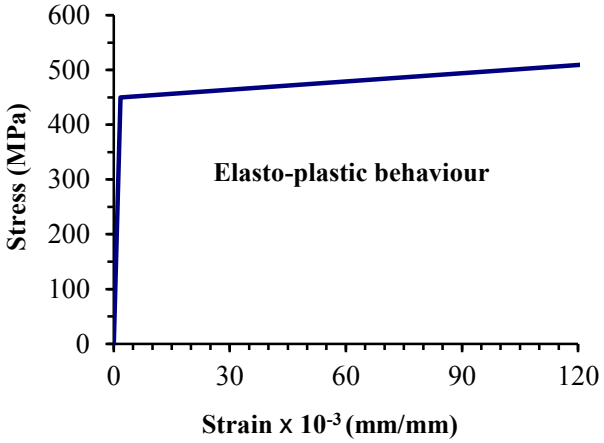

Figure 3-2 Adopted constitutive law for steel within deck and tower

3.3 Description of materials, geometry and loads

3.3.1 Material properties and geometry of the bridge

The dimensions of the bridge and geometry of sections as well as the configuration of cables for the bridge considered in this chapter are shown in Figure 3-3. The bridge is symmetrical and has a main-span length of 600 m supported by two 140 m tall towers and 60 pairs of cables. All cables, except the first and the last four back stays (i.e. cables no. 1-4 and 57-60), are regularly spaced (20 m apart) along the deck (Figure 3-3a).

Regarding the back stays no. 1-4 and 57-60 (see Figure 3-3b), a 2.5 m spacing along the deck was considered. Furthermore, all cables are regularly spaced (4 m apart) over the pylons height over a distance of 56 m from the top of the pylon. The bridge deck is 25.6 m wide (8 traffic lanes according to AS5100.2 (2004) and 2 m deep and is made of a multi-cell steel box girder as depicted in Figure 3-3c. This bridge deck is restrained by a pin support at the far left end and by a roller support at the far right end (Figure 3-3a), and there is no direct connection between the deck and the pylons. The cross section of each leg of the pylons which are fully fixed at the ground level is shown in Figure 3-3d.

The modulus of elasticity, E, and the yield stress of steel, σ_y, as well as the geometrical properties of the deck, including the second moment of area, I, and cross sectional area, A, are given in Table 3-1. Three different sizes of stays are used as given in

Table 3-1. Further, the axial force and bending moment corresponding to the first yield of material for the cables, deck and towers are calculated and summarized in Table 3-1.

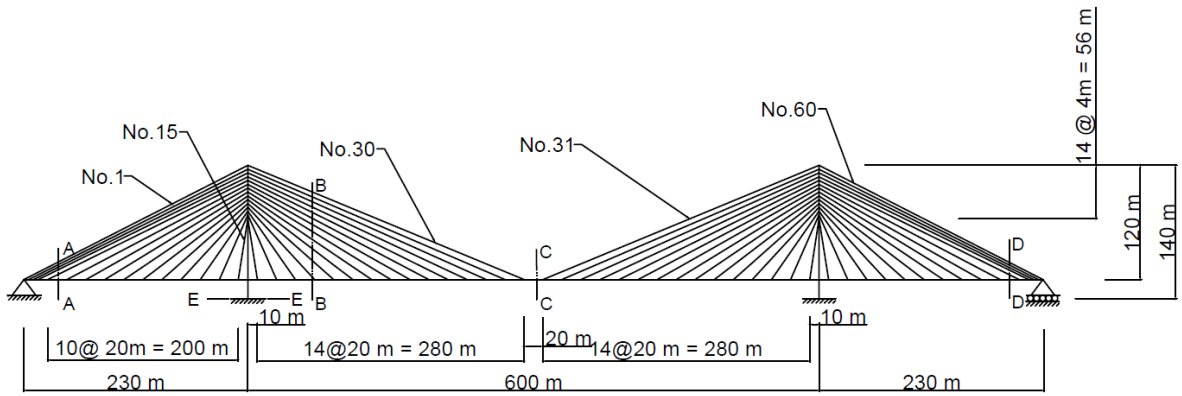

(a) Bridge configuration and location of critical sections

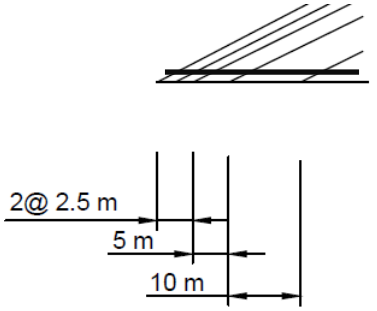

(b) Cable spacing at the end supports

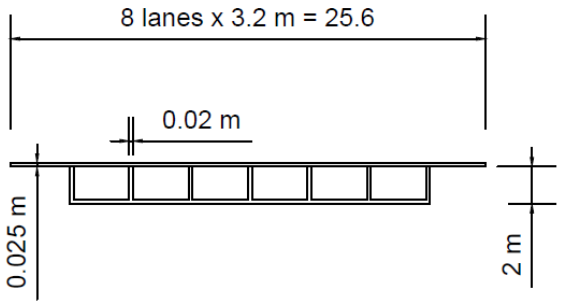

(c) Cross section of the deck

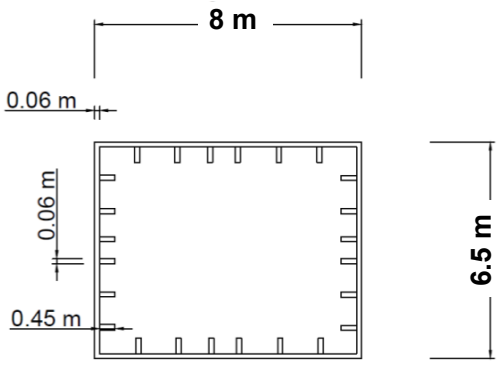

(d) Cross section of the tower

Figure 3-3 Bridge elevation and principal dimensions.

3.3.2 Design loads

The bridge considered in this chapter has been designed for gravity loads (i.e. permanent and traffic loads) as well as the post-tensioning forces determined according to Australian Standard AS5100.2 (2004). The permanent load includes the self-weight of the structural elements as well as the wearing surface of the road (see Figure 3-3c).

The adopted traffic load is S1600 stationary traffic load which contains a uniform distributed load and heavy truck loads as defined in AS5100.2 (2004) and shown in Figure 3-4.

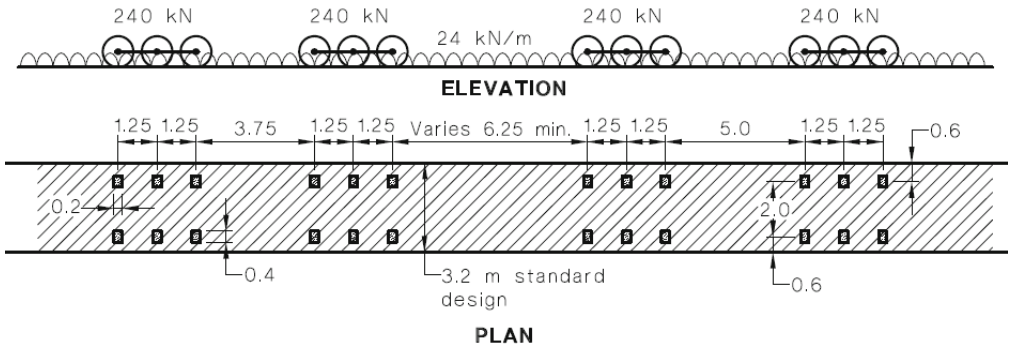

Figure 3-4 S1600 stationary traffic load according to AS5100.2 (2004).

The post-tensioning forces in the cables were calculated based on serviceability design requirements and maximum mid-span deflection due to traffic load as specified by AS5100.2 (2004). Furthermore, the post-tensioning forces in the cables were adjusted according to 'zero displacement method' to achieve the desired profile for the bridge deck (Wang et al., 1993).

In design, it was assumed that local buckling would not occur and the ultimate loading capacity of members is governed by yielding of the material according to AS5100.6 (2004) requirements. Furthermore, the maximum stress induced in the deck and towers due to service load (permanent action + S1600 traffic load) plus the post-tensioning forces is always less than $0.5\sigma_y$ and the maximum stress in the cables is limited to $0.45\sigma_y$ in accordance to JSCE (1990) design requirements.

3.3.3 Cable loss scenarios

With regard to existing guidelines (PTI, 2007) for anti-progressive collapse design of cable stayed bridges, only considering the scenarios associated with loss of a single cable is adequate, however, some researchers believe that scenarios in which more than one cable is lost should not be ignored (Wolff and Starossek, 2010). Accordingly, in this study, three different scenarios corresponding to loss of only one cable and simultaneous loss of two and three cables are considered. In the first scenario (when only one cable is lost) four different cases which are potentially the most critical ones are investigated (Wolff and Starossek, 2010, Aoki et al., 2011). In case-1 and -4 the loss of cables no. 1 and 60, respectively, connected to the end supports (Figure 3-3a) are studied, in case-2 loss of the shortest cable adjacent to the left tower (cable no. 15) is considered and in case-3, the longest cable connected to mid-span (cable no. 30) is lost. In the second scenario (loss of a pair of cables) two different cases are analysed. In case-1, the longest cables connected to the pin support (cables no.1 and 2) are lost, and loss of cables connected to the mid span (cables no.30 and 31) is considered in case-2.

In the third scenario only one case is considered in which the three cables connected to the pin support (cables no.1, 2 and 3) are lost. The scenarios considered in conjunction with different loading patterns are listed in Table 3-2. LC-1 and LC-2 in table are different load cases which are explained in following section.

Table 3-2 Scenarios considered.

Scenario Name	Lost cable no.	Load case (Figure 3-5)
scenario -1/LC-1, case-1	1	LC-1
scenario -1/LC-1, case-2	15	
scenario -1/LC-1, case-3	30	
scenario -1/LC-1, case-4	60	
scenario -1/LC-2, case-1	1	LC-2
scenario -1/LC-2, case-2	30	
scenario -2/LC-2, case-1	1 & 2	
scenario -2/LC-2, case-2	30 & 31	
scenario -3/LC-2, case-1	1 & 2 & 3	

3.3.4 Finite element model

A 2D finite element model of the bridge is developed in ANSYS (2009). The structural elements are modelled by frame elements and the cables are treated as only tension members with limited tensile capacity. The material is assumed to be elasto- plastic (see Figure 3-2), and the effects of large displacements and geometrical nonlinearities are taken into account by activating the required solution algorithm of the ANSYS software (2009). The demand-to-capacity ratio (*DCR*) calculated at the most critical cross sections of the deck, pylons and cables are employed to verify the adequacy of the adopted linear elastic material behaviour.

3.3.5 Load combinations adopted for progressive collapse assessment

In conjunction with the abovementioned cable loss scenarios, two different load combinations are considered as shown in Figure 3-5. In load combination LC-1 (Figure 3-5a) the distributed component of the traffic load along with dead load is applied over the entire bridge length whereas in LC-2 (Figure 3-5b) the distributed component of the traffic load as well as the heavy truck loads are only placed on the middle span and the back spans are only under permanent action (dead load). The preliminary investigations based on influence line theory showed that LC-2 is more critical than LC-1.

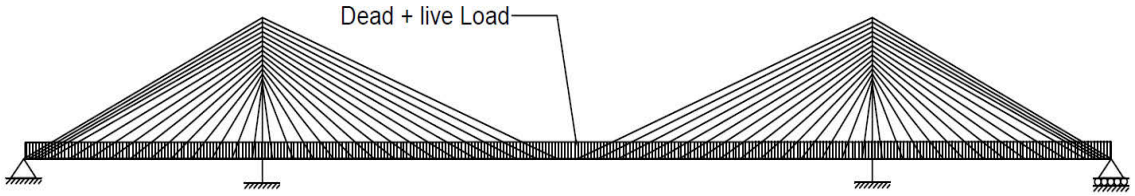

(a) LC-1

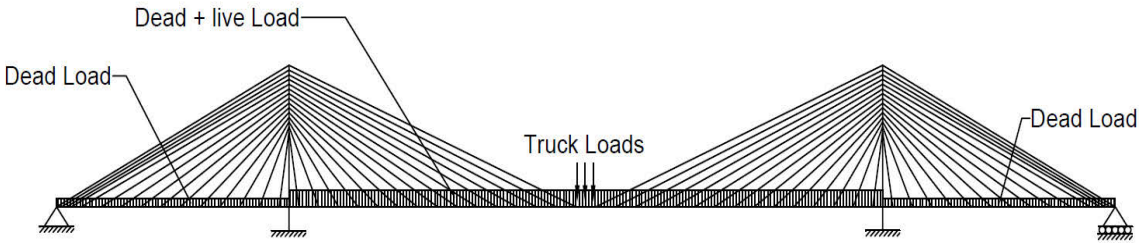

(b) LC-2

Figure 3-5 Applied load cases.

For the cable loss scenarios, adopted load factors are as recommended by PTI (2007),

$$1.1DC + 1.35DW + 0.75\,(LL+IM) + 1.1CLDF \tag{3-5}$$

where, *DC*= dead load of structural components and non-structural attachments, *DW*= dead load of wearing surfaces and utilities, *LL*= full vehicular live load placed in actual stripped lanes, *IM*= vehicular dynamic load allowance taken equal to zero in this study and *CLDF*= cable loss dynamic forces.

In the example considered in this chapter, the exact value of cable internal forces are available, and accordingly the load factor of 1.1 on the cable loss dynamic forces that accounts for a variation of final cable force in construction has been ignored.

3.3.6 Cable removal method and type of analysis

In progressive collapse assessment of structures/bridges based on alternate load path (ALP), the time over which the critical members (i.e. columns or cables) are removed can significantly affect the response of the structures. If the member is removed over a longer period of time (typically longer than the first natural period of structure) a static analysis is deemed adequate, however, removing the members (i.e. columns or cables) over a shorter period of time warrants a dynamic analysis. For analysis of cable stayed bridges against progressive collapse, the cables can be removed through a static or dynamic procedure and the FE model should be analysed accordingly. In this chapter, for dynamic analysis a consistent mass matrix with a proportional damping is adopted (Bathe, 1996) and Newmark constant acceleration method, which is unconditionally stable, is used for time integration.

3.3.7 Discussion on the adequacy of the proposed 2D model

Due to lack of experimental data, the proposed 2D models in this study cannot be validated directly; however, the adequacy and accuracy of the proposed FE models and adopted constitutive laws for steel can be verified against other softwares and more complex 3D finite element (FE) models.

In the first step, a 2D FE model of the bridge was developed using Microstran Software and the results obtained from this model for the healthy bridge under LC-1 were compared with the results obtained from 2D FE model developed in ANSYS software (see Figure 3-6).

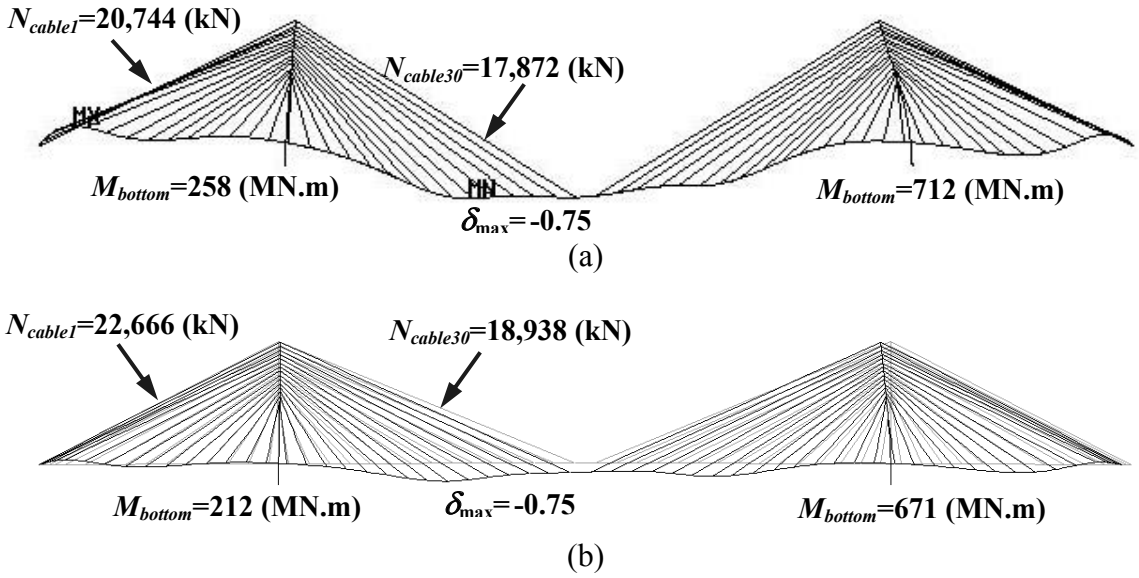

Figure 3-6 Comparison of results obtained from 2D models developed in (a) ANSYS and (b) MicroStran for the healthy bridge under LC-1.

From this comparison, it can be observed that the response (including internal force in the cables and towers and the maximum deflection at the mid-span) obtained from ANSYS model correlates very well with Microstran results. In addition, a 3D FE model of the bridge was developed using shell elements in ANSYS. In the 3D model all material and geometrical nonlinearities were considered and element sizes varied between 0.3-1.0 m. Outline of the 3D FE mesh is shown in Figure 3-7a. Regarding material nonlinearity, Von Mises yield criterion with perfect plastic behaviour (i.e. no strain hardening) was adopted (see Chapter 4). Comparison between 3D and 2D model predictions for the healthy bridge under LC-1 is shown in Figures 3-7b and c that show a very good correlation. Furthermore, comparison of 2D and 3D FE model predictions for the mid-span deflection time history due to loss of cable no. 1 (under LC-1 load case) is shown in Figure 3-8, that clearly demonstrates the adequacy of the proposed 2D model for predicting the global response of the cable-stayed bridges.

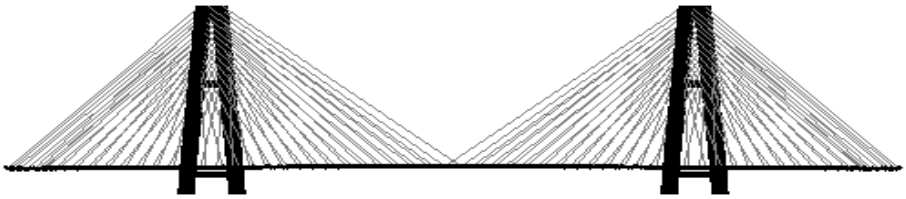

(a)

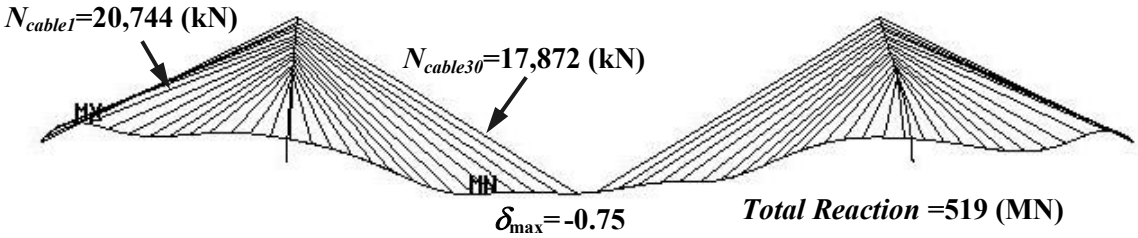

(b)

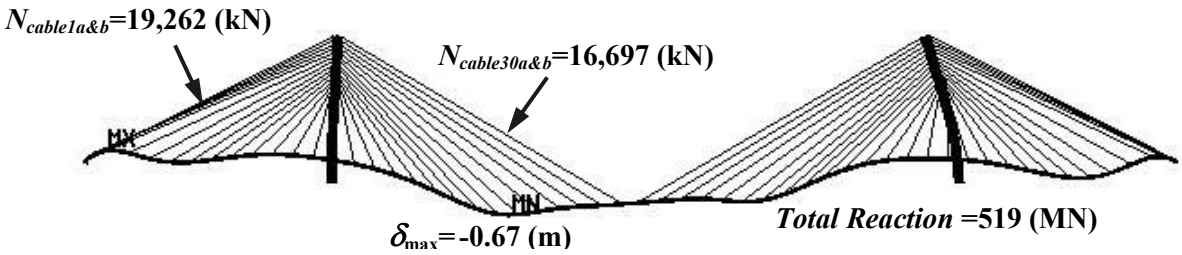

(c)

Figure 3-7 Outline of the (a) 3D FE model and internal force and deflections predicted by a (b) 2D linear-elastic model (c) 3D model with material & geometrical nonlinearity.

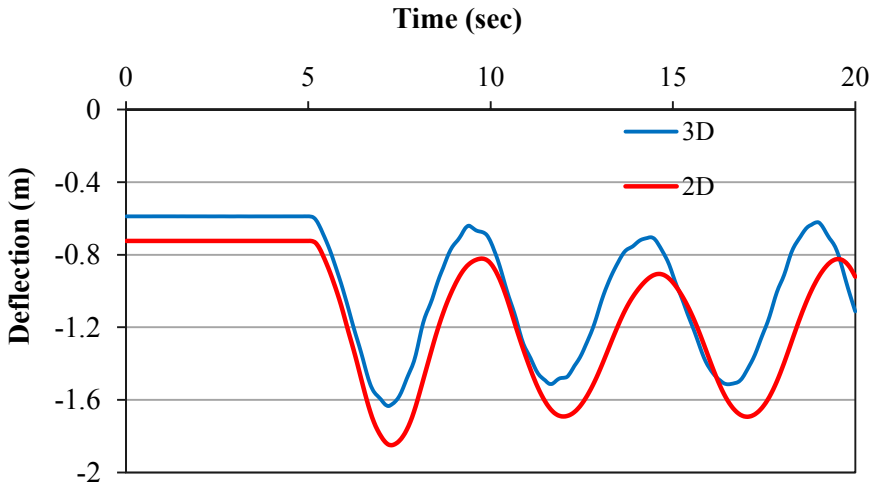

Figure 3-8 Time history of mid-span deflection predicted by 2D and 3D FE models for the bridge subjected to loss of cable no. 1 and LC-1.

3.4 Parametric studies and discussion

A parametric study is undertaken and parameters influencing *DAF* and *DCR* such as the time over which the cable is removed, damping ratio and geometrical nonlinearities (large displacements) are studied. Moreover, different cable loss scenarios are examined and the most critical ones which lead to the maximum *DAF* and *DCR* are identified. The results are presented in Tables 3-3 to 3-5. In these tables, 'Ekill' represents the instantaneous removal of the cables over a time step, i.e. within 0.01 seconds.

3.4.1 Time step over which the cable is removed (cable removal time step)

For dynamic simulation of a cable loss scenario, the bridge without the lost cable is modelled first and the initial force in the lost cable, F_{init} , is gradually applied on the tower and deck (see Figure 3-9a), then the bridge is allowed to reach the equilibrium state which is basically equivalent to the healthy bridge.

After the bridge reaches the equilibrium state, the cable loss scenario is simulated by reducing the force, F_{init}, down to zero over a time step of Δt_{f} (see Figure 3-9b). Alternatively, the cable loss scenario can be achieved by activating a special solution procedure in ANSYS by applying the "EKILL" command. It is noteworthy that the EKILL command deactivates the lost cable element over an integration time step (Δt = 0.01 sec) whereby the element contributes a near-zero stiffness value to the overall stiffness and mass matrix.

Since the time step over which the cable is removed, Δt_{f} , can affect the dynamic response of the bridge, in this part of the parametric study, sensitivity of the dynamic response in relation to Δt_{f} is examined. Four different cases corresponding to removal of cable no. 30 (see Figure 3-9a) $\Delta t_{\text{f}} = 8$ sec, 1 sec, 0.1 sec and application of EKILL command are considered (Figure 3-9b). The time history of bending moment in scenario-1, case-3 at section C-C (Figure 3-3a) for four different cases (i.e. $\Delta t_{\text{f}} = 8$ sec, 1 sec, 0.1 sec and EKILL) are shown in Figure 3-10 and it is observed that dynamic responses (particularly the maximum and minimum values) provided by different Δt_{f} ,

more or less have the same magnitude except for the case in which the cable is removed over 8 sec. The maximum *DCR* and corresponding *DAF* values calculated for one, two and three cable loss scenarios are given in Tables 3-3 to 3-5, respectively.

Table 3-3 Maximum *DCR* and corresponding *DAF* values for scenario-1/LC-1 in which one cable is lost (Gravity load case 1- critical damping ratio is taken as 0.5%).

Lost Cables No.	**Duration Δ_{t_f} (Sec)**	**Geometrical nonlinearity**	***DAF*** (*equivalent DAF*)**	***DCR****
1 (scenario-1/LC-1, case-1, Section A-A)	**8**	on	1.1 (0.5)	40%
		off	1.1 (0.5)	40%
	1	on	1.7 (0.8)	46%
		off	3.8 (1.8)	46%
	0.1	on	1.8 (0.8)	48%
		off	7.9 (3.8)	48%
	Ekill	on	1.8 (0.8)	48%
15 (scenario-1/LC-1, case-2, Section B-B)	**8**	on	1.7 (0.8)	28%
		off	2.4 (1.0)	28%
	1	on	9.4 (4.1)	28%
		off	9.7 (4.3)	28%
	0.1	on	60 (26)#	29%
		off	78 (35)#	29%
	Ekill	on	83 (36)#	30%
30 (scenario-1/LC-1, case-3, Section C-C)	**8**	on	1.1 (0.6)	27%
		off	1.0 (0.5)	26%
	1	on	2.4 (1.2)	30%
		off	2.0 (1.1)	29%
	0.1	on	2.7 (1.3)	31%
		off	2.3 (1.4)	31%
	Ekill	on	2.6 (1.3)	31%
60 (scenario-1/LC-1, case-4, Section D-D)	**8**	on	1.1 (0.6)	34%
		off	1.1 (0.5)	33%
	1	on	1.6 (0.8)	39%
		off	1.6 (0.7)	37%
	0.1	on	1.6 (0.9)	40%
		off	1.6 (0.7)	37%
	Ekill	on	1.7 (0.9)	40%

Table 3-4 Maximum *DCR* and corresponding *DAF* values for scenario-2/LC-2 in which two cables are lost (Gravity load case 2- critical damping ratio is taken as 0.5%).

Lost Cables No.	**Duration Δ_{tf}(sec)**	**Geometrical nonlinearity**	***DAF*** (*equivalent DAF*)**	***DCR****
1&2 (scenario-2/LC-2, case-1, Section A-A)	**8**	on	1.2 (0.6)	69%
		off	1.1 (0.5)	64%
	1	on	2.7 (1.3)	84%
		off	14 (7.1)	74%
	0.1	on	5.1 (2.4)	90%
		off	4.0 (2.0)	83%
	Ekill	on	5.7 (2.7)	91%
30&31 (scenario-2/LC-2, case-2, Section C-C)	**8**	on	1.9 (0.7)	45%
		off	1.0 (1.0)	44%
	1	on	20# (7.5)	60%
		off	1.1 (1.1)	59%
	0.1	on	35# (13)	64%
		off	1.3 (1.3)	64%
	Ekill	on	36# (14)	63%

* *DCR* values are calculated based on combination of axial force and bending moment at different critical sections (with maximum bending moment) along the deck (see Figure 3-3a for location of critical sections).

** *DAF* values were calculated based on maximum bending moment except the ones with # superscript.

DAF value was calculated based on maximum axial force and is a large value due to small static response.

Table 3-5 Maximum *DCR* and corresponding *DAF* values for scenario-3/LC-2 in which three cables are lost (Gravity load case 2).

Lost Cables No.	Duration Δ_{tf} (sec)	Geometrical nonlinearity	Damping	***DAF*** ** (***equivalent DAF***)	***DCR*** *
1 & 2 & 3 (scenario-3/LC-2, case-1, Section A-A)	**8**	on	0.5%	1.2 (0.7)	81%
		off		1.1 (0.6)	78%
	1	on		1.9 (1.1)	108%
		off		1.8 (0.9)	104%
	0.1	on		3.1 (1.4)	117%
		off		2.4 (1.2)	111%
	Ekill	on		3.2 (1.5)	120%
	8	on	1.0%	1.2 (0.7)	81%
		off		1.1 (0.6)	78%
	1	on		1.9 (1.1)	107%
		off		1.8 (0.9)	104%
	0.1	on		2.5 (1.2)	114%
		off		1.9 (1.0)	109%
	Ekill	on		2.7 (1.2)	116%
	8	on	2.0%	1.2 (0.7)	80%
		off		1.1 (0.6)	78%
	1	on		1.9 (1.1)	106%
		off		1.8 (0.9)	102%
	0.1	on		2.0 (1.2)	110%
		off		1.9 (1.0)	106%
	Ekill	on		2.0 (1.2)	112%

With regard to Tables 3-3 to 3-5, it is observed that *DAF* and *DCR* values are quite sensitive to Δt_f (particularly when two cables are lost) and for accurate estimation of *DAF* and *DCR* a fairly small Δt_f (about 0.001-0.1 sec) is required, which is consistent with the recommendations of some guidelines for progressive collapse analysis of framed structures (DoD, 2005, GSA, 2003). It should be noted that removing the cable over 8 sec or 1 sec in this example cannot adequately simulate the sudden loss of cable and produces a quasi-static scenario rather than a dynamic one.

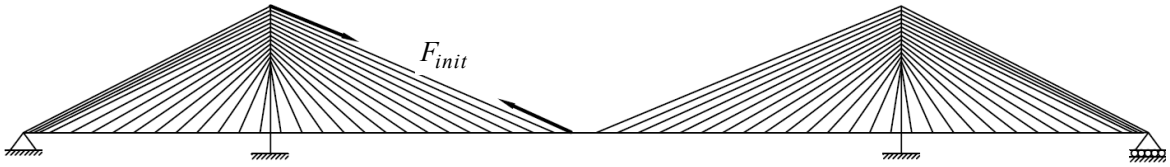

(a) Cable loss scenario considered for sensitivity analysis with respect to removal time step Δt_f.

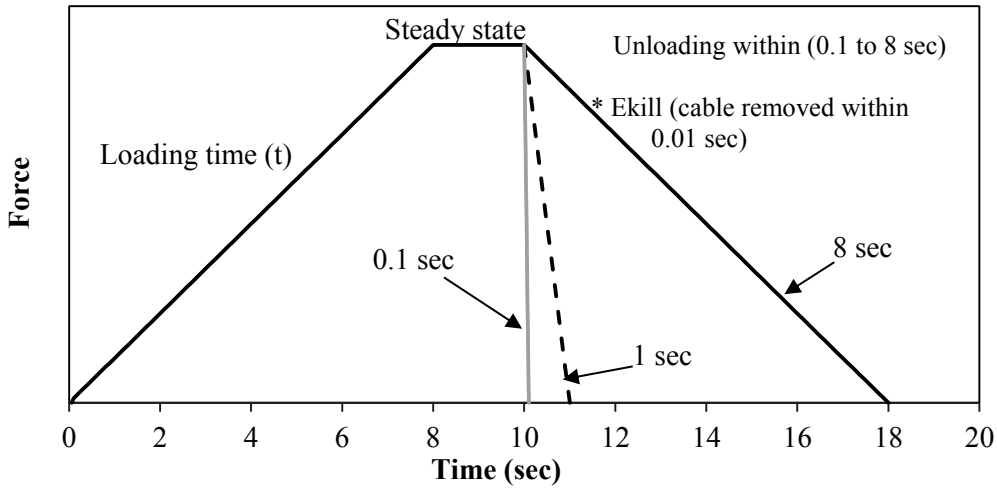

(b) Loading curve

Figure 3-9 (a) Load direction in the lost cable and (b) cable force versus time schemes adopted for dynamic removal of cables.

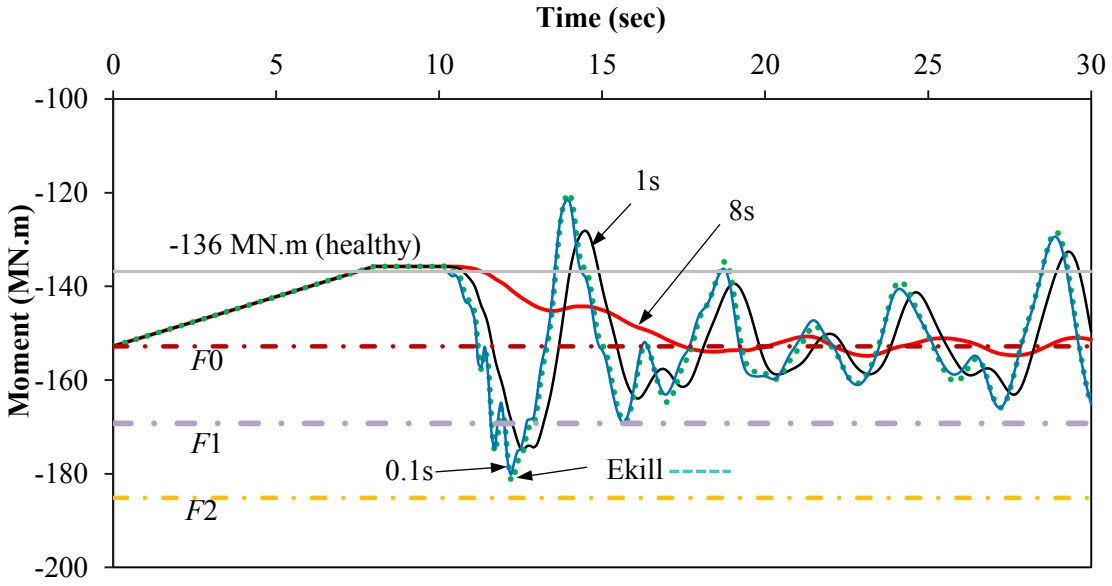

Figure 3-10 Time history of bending moment in scenario-1, case-3 at section C-C of the deck after removing cable no. 30

3.4.2 Structural damping

Mozos and Aparisio (2010b) identified the structural damping ratio as one of the factors that can significantly influence the progressive collapse response of the bridge and *DAF* values, however, they do not provide any details in this regard. Accordingly, the importance of damping ratio and its impact on *DAF* and *DCR* values are investigated in this section. For parametric study, three different levels of damping, i.e. 0.5%, 1% and 2% of critical damping within the acceptable range for steel structures are adopted (Clough and Penzien, 1993). For the triple cable loss scenario, i.e. scenario-3, the time history of bending moment at Section A-A (refer to Figure 3-3a) for three different levels of damping (i.e. 0.5%, 1% and 2% of critical damping) are shown in Figure 3-11 and it is observed that the time history and the maximum/minimum values are very similar for all adopted damping ratios.

The maximum *DCR* and corresponding *DAF* values calculated for the scenarios with three cable losses are given in Table 3-5. The results provided in Table 3-5 clearly show that *DAF* and *DCR* values are not sensitive to the level of damping ratio adopted for dynamic analysis. Furthermore, it can be concluded that the damping ratio within the range considered (i.e. 0-2% of critical damping), has a minor impact on the potential progressive collapse response of the cable stayed bridges.

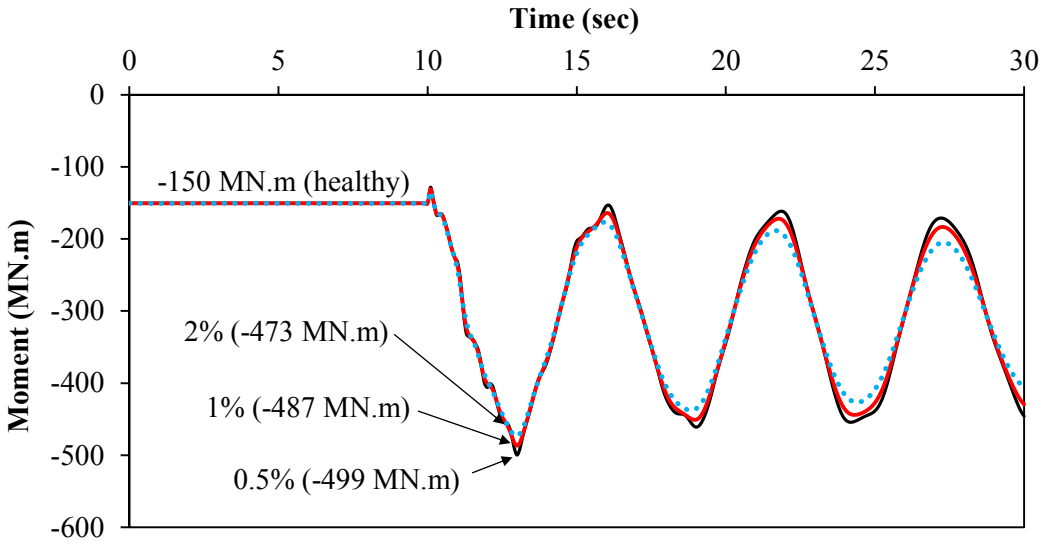

Figure 3-11 Time history of bending moment in scenario-3 at section A-A of the deck obtained from dynamic analysis with different damping ratios.

3.4.3 Geometrical nonlinearities

Effect of geometrical nonlinearity should be taken into account when the deflections of the structure are large enough compared with the size of structural members. Furthermore, for compressive structural members such as columns or pylons the second order $P-\Delta$ effects can reduce the stiffness and loading capacity of the members, particularly in cable stayed bridges, the $P-\Delta$ effects can be quite significant for pylons/towers subjected to lateral air blast pressure (Son and Lee, 2011). The general understanding is that during cable loss scenarios, geometrical nonlinearities can affect the response of the cable stayed bridges and therefore they should be taken into account (Mozos and Aparicio, 2010a, Wolff and Starossek, 2010), however, there is no comprehensive study to clearly demonstrate the contribution of the geometrical nonlinearities to *DAF* values and the progressive collapse response of the cable stayed bridges. The maximum *DAF* and *DCR* values calculated for different cable loss scenarios with and without geometrical nonlinearities included are summarised in Tables 3-3 to 3-5. It is observed that for the bridge under consideration, the effect of geometrical nonlinearities on *DAF* is considerable and the major contribution of geometrical nonlinearity to *DAF* comes from the dynamic analysis $S_{dyn\,(t)}$; in particular, inclusion of geometrical nonlinearities for scenario-1, case-1 in which cable No. 1 is lost has led to a 200% to 400% increase in *DAF*. Among investigated cable loss scenarios, the scenarios involving loss of cable No. 1 (back stay connected to the hinge support) are the most critical ones in terms of significance of geometrical nonlinearity. With regard to Tables 3-3 to 3-5 it is concluded that the maximum and minimum *DCR* values for towers, deck and cables are not really sensitive to geometrical nonlinearity and geometrical nonlinearities have a minor role (for this example less than 7%) in driving the structural members towards their ultimate state during cable loss scenarios.

3.4.4 Cable removal scenarios

In this part, dynamic progressive collapse response of the bridge due to different cable loss scenarios is investigated. The configuration of gravity load cases applied on the deck is shown in Figure 3-5 and a constant damping of 0.5% of critical damping is adopted for dynamic analyses.

Single cable loss

For the sake of comparison, in the single cable loss scenarios two different gravity load cases (i.e. LC-1 and LC-2) are considered (Figure 3-5).

LC-1

Figure 3-12 shows the time history of the bending moment at section E-E, which is the bottom of left tower (see Figure 3-3a), for different cases within scenario-1/LC-1, in which cables no.1, 15, 30 and 60 are removed. It is observed that loss of cables 1, 30 and 60 can significantly affect the magnitude of bending moment at the bottom of left tower, whereas loss of cable no.15 has a minor effect. Among four different cases considered under scenario-1/LC-1, loss of cable no.1 (the longest back stay) is the most critical in terms of maximum bending moment induced in the bottom of the tower.

For scenario-1/LC-1, the value of *DAF* and *DCR*, calculated based on maximum bending moment at the most critical sections along the deck (see Figure 3-3a) are given in Table 3-3. Furthermore, the maximum *DCR* values and corresponding *DAF* observed in the deck, towers and cables for scenario-1/LC-1 are given in Table 3-6. With regards to Table 3-6, it can be concluded that *DAF* can take values higher than 2.0, however the *DCR* values are still well below 100% (no yielding has occurred).

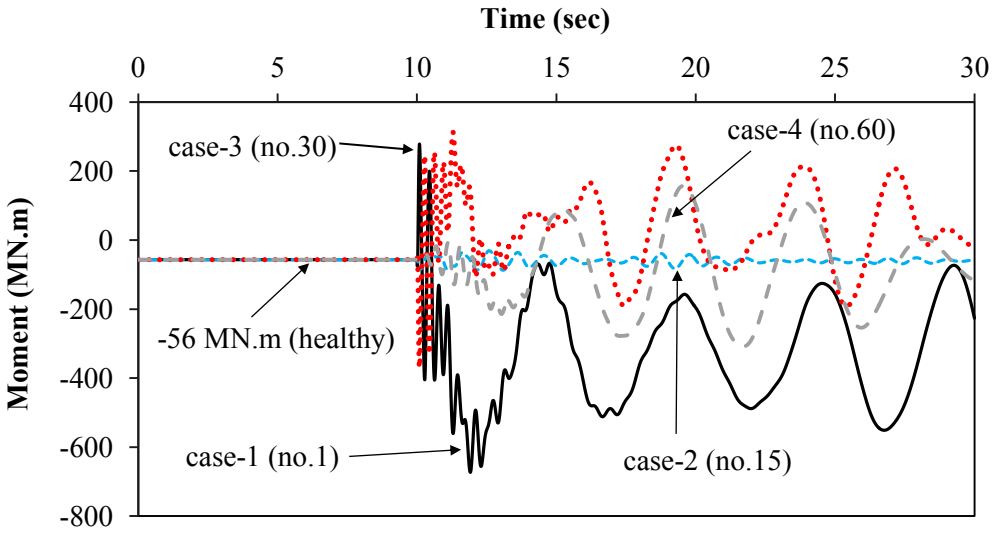

Figure 3-12 Time history of bending moment at the bottom of the left tower for different cable loss cases under scenario-1/LC-1 (only one cable is lost).

In addition, for all structural components, it is concluded that loss of cables no. 1 and 30 are more critical than the other cases under scenario-1/LC-1 and accordingly for scenario-1/LC-2 only loss of these cables will be considered.

Table 3-6 Maximum *DCR* and corresponding *DAF* values in towers, deck and cables under scenario-1/LC-1 (Gravity load case 1 – critical damping ratio is taken as 0.5%).

Lost Cables No.	**Component**	***DAF* (*equivalent DAF*)**	***DCR***
1 (scenario-1/LC-1, case-1)	**Left tower (bottom)**	2.3 (1.1)	25%
	Right tower (bottom)	6.8 (3.0)	25%
	Deck (section A-A)	1.8 (0.8)	48%
	Cable (Cable no. 2)	1.7 (0.8)	36%
15 (scenario-1/LC-1, case-2)	**Left tower (bottom)**	8.2 (4.7)	14%
	Right tower (bottom)	122# (30#)	14%
	Deck (section B-B)	83# (36#)	30%
	Cable (cable no. 14)	1.9 (1.0)	40%
30 (scenario-1/LC-1, case-3)	**Left tower (bottom)**	2.6 (1.4)	18%
	Right tower (bottom)	2.7 (1.3)	18%
	Deck (section C-C)	2.7 (1.3)	31%
	Cable (cable no. 31)	1.5 (0.7)	33%
60 (scenario-1/LC-1, case-4)	**Left tower (bottom)**	7.8 (4.1)	18%
	Right tower (bottom)	1.2 (0.6)	17%
	Deck (section D-D)	1.7 (0.9)	40%
	Cable (cable no. 59)	1.6 (0.8)	35%

DAF value was calculated based on maximum axial force and is a large value due to small static response.

LC-2

The time history of the bending moment at the bottom of the left tower for different cases within scenario-1/LC-2 is given in Figure 3-13 that clearly shows loss of cable no. 1 is more critical than other cases in terms of maximum dynamic bending moment induced at the bottom of the tower. For scenario-1/LC-2, the value of *DAF* and *DCR* calculated at the most critical sections along the deck (section with maximum bending moment) are given in Table 3-7. Furthermore, the maximum *DCR* values and corresponding *DAF* observed in the deck, towers and cables for scenario-1/LC-2 are given in Table 3-8 which shows *DAF* can take values higher than 2.0, however, the *DCR* values are still well below 100% (no yielding has occurred).

Loss of two cables

Among different possible scenarios in which two cables are simultaneously lost, the most critical ones are related to simultaneous loss of cables no. 1 and 2 (case-1) and cables no. 30 and 31 (caes-2) which are investigated in this part of the parametric studies. The time history of bending moment at section A-A for case-1 and -2 within scenario-2 are shown in Figure 3-14.

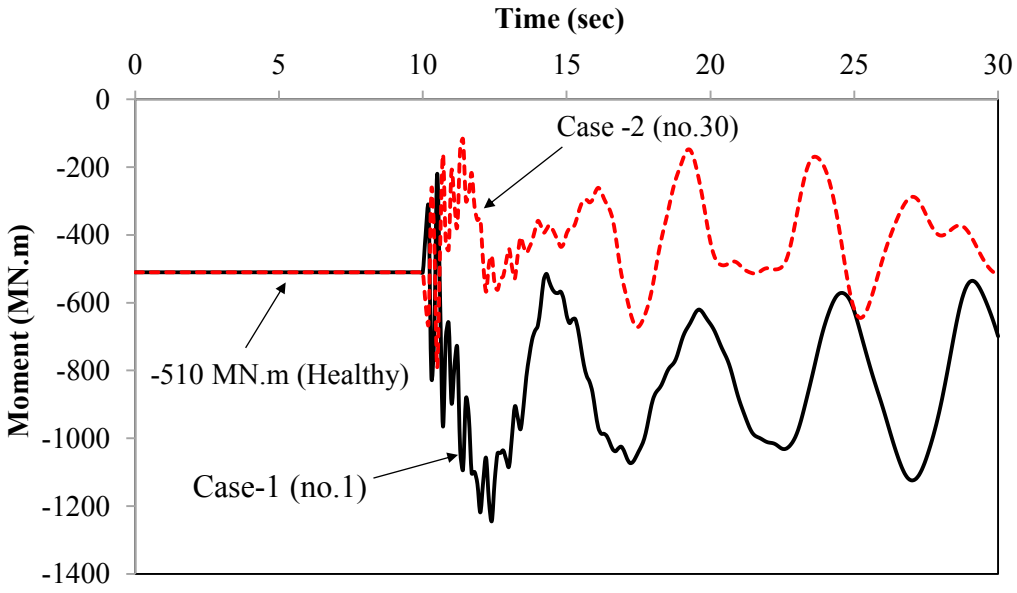

Figure 3-13 Time history of bending moment at the bottom of the left tower for different cable loss cases under scenario-1/LC-2 (only one cable is lost).

Table 3-7 Maximum *DCR* and corresponding *DAF* values for scenario-1/LC-2 in which one cable is lost (Gravity load case 2 - critical damping ratio is taken as 0.5%).

Lost Cables No.	Duration Δ_{tf} (sec)	Geometrical nonlinearity	*DAF* (*equivalent DAF*)	*DCR*
1 (scenario-1/LC-2, case-1, Section A-A)	**8**	on	1.1 (0.6)	55%
		off	1.0 (0.5)	52%
	1	on	4.0 (2.0)	62%
		off	3.0 (1.6)	57%
	0.1	on	7.1 (3.7)	63%
		off	6.1 (3.2)	60%
	Ekill	on	8.2 (4.2)	64%
30 (scenario-1/LC-2, case-2, Section C-C)	**8**	on	1.1 (0.6)	43%
		off	1.1 (0.5)	40%
	1	on	2.4 (1.2)	47%
		off	2.3 (1.0)	44%
	0.1	on	2.8 (1.3)	49%
		off	3.0 (1.3)	46%
	Ekill	on	2.7 (1.3)	49%

Table 3-8 Maximum *DCR* and corresponding *DAF* values in towers, deck and cables under scenario-1/LC-2 (Gravity load case 2 - critical damping ratio is taken as 0.5%).

Lost Cables No.	Component	*DAF* (*equivalent DAF*)	*DCR*
1 (scenario-1/LC-2, case-1)	**Left tower (bottom)**	2.4 (0.8)	36%
	Right tower (bottom)	0.6 (0.3)	37%
	Deck (section A-A)	8.2 (4.2)	64%
	Cable (cable no.2)	1.1 (0.6)	38%
30 (scenario-1/LC-2, case-2)	**Left tower (bottom)**	8.2 (0.9)	27%
	Right tower (bottom)	0.6 (1.2)	17%
	Deck (section C-C)	2.8 (1.3)	49%
	Cable (cable no.31)	2.3 (1.1)	36%

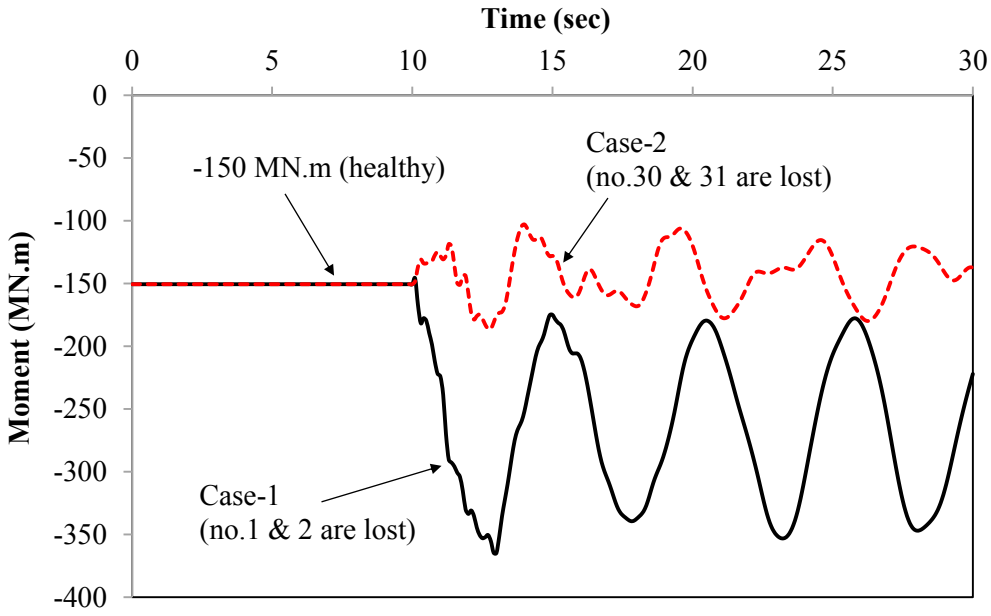

Figure 3-14 Time history of the bending moment at section A-A of the deck under scenario-2/LC-2 (two cables are lost).

It is observed that scenario-2/case-1 corresponding to loss of two back stays (cables no. 1 and 2) is the most critical one in terms of maximum dynamic bending moment induced in the deck. Accordingly, the maximum *DCR* values and corresponding *DAF* observed at different locations in the deck, towers and cables for scenario-2/case-1 are given in Figure 3-15.

Moreover, for scenario-2/LC-2, *DAF* and *DCR* values determined at the most critical sections (based on maximum bending moment) along the deck are given in Table 3-4.

With regard to the results obtained for scenario-2, it is concluded that similar to scenario-1, *DAF* can take values higher than 2.0, however the *DCR* values are still below 100% (no yielding has occurred) and accordingly no potential progressive collapse due to material nonlinearity is expected.

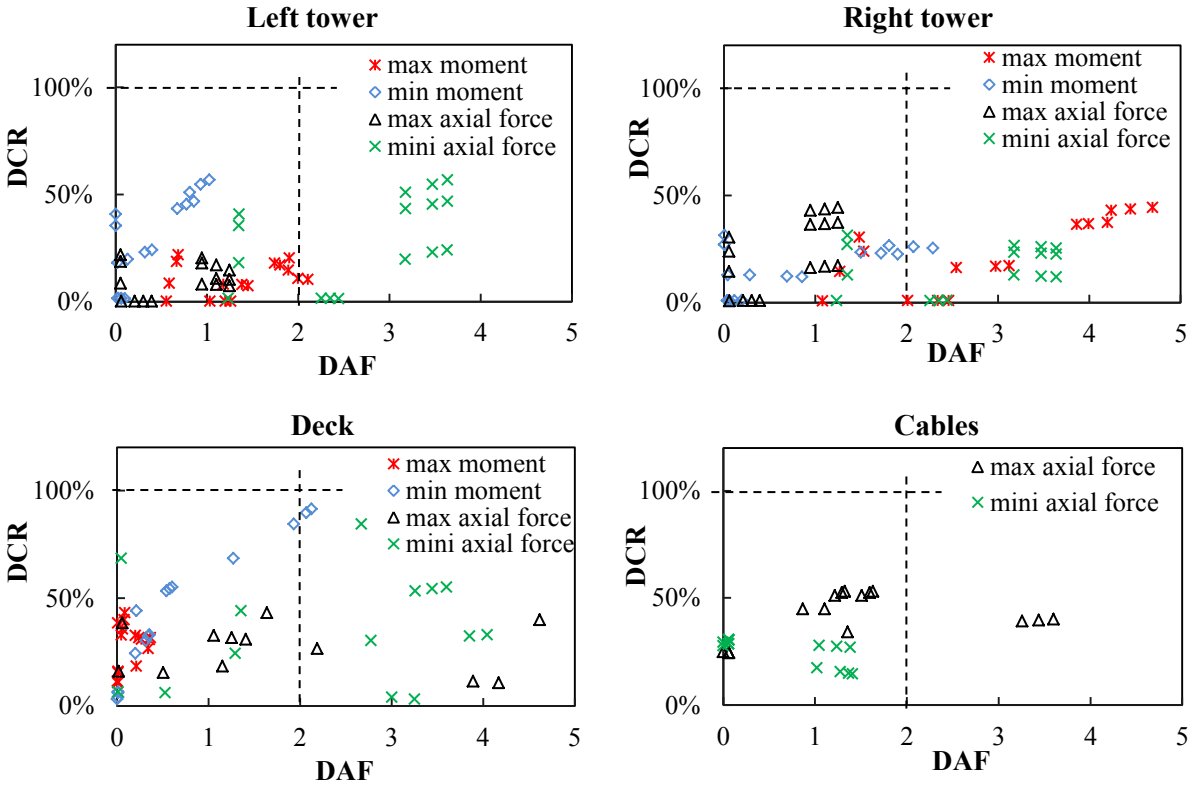

Figure 3-15 *DAF* versus *DCR* values for scneaio-2 (LC-2, loss of cables no. 1 and 2).

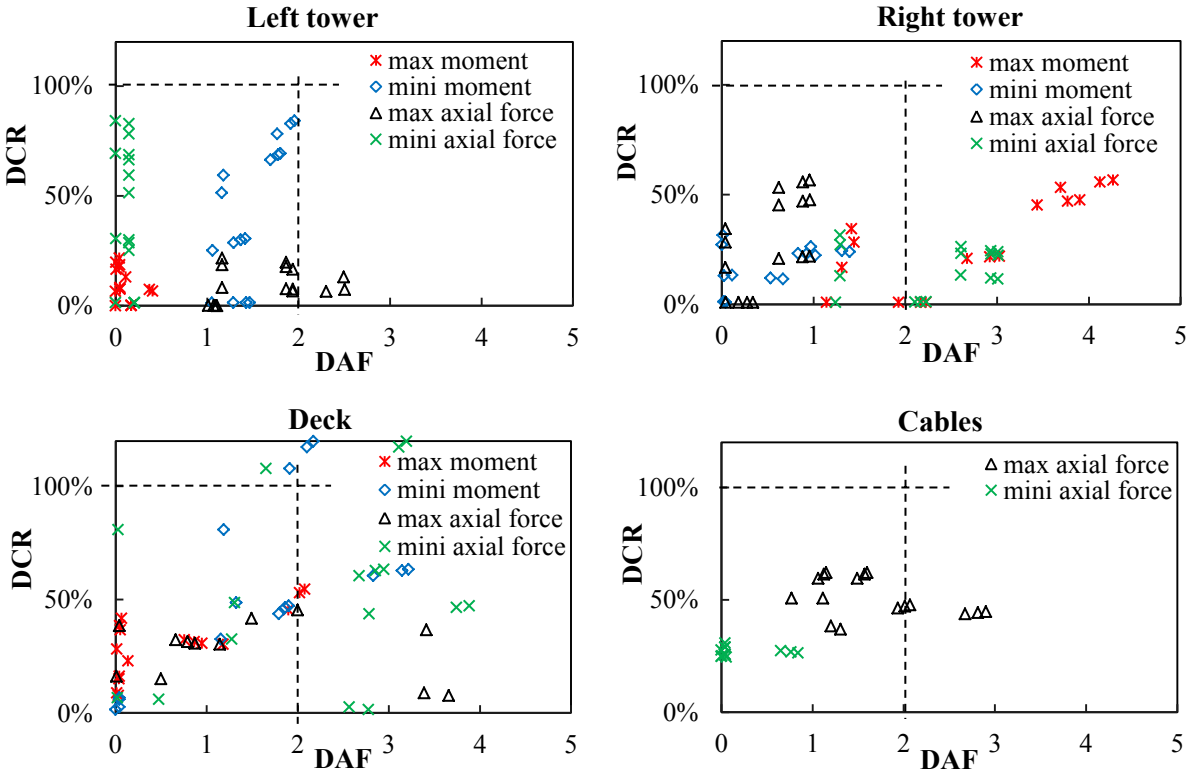

Figure 3-16 *DAF* versus *DCR* values for scneaio-3 (LC-2, loss of cables no. 1, 2 & 3).

Loss of three cables

With regard to the results obtained from the previous scenarios, it can be concluded that scenarios associated with loss of back stays connected to the pin support are the most critical ones. Accordingly, simultaneous loss of cables no. 1, 2 and 3 is only considered in this part. For scenario-3/LC-2, *DAF* and *DCR* values determined based on maximum bending moment at the most critical sections along the deck are given in Table 3-5. In addition, the maximum *DCR* and corresponding *DAF* values observed in the deck, towers and cables for scenario-3/LC-2 are given in Figure 3-16. The maximum *DAF* calculated within this scenario is about 4.5 and related to the maximum moment in the right tower. In scenario-3, *DCR* takes values greater than 100% (yielding may occur due to combination of bending moment and axial load in the deck, see Table 3-5). However, even in the event of formation of a plastic hinge at one location of the deck, the redundancy provided by the supports through the remainder of the cables will prevent the progressive collapse of the bridge.

3.5 Concluding remarks

A numerical study on the potential progressive collapse of cable stayed bridges due to different cable loss scenarios was carried out in this chapter. A comprehensive parametric study was undertaken and effect of location, duration and number of lost cables, as well as applied load case and the structural damping ratio on the dynamic amplification factor (*DAF*) and demand-to-capacity ratio (*DCR*) in different structural members (towers, deck and cables) are investigated. With regard to the parametric studies undertaken in this chapter, the following conclusions are drawn;

- Among different cable loss scenarios considered for potential progressive collapse of the cable stayed bridge, the ones associated with loss of the longest back stays are the most critical ones (the highest *DCR* values were observed for all structural components).

- The *DAF* for the bending moment and axial force at different sections along the

deck, towers and cables can take values much higher than 2 (typically adopted by different guidelines as the maximum value), however, the corresponding *DCR* values were usually less than 100%. In other words, material nonlinearity has minor effect on the global progressive collapse response of the bridge due to cable loss, and it is not un-conservative to allow a *DAF* of greater than 2 as long as *DCR* remains below 1.

- The *DAF* values alone, do not provide any information about the progressive collapse response of the cable stayed bridge under investigation, whereas *DCR* values at different locations of the structure can be used as an indicator of material nonlinearity and formation of plastic hinges.

- Damping ratio has a minor impact on the dynamic progressive collapse response of the cable stayed bridges as long as the adopted value of the damping ratio is within the acceptable range (less than 2% of critical damping for the steel bridge considered in this study).

- The developed FE model for the bridge was analysed with and without geometrical nonlinearities included to demonstrate the effect of geometrical nonlinearities on the global progressive collapse response of the bridge. It was shown that for the cases studied in this paper, the effect of geometrical nonlinearities on the progressive collapse response (due to cable loss), for a properly designed bridge is limited (less than 7% for the cases considered in this study).

- The value of *DAF* is highly sensitive to the time step over which the cables are removed.

- The value of *DAF* for bending moment and axial force in the towers and deck is larger than the *DAF* that should be applied for axial force in the cables.

- For all cases and scenarios studied in this chapter, values of *DAF* for axial force in the cables are generally less than 2.

Chapter 4 : Model verification - A Comparative Study of 2D and 3D FE Models of a Cable-Stayed Bridge Subjected to Sudden Loss of Cables

Summary of chapter

In the previous chapter, *DAF*s and *DCR*s were determined by using 2D linear elastic models, mainly because the sudden loss of cables is typically analysed by 2D linear-elastic models in design of cable-stayed bridges. However, cable loss scenarios are associated with material as well as geometrical nonlinearities which may trigger progressive collapse of the entire bridge. Accordingly, a non-linear 3D bridge model is required to adequately investigate the cable loss scenarios. The non-linear 3D model to be developed in this chapter can be used to analysis the unsymmetrical cable loss scenarios as well as loss of cables subject to blast loading. However, this chapter only focus on the correlation between results of nonlinear 3D and 2D linear-elastic finite element (FE) models. The results of this comparative study are employed to determine the adequacy of linear elastic models for potential progressive collapse assessment of cable stayed bridges. In this chapter, 2D and 3D finite element models of a cable-stayed bridge with and without considering material and geometrical nonlinearities are developed and analysed. The progressive collapse response of the bridge subjected to two different cable loss scenarios at global and local levels are investigated. For the cases studied in this chapter, it is shown that the linear elastic 2D FE models can adequately predict the dynamic response (i.e. deflections and main stresses within the deck, tower and cables) of the bridge subjected to cable loss. Material nonlinearities occurred at different locations are found to be localized and unlikely to trigger the progressive collapse of the entire bridge.

4.1 Introduction

The finite element models employed for progressive collapse analysis of structures can be classified to 2D or 3D models. The 2D models have been successfully used for capturing the global response of the cable-stayed bridges as well as identifying the most

critical structural components. For example, using a 2D finite element (FE) model, the back stays connected around the pin-support and also the stays connected to the mid-span have been identified as the most critical cables as presented in the previous chapter as well as previous studies (Aoki et al., 2012a, Aoki et al., 2012b, Kao and Kou, 2010). The 2D models, however, cannot capture the effects of out-of-plane unsymmetric cable loss scenarios that may have a significant influence on the response (particularly the torsional response) of the bridges.

The cable-stayed bridge adopted in this study has a steel box deck designed according to Australian Standards AS5100 (2004) requirements. The 2D and 3D FE models of the bridge were developed and analysed under gravity loads and subjected to different cable loss scenarios using SAP2000 (2004) and ANSYS software (2009), respectively. The nonlinear 3D FE models are developed to provide the benchmark data required for assessing the accuracy of 2D FE models commonly developed assuming a linear elastic material behaviour. The developed 3D FE models can take account of material non-linearity as well as geometrical non-linearity. Using the 2D and 3D FE models, the effect of location of lost cables on the potential collapse response of the bridge is studied and also the significance of material nonlinearities on the potential collapse response of the considered cable stayed bridge is investigated.

4.2 Principal Assumptions

4.2.1 Geometry and material properties

The dimensions of the bridge and the configuration of cables for the bridge considered in this chapter are the same as the bridge used in Chapter 3 as shown in Figure 4-1a. The cross sectional area of deck and towers has been re-designed in order to prevent premature local buckling of plates before yielding of steel. The slenderness of unsupported length of plates, $(b/t)\sqrt{\sigma_y / 250}$, was limited to the yield limit slenderness ratio λ_{ey} (45 for plates supported on one edge and 32 for plates supported on both edges of deck) according to AS 5100.6 (2004) requirements. The geometry of the deck, towers and configuration of cables are shown in Figure 4-1b and 4-1c, respectively.

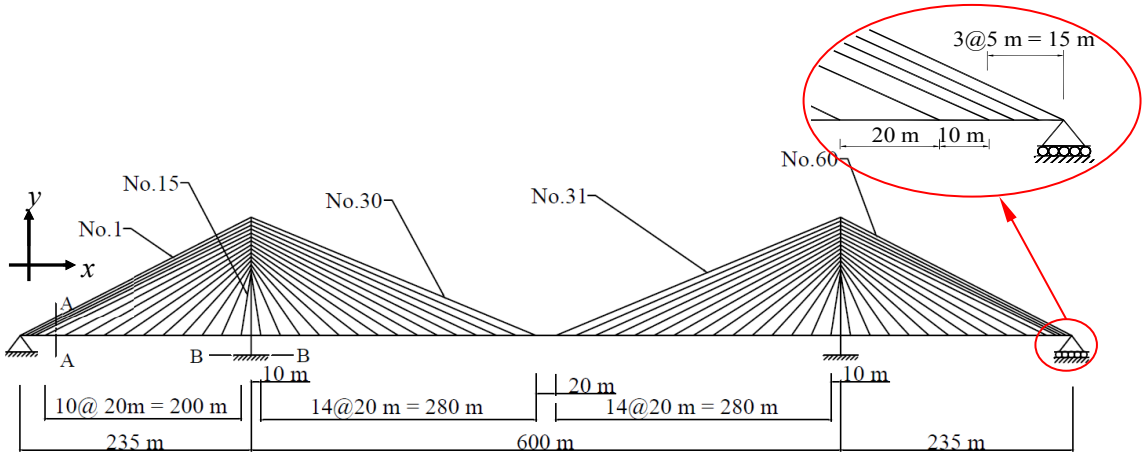

(a) Bridge configuration

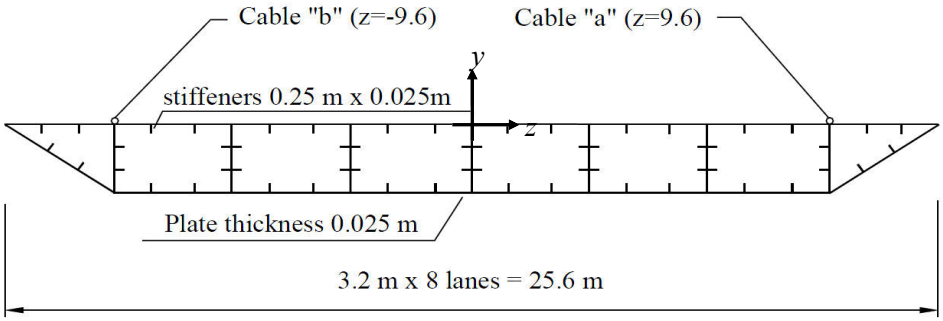

(b) Cross section (A-A) of deck

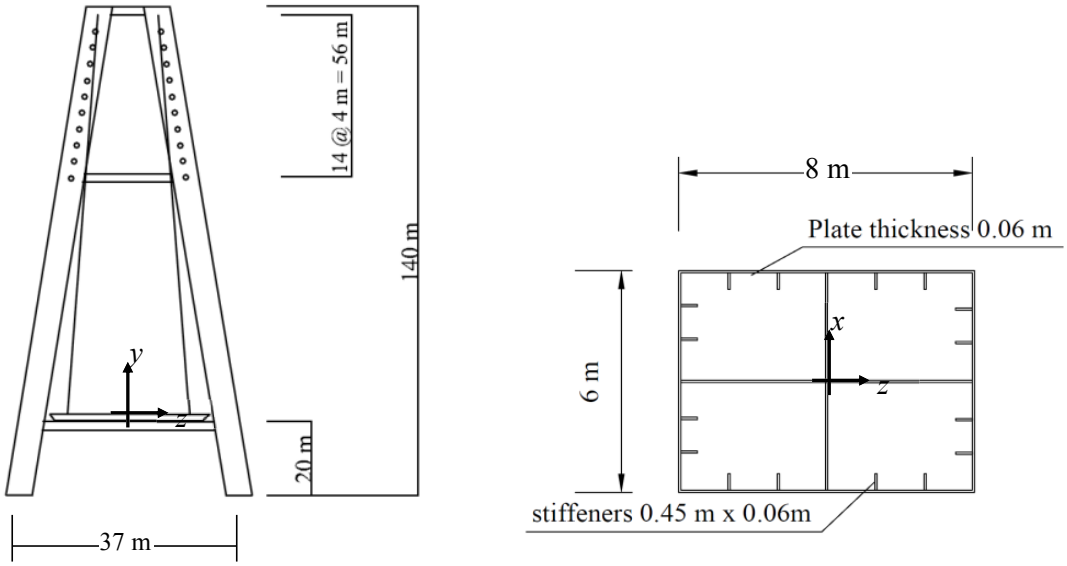

(c) Tower

Figure 4-1 Geometrical outline of the bridge and cross-sections of deck and tower.

The adopted material properties (i.e. E, σ_y, σ_u and E_{sh}), initial post-tensioning strain in cables ε_{i-PT}, and the geometrical properties of members (i.e. cables, deck and tower) including second moment of area, I, and cross sectional area, A adopted in 2D FE models are given in Table 4-1. The material is assumed to be linear elastic in 2D models, whereas in 3D models a linear elasto-plastic hardening stress-strain relationship with Von Mises yield surface is adopted for deck and tower (Figure 4-2a). The cables are assumed to be linear elastic-brittle in 2D and 3D FE models (Figure 4-2b).

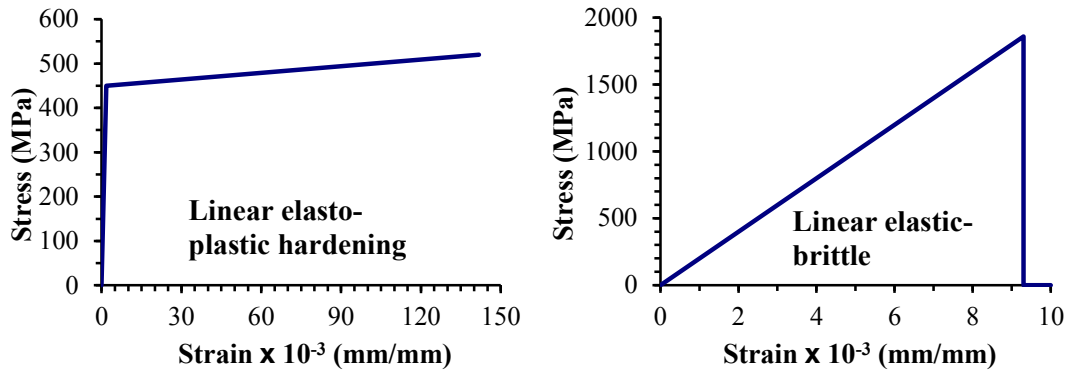

(a) (b)

Figure 4-2 Adopted stress-strain model for steel in the (a) tower and deck and (b) cables.

Table 4-1 Material and geometrical properties of the deck, towers and cables.

Structural component		E (MPa)	σ_y (MPa)	σ_u (MPa)	E_{sh} (MPa)	A (m^2)	I (m^4)	ε_{i-PT}
Box Girder		200	350	420	500	1.91	1.36	-
Tower		200	350	420	500	6.09	47.41	-
Cable No.	**1-5, 26-35, 56-60**	200	1860	1860	-	0.0327	-	0.0033
	6-10,21-25,36-40, 51-55	200	1860	1860	-	0.0219	-	0.0033
	11-20, 41-50	200	1860	1860	-	0.0165	-	0.0037

E is the modulus of elasticity, σ_y and σ_u denote the yield and ultimate strength and E_{sh} is the hardening modulus of steel.

4.2.2 Modelling and analysis

For both static and dynamic analyses of the cable stayed bridge under investigation, the effects of large displacements and geometrical nonlinearities are taken into account in both 2D and 3D FE models. Furthermore, in the dynamic analysis, a proportional damping with stiffness and mass multipliers of $\alpha = \beta = 0.5\%$ is adopted (Clough and Penzien, 1993).

In the 3D FE model, the deck and towers are modelled by shell elements, whereas 2D FE models take advantage of beam elements. The cables are modelled by link-elements which are treated as tension-only members with limited tensile capacity. The outline of the 2D and 3D FE models are shown in Figure 4-3. In the 2D models, the eccentricity of cables with respect to the centroidal axis of the deck and pylons was modelled by rigid constraints (see Figure 4-3a).

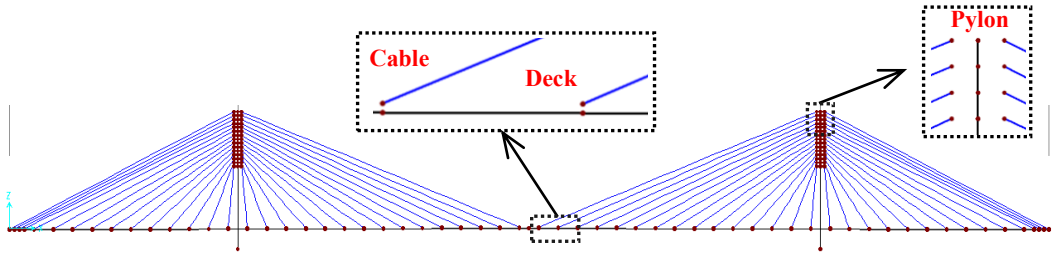

(a) 2D model

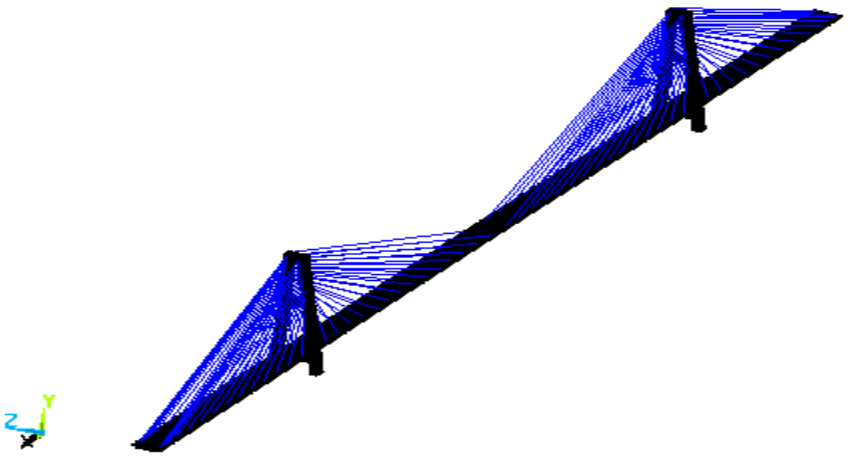

(b) 3D model

Figure 4-3 Outline of the (a) 2D and (b) 3D finite element model.

In this research project, shell element SHELL181, which is suitable for analysing thin to moderately-thick shell structures is used for modelling steel plates. SHELL181 is a four-node element with six degrees of freedom at each node. Also, SHELL181 is well-suited for linear, large rotation, and/or large strain nonlinear applications. This element supports uniform reduced integration, full integration, and full integration with incompatible modes. In this research, full integration (five points of integration through the thickness of the shell) is used.

In addition, for SHELL181 element, the default orientation has shell surface coordinate (called as S_1) axis aligned with the first parametric direction of the element at the centre of the element. In the most general case, the S_1 axis can be defined as follows

$$S_1 = \frac{\frac{\partial \{x\}}{\partial s}}{\left| \frac{\partial \{x\}}{\partial s} \right|} \tag{4-1}$$

where

$$\frac{\partial \{x\}}{\partial s} = \left(\frac{1}{4}\right)\left[-\{x\}^I + \{x\}^J + \{x\}^K - \{x\}^L \right] \tag{4-2}$$

and $\{x\}^I$, $\{x\}^J$, $\{x\}^K$ and $\{x\}^L$ are global coordinates of the nodal points.

In the 3D continuum-based FE models, LINK10 is used for modelling cables. It is a 3D spar element having the unique feature of a bilinear stiffness matrix resulting in a uniaxial tension-only element. With this option, the stiffness is removed if the element goes into compression (simulating a slack cable or slack chain condition. LINK10 element has three degrees of freedom at each nodal point. No bending stiffness is included in the LINK10 element that is consistent with the real behaviour of cables.

4.2.3 Design Loads

The loads considered for collapse assessment of this bridge are gravity loads including the self-weight of the structure (Dead) plus the surfacing asphalt (Superimposed Dead) and the traffic load (S1600 as shown in Figure 4-4) according to AS5100.2 (2004).

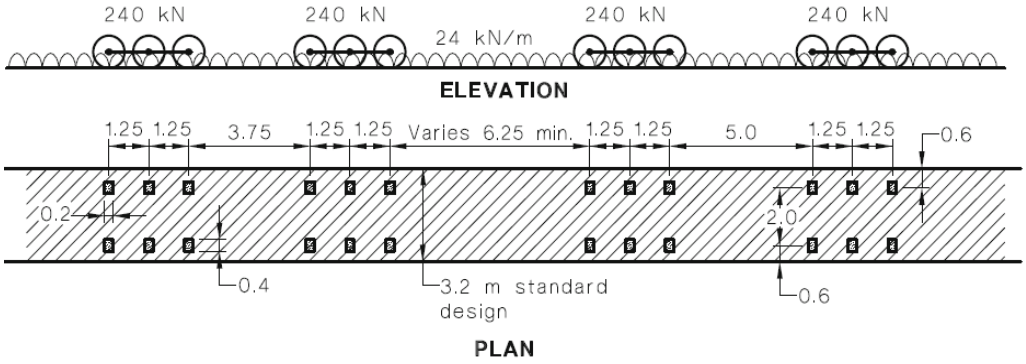

Figure 4-4 S1600 stationary traffic load according to AS5100 (2004).

Applied post-tensioning forces in the cables were calculated according to AS5100.2 (2004) provisions for ultimate and serviceability design requirements as well as allowable mid-span deflection due to traffic loads. Further, the maximum stress induced in the deck and towers due to service load (i.e. Permanent + Traffic + Post-tensioning forces) was kept below $0.5\sigma_y$ and the maximum stress in the cables is limited to that considered consistent with JSCE (2010) design provisions.

4.2.4 Calibration of 2D and 3D FE models

The correlation between the 2D and 3D FE models developed in this study was verified by comparing the total self-weight, cable initial forces and global deflection of the deck obtained from the FE models. The total weight of the bridge obtained from 2D and 3D FE models under progressive collapse load combination of (1.1xDead + 1.35xSuperimposed Dead + 0.75xTraffic) are 647 MN and 656 MN, respectively. Furthermore, the vertical deflection, the stress in the cables and σ_{xx} stress on top surface of the bridge deck obtained from 2D and 3D FE models are compared in Figure 4-5 that demonstrates a good correlation between 2D and 3D FE results. The σ_{xx} stress

at each section in 2D FE models were calculated from $\sigma_{xx} = N/A \pm My/I$; where N and M are the axial force and bending moment, respectively, y is the distance from the neutral axis and A denotes the cross-sectional area and I denotes the moment of inertia of the section (see Table 4-1).

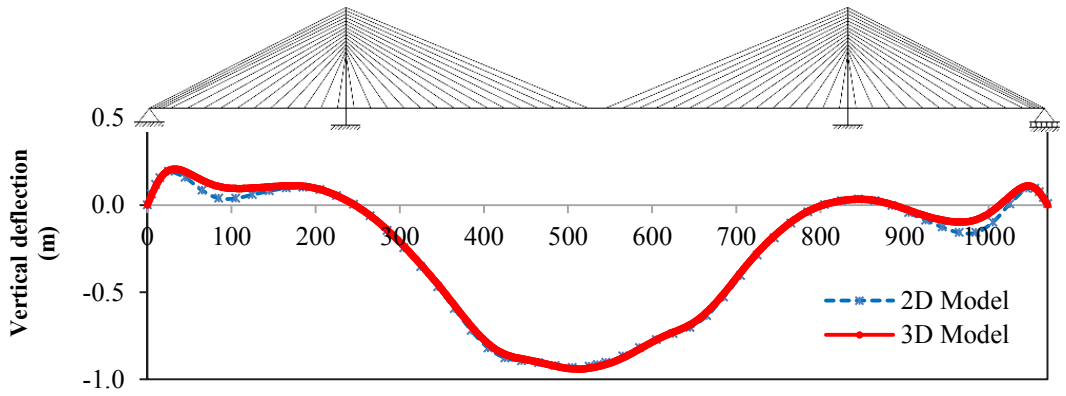

(a) Vertical displacements along the deck

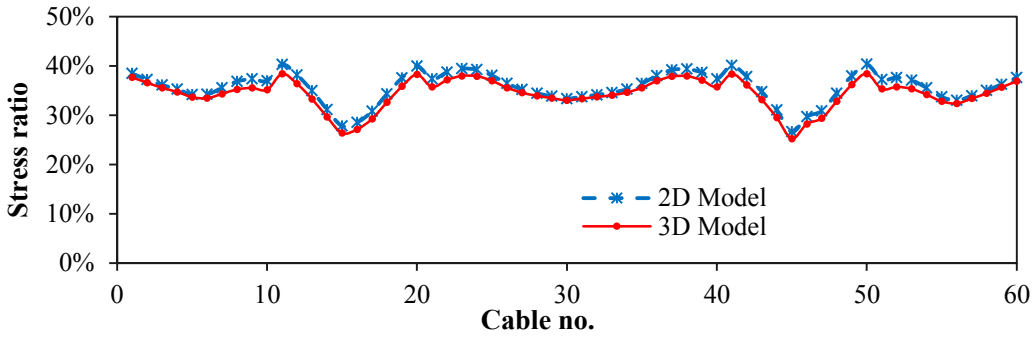

(b) Ratio of the axial force (stress) over breakage load (stress) for stays (under service load).

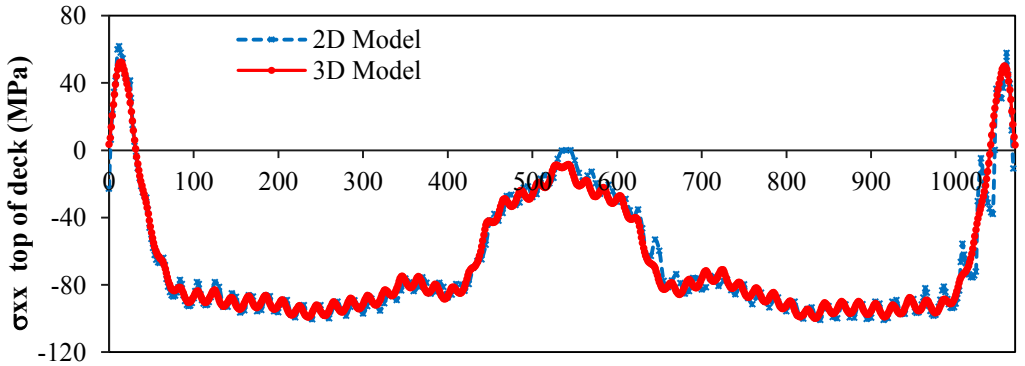

(c) σ_{xx} Stress component on top surface of the deck.

Figure 4-5 Comparison between results of 2D and 3D finite element models.

In addition, the periods of the first five in-plane natural vibration modes obtained from Eigen value analyses of the 2D and 3D FE models are given in Table 4-2 and a maximum of 13% difference between the 2D and 3D FE predictions is observed. For all modes of vibrations, the periods associated with the 3D model are smaller than those for the 2D model.

During the process of modelling and calibration of 2D versus 3D models, the eccentricity of cables with respect to the centroidal axis of the deck and towers was found to be important and accordingly should be considered for proper calibration of the 2D FE models (see Figure 4-3a).

Table 4-2 The periods of the first five in-plane global natural modes of vibration.

Mode no.	2D Model (sec)	3D Model (sec)
1st	5.68	5.15
2nd	4.59	4.22
3rd	2.95	2.64
4th	2.63	2.36
5th	2.51	2.22

4.3 Cable Loss Scenarios

4.3.1 Cable removal method

For dynamic analysis, the unconditionally stable Newmark constant acceleration method is used for time integration (Paz, 2004). The cables are removed over an integration time step, Δt, which is short enough compared with the 1st natural period of the bridge to warrant the adequacy of dynamic analysis for alternate load path (ALP) method (Ellingwood et al. 2007).

4.3.2 Load combinations adopted for progressive collapse assessment

For collapse assessment, the distributed component of the traffic load, as well as the dead load, is applied along the entire bridge deck (Figure 4-6a). The adopted load factors are as recommended by PTI (2007),

$$1.1DC + 1.35DW + 0.75(LL + IM) + 1.1CLDF \quad (4\text{-}3)$$

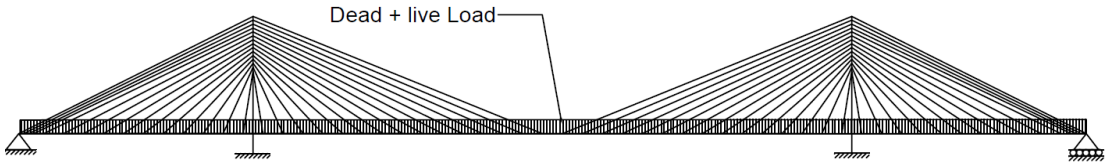

(a) UDL along the deck

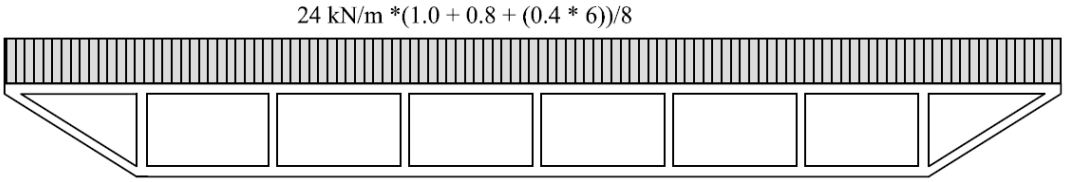

(b) Symmetric loading pattern

Figure 4-6 Pattern of (a) gravity loads along the bridge deck (Dead + traffic) (b) traffic loads across the deck including accompanying lane factors for progressive collapse assessment

In Equation (4-3), *DC* is the dead load of the structural components and non-structural attachments, *DW* is the dead load of the wearing surfaces and utilities, *LL* is the full vehicular live load placed in the actual stripped lanes, *IM* denotes the vehicular dynamic load allowance taken equal to zero in this study and *CLDF* is the cable loss dynamic forces. In this study, the wearing surface is a 200 mm thick layer of asphalt concrete (γ=24.5 kN/m^3). According to AS5100.2 (2004), for scenarios in which more than one lane is subjected to traffic loads, applied traffic loads should be multiplied by an accompanying lane factor (1.0 for first lane, 0.8 for second lane and 0.4 for third and subsequent lanes (see Figure 4-6b).

4.3.3 Cable loss scenarios

Based on PTI (2007) guidelines, for progressive collapse assessment of cable stayed bridges, only the scenarios associated with loss of a single cable are adequate, however, some researchers believe that scenarios in which more than one cable is lost should not be ignored (Aoki et al., 2011, Wolff and Starossek, 2010). Two different scenarios (i.e. S1 and S2) which are considered to be the most critical ones (see Chapter 3) are studied here. In the 2D model, cable no.1 (connected to the pin support) and cable no.30 (the

longest cable connected to the mid-span) are subject to loss. These scenarios are referred to as scenario-S1 (2D) and scenario-S2 (2D), respectively. The corresponding symmetrical cable loss scenarios in 3D FE models are scenario-S1 (3D) and S2 (3D) in which a pair of cables (1a and 1b) and (30a and 30b) are simultaneously removed (see Figure 4-1a). The considered cable loss scenarios are listed in Table 4-3.

Table 4-3 Cable loss scenarios considered in this chapter.

Scenario name	Lost cable no.	Model type 2D/3D	Cable loss pattern	Traffic loading pattern
S1(2D)-SL	1	2D	Symmetric	Symmetric (see Figure 4-6b)
S2(2D)-SL	30			
S1(3D)-SL	1a & 1b	3D	Symmetric	
S2(3D)-SL	30a & 30b			

4.3.4 Equivalent Modulus of Elasticity for Cables

The shape (geometry) of stays in cable-stayed bridges can change due to variation of stress levels and a simple approach to account for this geometrical nonlinearity is to adjust the modulus of elasticity (JSCE, 2010, Walther, 1999, Gimsing and Georgakis, 2011). The equivalent modulus of elasticity is determined by the following equation which was established by H.J. Ernst (JSCE, 2010, Walther, 1999)

$$\overline{E} = \frac{E}{1 + \frac{\left(\gamma\, l\right)^2 E}{12\sigma^3}} \tag{4-4}$$

where, $\overline{E}$ is the equivalent modulus of elasticity, E is material modulus of elasticity, γ is density of the cable, l is the horizontal span (x coordinate) and σ is the stress in the cable. For the longest cable connected to the mid-span, $E_e = 200\,\text{GPa}$, $\gamma = 78\,\text{kN/m}^3$, $l \cong 314\,\text{m}$ and $\sigma \cong 0.33\sigma_u = 613\,\text{MPa}$, the equivalent modulus of elasticity is $\overline{E} = 0.96E_e$ that would have small effect on the results and, hence, actual modulus value (instead of the equivalent modulus) is used in subsequent analyses.

4.4 Results

Analysis results for symmetrical cable loss scenarios S1 and S2 obtained from 2D and 3D FE models are compared in this section.

4.4.1 Deck and Towers

Time-history of vertical deflection at the mid-span of deck (i.e. x=535 m) and σ_{xx} stress component on top and bottom of the deck (at the maximum stress instant) for scenarios S1 and S2 are shown in Figures 4-7 and 4-8, respectively.

The magnitude and location of maximum vertical deflection within the deck as well as the maximum σ_{xx} longitudinal stress on top and bottom surface of the deck obtained from 2D and 3D FE models are compared in Table 4-4. It is observed that the difference between 2D and 3D FE models in terms of predicted σ_{xx} stress is limited to 8% and for predicted deflections the maximum difference between 2D and 3D model is around 6%.

Furthermore, it is seen that the major longitudinal flexural stresses along the deck (see Table 4-4) are well below the yield strength of steel, i.e. $\sigma_y = 350MPa$ and accordingly neither cable loss scenario S1 nor S2 will lead to formation of plastic hinge along the deck. The deflected configuration (elastic curve) of the deck at the maximum vertical displacement instant for scenarios S1 and S2 is shown in Figure 4-9a and time history and maximum lateral drift on top of left tower obtained from 2D and 3D models are compared in Figure 4-9b and Table 4-4, respectively. It is observed that the calibrated 2D model can adequately capture the global response (i.e. deflection and major flexural stresses in the deck and towers) of the bridge during cable loss scenarios.

Table 4-4 Material and geometrical properties of the deck, towers and cables.

Scenario (FE model)	Deflection in deck (m)		Max. drift on top of the left tower (m)	Max. σ_{xx} stress in deck (MPa)	
	Mid span	Max. @ x (m)		Top of deck	Bottom of deck
S1 (2D)	1.81	2.04 @ 485	0.69	137	233
S1 (3D)	1.88	2.17 @ 485	0.68	129	227
S2 (2D)	1.83	1.86 @ 530	0.16	55	185
S2 (3D)	1.86	1.81 @ 540	0.16	51	206

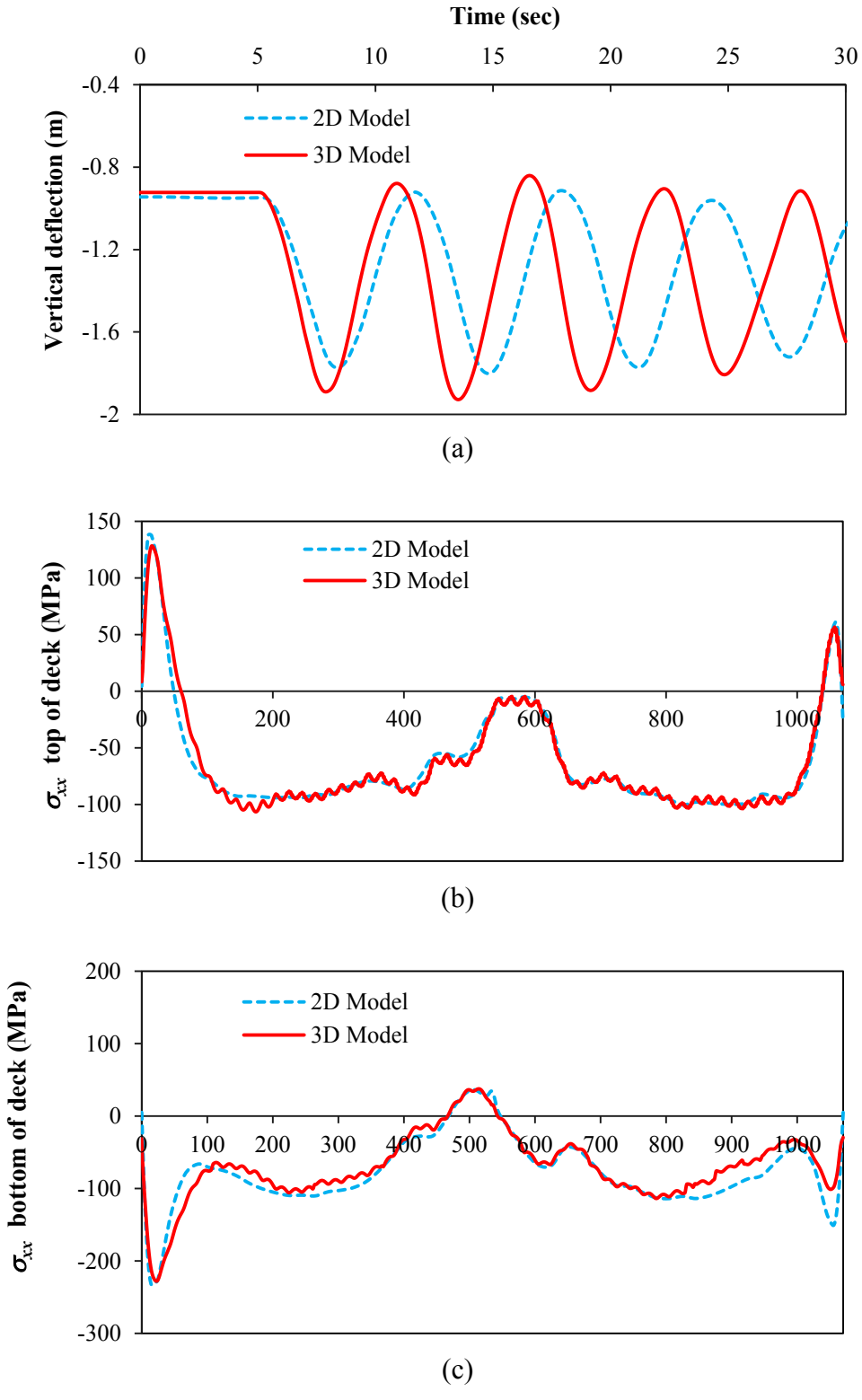

Figure 4-7 Time history of (a) vertical deflection at mid-span (x= 535 m) and σ_{xx} stress component on the (b) top and (c) bottom surface of the deck for scenario-S1.

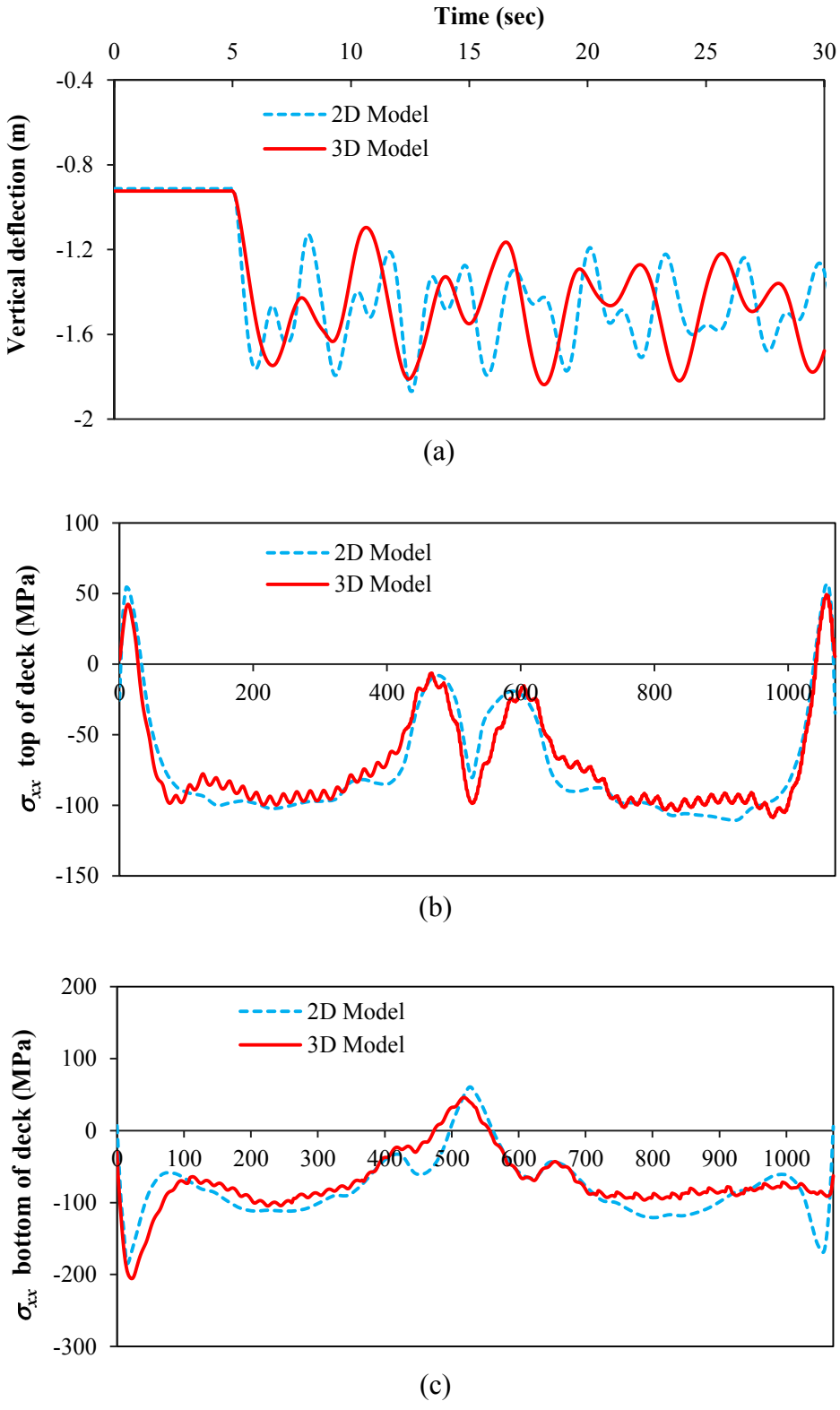

Figure 4-8 Time history of (a) vertical deflection at mid-span (x= 535 m) and σ_{xx} stress component on the (b) top and (c) bottom surface of the deck for scenario-S2.

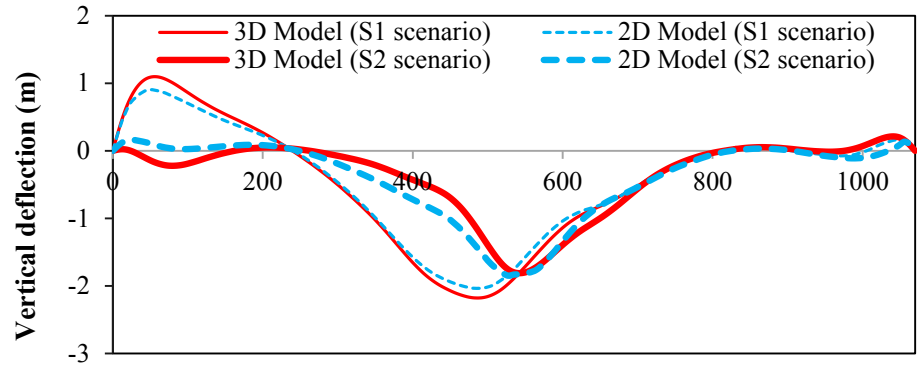

(a)

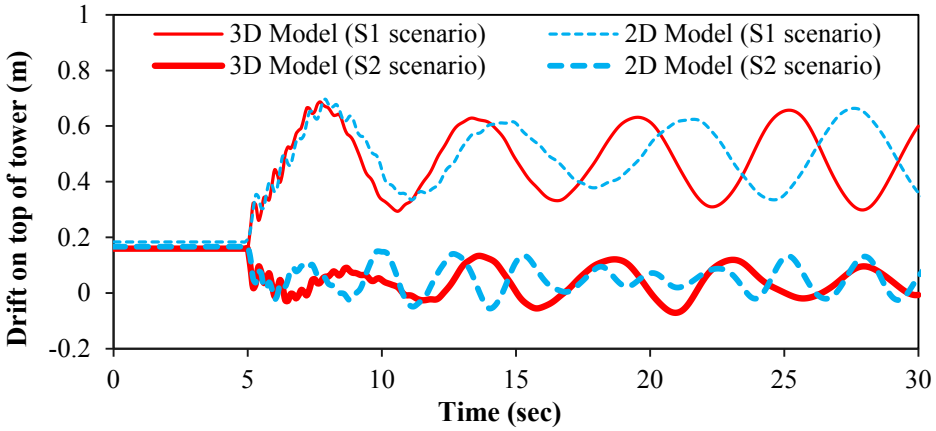

(b)

Figure 4-9 (a) Deflected configuration of the deck when maximum vertical displacement has occurred (b) time history of lateral displacement on top of left tower.

4.4.2 Cables

The envelops of maximum tensile stress in the cables, expressed as a percentage of cable ultimate strength ($\sigma_u = 1860$ MPa) within scenarios S1 and S2 are shown in Figure 4-10. Comparison between maximum tensile stress (force) in cables predicted by 2D and 3D models shows excellent correlation between 2D and 3D FE results. Furthermore, it is seen that the maximum tensile stress in the cables during scenarios S1 and S2 is limited to $0.6\sigma_u$ (in cable 2 during scenario S1) which is well below the breakage stress of the cables and therefore, in the cable stayed bridge under consideration, no zipper-type progressive collapse is expected to occur due to loss of either first back stay or the cable connected to the mid-span.

The ratio of minimum tensile stress over ultimate strength, $\sigma_u = 1860$ MPa, of cables during scenarios S1(3D) and S2(3D) are shown in Figure 4-11a. These minimum axial stresses in the cables are used for calculating the minimum equivalent modulus of elasticity $\overline{E}$ (Ernst's modulus of cables) for cables which is shown in Figure 4-11b. It is seen that with reasonable accuracy $\overline{E} \cong E$. In other words, the fluctuation of axial tensile force in the cable (due to cable loss) is so small that has a negligible influence on the stiffness of cables.

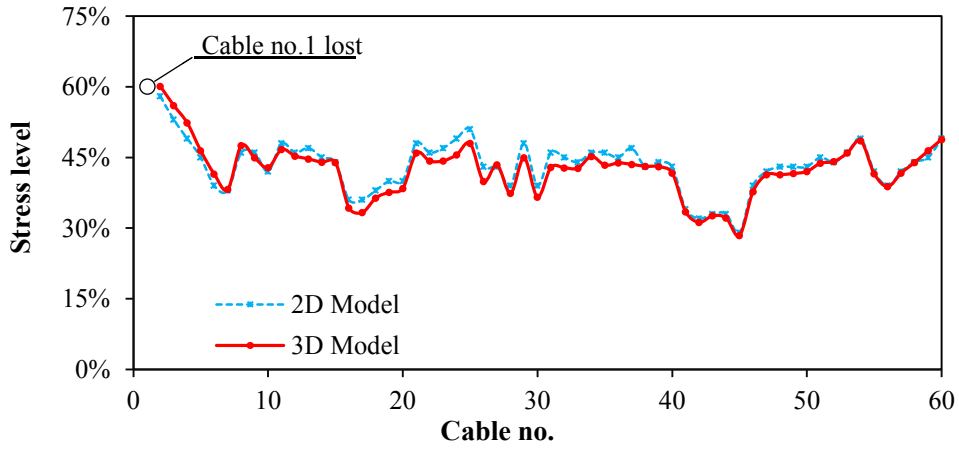

(a)

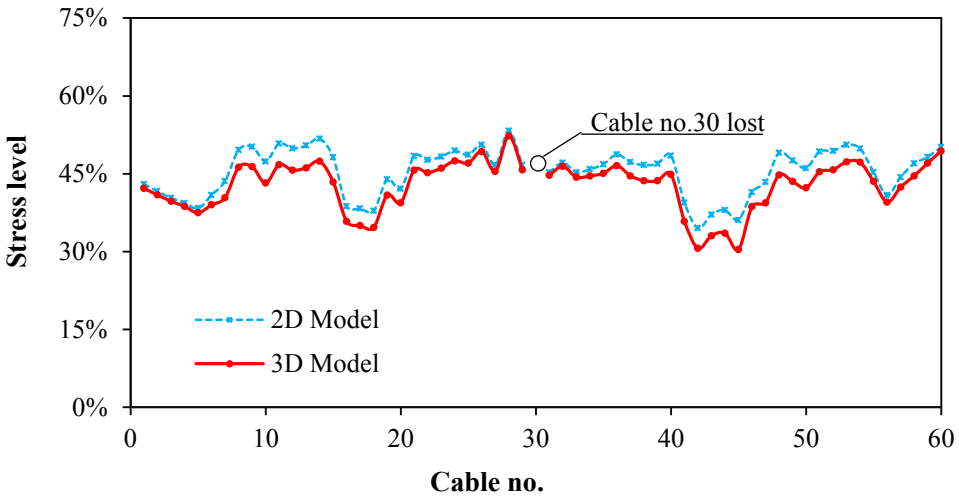

(b)

Figure 4-10 Envelops of the maximum tensile stress in the cables for (a) Scenario S1 and (b) Scenario S2 (expressed as a percentage of ultimate strength $\sigma_u = 1860$ MPa).

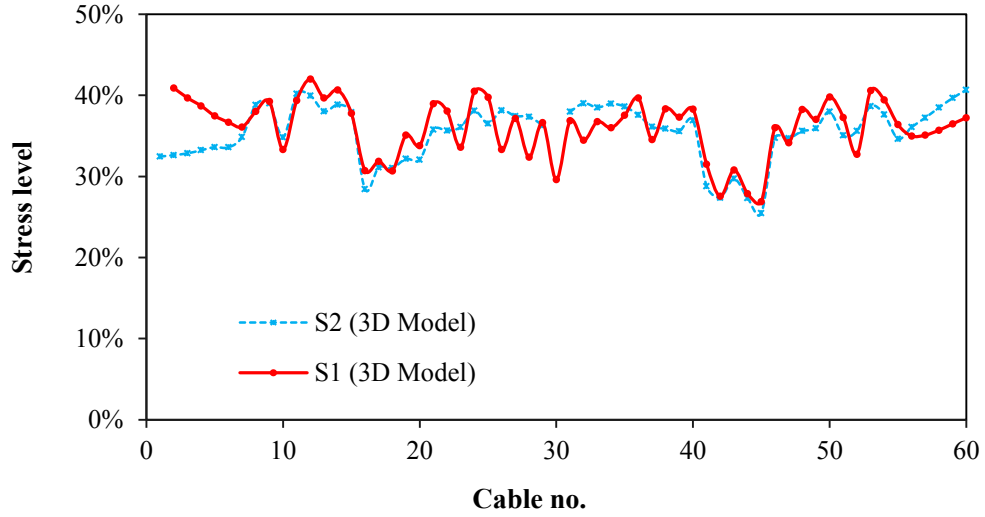

(a)

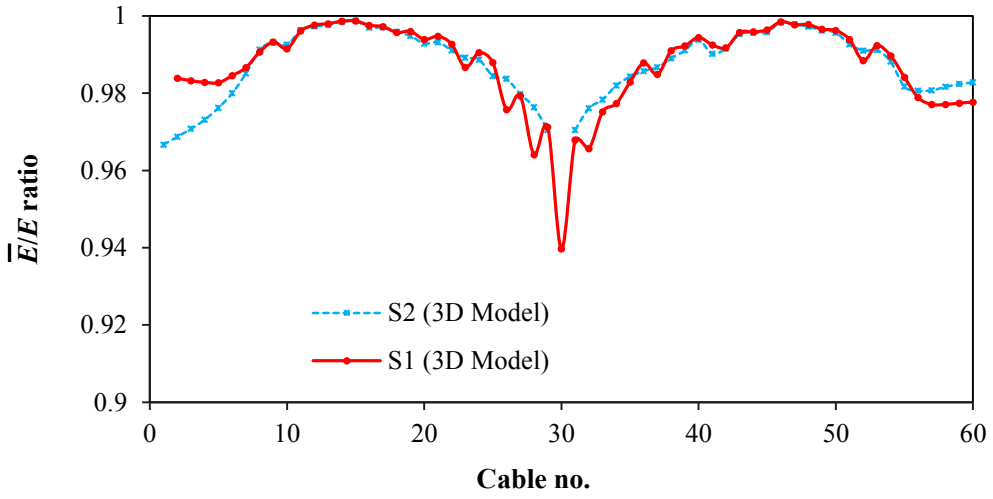

(b)

Figure 4-11 (a) Ratio of the minimum tensile stress over ultimate strength for cables (b) the minimum equivalent modulus of elasticity $\overline{E}$ (Ernst's modulus of cables) expressed as a percentage of modulus of elasticity E.

4.5 Conclusions and Discussion

In this chapter, 2D and 3D nonlinear finite element (FE) models of a cable stayed bridge with steel box deck and towers were developed and analysed under gravity loads and subjected to two different cable loss scenarios (i.e. loss of a back stay connected to the hinge support and/or loss of a cable connected to the mid-span).

The 2D models were developed using linear elastic frame elements whereas the 3D FE models were developed using shell elements and can take account of material non-linearity as well as geometrical non-linearity. A comparative study of 2D and 3D FE models was undertaken and based on the finite element (FE) analyses results, the following conclusions for the bridge considered in this chapter are drawn;

- The 2D FE models can adequately capture the global response (e.g. time history and maximum deflection in the deck, lateral drift on top of tower and maximum flexural longitudinal stresses in the deck and tower) of cable stayed bridges subjected to critical cable loss scenarios.

- The deflection elastic curve, longitudinal flexural stresses within the deck and axial force/stress in the cables were used for validating and calibration of the 2D against 3D FE model, and the eccentricity of cables with respect to the centroidal axis of the deck and towers was found to be important for proper calibration of the 2D FE models against the full 3D FE models.

- Between two different cable loss scenarios considered in this study (i.e. S1 and S2) the scenario corresponding to the loss of back stay connected to the hinge support (scenario S1) is the most critical one in terms of maximum deflection and stresses induced in the deck and towers.

- The variation of equivalent modulus of elasticity (Ernst's modulus) for cables during cable loss scenarios was found to be small (less than 5%) and hence negligible.

- In the results of full nonlinear 3D finite element model no sign of material nonlinearity (yielding of steel) or buckling of steel plates were observed and instantaneous loss of two cables (one on each side of deck) neither triggered the zipper-type collapse nor led to formation of any plastic hinge within the deck and towers.

Chapter 5 : Effect of loading pattern and deck configuration on the progressive collapse response of cable-stayed bridges

Summary of chapter

In Chapter 3, the DAFs related to sudden loss of cable(s) were determined by using linear-elastic 2D model and onset of material non-linearity (i.e. yielding of steel and/or rupture of cable) was investigated by adopting the *DCR* (Demand-to-Capacity Ratio) concept. Furthermore, in the potential progressive collapse analyses undertaken in Chapter 3, only symmetric load combinations and cable loss scenarios were considered. Accordingly, in this chapter, a parametric study is undertaken and effect of unsymmetric cable loss scenarios, deck configurations (i.e. steel box girder and open orthotropic deck) and number of lost cables on the progressive collapse response of the bridge is investigated by the nonlinear continuum-based finite element model described in Chapter 4. With regard to the results of parametric study, it is concluded that the deck configuration has a minor influence on the potential progressive collapse response of cable-stayed bridges. Also, it is shown that localised yielding of steel may occur following loss of more than one cable, however, such localised plastic strains cannot trigger the progressive collapse of the entire bridge. During cable loss scenarios, the reduction in post-tensioning stress and subsequently stiffness of the remaining cables (reflected in Ernst's modulus) is found to be around 12% that warrants designers taking into account the effect of geometrical nonlinearities within the cables.

5.1 Introduction

According to the previous chapters, application of a full dynamic analysis for progressive collapse assessment of bridges subject to cable loss is highly recommended. In addition, using the results of dynamic finite element analyses, the back stays connected around pin-support and cables connected to the mid-span have been

identified as the most critical cables where their loss can significantly affect the entire bridge. However, a 2D linear-elastic model presents some limitations in regards to unsymmetric loading patterns and cable loss scenarios. Furthermore, the linear-elastic models cannot adequately capture the local effects associated with buckling of slender elements (plates) and yielding of materials.

In this chapter, the 3D continuum-based FE model developed in Chapter 4 is employed to undertake a parametric study in which particular emphasis is placed on the effect of un-symmetric cable loss and traffic loading patterns that induce torsional vibrations, in conjunction with configuration of the deck (i.e. box girder vs open orthotropic deck). As described in Chapter 4, the adopted 3D FE models can take account of material and geometrical non-linearity, including large strains and displacements.

5.2 Adopted assumptions

The adopted assumptions such as over dimensions of the bridge deck and towers, material properties as well as the 3D FE model, analysis methods and design loads are as given in Chapter 4, Sections 4.2 and 4.3.

In this chapter, two types of decks are considered (see Figure 5-1); the first one is a multi-cell steel box girder with 56 stiffeners (Deck-1) and the second one is an open orthotropic steel deck with 46 stiffeners (Deck-2). Both decks are 25.6 m wide and comprise 8 standard traffic lanes according to AS5100.2 (2004).

For progressive collapse assessment, the distributed component of the traffic load, as well as the dead load, is applied along the entire bridge deck (Figure 5-2a) with the adopted load factors as recommended by PTI (2007) and shown in Section 4.3.2. Two types of loading patterns (i.e. symmetrical and un-symmetrical) for traffic loads are considered (see Figure 5-2b and 5-2c) assuming that in 3D FE models the un-symmetrical load cases in conjunction with un-symmetrical cable loss scenarios can excite torsional modes and consequently generate more critical scenarios.

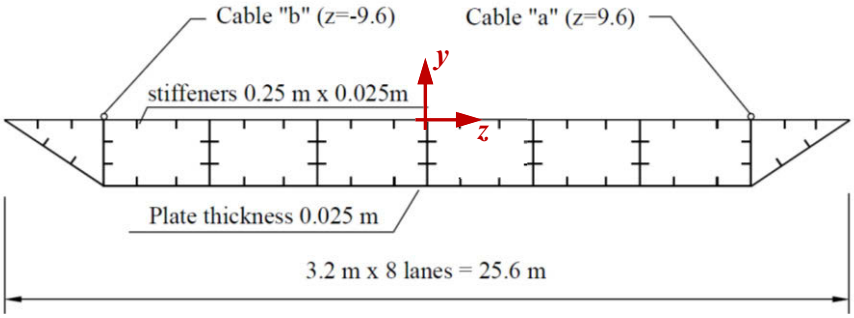

(a) Deck-1

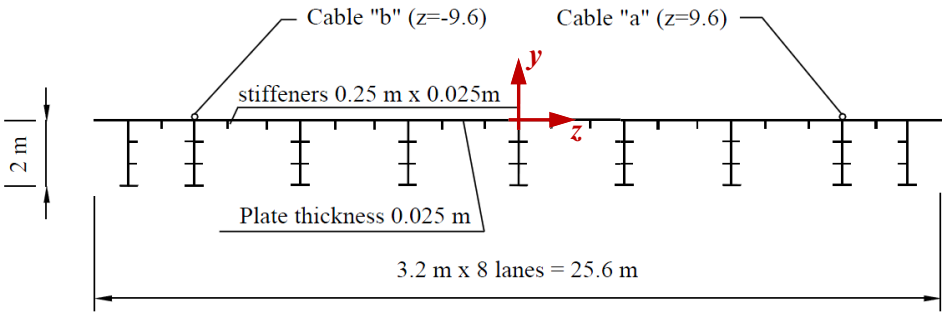

(b) Deck-2

Figure 5-1 Cross section of the deck (a) box girder (b) open orthotropic deck.

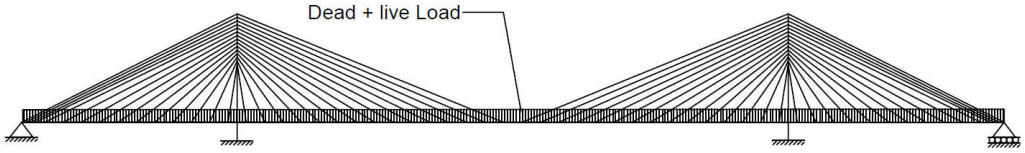

(a) UDL along the deck

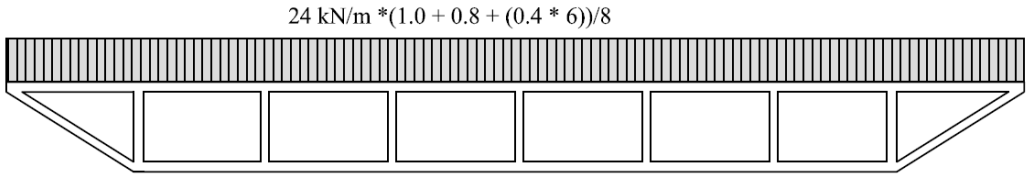

(b) Symmetrical pattern

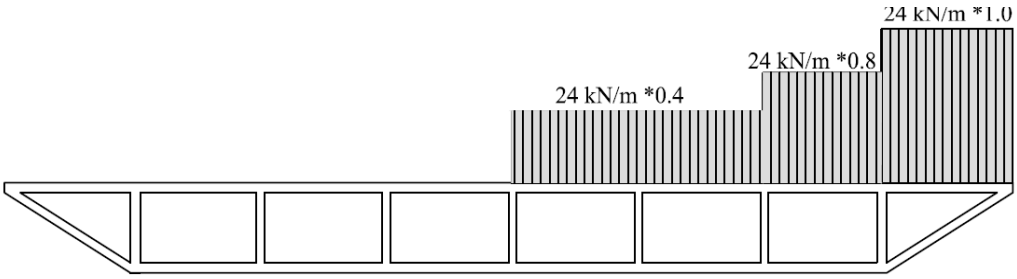

(c) Un-symmetrical pattern

Figure 5-2 Gravity loads applied (a) along the bridge deck and in a (b) symmetrical and (c) un-symmetrical pattern across the deck (accompanying lane factors included).

It is noteworthy that in the multi-lane traffic loading scenarios (symmetric and unsymmetric) shown in Figures 5-2b and 5-2c, the accompanying lane factor is applied according to AS5100.2 (2004). In the case of multi-lane events the accompanying load factor predicts that an extreme event in one lane is combined with a typical event in the adjacent lanes. Simulations of multi-lane queues of traffic confirmed that the accompanying load factor can adequately simulate the effects of queues in two or more heavily trafficked lanes.

5.3 Cable loss scenarios

The nonlinear dynamic analysis with direct time integration is employed to simulate the cable loss scenarios. The FE modelling and analyses are conducted using ANSYS software (2009) and the cable loss scenarios are simulated using Ekill command available in ANSYS. The Ekill command deactivates the lost cable over a time integration step, Δt.

Based on PTI (2007) provisions for progressive collapse assessment of cable stayed bridges, only the scenarios associated with loss of a single cable are adequate, however, some researchers believe that scenarios in which more than one cable is lost should not be ignored (Wolff and Starossek, 2010). In this chapter, both symmetrical and unsymmetrical cable loss scenarios as well as scenarios with more than one lost cables are considered. Moreover, the geometrical nonlinearity associated with fluctuation of post-tensioning force in the cables is investigated by using the equivalent modulus of elasticity that initially introduced by Ernst (1965) and later adopted by different standards (JSCE, 2010, Walther, 1999).

The list of considered scenarios along with the lost cable(s) and loading patterns in conjunction with different deck configurations are given in Table 5-1. Apart from

Table 5-1 Cable loss scenarios and loading patterns considered in this study.

Scenario	Lost cable No.	Deck	Cable loss pattern	Traffic loading pattern
S1-SL_D1	1a,1b	**Deck-1**	**Symmetrical**	**Symmetrical**
S1-SL_D2	1a,1b	**Deck-2**		
U1-UL_D1	1a	**Deck-1**	**Unsymmetrical**	**Unsymmetrical**
U2-UL_D1	2a			
U3-UL_D1	30a			
U4-UL_D1	1a,2a			
U1-UL_D2	1a	**Deck-2**		
U2-UL_D2	2a			
U3-UL_D2	30a			
U4-UL_D2	1a,2a			

5.4 Analysis Results

5.4.1 Healthy bridge (before loss of cables)

The longitudinal profile of the deck, cable stresses (as percentage of ultimate strength) and σ_{xx} stress on top surface of the deck obtained from static FE analysis of the healthy bridge subject to SL (symmetrical traffic load pattern) and UL (unsymmetrical traffic load pattern) are shown in Figures 5-3 and 5-4, respectively. The difference between maximum deflection of Deck-1 and Deck-2 is around 8% for symmetrical load pattern and 4% for unsymmetrical load pattern.

In SL scenario, the cable stresses for Deck-1 and Deck-2 are almost the same whereas for UL scenario the cables of the bridge with Deck-2 have lower stresses than Deck-1. In terms of predicted σ_{xx} stress on top surface of the decks, the difference between Deck-1 and Deck-2 is limited to18%. The discrepancy between the responses of Deck-1 and Deck-2 can be attributed to slightly lower stiffness of Deck-2 compared with Deck-1 and slightly higher self-weight of Deck-1 compared with Deck-2.

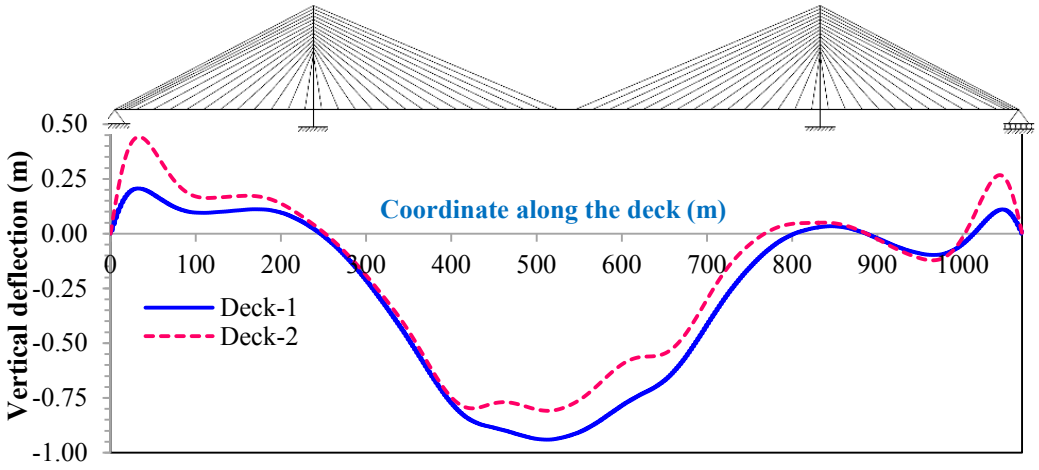

(a) Vertical deflection

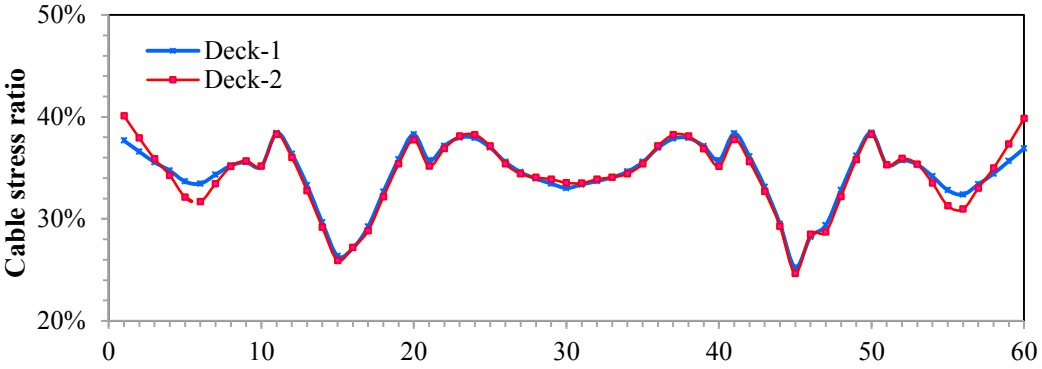

(b) Cable forces

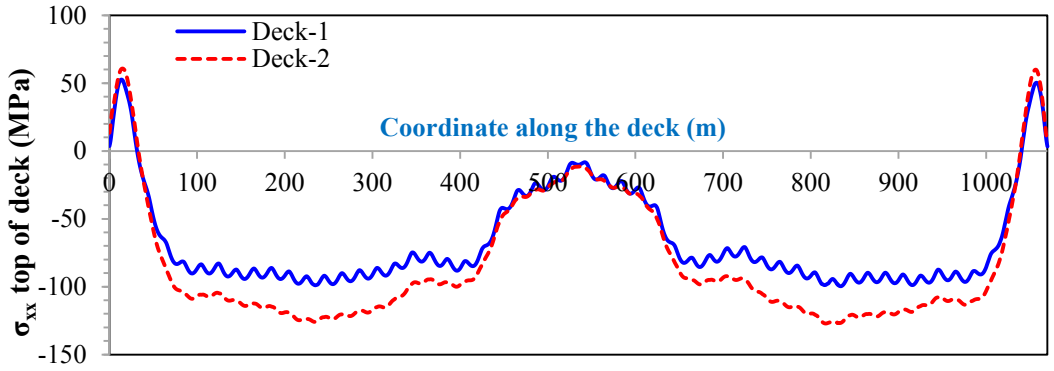

(c) σ_{xx} stress component on top surface of the deck

Figure 5-3 Comparison between responses of cable stayed bridges with Deck-1 and Deck-2 under symmetrical load (SL) pattern (a) vertical displacements along the deck (b) ratio of axial force (stress) over breakage load (stress) for stays and (c) σ_{xx} stress component on top surface of the deck.

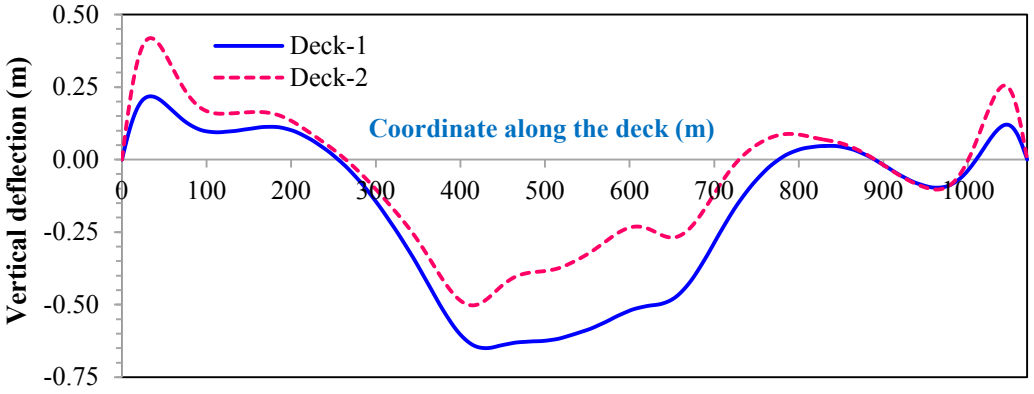

(a) Vertical deflection

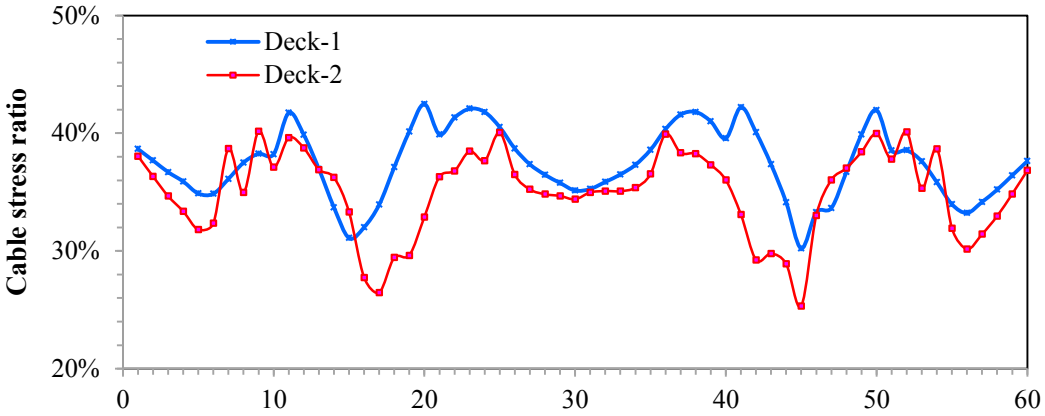

(b) Cable forces

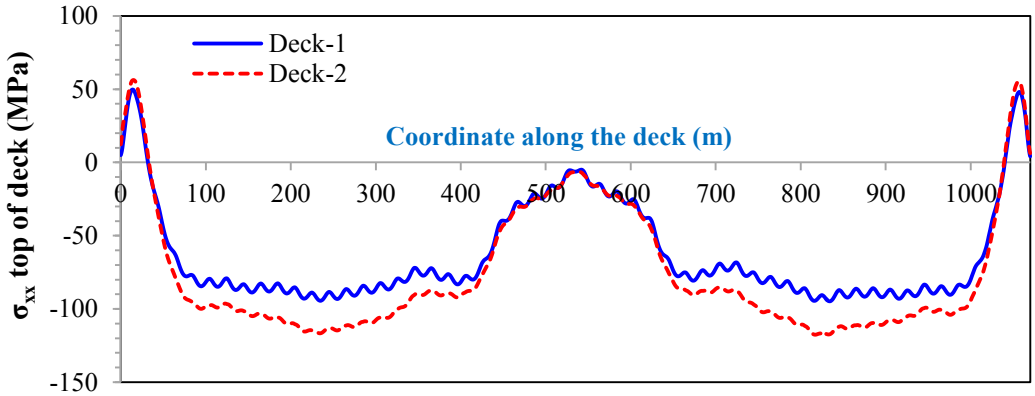

(c) σ_{xx} stress component on top surface of the deck

Figure 5-4 Comparison between responses of cable stayed bridges with Deck-1 and Deck-2 under unsymmetrical load (UL) pattern (a) vertical displacements along the deck (b) ratio of axial force (stress) over breakage load (stress) for stays and (c) σ_{xx} stress component on top surface of the deck.

5.4.2 Deck and Tower

Time-history of the vertical deflection at the mid-span of deck (i.e. x = 535 m), the deflected configuration of the deck (when maximum vertical displacement has occurred) and profile of σ_{xx} stress component on the top surface of the deck (when maximum σ_{xx} stress has occurred) for SL scenario is shown in Figure 5-5. Furthermore, deflected configuration and average σ_{xx} stress component on top surface of the deck (when maximum vertical displacement has occurred) for different unsymmetrical (UL) scenarios are shown in Figures 5-6 and 5-7, respectively. The maximum twist of the deck $\theta_{\max}$ (see Figure 5-8), maximum nodal σ_{xx} stress on the deck, maximum lateral drift on top and maximum equivalent stress σ_{eqv} on the bottom of the right tower for unsymmetrical (UL) scenarios are given in Table 5-2.

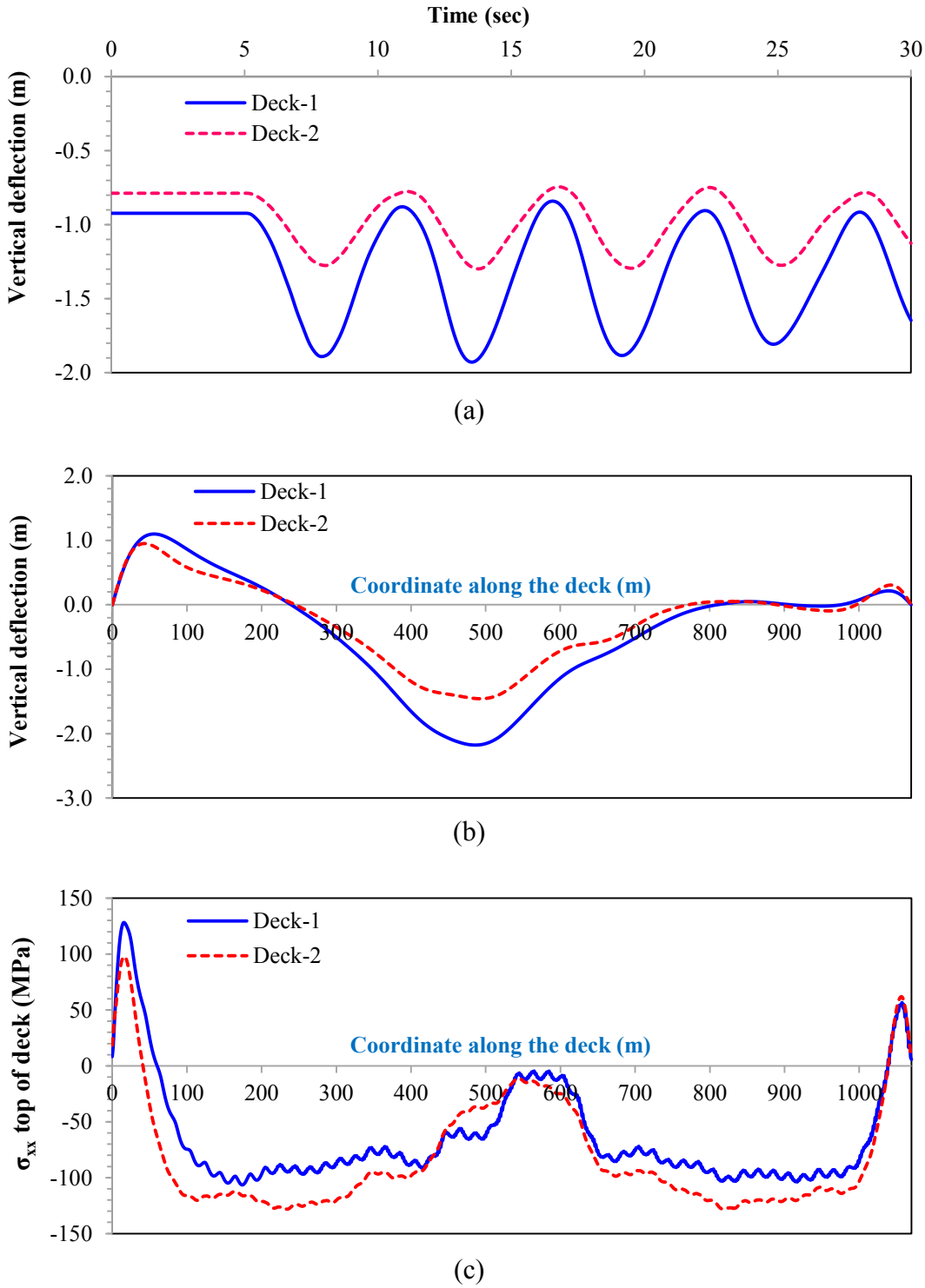

Figure 5-5 Time history of (a) vertical deflection at mid-span (x= 535 m) (b) deflected configuration of the deck (when maximum vertical displacement has occurred) (c) σ_{xx} stress component on the top surface of the deck (when maximum σ_{xx} stress has occurred) for symmetrical (SL) cable loss and loading scenarios.

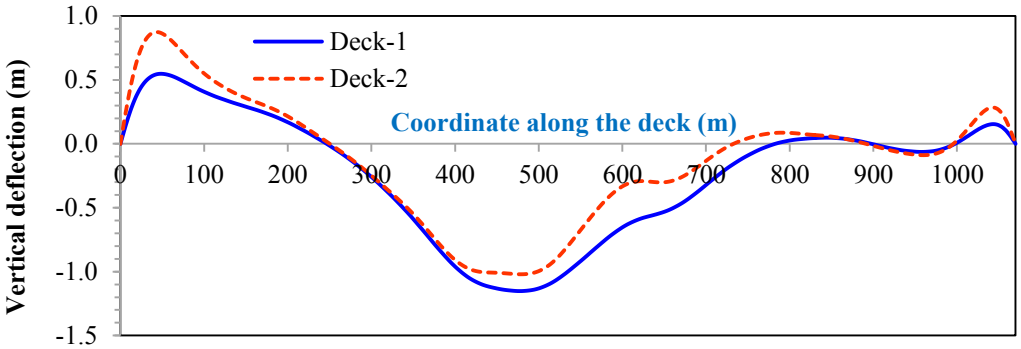

(a) U1-UL

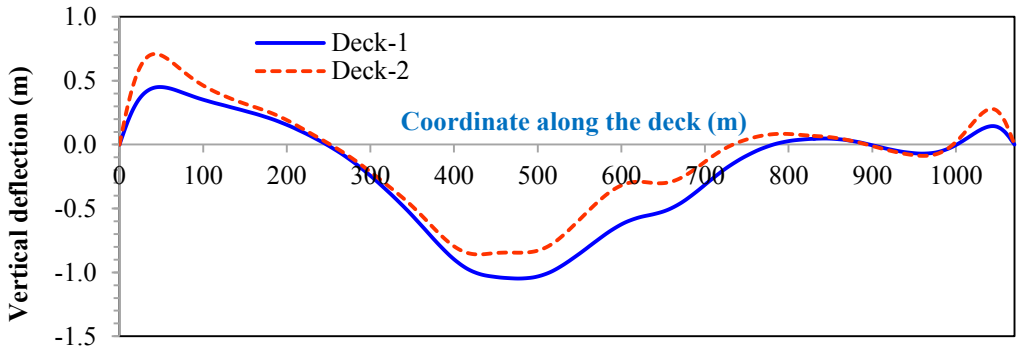

(b) U2-UL

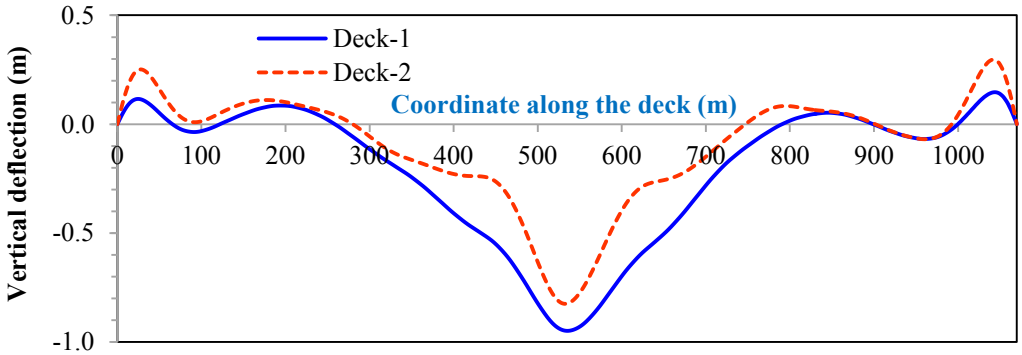

(c) U3-UL

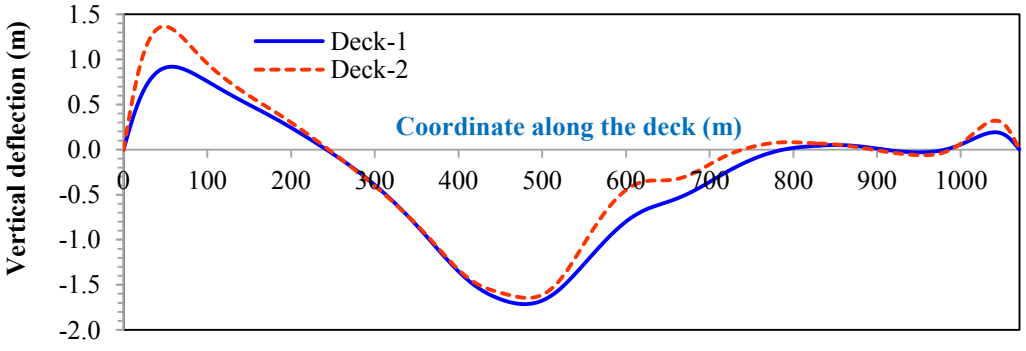

(d) U4-UL

Figure 5-6 Deflected configuration of the deck (when maximum vertical displacement has occurred) for different unsymmetrical (UL) cable loss and loading scenarios.

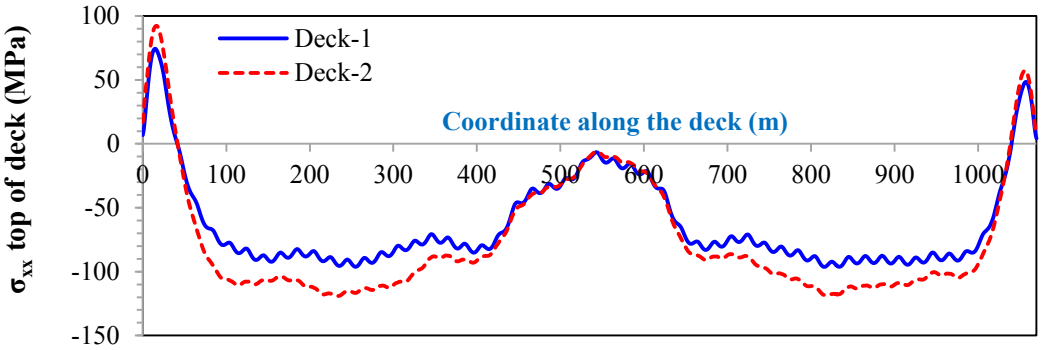

(a) U1-UL

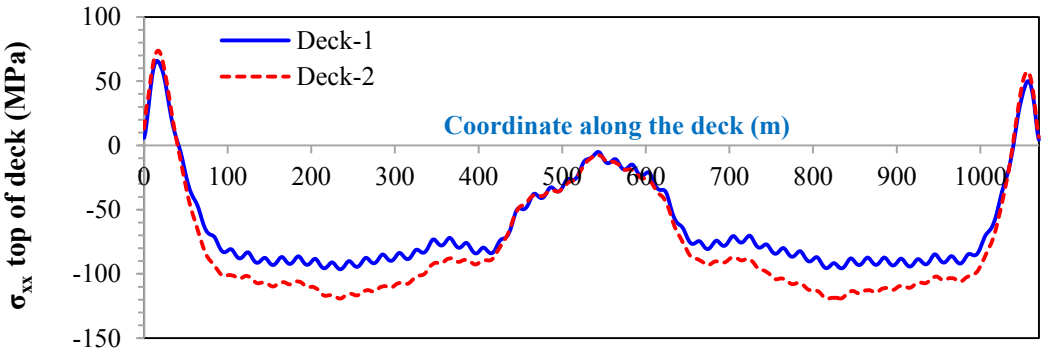

(b) U2-UL

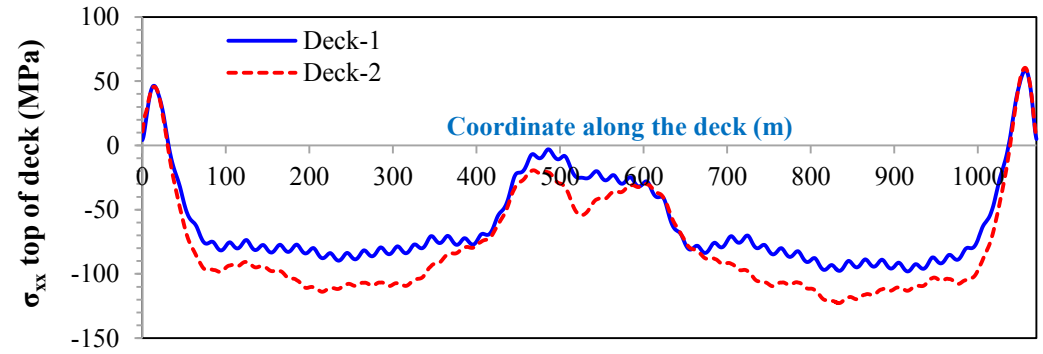

(c) U3-UL

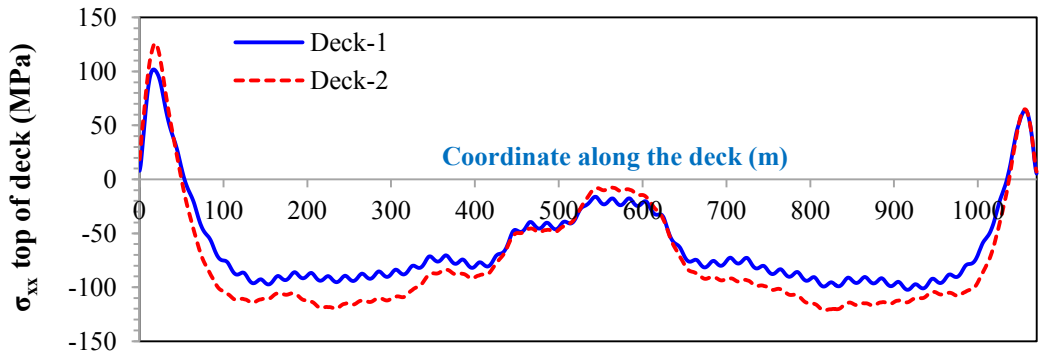

(d) U4-UL

Figure 5-7 Average σ_{xx} stresses (when maximum vertical displacement has occurred) for different unsymmetrical (UL) cable loss and loading scenarios.

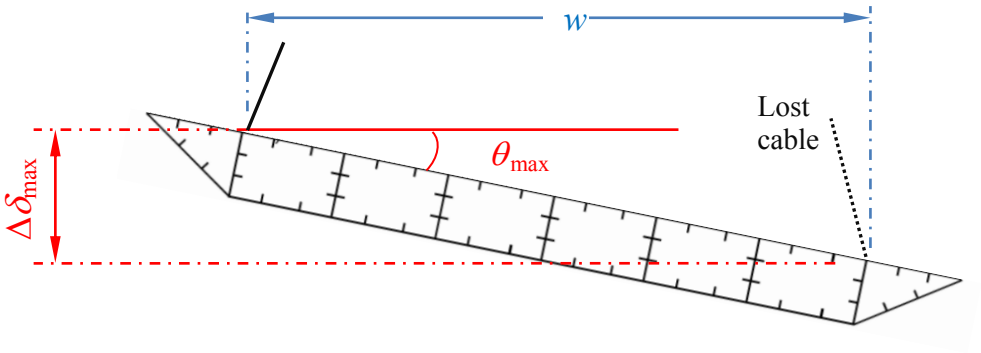

Figure 5-8 Maximum twist of the deck due to unsymmetrical cable loss.

Table 5-2 Summary of the maximum twist (θ_{max}), maximum stresses within the deck, maximum drift on top and maximum equivalent stresses on the bottom of the right tower obtained from unsymmetrical load pattern and cable loss scenarios.

Scenario		**Deck**			**Tower**	
		θ_{max} (rad)	σ_{xx} # (MPa)	Normalised σ_{xx} ##	Drift on top (m)	σ_{eqv} # on bottom (MPa)
U1-UL	**Deck-1**	1.67×10^{-4}	363.2	3.63	-0.56	161.4
U2-UL		1.08×10^{-3}	382.3	3.82	-0.53	158.2
U3-UL		2.71×10^{-2}	358.3	3.58	-0.53	161.2
U4-UL		8.33×10^{-4}	384.7	3.84	-0.68	179.2
U1-UL	**Deck-2**	1.67×10^{-4}	458.7	3.60	-0.45	157.9
U2-UL		2.47×10^{-3}	429.2	3.37	-0.43	150.8
U3-UL		7.92×10^{-2}	426.3	3.34	-0.41	161.2
U4-UL		1.48×10^{-2}	464.1	3.64	-0.49	166.9

Maximum nodal values.

Maximum nodal values normalised with respect to the average σ_{xx} stress in the deck of the healthy bridge.

Based on the results given in Table 5-2, it is concluded that scenario U4-UL associated with loss of back stays 1a and 2a lead to maximum stress and deflection compared with other scenarios, whereas the U3-UL scenario induces the maximum torsion/twist in the deck. For the bridge with Deck-2, during scenarios U1-UL and U4-UL, the maximum nodal stress exceeds the yield strength of the steel (i.e. 450MPa), however, the average longitudinal flexural stresses σ_{xx} along the deck (see Figures 5-5c and 5-7) are well below the yield strength of steel and accordingly neither cable loss scenario (SL) nor (UL) lead to formation of a plastic hinge within the deck.

Overall, the stresses induced in the bridges with Deck-1 and Deck-2 during unsymmetrical cable loss scenarios have the same magnitude. In order to further assess the effect of deck configuration on the potential progressive collapse response during different cable loss scenarios, the maximum stress induced in Deck-1 and Deck-2 are normalised with respect to the maximum stress occurred in the healthy bridge and the values are reported in Table 5-2 that demonstrate the minor influence of the deck configuration on the response of the deck following different cable loss scenarios.

5.4.3 Cables

Envelop of maximum and minimum tensile stresses in the cables for symmetrical (SL) scenarios are shown in Figures 5-9a and 5-9b, respectively. It is seen that the axial stress in the cables is well below the breakage stress ($\sigma_u = 1860\ \text{MPa}$) of the cables. In addition, the minimum axial stresses in the cables are used for calculating the minimum equivalent modulus of elasticity $\overline{E}$ (Ernst's modulus) of cables which are shown in Figure 5-9c. It is seen that for the longest cables connected to the mid-span $\overline{E} \cong 0.94E$ which would have a minor influence on the response of the bridge.

Envelops of the maximum tensile stress in the cables "a" and "b" (see Figure 5-1) during unsymmetrical (UL) scenarios are shown in Figures 5-10 and 5-11, respectively. It is observed that the axial stress in the cables for the considered unsymmetrical cable loss scenarios is well below the breakage stress ($\sigma_u = 1860\ \text{MPa}$) of the cables and accordingly in the cable stayed bridge under consideration, no zipper-type progressive collapse is expected to occur due to symmetrical or unsymmetrical loss of two cables. In addition, the minimum equivalent modulus of elasticity $\overline{E}$ (Ernst's modulus of cables) expressed as a ratio of modulus of elasticity E during unsymmetrical (UL) scenarios for Deck-1 and Deck-2 are shown in Figure 5-12. It is seen that for the bridge with Deck-2 subjected to unsymmetrical (U4-UL) scenario, the minimum $\overline{E}$ is as low as $0.88E$ for cable 30 (see Figure 5-12d) that can affect the dynamic response and accordingly should not be ignored in the progressive collapse assessment of the bridge.

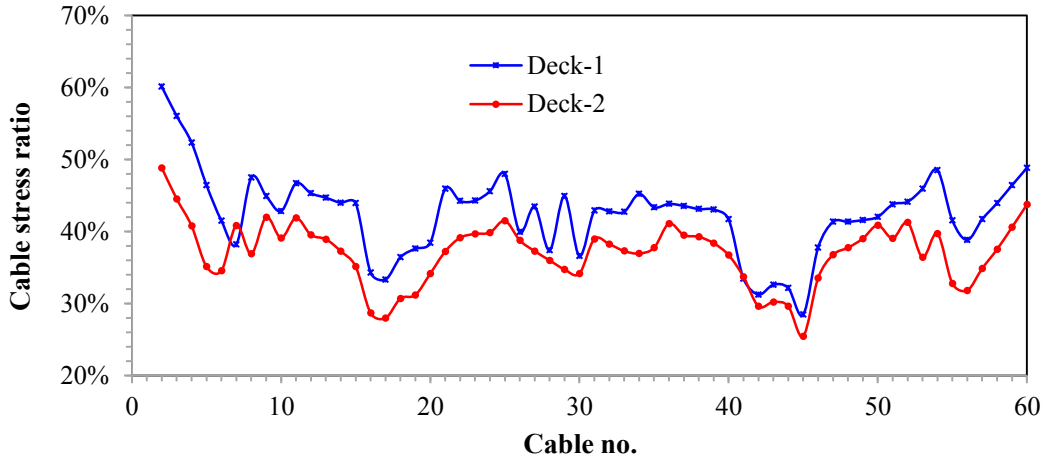

(a)

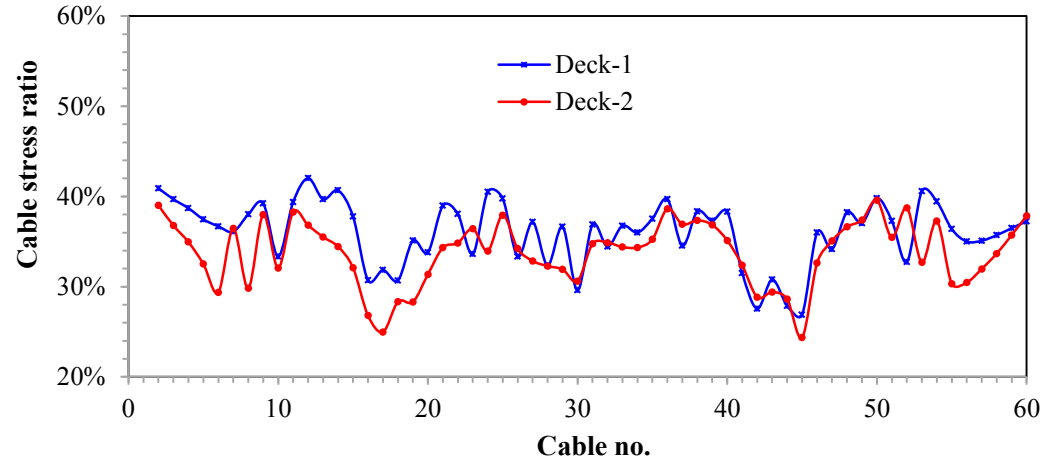

(b)

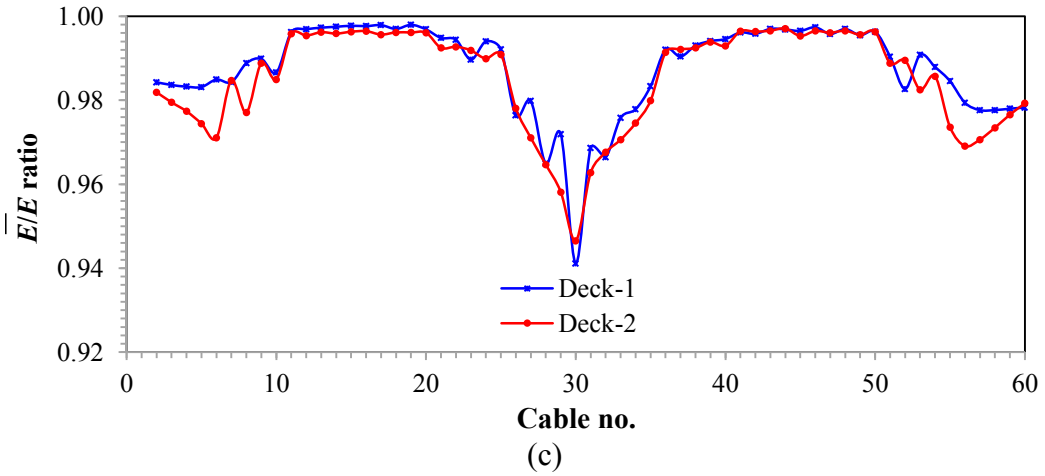

(c)

Figure 5-9 Envelop of the (a) maximum tensile stress over ultimate strength (b) minimum tensile stress over ultimate strength and (c) the minimum equivalent modulus of elasticity $\overline{E}$ (Ernst's modulus of cables) expressed as a percentage of modulus of elasticity E in the cables during symmetrical (SL) cable loss and loading scenarios.

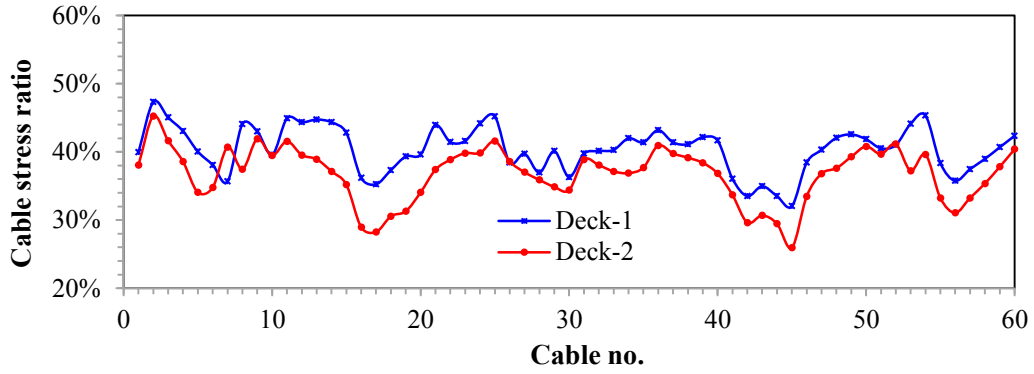

(a) U1-UL

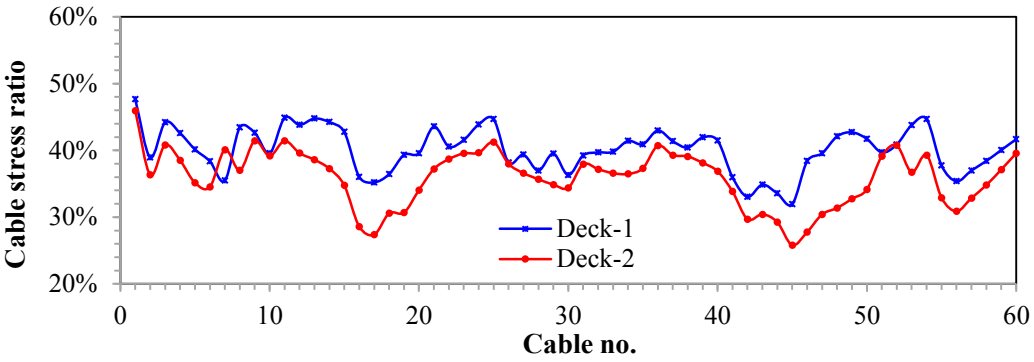

(b) U2-UL

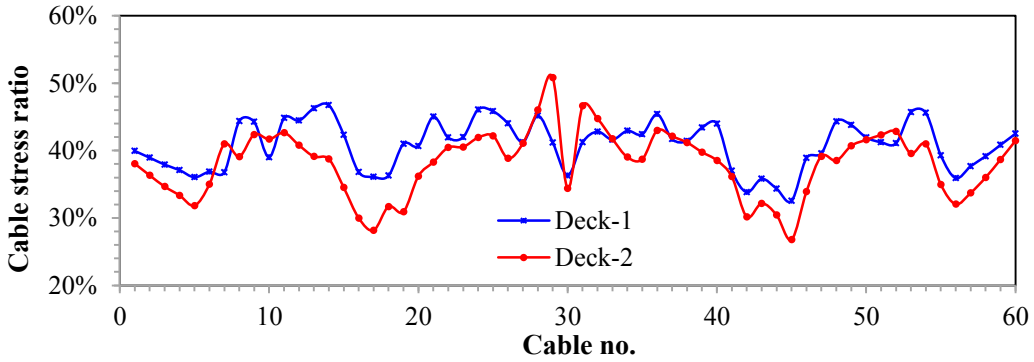

(c) U3-UL

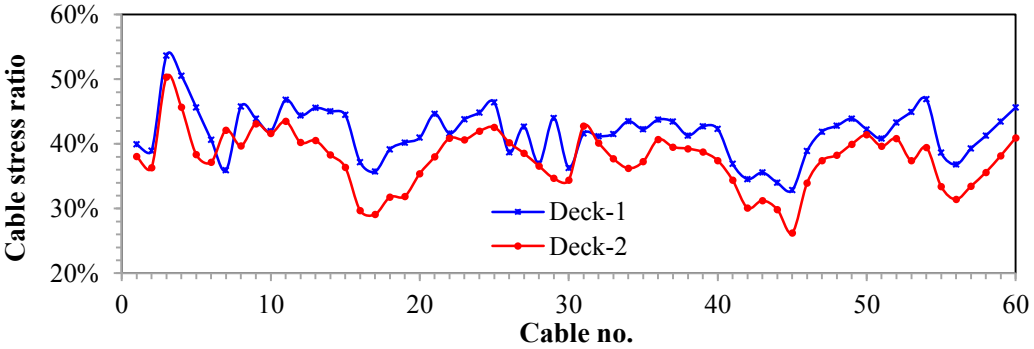

(d) U4-UL

Figure 5-10 Envelop of the maximum tensile stress in cables “a” (z=9.6) during unsymmetrical (UL) scenarios.

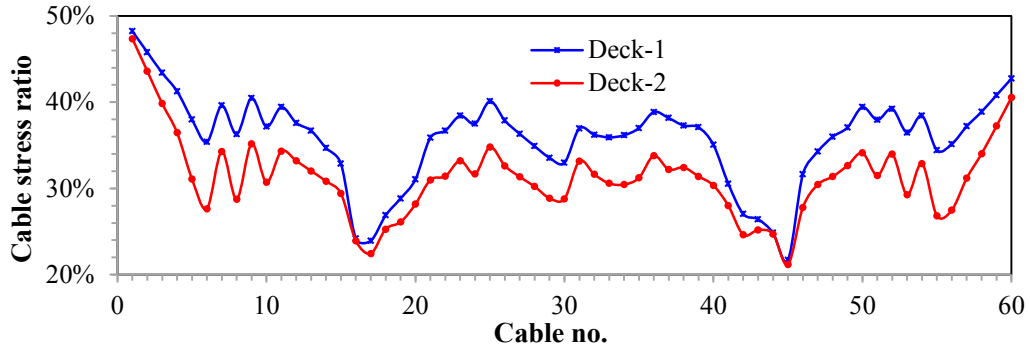

(a) U1-UL

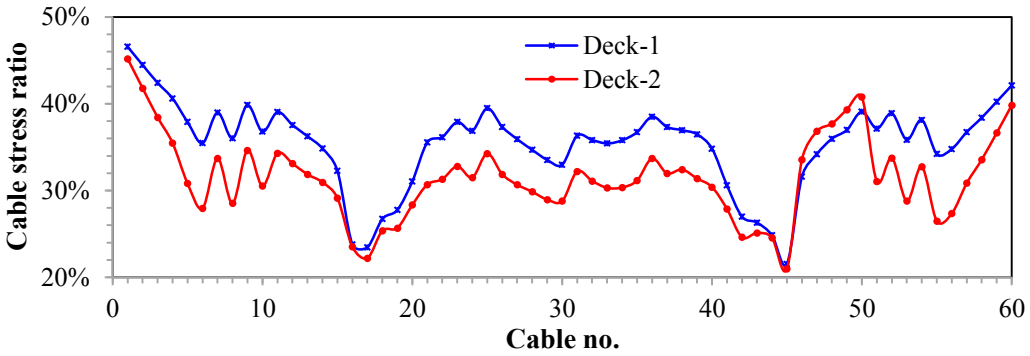

(b) U2-UL

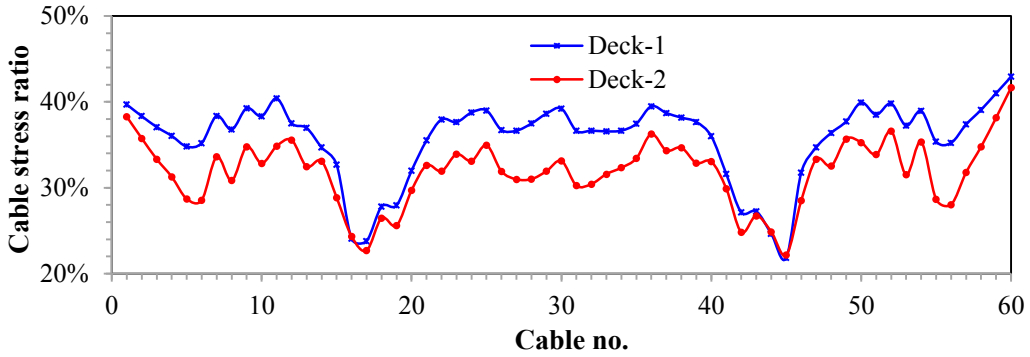

(c) U3-UL

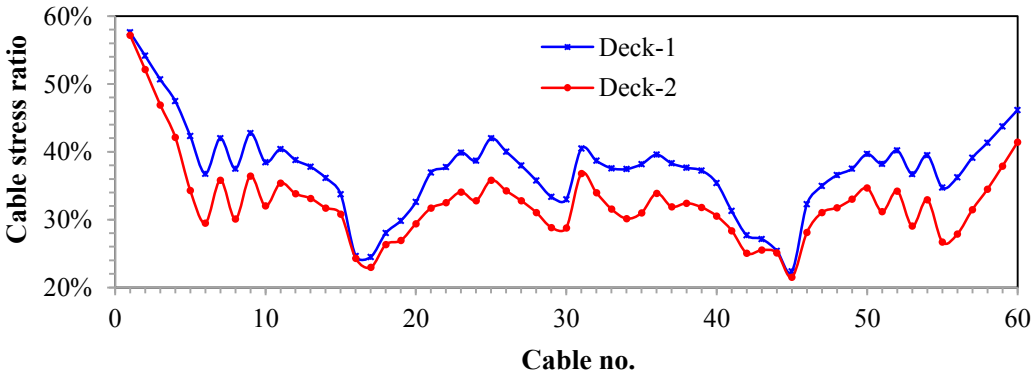

(d) U4-UL

Figure 5-11 Envelop of the maximum tensile stress in cables “b” (z=-9.6) during unsymmetrical (UL) scenarios.

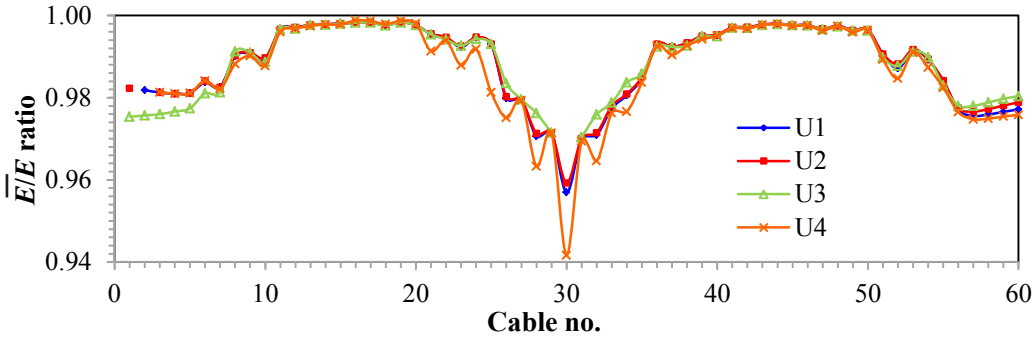

(a) Cables "a" (z=9.6) –Deck1

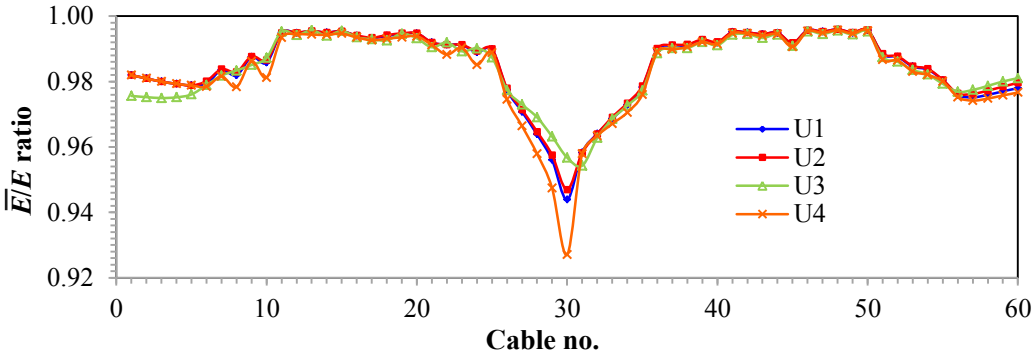

(b) Cables "b" (z=-9.6) –Deck1

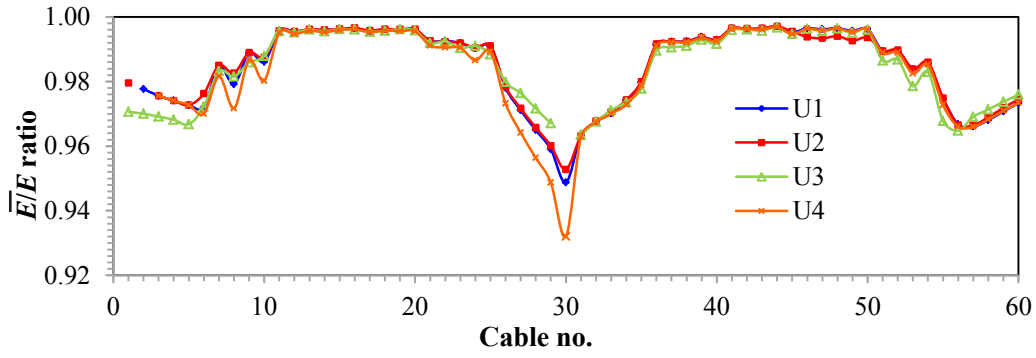

(c) Cables "a" (z=9.6) –Deck2

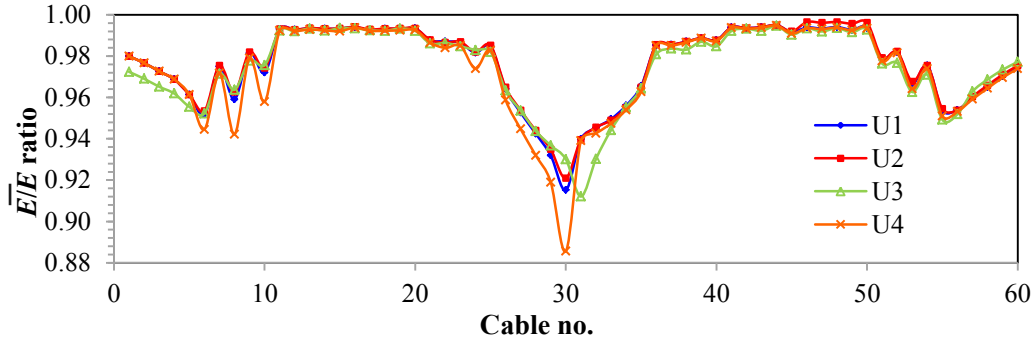

(d) Cables "b" (z=-9.6) –Deck2

Figure 5-12 The minimum equivalent modulus of elasticity $\overline{E}$ (Ernst's modulus of cables) expressed as a ratio of modulus of elasticity E during unsymmetrical (UL) scenarios.

5.4.4 Sensitivity Analysis

With regard to the variability in strength and stiffness of materials, a sensitivity analysis is carried out to demonstrate the robustness of the FE results and also evaluate the influence of mechanical properties of steel (i.e. yield strength σ_y and elastic modulus E) on the potential progressive collapse response of the cable stayed bridge. The scenario U4-UL (loss of cables No. 1a and 2a) that led to maximum vertical deflection and maximum stresses in the structural components (i.e. deck and cables) and ±10% variability in the steel modulus of elasticity E is considered in this sensitivity analysis. The sensitivity of deflection response (along the deck) with respect to the yield strength σ_y and elastic modulus E of the steel during scenario U4-UL is shown in Figure 5-13.

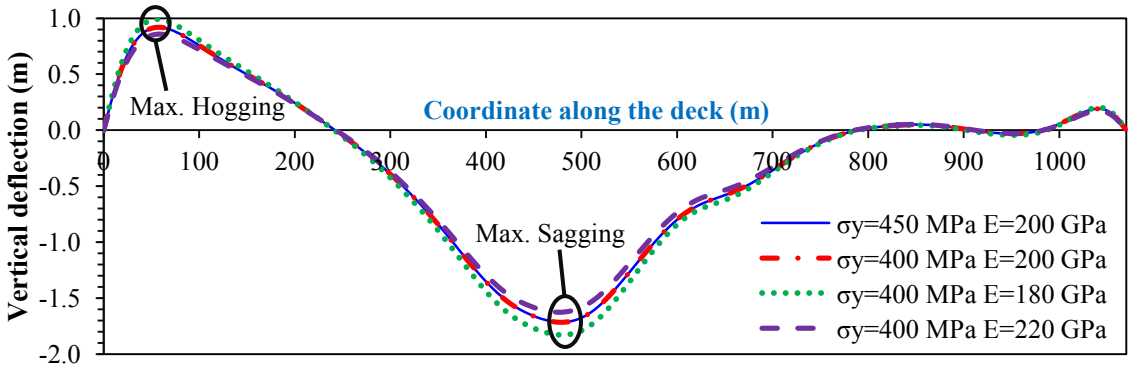

(a) Deck-1

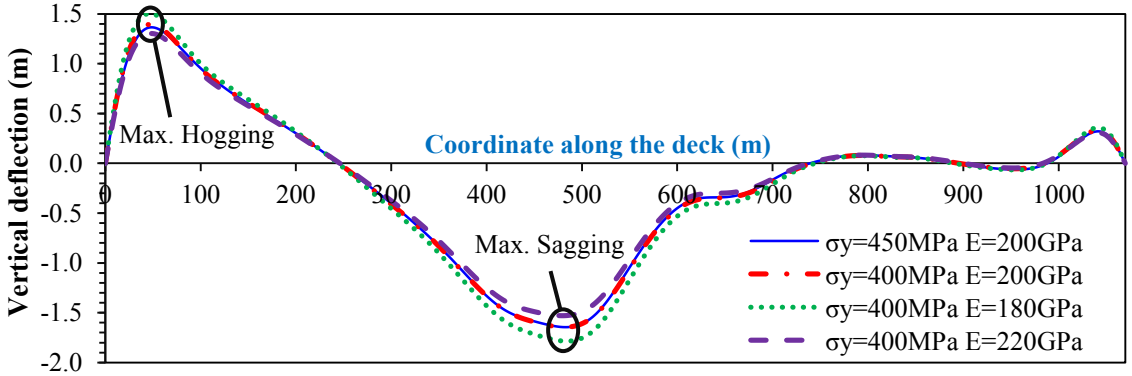

(b) Deck-2

Figure 5-13 Sensitivity of the deflected configuration of the deck (when maximum vertical displacement has occurred in scenario U4-UL) with respect to steel yield strength σ_y and elastic modulus E.

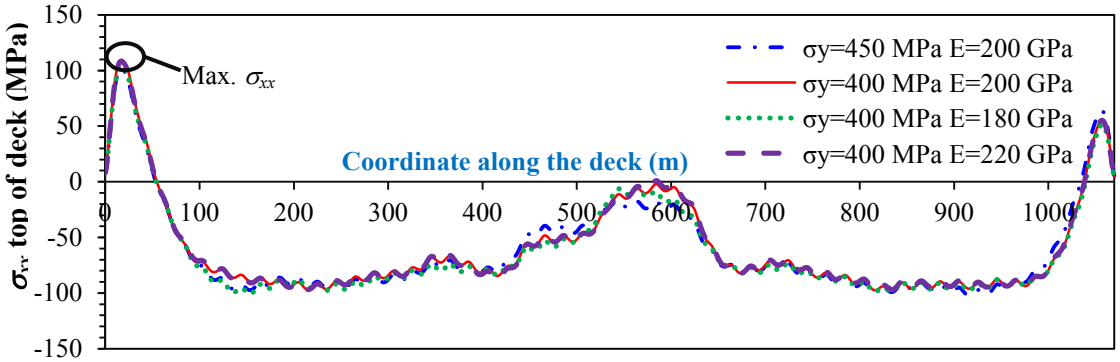

(a) Deck-1

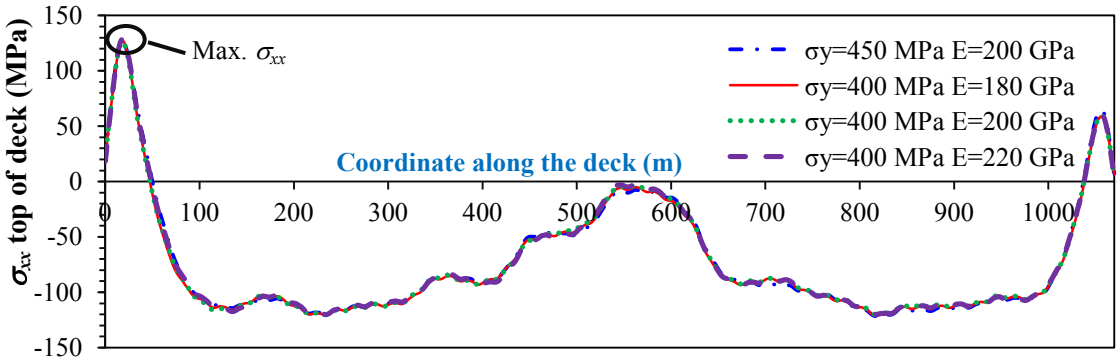

(b) Deck-2

Figure 5-14 Sensitivity of average σ_{xx} stress component on top surface of the deck (when maximum vertical displacement has occurred in scenario U4-UL) with respect to steel yield strength σ_y and elastic modulus E.

In addition, the sensitivity of average σ_{xx} stress component on top surface of the deck (when maximum vertical displacement has occurred) with respect to the yield strength and elastic modulus of the steel during scenario U4-UL is shown in Figure 5-14. It is observable that the variation of response (i.e. vertical deflection and σ_{xx} stress) is within the range of variability assumed for mechanical properties of steel.

With regard to the results shown in Figures 5-13 and 5-14, it is seen that the deflected configuration of the deck (locations of maximum sagging and hogging deflection) and the variation of σ_{xx} stress along the deck (locations of maximum σ_{xx}) are not sensitive to the yield strength and elastic modulus of steel. This is clearly demonstrative of the robustness as well as adequacy of the results obtained from the FE models.

5.5 Conclusions and Discussion

A detailed nonlinear 3D finite element model of a cable-stayed bridge with two different configurations of deck (i.e. steel box girder vs open orthotropic girder) was developed in this chapter. The results of 3D FE model, including axial stress on top surface of the deck, deflected profile of the deck, and tensile stress in cables, are compared with corresponding 2D FE models and validated. The developed 3D FE model was used for progressive collapse assessment of the bridge subjected to symmetrical and unsymmetrical cable loss scenarios with lost cables at different locations. Especially, the scenarios associated with loss of two back stays connected around the supports were studied in more details. With regards to the parametric studies undertaken in this chapter, the following conclusions for the cable stayed bridge under consideration can be drawn;

- The configuration of the deck (e.g. box girder or orthotropic open girder) as well as the torsional stiffness of the deck was found to have minor influence on the potential collapse response of the cable stayed bridge following loss of one or two cables.
- The cable loss scenarios associated with loss of back stays (cable 1a and 2) were the most critical scenarios that lead to maximum stress and deflection compared with other scenarios. This observation is consistent with the results obtained from detailed linear elastic 3D FE models (Aoki et al., 2012b).
- The stresses induced in the deck by the torsional mode of vibration were shown to have minor influence on the response of the bridge (no buckling or yielding of steel was observed). Also, a sensitivity analysis was carried out and it was shown that the yield strength of steel has no influence on the potential progressive collapse response of the cable stayed bridge investigated in this paper.
- The tensile stress in the stays following the cable loss scenarios remained well below the breakage stress of the cables and accordingly for the cable stayed bridge considered in this paper, loss of one or even two cables cannot trigger a zipper-type progressive collapse.

- The change in shape (geometry) and the reduction in axial stiffness of the stays due to variation of stress levels in the cables were evaluated with respect to Ernst's modulus. The variation of Ernst's modulus in the longest stays was found to be less than 12% and this is demonstrative of the magnitude of geometrical nonlinearities in the cables during progressive collapse assessment of the cable stayed bridges.
- In the analysed bridge, material nonlinearity (yielding of steel) and buckling of steel plates did not occur at global as well as local levels. Accordingly, it was concluded that the zipper-type collapse triggered by formation of plastic hinges is unlikely to happen in the cable stayed bridges that have lost two cables or less.

Chapter 6 : Cable-Stayed Bridges and Blast Loads

Summary of chapter

One of the reasons for loss of cable(s) in cable –stayed bridges can be blast loading that has become a major concern after the 911 terrorist attacks. In this chapter, a detailed nonlinear 3D finite element model is used to simulate the effect of blast loadings with different amounts of explosives at different locations along the deck, to determine the number of potential cable losses due to explosion. Moreover, the results obtained from the direct cable loss analyses due to blast loadings are compared with simple cable loss scenarios (presented in previous Chapters 3 to 5) according to alternate load path (ALP) approach. Finally, the potential of the progressive collapse of the bridge at global and local levels is investigated. With regard to the results of FE analyses, it is concluded that up to a maximum of three stays could be lost if a large enough TNT equivalent charge is detonated in the critical region around the end supports. However, loss of three cables with damage to the anchorage zone area within the end support did not trigger the progressive collapse of the entire bridge. It is shown that the simple cable loss analysis based on ALP can adequately capture the response (i.e. deformation along the deck and tower, and maximum stress levels in the regions sufficiently away from the explosion) of the cable stayed bridge following cable loss due to direct blast load. The short cables near the tower are identified as the most sensitive cables in which the stress level is significantly influenced by the blast loadings. However, these short cables are not sensitively influenced by the simple cable loss analysis.

6.1 Introduction

In previous 3 chapters (Chapters 3 to 5), the effect of loss of cable(s) were studied by using alternate load path (ALP) method. Linear as well as nonlinear dynamic analyses following different cable loss scenarios were conducted and dynamic amplification factor (*DAF*) for different structural components were determined.

A wide range of loading scenarios such as corrosion, collision of vehicles, earthquake and blast can lead to cable loss and subsequently catastrophic progressive collapse of the entire bridge. Among different extreme loading scenarios, however, the loss of cables due to air blast and explosion has become a major concern since 911 terrorist attacks.

The progressive collapse assessment of structures prone to terrorist attacks can be carried out by directly simulating the explosion or alternatively applying the air blast pressure on the structure and obtaining the structural response (Shi et al., 2010). This approach is accurate, however, it is computationally demanding. On the other hand, there are simplified progressive collapse analysis methods based on alternate load path (ALP) approach, in which, the load carrying structural components such as columns and/or cables are removed in some hypothetical scenarios to simulate the implications of critical member loss due to blast loadings. However, some researchers claim that the simplified method based on ALP cannot adequately predict the progressive collapse response of the structure subject to blast loading (Shi et al., 2010).

Therefore, in this research, these two methods will be applied to a cable-stayed bridge and compared to determine the accuracy of simplified method since many research works have been conducted using the simplified method.

In this study, nonlinear 3D FE models of a cable stayed bridge is developed using LS-DYNA (2007) and ANSYS software (2009). The developed FE models can take account of material and geometrical non-linearity including large strains and displacements. Using the developed 3D FE model in LS-DYNA, blast load analysis was carried out to determine the air blast pressure. Then, the air blast pressure is automatically applied on the bridge to determine the extent of the damage in the deck as well as the lost (fully damaged) cable(s). Furthermore, the dynamic response of the bridge following loss of fully damaged cables is captured by the LS-DYNA model and the results are compared with the FE model predictions in which the ALP method is used to assess the potential progressive collapse response of the bridge following cable loss due to explosion.

6.2 Adopted assumptions

6.2.1 Geometry, material properties and design loads

The adopted assumptions including bridge configuration, material properties, 3D FE model used in conjunction with ALP method and design loads in this chapter are as given in Chapter 4, Sections 4.2 and 4.3.

6.2.2 Modelling and analysis

Similar to previous chapters, the developed FE models can take account of large displacements and geometrical nonlinearities. Furthermore, for dynamic analysis a proportional damping with mass and stiffness multipliers of $\alpha = \beta = 0.5\%$ is adopted, which is within the acceptable range for steel structures (Clough and Penzien, 1993).

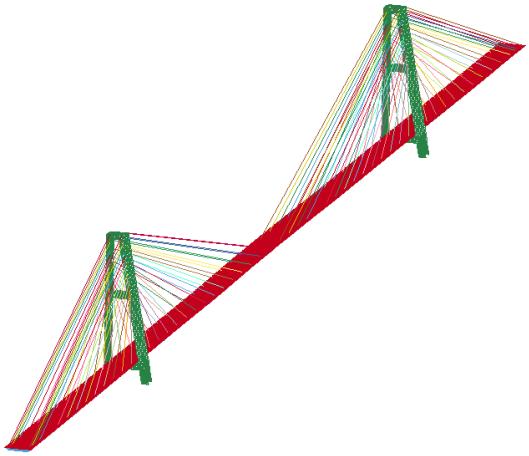

(a) Explicit model (LS-DYNA)

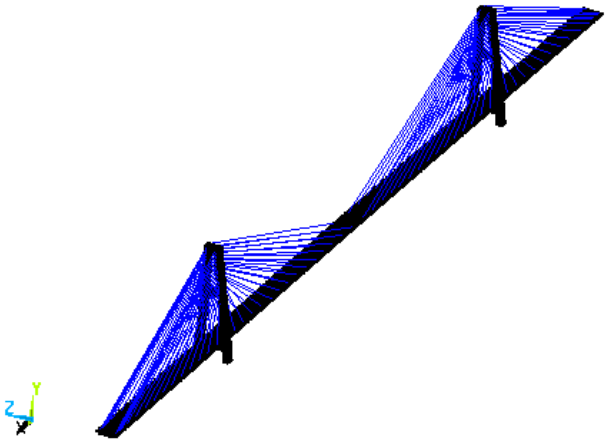

(b) Implicit model (ANSYS)

Figure 6-1 Outline of the 3D finite element models.

In this chapter, the bridge model was developed using both LS-DYNA and ANSYS software (see Figure 6-1). The LS-DYNA model with an explicit solver was employed for blast analysis and capturing the local/global response of the bridge subject to air blast pressure, whereas the ANSYS model with an implicit solver was used to capture the local/global response of the bridge following sudden loss of cable(s) based on ALP approach.

In LS-DYNA 3D model (Figure 6-1a), the deck and tower are modelled by shell element (Belytschko-Tsay element formulation). This shell element is defined by 8 nodes with 6-dofs at each node and it takes advantage of a reduced integration scheme with 2 integration points over the thickness of the element. The material model used in conjunction with this shell element to capture the nonlinear behaviour of steel plates is material number 24 which is MAT_PIECEWISE_LINEAR_PLASTICITY. This is an elasto-plastic material for which failure mode based on plastic strain can be defined by a bilinear stress strain curve. In this research, steel plastic strain failure value was set as 0.06 (see Figure 4-2 in Chapter 4). When the plastic strain within an element reaches this value, the element is removed from the numerical model. Moreover, cables in LS-DYNA were modelled by discrete beam/cable elements with 2 Gauss points. The material type 71 called MAT_CABLE_DISCRETE_BEAM was used for modelling cables. This beam element can model an elastic cable without compressive force (tensile only). This beam/cable element also has the ability to take account of the cable pre-tensioning force at the start of the analysis. The initial pre-tensioning strains induced in the cables were given in Table 4-1 in chapter 4.

The 3D FE model developed in ANSYS (Figure 6-1b) is analysed using an implicit solver. In ANSYS, the deck and towers are modelled by shell elements, whereas the cables are modelled by link-elements which are treated as tension-only members with limited tensile capacity. More details on the element type and material constitutive laws adopted in ANSYS model were provided in Section 4.2.2 of Chapter 4.

Explicit versus implicit analysis

Typically direct step-by-step integration schemes are used for time discretisation of differential equations governing dynamic response of structures (Cook et al., 2002),

$$[M]\{\ddot{D}\}_n + [C]\{\dot{D}\}_n + [K]\{D\}_n = \{R^{ext}\}_n \tag{6-1}$$

where, $[M]$, $[C]$ and $[K]$ are mass, damping and stiffness matrix of the structure, respectively. $\{\ddot{D}\}_n$, $\{\dot{D}\}_n$ and $\{D\}_n$ denote current nodal acceleration, velocity and displacement vectors and $\{R^{ext}\}_n$ is the current vector of external dynamic load.

A wide range of time discretisation techniques for solving Equation (6-1) have been proposed to date. These time discretisation methods mostly take advantage of finite difference schemes and accordingly they are categorised to explicit and implicit methods (Cook et al., 2002). In the explicit schemes the unknown displacement vector $\{D\}_{n+1}$ is an explicit function of acceleration, velocity and displacement vectors of previous steps

$$\{D\}_{n+1} = f\left(\{D\}_n, \{\dot{D}\}_n, \{\ddot{D}\}_n, \{D\}_{n-1}, \ldots\right) \tag{6-2}$$

whereas in an implicit solution scheme

$$\{D\}_{n+1} = f\left(\{\dot{D}\}_{n+1}, \{\ddot{D}\}_{n+1}, \{D\}_n, \{\dot{D}\}_n, \{\ddot{D}\}_n, \ldots\right) \tag{6-3}$$

Accordingly, implicit methods should use iterative schemes for capturing nonlinear behaviour of structures. The major differences between explicit and implicit methods are stability and economy. The time step is a critical factor in both methods, however, the required time step for explicit solvers is much smaller than the implicit schemes. The explicit solvers need to use a large number of time steps, but the process involves solving the simultaneous set of governing equations is very fast because the coefficient matrix of $\{D\}_{n+1}$ can be made diagonal. On the other hand, in implicit methods the number of time steps is fairly small, but at each step a few iterations are required to adequately satisfy the equilibrium and compatibility conditions (Cook et al., 2002).

In summary, explicit schemes are appropriate for wave propagation problems including blast or impact loadings, whereas implicit schemes are suitable for structural dynamics problem such as analysis of structures subject to seismic actions.

6.2.3 Verification and calibration of LS-DYNA model (Explicit Solver)

In this section, the results obtained from the LS-DYNA model with an explicit solver is compared with the results predicted by ANSYS model that takes advantage of an implicit solver. The main objective is to calibrate the explicit solver and verify its adequacy compared with the more reliable implicit solver. The cable initial force over the cable breakage load and σ_{xx} stress on top surface of the healthy bridge deck predicted by LS-DYNA, ANSYS and 2D FE models are compared in Figure 6-2 that demonstrates a good correlation among the three sets of FE models. Furthermore, the total weight of the bridge obtained from 2D, 3D-implicit and 3D-explicit FE models under progressive collapse load combination of (1.1xDead+1.35xSuperimposed Dead+0.75xTraffic) are 647 MN, 656 MN and 641MN, respectively.

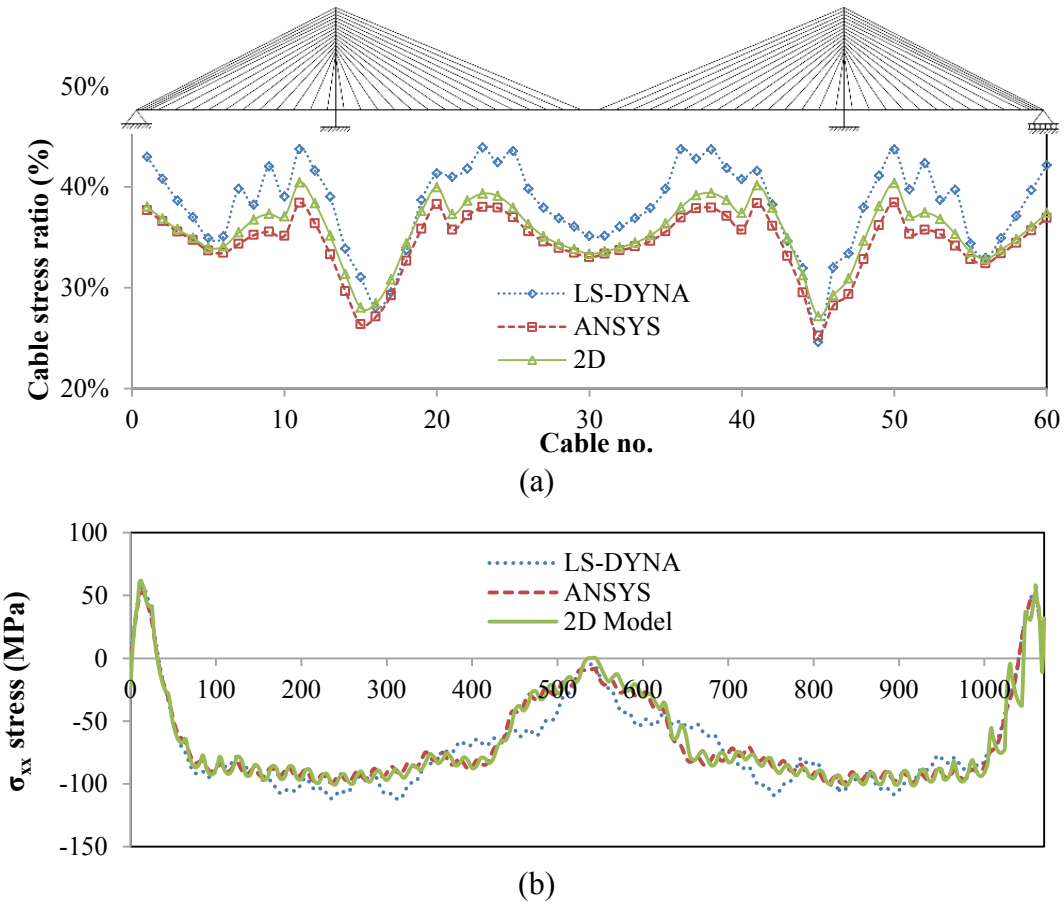

Figure 6-2 Comparison between results of 2D, implicit (ANSYS) and explicit (LS-DYNA) 3D FE models (a) ratio of axial force (stress) over breakage load (stress) for stays (under service load) (b) σ_{xx} stress component on top surface of the deck.

6.3 Blast load analysis and sudden loss of cable

6.3.1 Blast load analysis by explicit analysis (LS-DYNA)

The blast load analysis adopted in this study is purely based on Lagrangian approach, in which the surface of the shell elements (set by *SET_SEGMENT) is defined to receive the blast load pressure calculated according to CONWEP blast function. The code used for this method is *LOAD_BLAST_ENHANCED (Tabatabaei and Volz, 2012). By using this code, pressure loads caused by the explosion of conventional charge is defined as an air blast function that include treatment of reflected waves, moving warheads and multiple blast sources (LSTC, 2007).

To verify adequacy of the adopted blast load analysis method, a simple numerical steel column subjected to a direct air blast loading scenario was modelled by LS-DYNA and the LS-DYNA prediction was compared with other numerical results as well as the available experimental data.

The steel column considered in this verification study is 4.3 m in height, 0.36 m in width and 0.122 m in depth and made of Grade 345 steel. This steel column was originally tested by Lawver et al. (2003). Furthermore, McConnell and Brown (2011) developed a FE model of this column in LS-DYNA software using shell elements (same element formulation) and with *MAT_JOHNSON_COOK material model. The schematic outline of the FE develop by McConnell and Brown (2011) is shown in Figure 6-3a. As McConnell and Brown mentioned in their paper, Lawver's experimental work was insufficiently presented in their paper due to confidentiality of the experimental data. Accordingly, McConnell and Brown had to assume some of the input data such as the amount of TNT charge and the scaled distance. With regard to the data provided by McConnell and Brown (2011) and Lawver et al. (2003), the equivalent TNT charge and scaled distance were taken as 1,000 kg and 2.1 m, respectively.

The maximum horizontal deflection at different height along the column obtained from the LS-DYNA model in this study is shown in Figure 6-3b along with predicted by McConnell and Brown's (2011) FE model predictions and Lawver's experimental data.

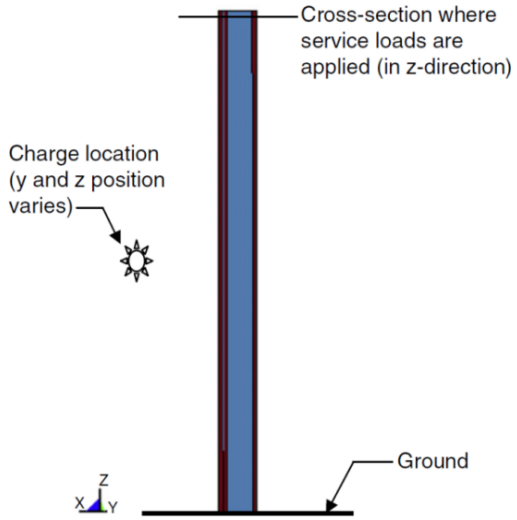

(a) FEA model (McConnell and Brown, 2011)

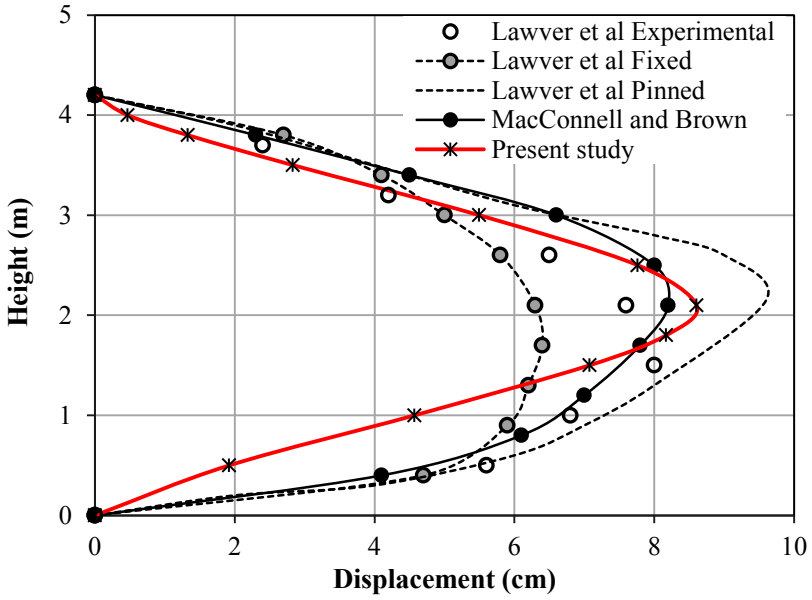

(b) Displacement

Figure 6-3 Comparison of validation model with other references

It is seen that the results of LS-DYNA model developed in this study correlates reasonably well with the test data. The maximum difference between the FE models is around 25%, however, the difference between maximum deflection predicted by the LS-DYNA FE model and the experimental results is less than 10%. This example demonstrates the adequacy of LS-DYNA FE models and explicit solvers for capturing the local and global response of structural members subjected to direct blast load.

6.3.2 Load combinations adopted for blast and sudden loss of cable analyses

For blast loading analysis, the distributed component of the traffic load, the dead load, and the accompanying lane factor from Australian standard AS5100.2 (2004) was applied along the entire bridge deck, which is the same as symmetrical loading pattern considered in Chapter 5 and shown in Figure 5-2a and b. The adopted load factors are as recommended by AASHTO LRFD bridge design specification reported in NCHRP (2003)

$$1.00DC + 0.5LL + 1.0EV \tag{6-4}$$

where, DC denotes the dead load of the structural components and non-structural attachments, LL is the full vehicular live load placed in the actual stripped lanes, and EV denotes extreme event load, which is the blast load in this chapter.

6.3.3 Scenario considered for Blast load analysis

In this chapter, three different charges of TNT are considered for blast load analysis, i.e. 1 tonne, 4.5 tonnes and 27 tonnes. The 1 tonne TNT equivalent explosive was adopted as the smallest possible charge for blast assessment of the bridge in accordance with a study undertaken by Hao and Tang (2010). The 4.5 and 27 tonnes TNT equivalent explosives are considered in this study as the maximum capacity of a small box van and a semi-trailer, respectively (Mahoney, 2007).

In the adopted blast analysis model of LS-DYNA, the contact surface has to be defined for applying the air blast pressure on the structure. Accordingly, a sensitivity analysis was carried out and the area of contact surface for blast loading was set as 25.6 m × 40 m and the detonation centre was placed at the middle of this contact surface. Within this contact surface, the element size is taken as 1/3 of the other part of the structure (approximately 0.25 m × 0.25 m elements). The cable element (link element) was too small to be subjected to the direct air blast pressure, thus, it was not defined as a contact surface.

There are eight locations where the blast load was applied (see Figure 6-4a and 6-4b); three locations near the pin-support (x=2.5, 5.0 and 7.5 m), two locations near the tower (x=225 and 235 m) and three locations around the mid-span (x=515, 525 and 535 m).

As shown in Figure 6-4c, the blast charge (detonation centre) was located at different heights depending on the scaled distance obtained from the following equation,

$$Z = \frac{R}{W^{\frac{1}{3}}} \tag{6-5}$$

where Z is the scaled distance (in m/kg$^{1/3}$), R is the distance between contact surface and the detonation centre and W is the equivalent TNT amount.

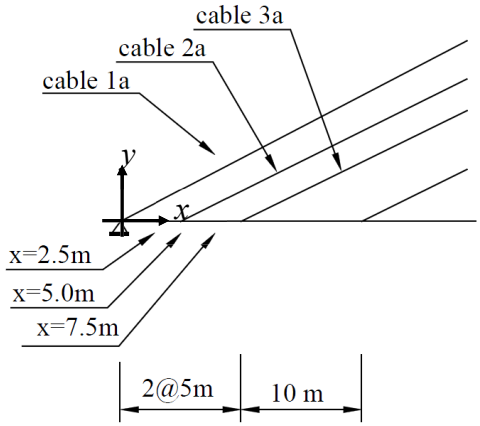

(a) Blast load location (x-distance from pin support [A-A])

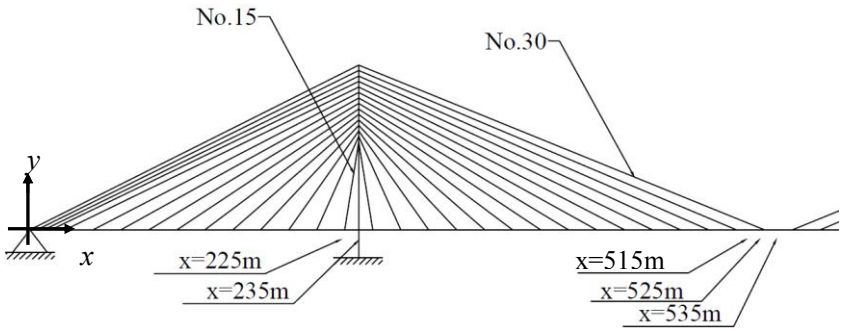

(b) Blast load location (x-distance from pin support)

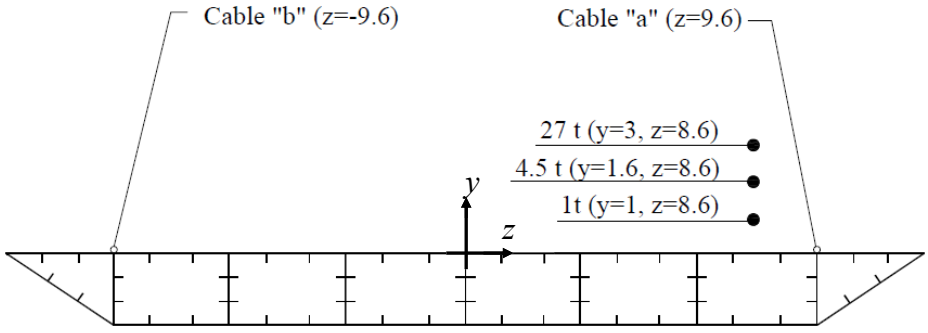

(c) Blast load location (y- and z-distances)

Figure 6-4 Locations of the applied blast loadings.

It is noteworthy that the CONWEP blast pressure function used in LS-DYNA for blast analysis is not applicable for very close range explosions and hence the scaled distance cannot be taken too small. In this study, Z is set equal to 0.1 and the R value is back calculated with respect to the amount of TNT equivalent explosive and based on Equation (6-5).

The cables are closely-spaced around the pin-support and these cables were found to be the most critical in terms of producing possible potential progressive collapse of the entire bridge (see in Chapter 3). Accordingly, three different sets of blast scenario with different amount of TNT equivalent explosive were considered assuming that explosions occur in the vicinity of pin-support. The TNT charge was placed in different locations to investigate the extent of damaged area and number of potential cable losses (total of 9 scenarios, i.e. Scenario: 1t_2.5m to Scenario: 27t_7.5m shown in Table 6-1). Apart from the blast scenarios around the pin-support, the 27-tonne TNT equivalent charge was placed at a location close to tower and mid-span (Scenario: 27t_515m to Scenario: 27t_235m). The list of considered blast scenarios along with the locations and amount of TNT equivalent explosive charges in each scenario are provided in Table 6-1 and Figure 6-4.

Table 6-1 Scenarios considered for blast load analysis (using LS-DYNA software).

	Scenario	Equivalent TNT (Tonnes)	Distance from pin-support (m)	scaled distance – Z (m/kg1/3)
Blast load analysis	Scenario:1t_2.5m	1	2.5	0.1
	Scenario:1t_5.0m		5	
	Scenario:1t_7.5m		7.5	
	Scenario:4.5t_2.5m	4.5	2.5	
	Scenario:4.5t_5.0m		5	
	Scenario:4.5t_7.5m		7.5	
	Scenario:27t_2.5m	27	2.5	
	Scenario:27t_5.0m		5	
	Scenario:27t_7.5m		7.5	
	Scenario:27t_515m		515	
	Scenario:27t_525m		525	
	Scenario:27t_535m		535	
	Scenario:27t_225m		225	
	Scenario:27t_235m		235	

6.3.4 Analysis of sudden cable loss using ALP approach and implicit solver (ANSYS)

A parametric study of cable losses by dynamic analysis using ANSYS software was presented in previous chapters. The EKILL command, available in ANSYS (2009) was used to remove the damaged cables and simulate the implications of possible cable losses due to blast load. In this chapter, the cable loss analysis using Ekill command (which is called hereafter "simple cable loss analysis") is compared with the FE simulations including the blast load analysis (i.e. LS-DYNA model). One cable loss (1a, 2a, 15a and 30a), two cable losses (1a and 2a) and three cable losses (1a to 3a) are considered as summarised in Table 6-2.

Table 6-2 Scenarios considered - equivalent cable loss analysis (simple cable loss analysis) -implicit analysis by ANSYS

	Scenarios	cable loss
Equivalent cable loss analysis	Scenario: 1a loss-ANSYS	1a
	Scenario: 2a loss-ANSYS	2a
	Scenario: 1a & 2a loss-ANSYS	1a & 2a
	Scenario: 1a,2a & 3a loss-ANSYS	1a, 2a & 3a
	Scenario: 30a loss-ANSYS	30a
	Scenario: 15a loss-ANSYS	15a

6.4 Results and discussion

6.4.1 Results of blast analysis (LS-DYNA)

The damaged area due to blast around the pin-support predicted by LS-DYNA model is shown in Figure 6-5. Furthermore, Table 6-3 summarises the damaged area and the corresponding loss of cables. In Figure 6-5a to 6-5c, the damaged area due to 1 tonne of TNT was about 4.8 m × 3.6 m with no cable losses. The most significant damage area and cable loss was created by 27 tonnes of TNT located at x=5.0 m (beside cable 2a) and 7.5 m (between cables 2a and 3a) and both scenarios led to loss of three cables.

It is noted that the damaged area is almost square shaped (straight lines). This is because of the stiffener plates used horizontally every 2.5 m apart along the whole bridge deck. The 27 tonnes of TNT equivalent charge damaged an area of 11 m × 11 m and if there

are cables within this damaged zone, obviously they would be lost. However, detonation of 27 tonnes of TNT around the tower and mid-span only led to damage in the anchorage zone and subsequently loss of only one cable. It is noteworthy that the cable losses happened due to damage in the anchorage zone of cables rather than the cable reaching its breaking stress point (see Figure 6-6).

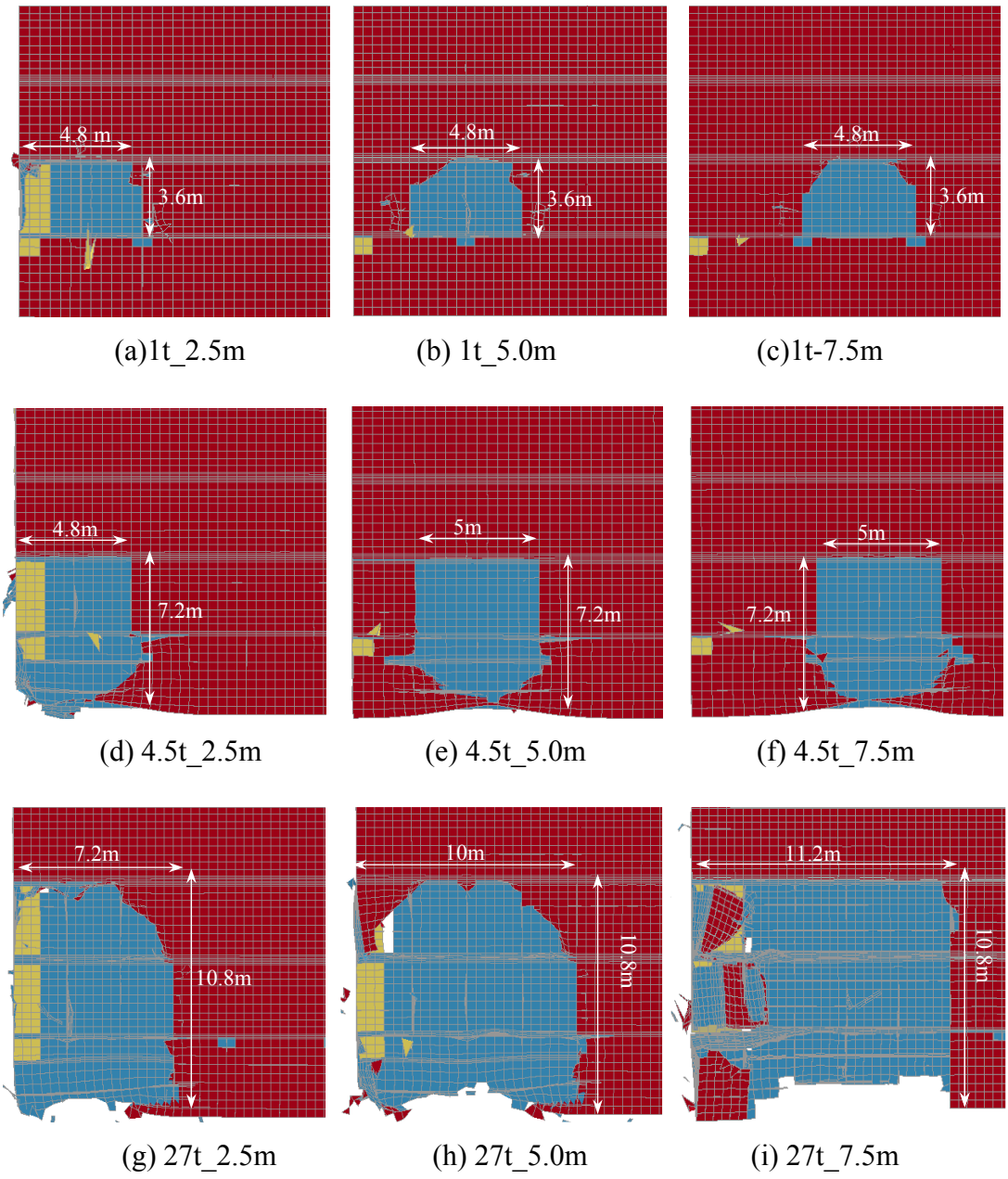

(a)1t_2.5m (b) 1t_5.0m (c)1t-7.5m

(d) 4.5t_2.5m (e) 4.5t_5.0m (f) 4.5t_7.5m

(g) 27t_2.5m (h) 27t_5.0m (i) 27t_7.5m

Figure 6-5 Damages of the deck under blast loadings (blast occurred around pin-support)

Table 6-3 Summary of the cable losses and damaged areas obtained from blast load analysis.

		Cable loss	Damaged area
Around pin-support	Scenario:1t_2.5m	None	4.8m x 3.6m
	Scenario:1t_5.0m		
	Scenario:1t_7.5m		
	Scenario:4.5t_2.5m	cable 1a	4.8m x 7.2m
	Scenario:4.5t_5.0m	cable 2a	5.0m x 7.2m
	Scenario:4.5t_7.5m	None	
	Scenario:27t_2.5m	cable 1a & 2a	7.2m x 10.8m
	Scenario:27t_5.0m	Cable 1a, 2a & 3a	10m x 10.8m
	Scenario:27t_7.5m	Cable 1a, 2a & 3a	11.2m x 10.8m
Mid-span	Scenario:27t_515m	None	11.2m x 10.8m
	Scenario:27t_525m	Cable 30a	
	Scenario:27t_535m	None	
Beside the tower	Scenario:27t_225m	Cable 15a	10m x 10.8m
	Scenario:27t_235m	None	

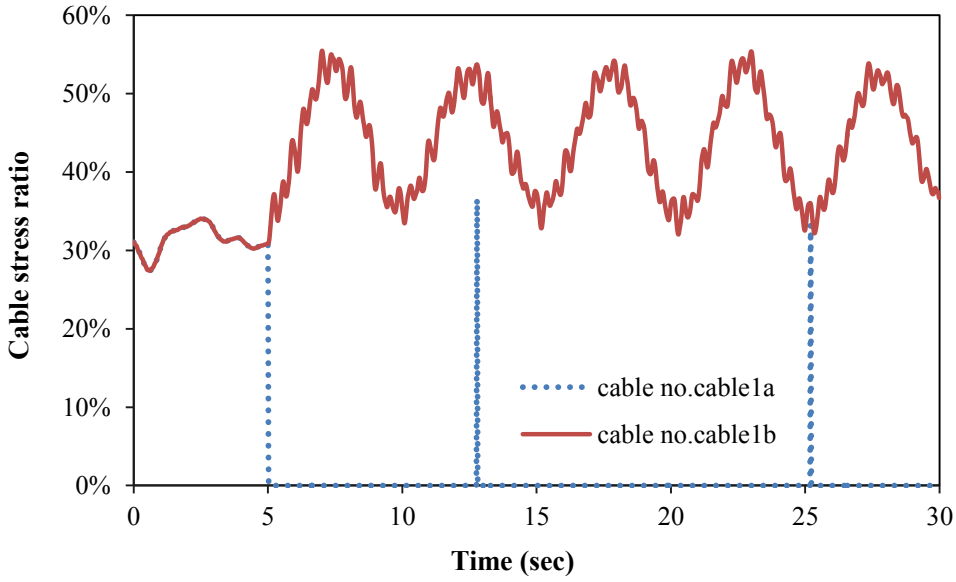

Figure 6-6 Time history of stress (expressed as a percentage of breakage stress) for cables No.1a and 1b (Scenario: 27t_7.5m).

6.4.2 Comparative study between blast load and simple cable loss according to ALP (blast around the pin support)

In this section, the effect of blast load impact and the local damage caused by air blast is investigated. Furthermore, the response of the bridge subjected to direct blast load and subsequent cable loss is compared with the response captured by simple cable loss analysis based on alternate load path (ALP) method to verify the adequacy of widely accepted ALP method. It should be noted that the blast load analysis provides information on cable loss as well as local damages, whereas the ALP method can only capture the structural implications of cable loss due to explosion.

With regard to the lost cables following blast scenarios around pin-support (see Table 6-3), Scenario: 4.5t_2.5m is compared with 1a_loss _ANSYS, and Scenario: 4.5t_5m is compared with 2a_loss_ANSYS, Scenario: 27t_2.5m is then compared with 1a & 2a_loss _ANSYS, and finally Scenario: 27t_5m and 27t-7.5m are compared with 1a to 3a_loss _ANSYS, respectively.

Deck and Tower

The magnitude of maximum vertical deflection within the deck, profile of the maximum σ_{xx} (longitudinal stress) on top and bottom surface of the deck, and maximum lateral drift on top and maximum equivalent stress σ_{eqv} at the bottom of the right tower obtained from blast analysis and simple cable loss analysis are compared in Table 6-4.

In addition, deflected configurations of the deck when maximum vertical displacement has occurred for each scenario are shown in Figure 6-7. It is observed that the deflections are predicted quite well in all cases. The average difference between the ALP and direct blast analysis is around 21% to 23%.

The average σ_{xx} stress component on the surface of the top and bottom of the deck (when maximum stress has occurred) for all scenarios are shown in Figures 6-8 and 6-9, respectively. The difference between σ_{xx} stress component predicted by ALP and direct blast analysis is around 7% and 11% for the top and about 17% for the bottom surface of the deck. With regard to the results given in Table 6-4, during scenarios 27t_2.5m and 27t_7.5m the maximum nodal stress σ_{xx} exceeds the yield strength of the steel (i.e.

450MPa), however, the average longitudinal flexural stresses σ_{xx} along the deck (see Figures 6-9c and 6-9d) are well below the yield strength of steel and accordingly neither blast analysis nor ALP cable loss analysis showed formation of any plastic hinges within the deck. Moreover, both analyses affected the tower drift and maximum equivalent stress σ_{eqv} at the bottom insignificantly, even with blast is occurring near the tower.

Cables

Comparison of cable stresses captured by two different methods, i.e. ALP and direct blast analysis is carried out for cables on left and right side of the deck. The cable stress envelops are shown in Figure 6-10 (side-a where blast occurred, see Figure 6-4c) and Figure 6-11 (side-b), respectively. It is observed that no cable exceeded the breakage stress and the maximum stress ratio was about 57% during Scenario: 27t_5m. In cables 10-20 and 40-50, the stresses obtained from the direct blast analysis are considerably higher than the results predicted by the ALP cable loss analysis. It can be concluded that the stress in these short cables is sensitive to the adopted choice of analysis.

Table 6-4 Summary of maximum deflection, stresses for deck and tower obtained from explicit analysis (blast loading analysis) and implicit analysis (loss of cable analysis)

Cable loss	**Scenarios**	**Deck**			**Tower**	
		$\delta_{y\text{-max}}$	$\sigma_{xx\text{-top}}$	$\sigma_{xx\text{-bot}}$	$\delta_{x\text{-max}}$	σ_{eqv}
1a	Scenario:4.5t_2.5m	-0.769	362.4	446.4	0.407	128.76
	Scenario: 1a loss-ANSYS	-0.876	323.2	337.4	0.438	119.68
2a	Scenario:4.5t_5.0m	-0.695	419.2	334.3	0.396	125.86
	Scenario: 2a loss-ANSYS	-0.783	321.3	332.2	0.417	116.29
1a & 2a	Scenario:27t_2.5m	-1.240	346.0	453.6	0.492	146.19
	Scenario: 1a&2a loss-ANSYS	-1.381	349.1	363.3	0.533	135.41
1a, 2a & 3a	Scenario:27t_5.0m	-1.730	392.7	411.4	0.646	153.87
	Scenario:27t_7.5m	-1.770	419.3	459.2	0.656	153.88
	Scenario: 1a, 2a&3a loss-ANSYS	-1.902	379.1	365.6	0.654	148.95
30a	Scenario:27t_525m	-0.589	277.6	313.1	0.371	124.60
	Scenario: 30a loss-ANSYS	-0.756	305.0	290.7	0.414	125.35
15a	Scenario:27t_225m	0.389	337.1	352.6	0.371	124.60
	Scenario: 15a loss-ANSYS	-0.473	297.2	273.4	0.349	104.95

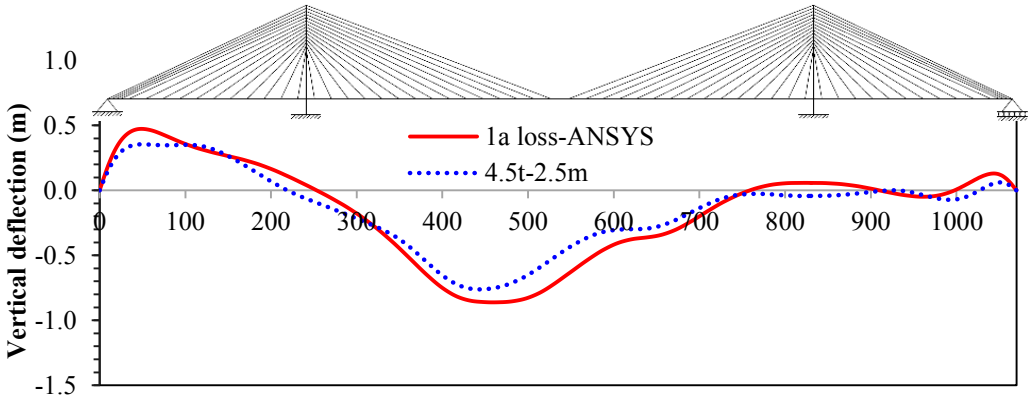

(a) 1 cable loss (1a)

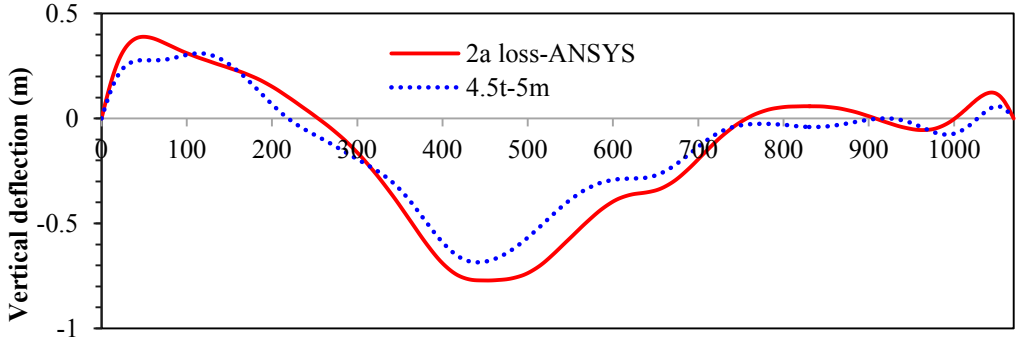

(b) 1 cable loss (2a)

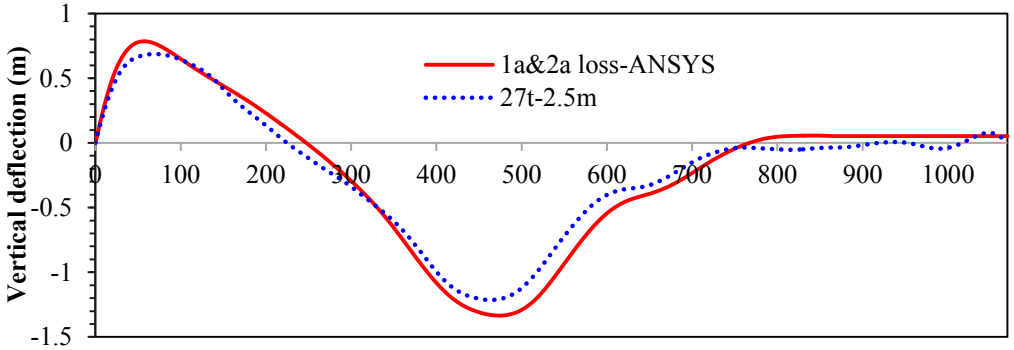

(c) 2 cable loss (1a and 2a)

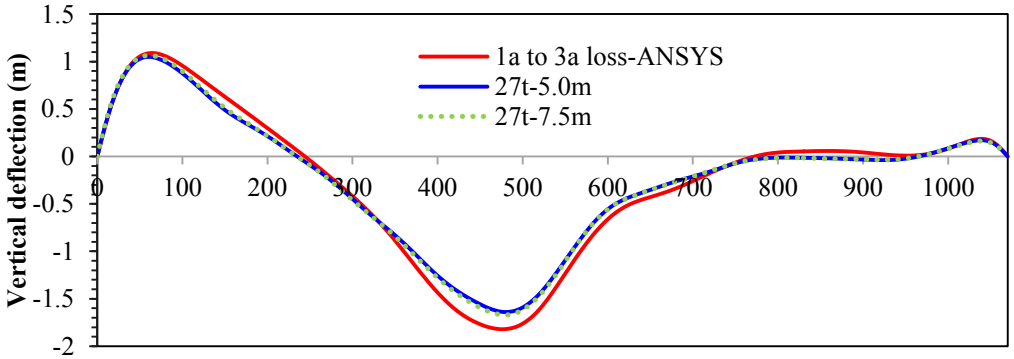

(d) 3 cable loss (1a-3a)

Figure 6-7 vertical displacements along the deck for scenarios with 1, 2 and 3 cable losses.

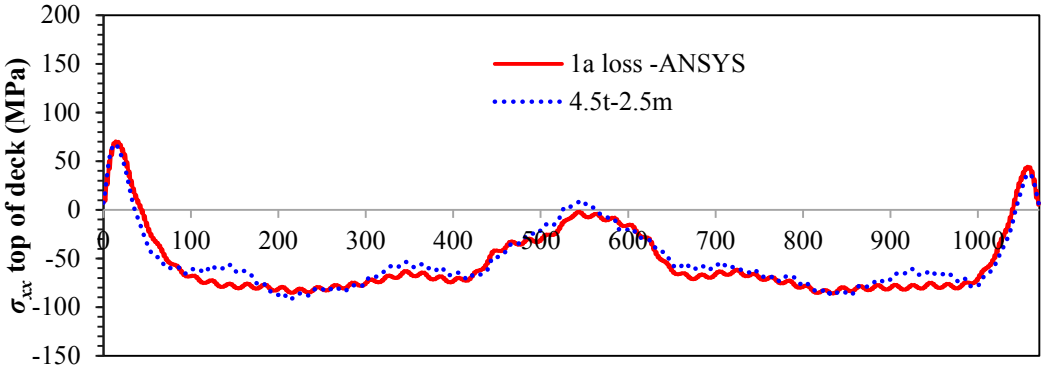

(a) 1 cables loss (1a)

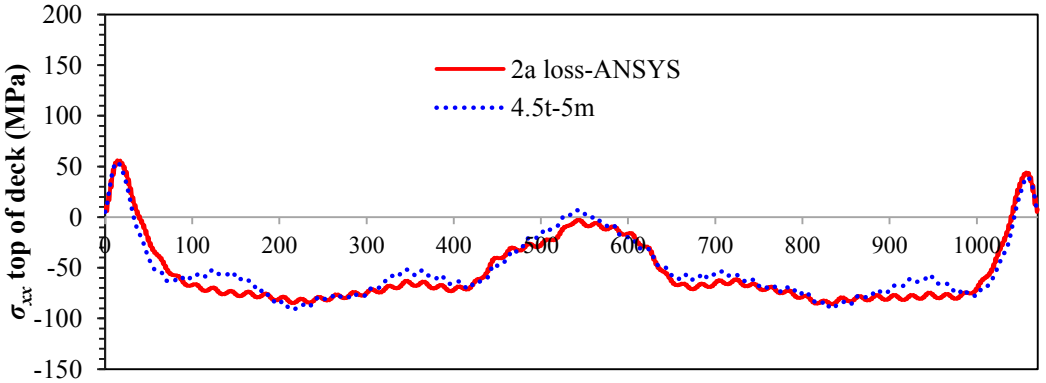

(b) 1 cable loss (2a)

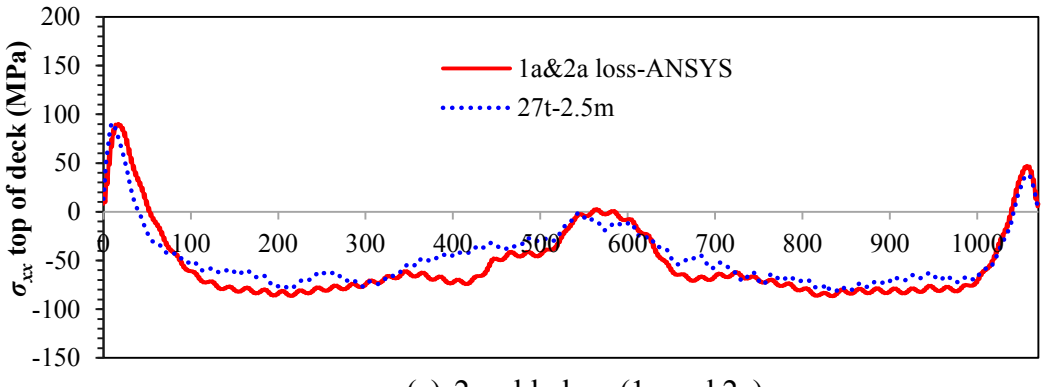

(c) 2 cable loss (1a and 2a)

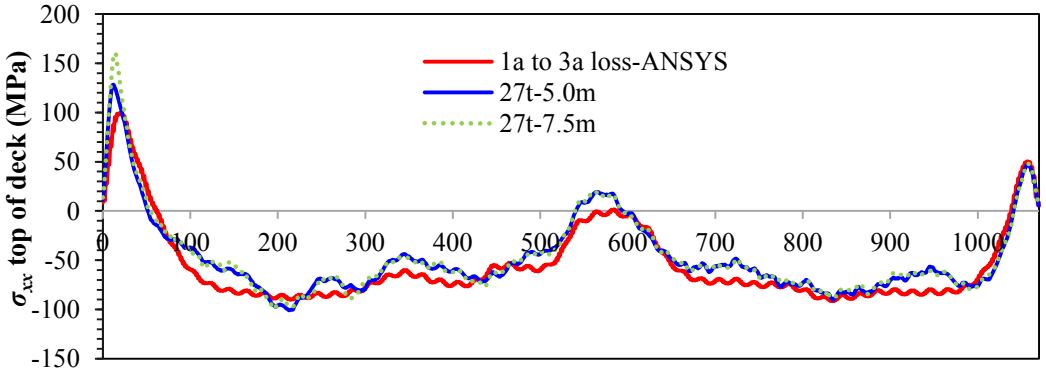

(d) 3 cables losses (1a, 2a and 3a)

Figure 6-8 σ_{xx} stress component on top surface of the deck for scenarios with 1, 2 and 3 cable losses.

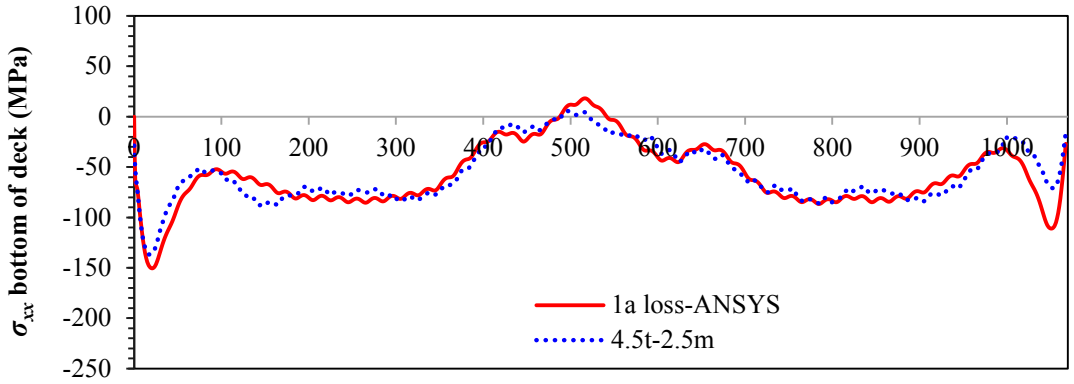

(a) 1 cables loss (1a)

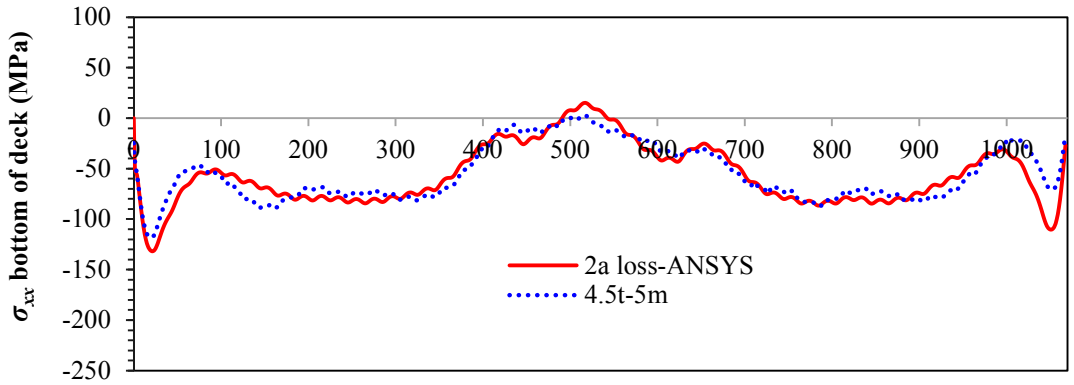

(b) 1 cable loss (2a)

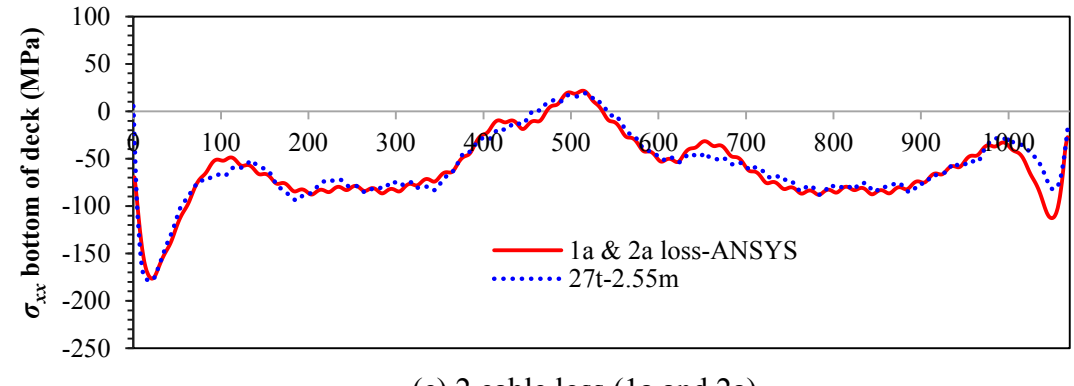

(c) 2 cable loss (1a and 2a)

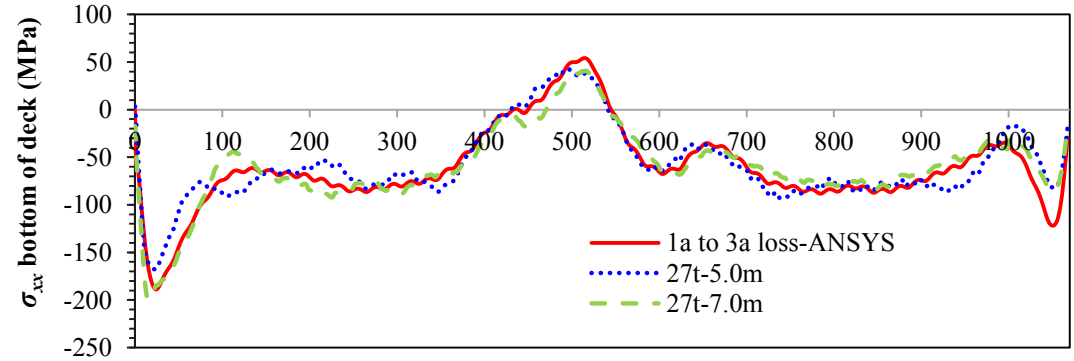

(d) 3 cable loss (1a, 2a and 3a)

Figure 6-9 σ_{xx} stress component on bottom surface of the deck for scenarios with 1, 2 and 3 cable losses.

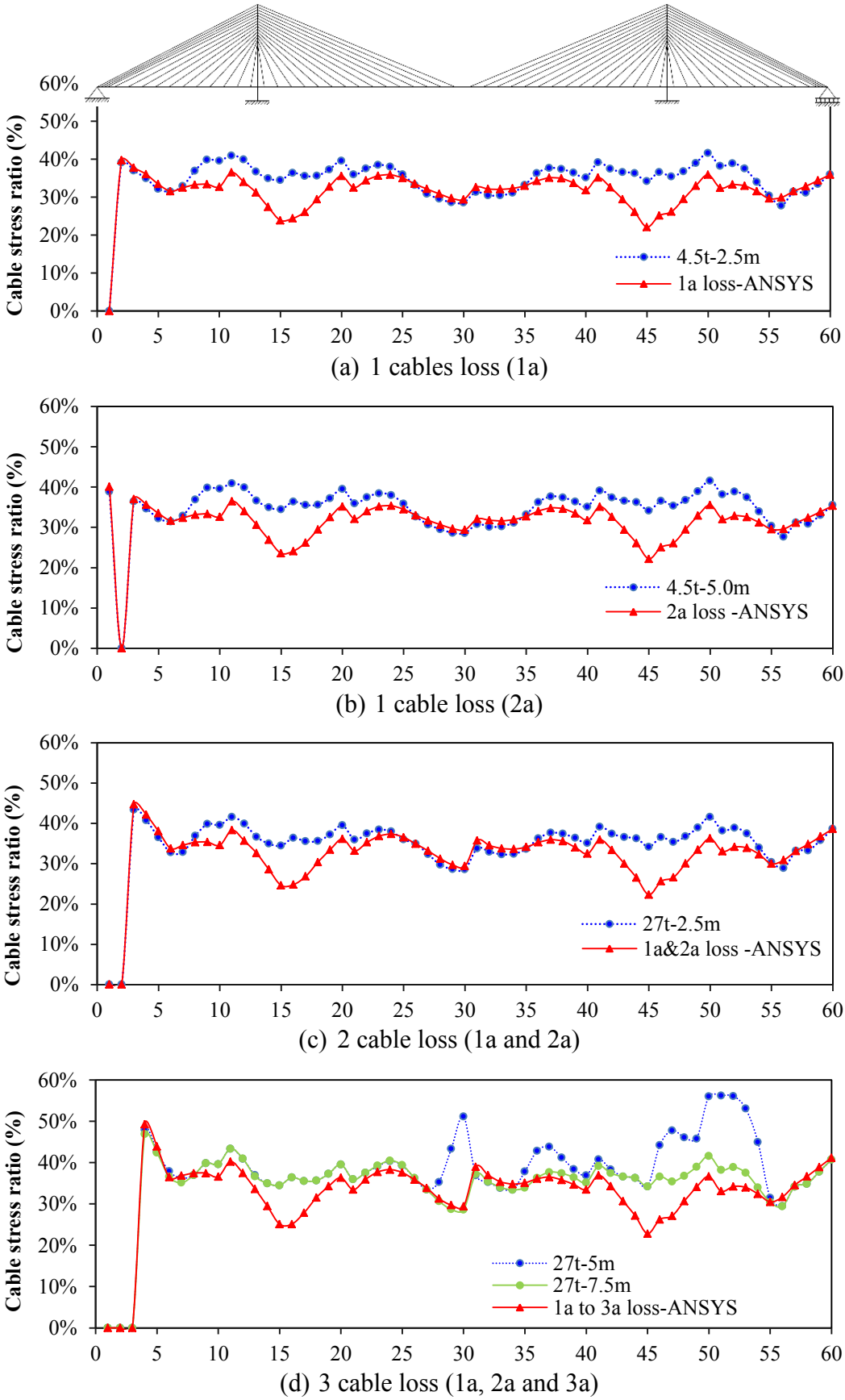

Figure 6-10 Envelop of the maximum tensile stress over breakage stress in the cables "a" (z=9.6).

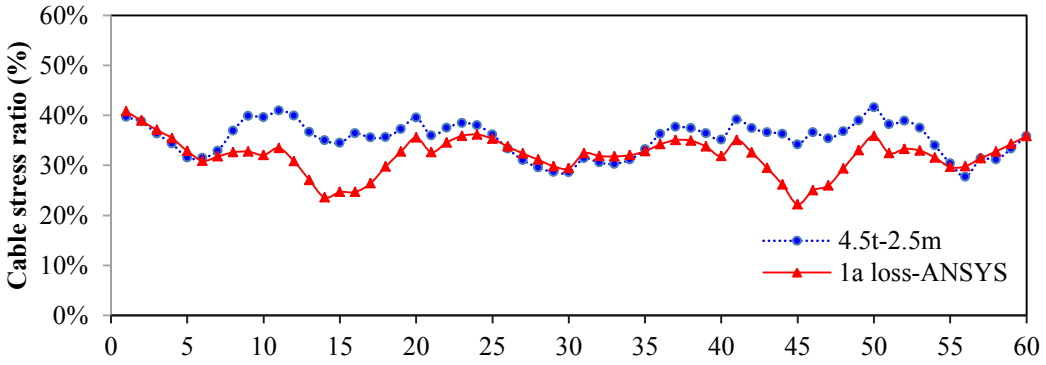

(a) 1 cables loss (1a)

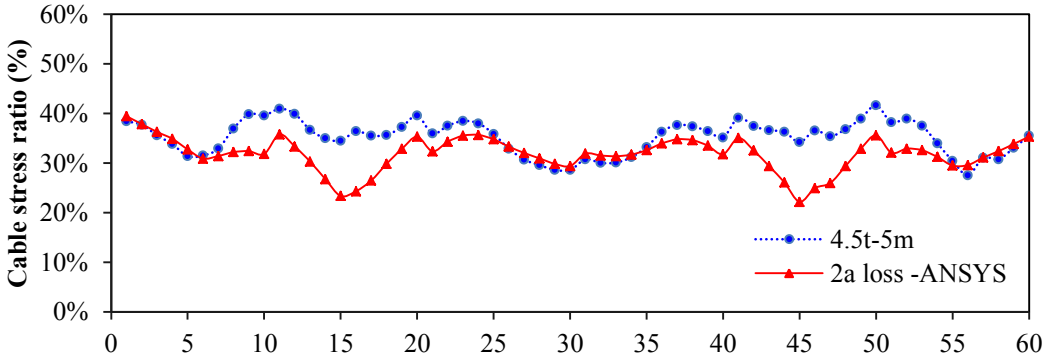

(b) 1 cable loss (2a)

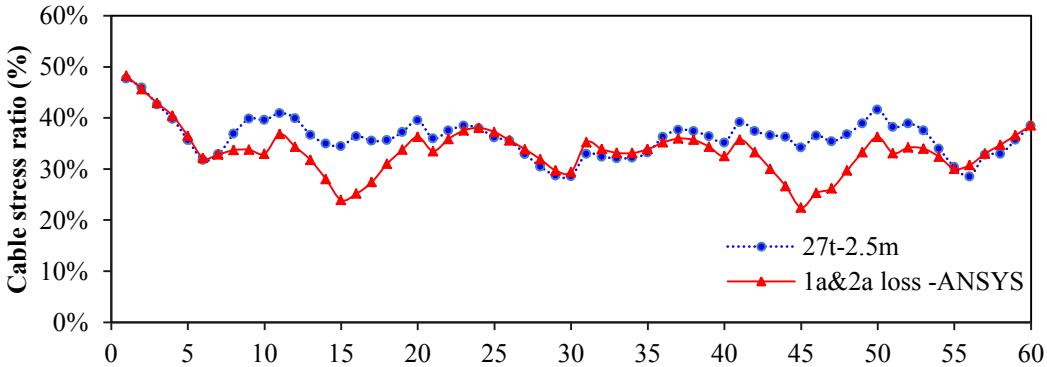

(c) 2 cable losses (1a and 2a)

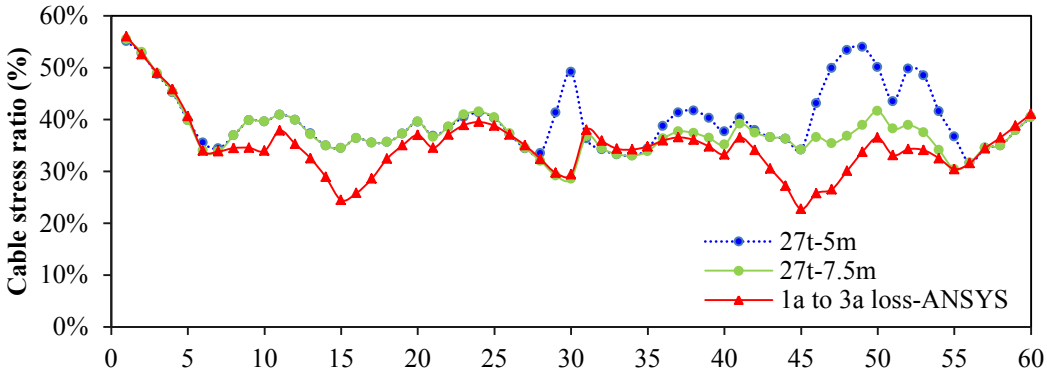

(d) 3 cable losses (1a, 2a and 3a)

Figure 6-11 Envelop of the maximum tensile stress over breakage stress in the cables "b" (z= - 9.6).

6.4.3 Comparative study between blast load and simple cable loss according to ALP (blast near tower and mid-span)

In this section, Scenario: 27t_525m (explosion in the vicinity of cable no. 30a) is compared with 30a_loss _ANSYS as one of the scenarios in which blast occurs around the mid-span. Furthermore, Scenario: 27t_225m (explosion in the vicinity of cable 15a) is compared with 15a_loss _ANSYS as one of the scenarios in which blast occurs around the tower, respectively.

Deck and Tower

Table 6-4 summarised the maximum deflection in the deck and lateral drift on top of the tower as well as the maximum σ_{xx} stress component on top and bottom surface of the deck and σ_{eqv} on the bottom of tower for all scenarios. Furthermore, deflected configurations of the deck when maximum vertical displacement has occurred, and average σ_{xx} stress component on the top and bottom surfaces of deck (when maximum stress has occurred) for blast scenarios with loss of one cable at mid-span and adjacent to tower are shown in Figures 6-12 (loss of 30a) and Figure 6-13 (loss of 15a), respectively. Overall, the ALP cable loss analysis has predicted the response of bridge with accuracy comparable with direct blast analysis. However, the localised large stresses occurred within the area directly affected by air blast cannot be adequately captured by the simplistic approach adopted in the alternate load path (ALP) method. For example, when the detonation centre was near the tower, the direct blast load analysis predicted σ_{xx} stress component on top surface of the deck which is twice as large the σ_{xx} predicted by ALP method (Figure 6-13b). The blast scenarios near mid-span and tower did not trigger the progressive collapse of the entire bridge according to ALP method as well as direct blast analysis.

Cable

The cable stresses for scenarios in which cable 30a and cable 15a are lost is presented in Figure 6-14 and the results are similar to the other scenarios in that no cable exceeded the breakage stress. Furthermore, cable stresses obtained from blast analysis for short cables (cable numbers between 10-20 and 40-50) are considerably larger than the results predicted by ALP cable loss analysis.

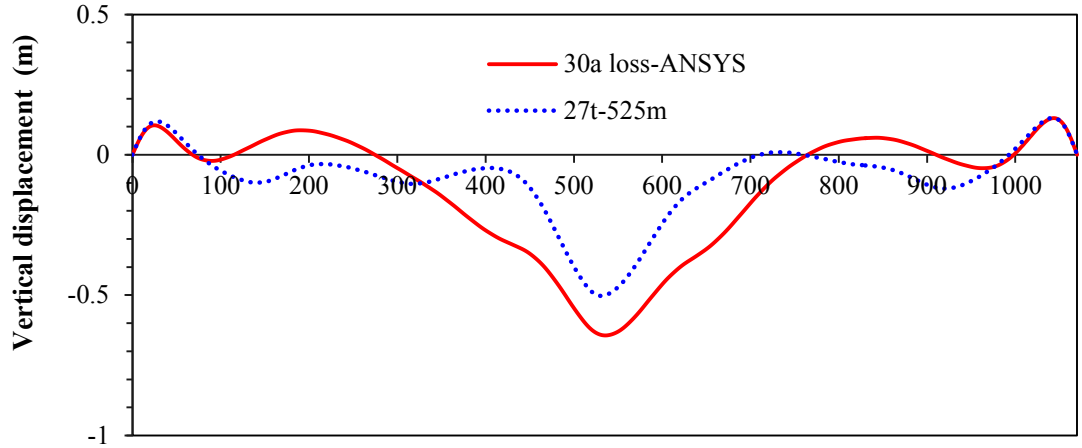

(a)

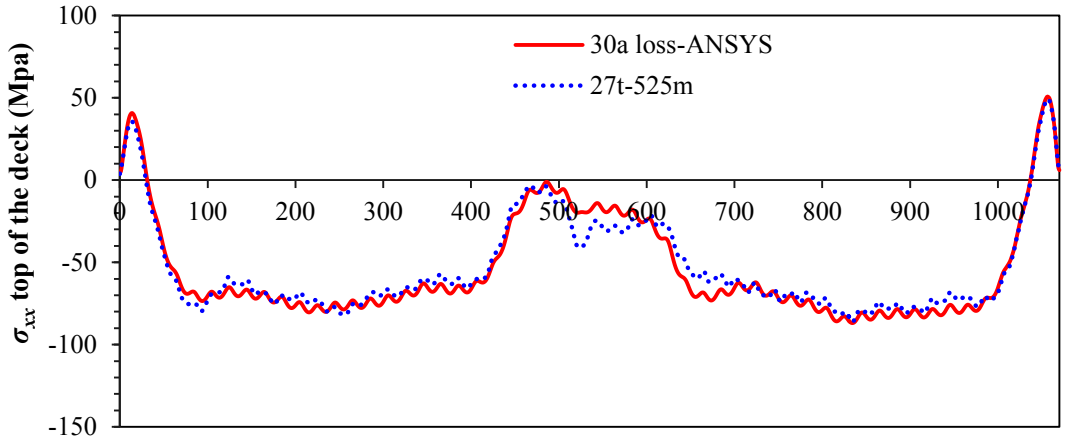

(b)

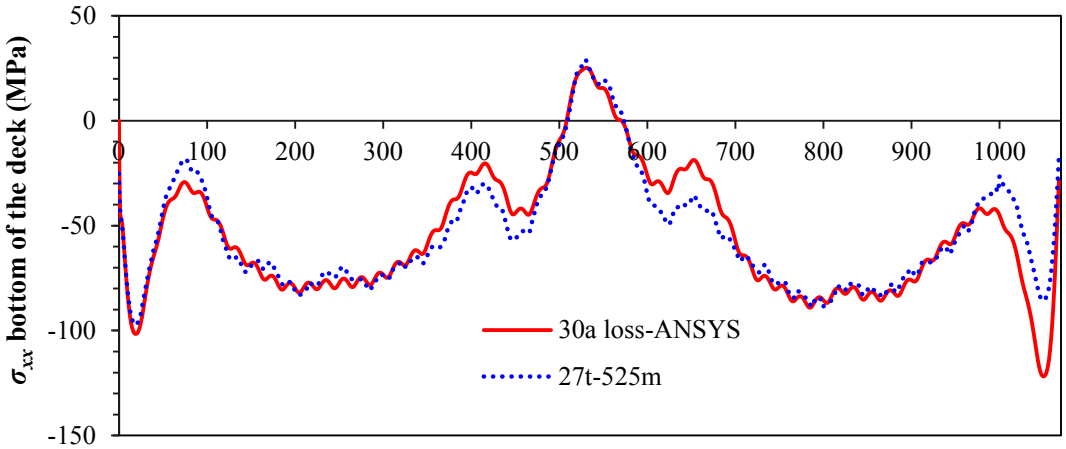

(c)

Figure 6-12 Maximum of (a) vertical deflection (b) σ_{xx} on top of the deck and (c) σ_{xx} on bottom of the deck (loss of cable 30a).

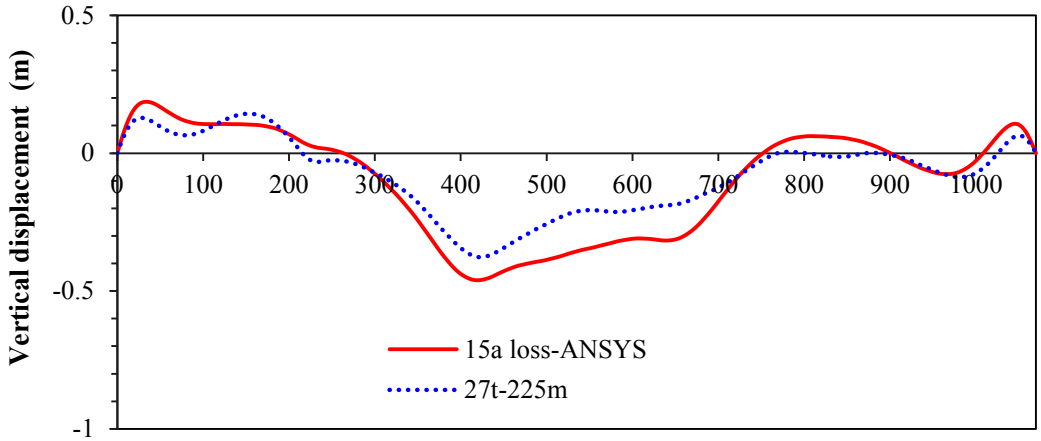

(a)

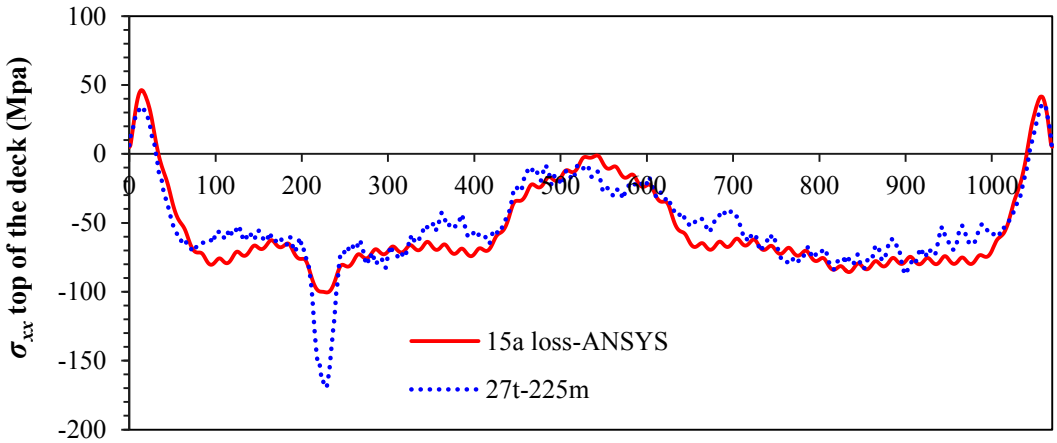

(b)

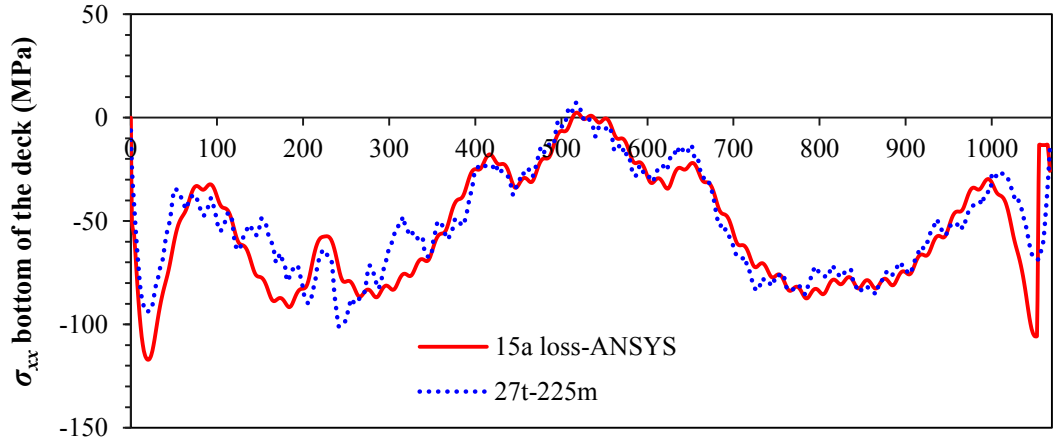

(c)

Figure 6-13 Maximum of (a) vertical deflection (b) σ_{xx} on top of the deck and (c) σ_{xx} on bottom of the deck (loss of cable 15a).

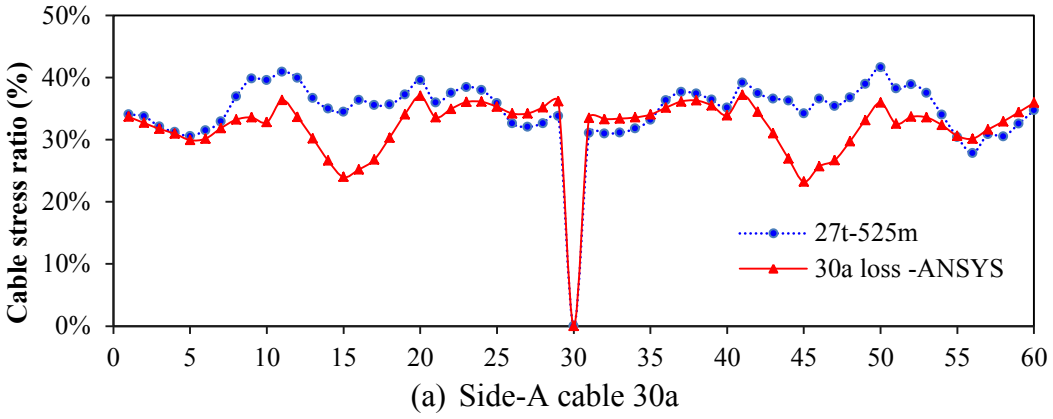

(a) Side-A cable 30a

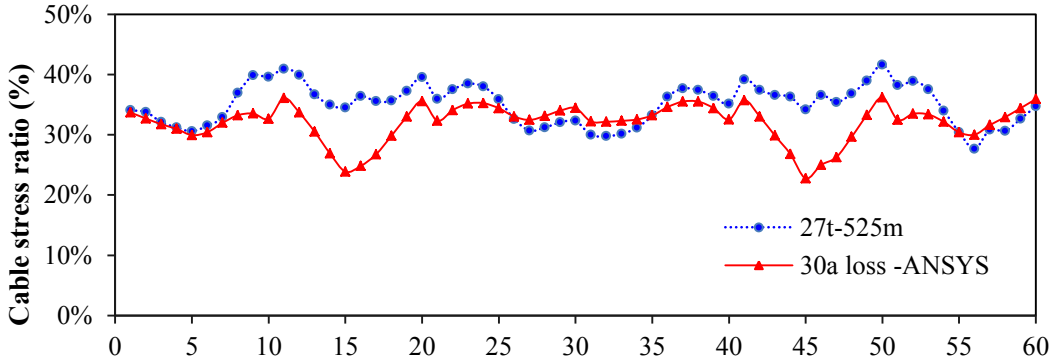

(b) Side-B cable 30a

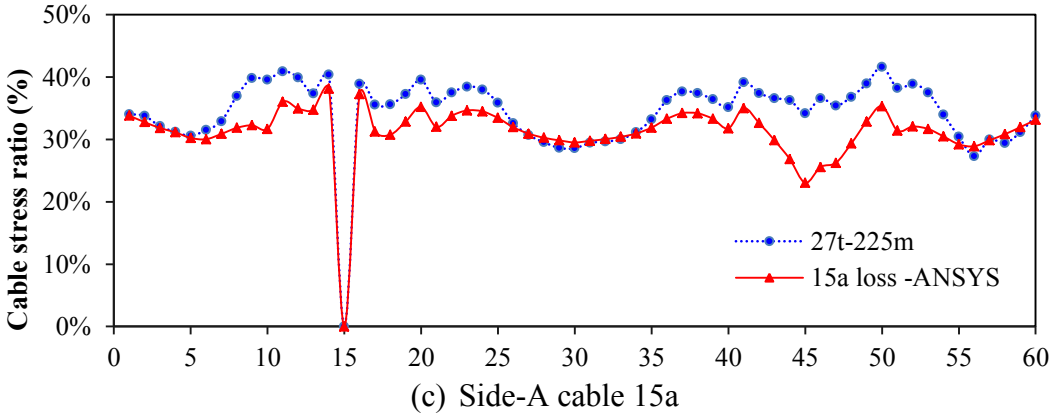

(c) Side-A cable 15a

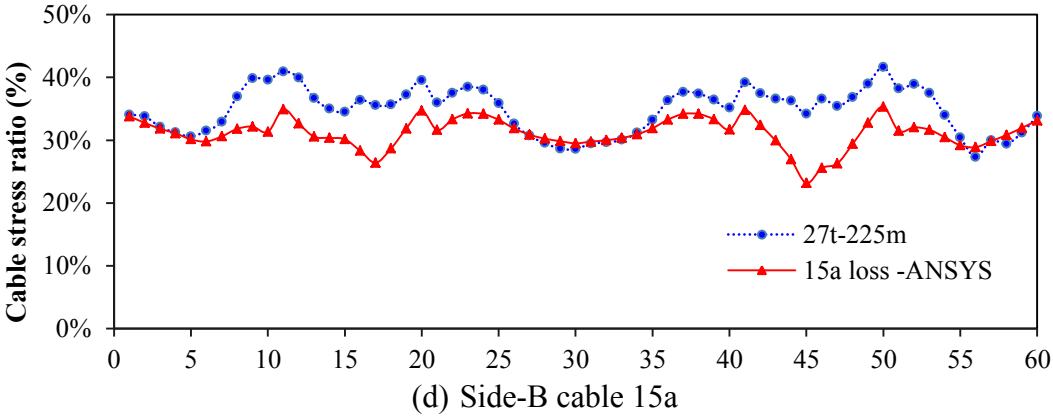

(d) Side-B cable 15a

Figure 6-14 Cable stress ratio (loss of cables 30a/15a).

6.5 Conclusions

A numerical study of the idealised cable-stayed bridge model subjected to blast loadings was carried out in this chapter. Also, the results obtained from the blast analysis were compared with the alternate load path (ALP) cable loss analyses. A comprehensive parametric study was undertaken and the importance of using a particular model under several blast loadings as well as sudden loss of cable(s) with non-linear effects was investigated. With regard to the numerical studies undertaken this chapter, the following conclusions may be drawn;

- For the bridge under consideration, 1 tonne of TNT equivalent explosive did not lead to any loss of cables, whereas detonation of 27 tonnes of TNT equivalent explosive near the end pin support led to loss of three cables.

- Cable(s) were lost due to damage at the anchorage zone rather than the damage of the cables themselves.

- The dynamic response of the entire cable stayed bridge following loss of the cables due to blast load can be adequately predicted by alternate load path (ALP) method regardless of the number of lost cables. The average difference between the results obtained from the direct blast and ALP cable loss analysis is around 15% to 25% depending on the location and type of structural components. However, the localised high stresses and deflections within the zone directly affected by the air blast cannot be adequately predicted by the ALP approach. This can be a critical factor when highly localised stresses lead to failure of a structural component that in turn will trigger the progressive collapse of the entire bridge.

- The response of the short cables adjacent to towers is sensitive to the choice of analysis. The stresses in short cables were significantly increased following blast loading scenarios, however, the stresses in short cables did not considerably change following different cable loss scenarios.

- For all scenarios, the σ_{xx} and σ_{eqv} at different components (i.e. deck and tower) captured by direct blast analysis and ALP cable loss were well below the yield

strength of steel and accordingly no plastic hinge formed within the deck and tower. Furthermore, loss of up to three cables (either by direct blast analysis or simple cable removal according to ALP procedure) did not trigger progressive collapse of the entire bridge.

Chapter 7 : Dynamic Response of a Cable-Stayed Bridge Subjected to Seismic Loading

Summary of chapter

Large seismic actions have caused severe damage including progressive collapse of bridge structures in the past, and are now recognised as one of the most important extreme loading cases that should be considered in bridge design. In this chapter, a detailed 3D nonlinear finite element model of a hypothetical cable-stayed bridge is developed and analysed. The developed FE models can take account of material and geometrical nonlinearities. A parametric study is undertaken and the effects of seismic loading scenarios (i.e. different types of earthquake acceleration in terms of frequency content and amplitude as well as direction) on the local as well as global and potential progressive collapse response of the bridge are investigated. For the bridge studied in this chapter, it is shown that the near field earthquakes applied along the bridge length have the most influence on the deck and cables. Moreover, LS-DYNA FE model and explicit solver are employed to analysis and capture the possible failure mode of the cable stayed bridge subjected to severe earthquake action along the bridge deck. It is shown that the failure mode of the cable stayed bridge under consideration is associated with development of high plastic strains around the pin support and this is consistent with the observed failure mode of real cable stayed bridges during past seismic actions.

7.1 Introduction

As discussed in Section 2-5 of Chapter 2, some bridges were damaged or even fully collapsed by severe past earthquakes. To prevent the catastrophic failure of bridges subject to earthquake actions, the existing design codes place particular emphasis on seismic design of bridges and also many studies have resorted to advanced computer-based simulations to provide a better understanding about the behaviour of bridges under earthquake attack.

With regard to high cost of undertaking field or lab test, one of the options for structural assessment of large scale bridges is to use advanced computer simulations (e.g. finite element models) that can properly capture the local and global response of the structure including material and geometrical nonlinearities.

In this chapter, using ANSYS package (ANSYS® 2009) as well as LS-DYNA (LSTC 2007), 3D FE models of the bridge are developed and analysed under gravity loads, traffic load and different seismic ground acceleration scenarios. Using the developed FE models, a comprehensive parametric study is carried out and structural response of the bridge under different peak ground accelerations and direction of earthquake attack is studied. Furthermore, the results obtained from a fully nonlinear 3D FE model are employed to identify the critical earthquake acceleration and direction range for each one of the structural components (i.e. deck, towers, cables and base shear).

With regard to lack of experimental data on cable-stayed bridge models, the preparations for future experimental works on a 1/60 scale cable-stayed bridge are presented in the final section of this chapter. The experimental work of this study follows previous shake table test of a 1/120 scale pre-stressed concrete cable stayed bridge model undertaken by Shoji et. al (2008).

7.2 Adopted assumptions

The adopted assumptions including bridge geometry and configuration, material properties including yield and ultimate strength of steel and ultimate strength of cable, 3D finite element (FE) models developed in ANSYS and LS-DYNA, analysis methods and design loads in this chapter are the same as those in Chapter 6, Sections 6.2.

To start the seismic analysis of the cable stayed bridge, an eigenvalue analysis was carried out and the frequency, period and mode shape of the first fifteen natural modes of vibration were extracted from the results of this eigenvalue analysis. The first six mode shapes of the bridge obtained from eigenvalue analysis of the 3D-implicit FE model developed in ANSYS software is shown in Figure 7-1. Furthermore, the natural frequency and period of the first fifteen modes of vibration are given in Table 7-1.

7.3 Seismic analysis scenarios

7.3.1 Seismic analysis method

Transient (time-history) analysis of the bridge was carried out using a direct time integration to determine the dynamic responses of the bridge model subjected to seismic loads. For the dynamic time marching, two different integration methods were used; i.e. Newmark constant acceleration method was used in conjunction with ANSYS implicit solver (ANSYS, 2009) and a central difference scheme was used in conjunction with LS-DYNA explicit solver (LSTC, 2007; Paz 2004). In both implicit and explicit models, a consistent mass matrix with proportional damping was adopted. In ANSYS software, "ACEL" command, which specifies the linear acceleration in the global Cartesian, x, y, and z coordinates, was used for applying the seismic load. Using this command, the same seismic acceleration was applied on all elements at the same time. In LS-DYNA program, "LOAD_BODY_option" code with a feature similar to "ACEL" commands of ANSYS was employed for applying the seismic action (ground acceleration); The "LOAD_BODY_option" can be used to activate the mass of the structure in conjunction with prescribed base accelerations in a Cartesian coordinate system.

Table 7-1 The natural frequency and period of the first fifteen modes of vibration.

Mode No.	Frequency (Hz)	Vibration Period (sec)
1	0.055	18.2
2	0.172	5.81
3	0.237	4.22
4	0.285	3.51
5	0.342	2.92
6	0.458	2.18
7	0.505	1.98
8	0.532	1.88
9	0.582	1.72
10	0.616	1.62
11	0.651	1.54
12	0.716	1.40
13	0.721	1.39
14	0.722	1.39
15	0.731	1.37

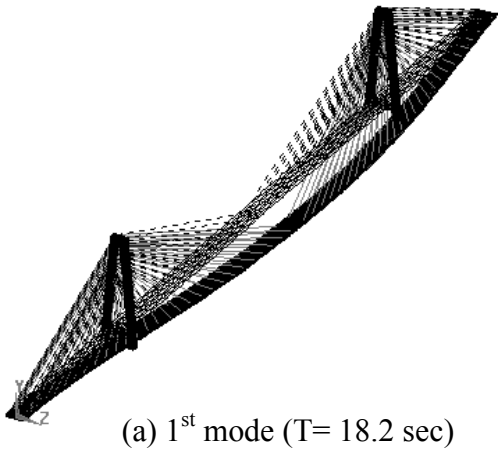

(a) 1st mode (T= 18.2 sec)

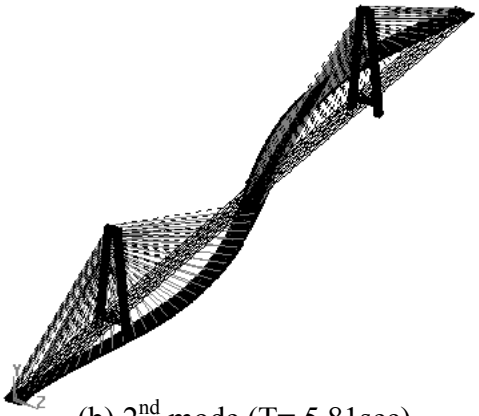

(b) 2nd mode (T= 5.81sec)

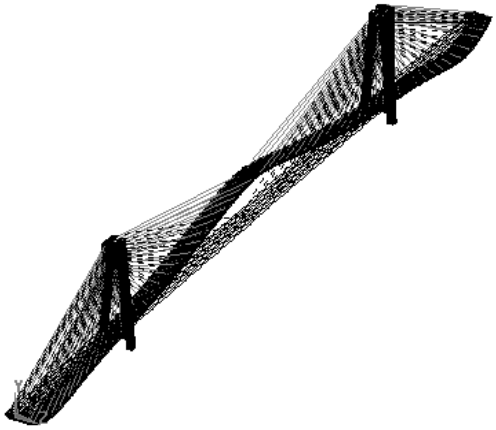

(c) 3rd mode (T=4.22 sec)

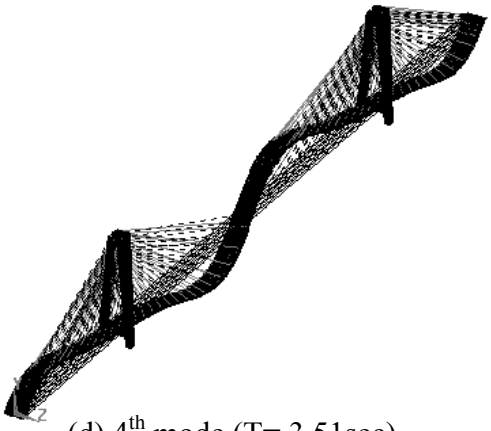

(d) 4th mode (T= 3.51sec)

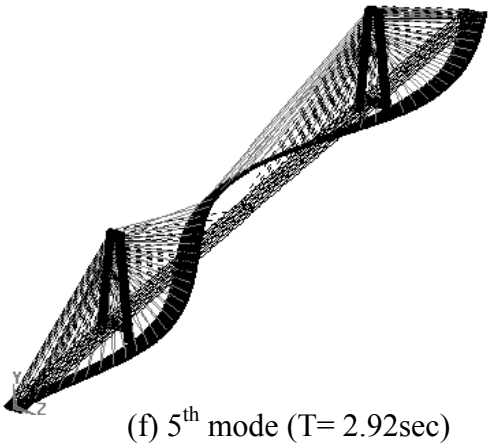

(f) 5th mode (T= 2.92sec)

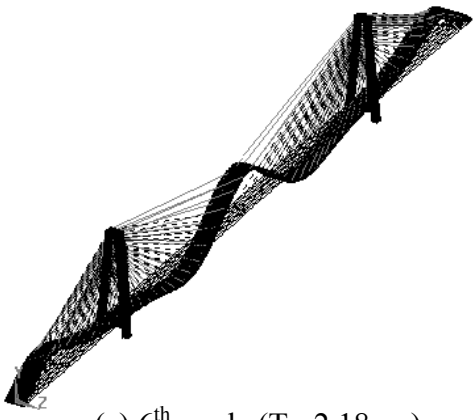

(e) 6th mode (T= 2.18sec)

Figure 7-1 The natural period and mode shapes for the first 6 natural modes of vibration.

7.3.2 Scenario considered for Earthquake load analysis

For seismic analysis, the distributed component of the traffic load as well as the dead load is applied along the entire bridge deck. The adopted load factors for dead, live and earthquake actions (loads) are as specified by AASHTO LRFD bridge design code and also reported in NCHRP (2003),

$$1.25DC + 0.25LL + 1.0EQ \quad (1)$$

where, DC is the permanent action (dead load) including self-weight of structural components and non-structural attachments, LL is the full vehicular live load placed in actual stripped lanes and EQ is the earthquake load. In this study, the wearing surface is assumed to be a 200 mm thick layer of asphalt concrete (γ=24.5 kN/m^3) which is considered as part of permanent action (dead load).

According to AS5100.2 (2004), for the loading scenarios in which more than one lane is subjected to traffic loads, the traffic loads should be multiplied by an accompanying lane factor (1.0 for first lane, 0.8 for second lane and 0.4 for third and subsequent lanes). In this chapter, the traffic loading pattern and accompanying lane factor are as specified in Figure 5-2b in Chapter 5.

7.3.3 Earthquake acceleration data

Both near-field and far-field earthquake records were used in this analysis; namely Kobe (Japan, 1995) and El-Centro (USA, 1940). Time-histories of ground accelerations, as well as acceleration response spectra for both earthquakes are shown in Figure 7-2a and 7-2b, respectively. In Figure 7-2a, Kobe record shows jerky high peak accelerations of over 8 m/s^2. This pulse-like ground motions normally create significant damage to the structures, including bridge structures (Liel, 2012, Moustafa and Takewaki, 2010, Jia and Ou, 2008). On the other hand, the frequency content of the El-Centro ground acceleration spreads over a wide range with less fluctuation. With regard to acceleration response spectra given in Figure 7-2b, it is concluded that the dominant frequency range possessing much of the seismic energy for Kobe earthquake is in the range between 0.5 to 3.5 Hz, whereas for El-Centro earthquake the range of dominant frequency content is between 0.5 to 7.5 Hz.

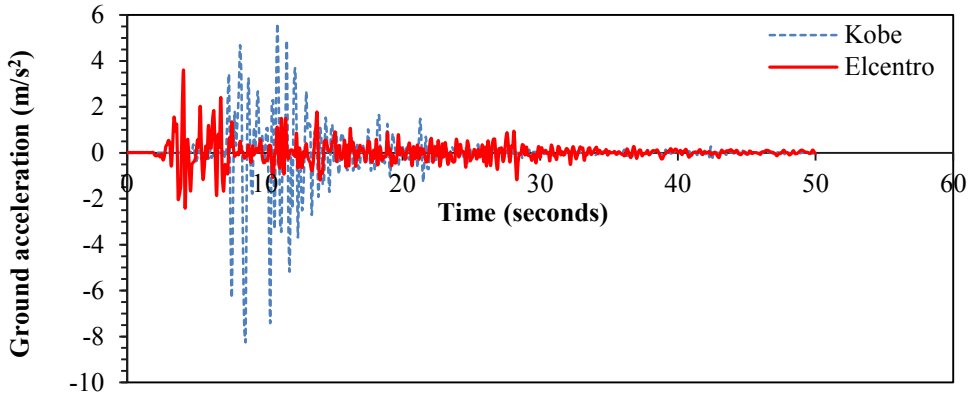

(a)

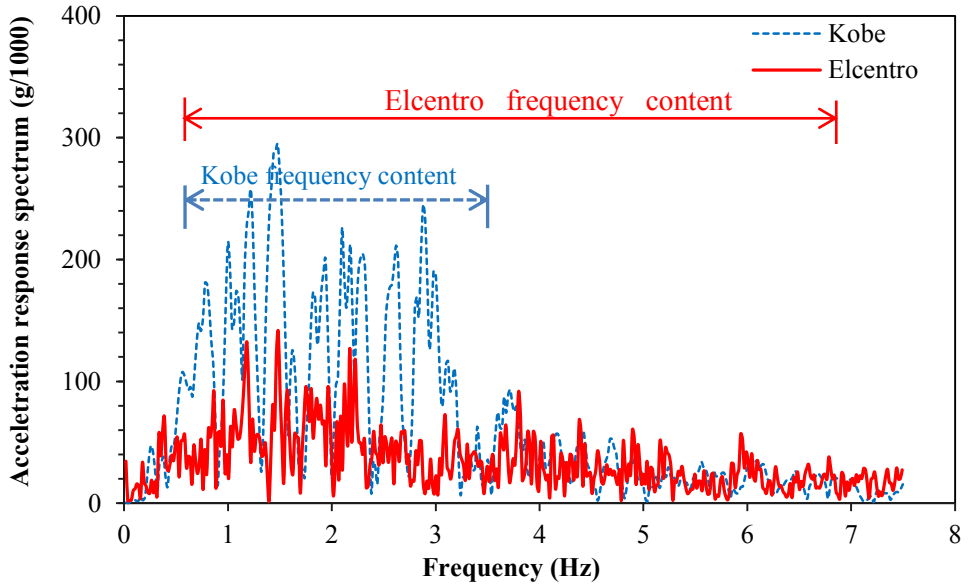

(b)

Figure 7-2 (a) ground acceleration time history (b) acceleration response spectrum.

7.3.4 Scenarios considered

A total of nine different seismic loading scenarios were considered in this study as summarised in Table 7-2. In the first five scenarios, i.e. Scenario-K1 to scenario-K5 Kobe earthquake ground acceleration is applied on the bridge and in the last four scenarios, i.e. scenario E1 to E4, the El-Centro earthquake is considered. In terms of magnitude and direction of ground acceleration, scenarios K1 and K5 are the same and the difference between these two scenarios is only related to the type of FE solver that will be explained later (see Table 7-2).The ground accelerations are applied horizontally to the bridge in different directions, i.e. along the deck (x-direction), perpendicular to the bridge deck (z-direction), 30 and 60 degrees between the x and z axes.

Table 7-2 Scenarios considered for applying seismic action.

Scenario No.	Name of earthquake	EQ Direction	FE method
Scenario-K1	Kobe	x	Implicit
Scenario-K2		z	Implicit
Scenario-K3		30° xz	Implicit
Scenario-K4		60° xz	Implicit
Scenario-K5		x	Explicit
Scenario-E1	El-Centro	x	Implicit
Scenario-E2		z	Implicit
Scenario-E3		30° xz	Implicit
Scenario-E4		60° xz	Implicit

7.4 Results and discussion

In this section, the analysis results produced by ANSYSS implicit model for Scenarios K2 to K4 and E1 to E4 are presented and discussed. The ANSNS implicit dynamic model stopped after 9.8 seconds into the Kobe earthquake applied along the bridge deck (Scenario-K1). A closer look to the ANSYS FE results showed large plastic strains in conjunction with large displacements occurring around the pin support that led to ill conditioning and subsequently lack of convergence in ANSYS implicit model. Accordingly, scenario K1 and the cause of convergence problem in ANSYS implicit model are discussed in details and the results of scenario K5 obtained from LS-DYNA explicit model are presented.

7.4.1 Results of implicit analysis (ANSYS model)

Deck and tower

Table 7-3 summarises the maximum deflections, maximum nodal σ_{xx} stresses on the deck and drift on top and σ_{eqv} stress at the bottom of the right tower occurring during each earthquake as well as the corresponding values for the healthy bridge (Scenario-SH) in the absence of seismic loads and only under gravity loads. Also, the deflected configurations (elastic curve) of the deck at the instant of maximum vertical displacement for all seismic load scenarios are shown in Figure 7-3. It is observed that scenario K3 can create significant hogging deflection (1.52 m uplift) in the back span at x= 150 m. Furthermore, it is seen that the major longitudinal flexural stresses along the deck (see Table 7-3) exceed the yield strength of steel (450MPa) in scenario-K series.

Accordingly, σ_{xx} stresses on top and bottom surface of the deck in scenario-K3 (most critical) are plotted in Figure 7-4. The zone in which the stress σ_{xx} exceeding the yield stress is quite localised and only limited to close proximity of the pin-support.

Table 7-3 Summary of the maximum vertical deflections, drift on top of right tower and σ_{xx} stresses within the deck obtained from implicit 3D ANSYS FE models.

	Deck			Tower		
	δ_{v+} (m)	δ_{v-} (m)	σ_{xx} (MPa)	δ_{topx} (m)	δ_{topz} (m)	$\sigma_{bot\ eqv}$ (MPa)
Scenario-SH#	0.22	-0.37	317.7 (C)	-0.33	0.00	91.6
Scenario-K1						
Scenario-K2	0.33	-0.49	508.9 (T)	-0.37	0.69	198.0
Scenario-K3	1.55	-1.07	558.4 (T)	-1.09	0.34	281.0
Scenario-K4	0.92	-0.73	535.3 (T)	-0.80	0.60	263.3
Scenario-E1	0.47	-0.50	319.3 (C)	-0.49	0.00	135.6
Scenario-E2	0.27	-0.42	436.4 (T)	-0.34	-0.14	115.0
Scenario-E3	0.43	-0.49	425.1 (T)	-0.47	-0.06	138.8
Scenario-E4	0.35	-0.45	467.5 (T)	-0.41	-0.10	130.4

Healthy bridge subject to gravity (dead load including wearing surface + traffic) load.

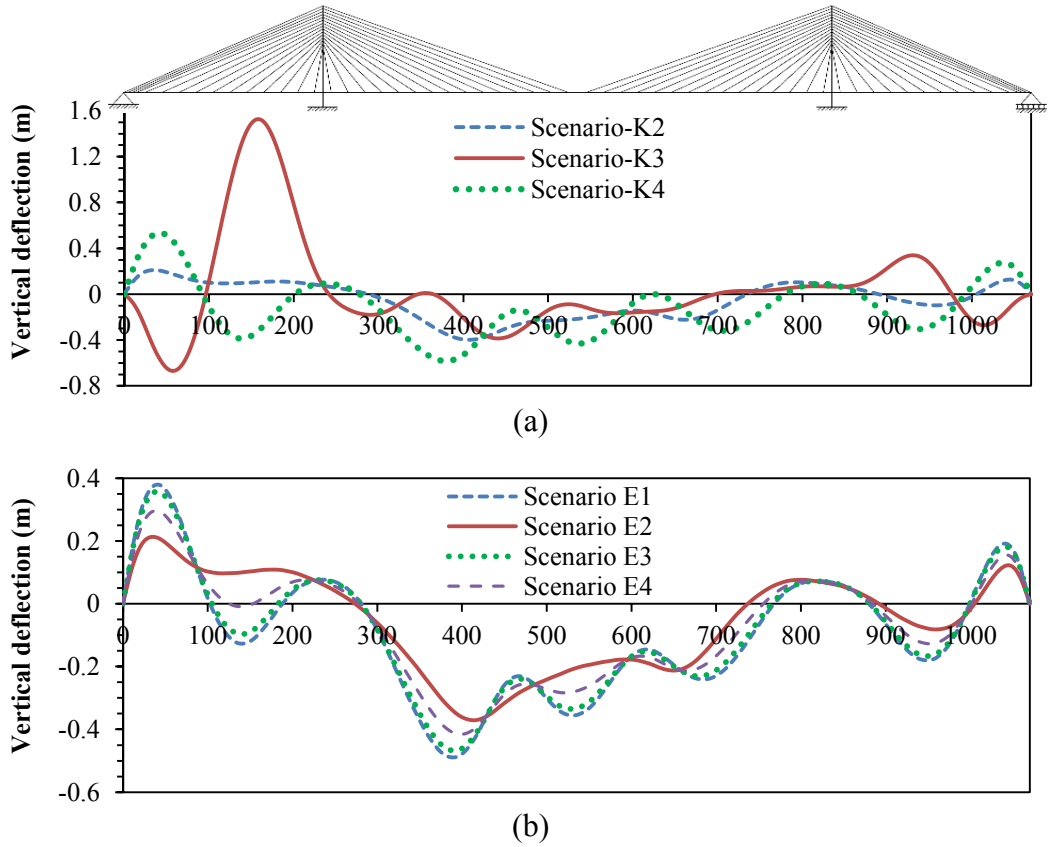

Figure 7-3 Vertical deflection along the deck (a) Scenario K2-K4 (b) Scenario E1-E4.

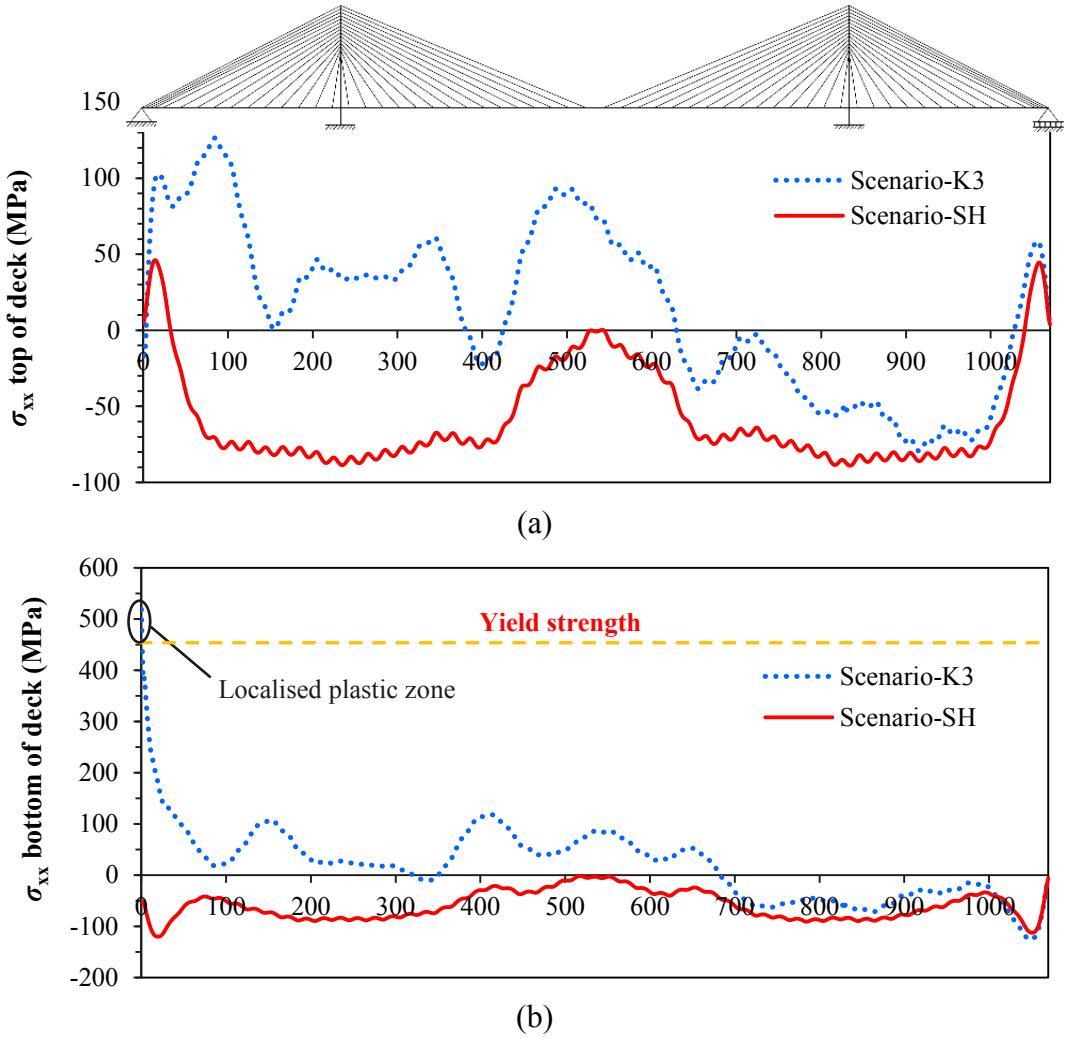

Figure 7-4 σ_{xx} stress component on the (a) top and (b) bottom surface of the deck for scenario-K3 compared with healthy structure

Cables

Envelope of maximum tensile stresses in the cables expressed as a percentage of cable ultimate strength for scenarios K2 to K4 and E1 to E4, as well as the healthy bridge under gravity load (i.e. scenario-SH) are shown in Figure 7-5. It is seen that the maximum tensile stresses in some of the cables during scenario K3 and K4 reached the 80% of cable breakage stress. The critical cables under the Kobe earthquake loading scenarios are amongst the short cables in the vicinity of towers (see Figure 7-5a).

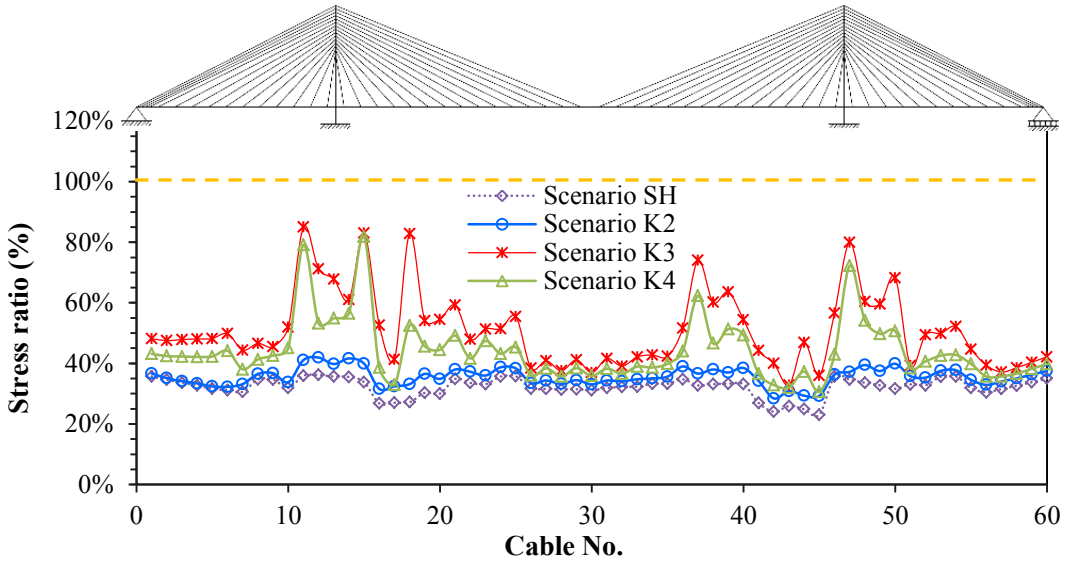

(a)

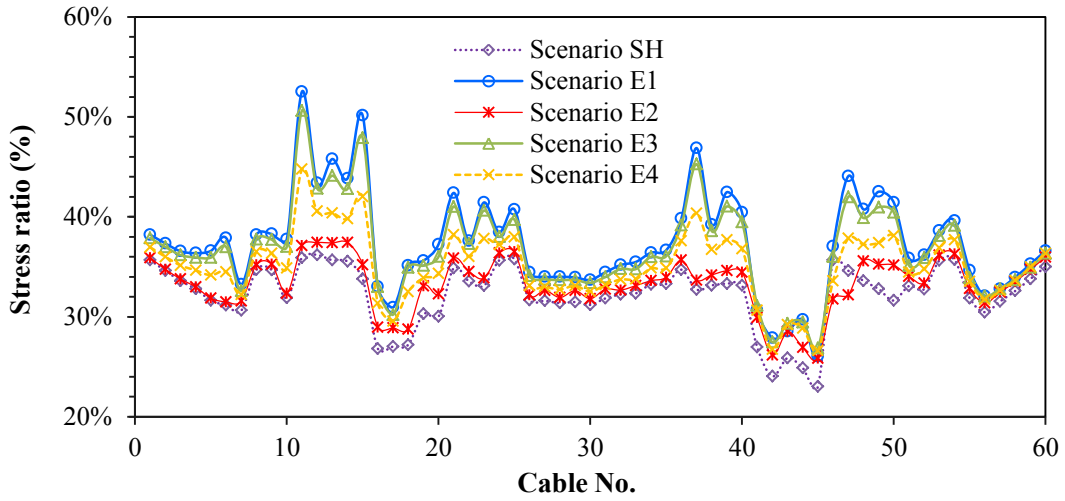

(b)

Figure 7-5 Envelop of the maximum tensile stress over ultimate strength in the cables (a) Scenarios K2-K4 and (b) Scenarios E1-E4.

7.4.2 Progressive collapse analysis – Scenario K1

Deck and tower

The deflected configuration (elastic curve) of the deck at 9.7 sec into seismic loading scenario-K1 (one step just before the occurrence of convergence problem in ANSYS implicit model) and the σ_{xx} stress on top and bottom surface of the deck for Scenario-K1 are shown in Figure 7-6.

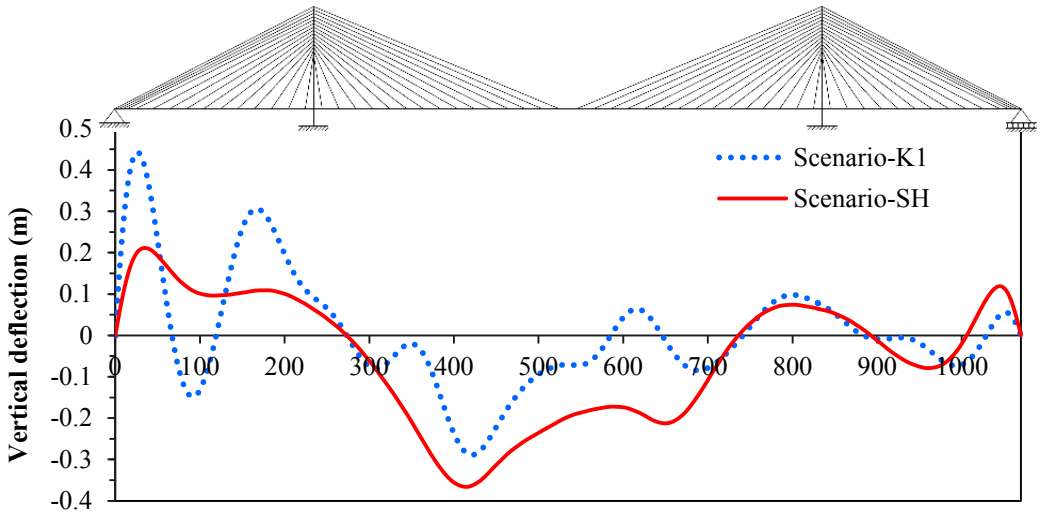

(a)

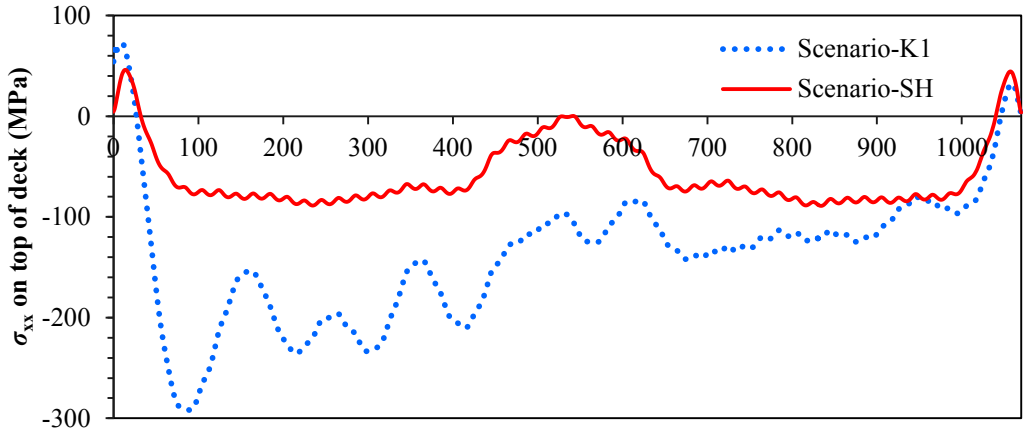

(b)

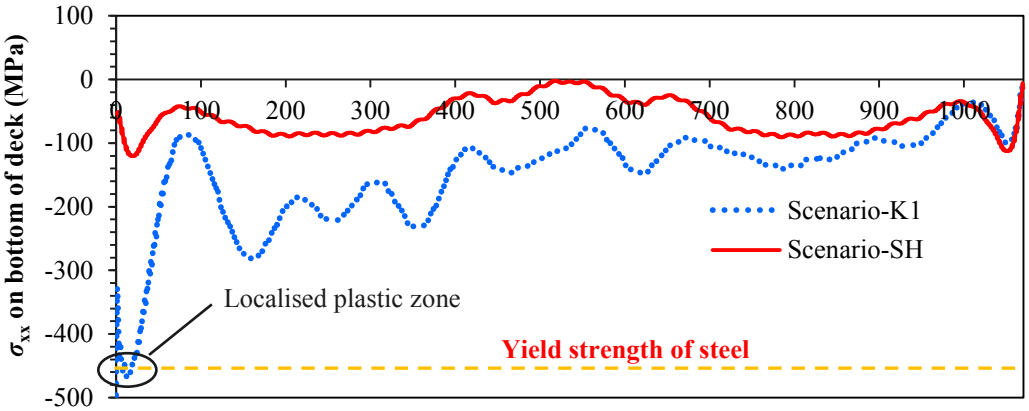

(c)

Figure 7-6 (a) has occurred along with σ_{xx} stress components on the (b) top and (c) bottom surface of the deck for scenario-SH (only gravity loads) and scenario-K1.

With regard to Figure 7-6a, it is observable that the deflections of deck occurred under seismic loading scenario-K1 are not that large compared with the deflections of deck only under gravity load (i.e. scenario-SH). The σ_{xx} stresses along the top surface of the deck (see Figure 7-6b) are not critical (well below the yield strength), whereas the σ_{xx} stresses on the bottom surface of the deck (Figure 7-6c) at the sections x= 7.5-17.5 m away from the pin-support exceeded the yield strength (450 MPa) of steel and led to formation of a plastic hinge at this section. The large plastic strains and rotations occurred at this plastic hinge must be the reason that ANSYS implicit model encountered convergence problem and stopped at 9.8 seconds into the seismic loading scenario-K1. To capture the possible collapse and failure mode of the structure, the bridge was modelled and analysed using LS-DYNA software and its explicit solver. The scenario-K5 in which the Kobe earthquake is applied along the bridge deck (x-direction) is considered in this section. As explained in Section 6.2.2 in Chapter 6, the elements in LS_DYNA will be deactivated when the plastic strain within the element reaches the plastic strain corresponding to failure of steel that is taken as 0.06 inhere. The results of σ_{xx} stress along the bottom of the deck at 9.7 seconds into the earthquake loading obtained from Scenarios K1 and K5 are compared and shown in Figure 7-7a that demonstrates a good correlation between the two FE models (i.e. ANSYS implicit and LS_DYNA explicit). Moreover, Figure 7-7b shows the time history of σ_{xx} stress at section x= 7.5 m away from the pin support, where the highest nodal σ_{xx} stresses were observed. It is seen that the stress at this location exceeds the yield strength a couple of times, however, after 12 seconds into seismic loading scenario, the σ_{xx} stress drops and fluctuates around 0 MPa.

The contour of stress and plastic strain on the bottom of the deck around pin-support (x= 0 to x= 40 m) at selected instants are shown in Figure 7-8. The stress and strain at 9.7 seconds, when the convergence criteria are still met in the ANSYS implicit FE model are shown in Figure 7-8a. The σ_{xx} stresses above yield strength of steel (i.e. 450MPa) are observable in Figure 7-8a, however, the plastic strains are still very small (close to zero) at this stage. At 11.65 seconds (Figure 7-8b), the plastic strains start to develop. Following that, at 11.82 seconds, two elements are eliminated since these

elements have reached the plastic strain corresponding to failure (taken as 0.06). At 11.95 seconds, four more elements were eliminated. After this stage, no element reached the failure point, however, the damaged zone was squeezed at around 30 seconds as shown in Figure 7-8e, that can be indicative of local buckling and large displacements/rotations (see Figure 7-8f). The failure mode predicted by the LS_DYNA explicit model (Figure 7-9a) is associated with significant up-lift around the pin support and also it correlates reasonably well with those observed in the Higashi-Kobe Bridge (Figure 7-9b) in the aftermath of Kobe earthquake.

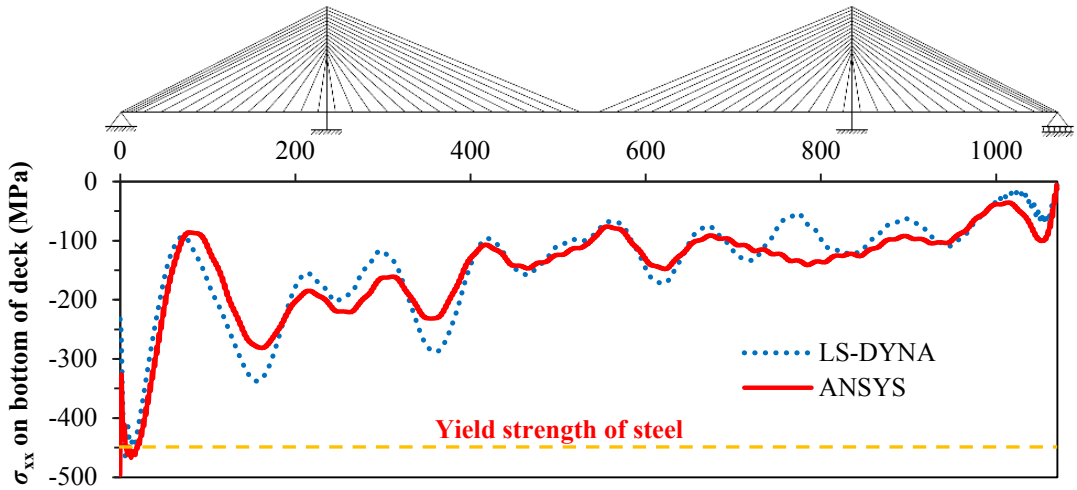

(a)

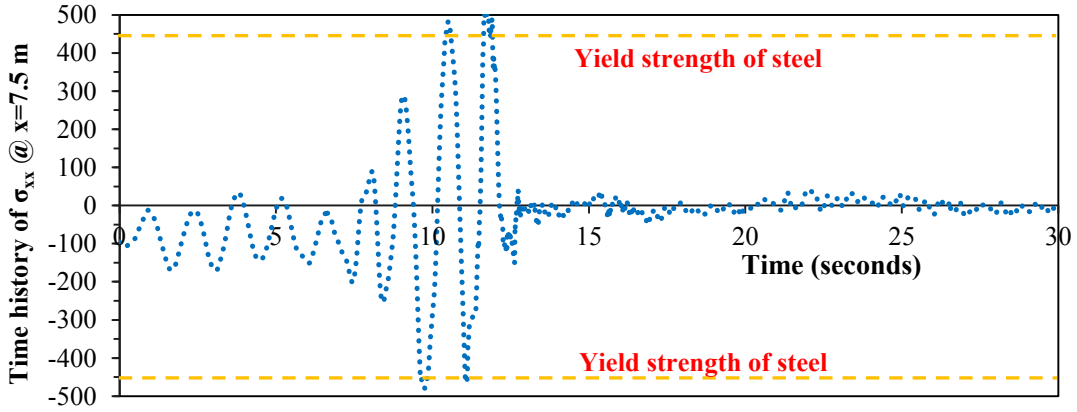

(b)

Figure 7-7 (a) σ_{xx} on bottom of the deck at 9.7 seconds and (b) time history of σ_{xx} at x= 7.5 m (stress exceeded the yield strength at 9.7 sec).

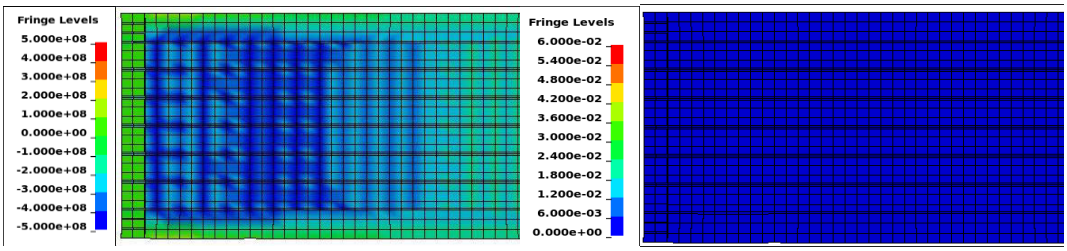

(a) 9.7 seconds

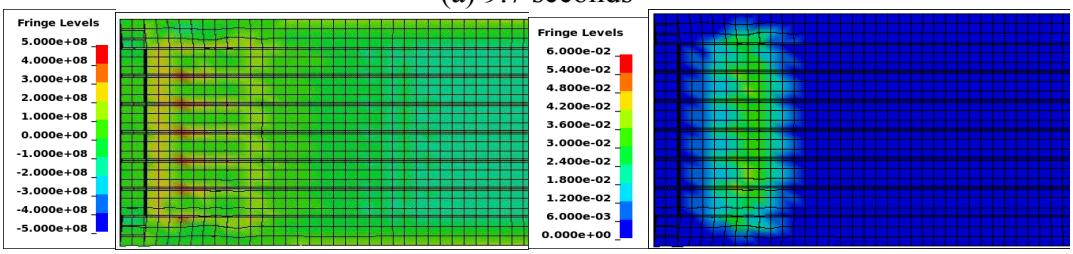

(b) 11.65 seconds

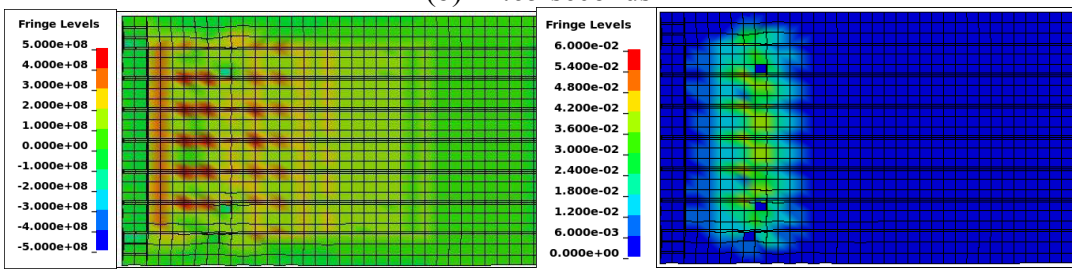

(c) 11.82 seconds

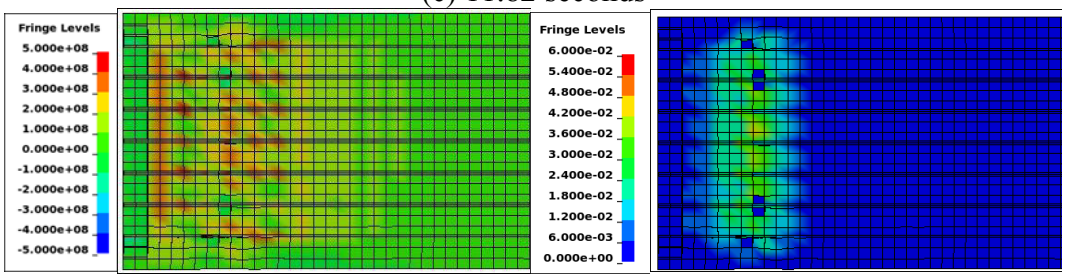

(d) 11.95 seconds

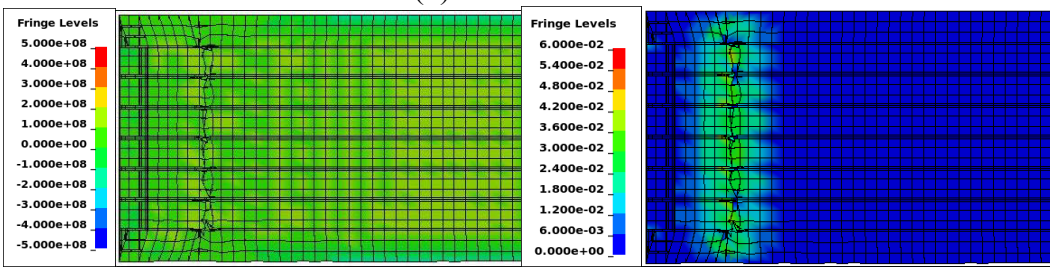

(e) 30 seconds

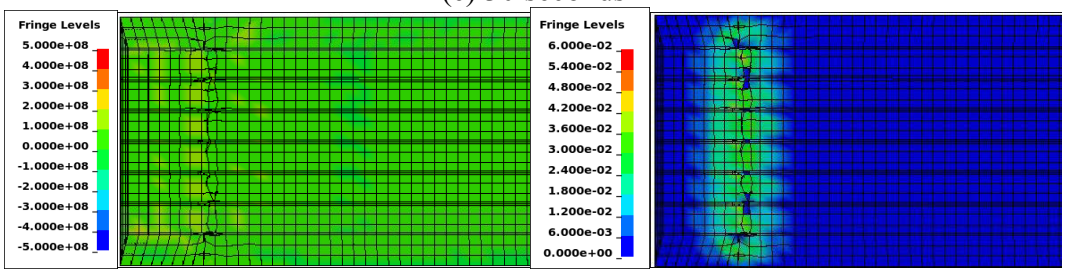

(f) 60 seconds

Figure 7-8 σ_{xx} and plastic strain around pin-support using ANSYS and LS DYNA

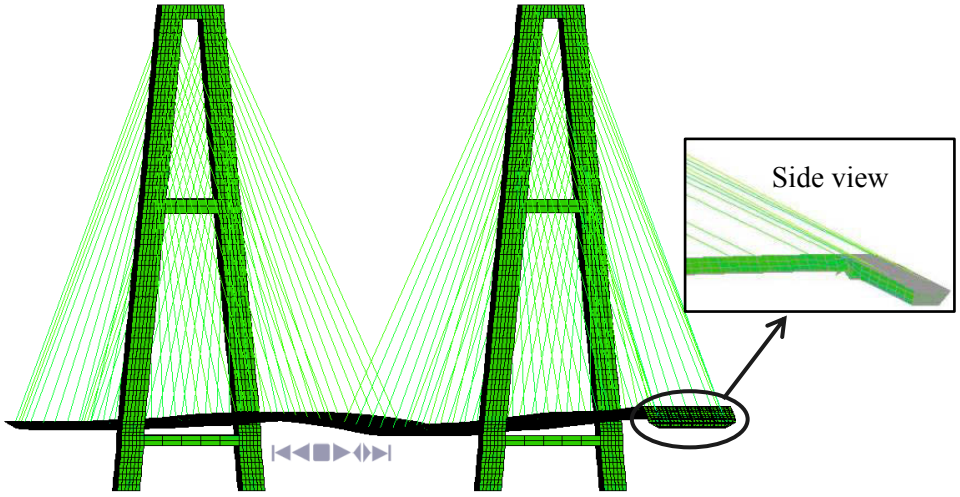

(a)

(b)

Figure 7-9 (a) Bridge configuration at 60 seconds (after earthquake) and (b) uplift of the deck around the pin-support, Higashi-Kobe Bridge after 1995 Kobe Earthquake.

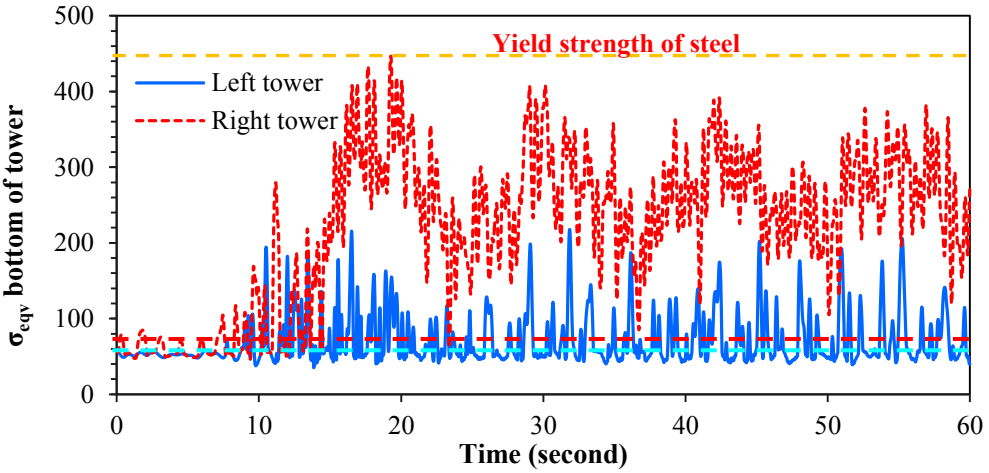

Figure 7-10 Time history of σ_{eqv} at the bottom of towers.

The time history of σ_{eqv} stresses at the bottom of the towers is plotted in Figure 7-10. In Figure 7-10, the blue dashed line (σ_{eqv} = 58 MPa) represents the maximum stress at the bottom of the left tower and the red dashed line (σ_{eqv} = 81 MPa) is the maximum stress at the bottom of right tower for the healthy bridge. It is observable that σ_{eqv} in both left and right tower is below the yield strength of steel, however, the right tower (the one closer to the hinge support) is more critical in terms of magnitude of σ_{eqv} stresses.

Cables

Envelop of maximum tensile stresses in the cables expressed as a percentage of cable ultimate strength within scenario K5 are shown in Figure 7-11a and the time history of tensile stress in cables No.1 and No. 48 is shown in Figure 7-11b.

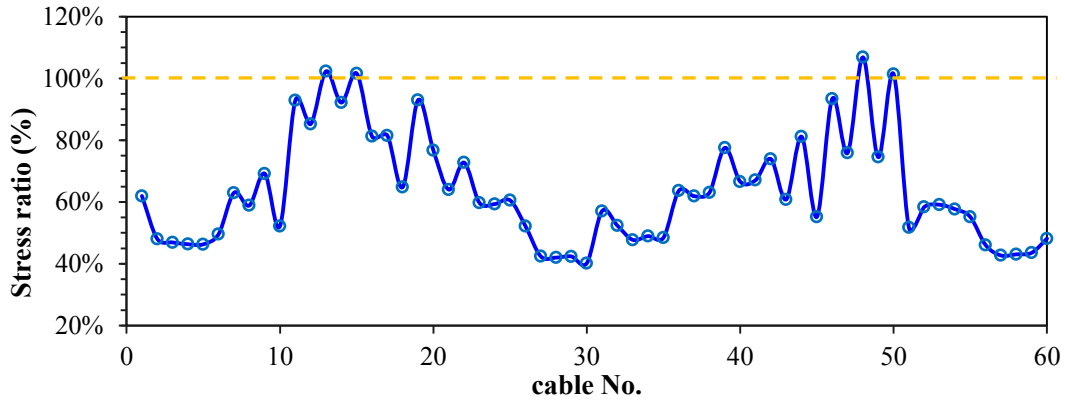

(a)

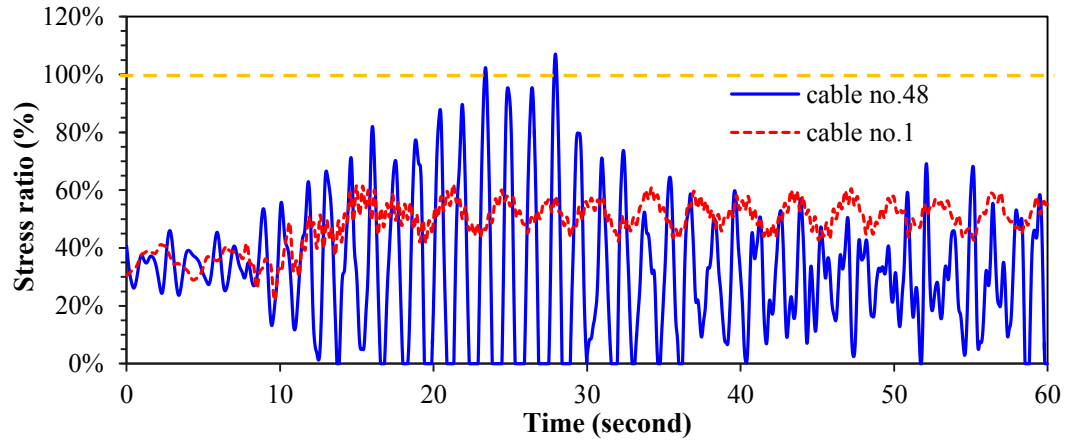

(b)

Figure 7-11 (a) Envelop of the maximum tensile stress in the cables and (b) time histories of tensile stress in cables No.1 and No. 48.

It is observable that in the earthquake loading scenario K5, the shorter cables (i.e. cables adjacent to the towers) are more critical than longer cables. The maximum tensile stress in the short cables (such as No. 13, 15, 48 and 50) has reached the breakage stress of the cables. However, the bridge model did not show any zipper type of collapse during this earthquake (i.e. scenario K5), because the most critical cables which their rupture can potentially trigger the progressive collapse of the cable stayed bridges are the ones connected to the pin support or mid-span (i.e. the longest cables such No.1 or 30). Also, the stress in the critical cables (e.g. No. 48) exceeds the breakage stress at only one instant.

7.5 Effect of traffic load distribution on the seismic response

In this section, the effect of traffic load distribution along the bridge deck on the potential progressive collapse response of the cable stayed bridge subject to seismic actions is investigated. The three different loading pattern (traffic load distribution) considered in this section is shown in Figure 7-12.

In conjunction with these loading patterns (see Figure 7-12), scenario-K5 (Kobe earthquake along the bridge deck) was considered to produce the maximum vertical deflection and maximum stresses in the structural components (i.e. deck and cables).

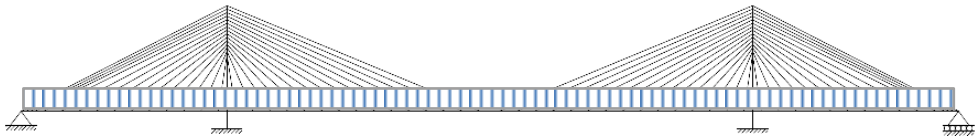

(a) Traffic load is distributed along the entire bridge (Entire Bridge)

(b) Traffic load is only acting on the middle span (Middle)

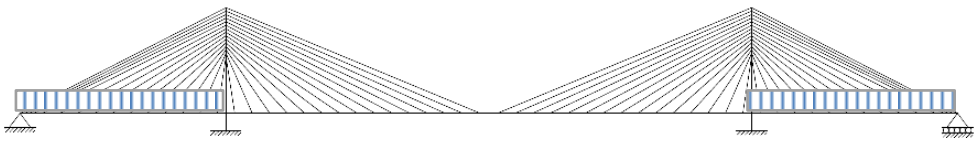

(c) Traffic load is only acting on the side spans (Side)

Figure 7-12 Traffic load distribution.

The average σ_{xx} stress on the bottom of the deck (along the deck) around 10 seconds into the earthquake (when the maximum stress occurred during the seismic event) for scenario-K5 is shown in Figure 7-13. Applying the traffic load on the entire bridge or on the side span led to the most critical scenarios in terms of maximum σ_{xx} stresses induced in the deck. When the traffic load was applied on the entire bridge, the compressive σ_{xx} stress reached the yield strength of steel at sections around the pin support, whereas applying the traffic load only on the side spans led to maximum tensile σ_{xx} stresses.

The envelop of vertical deflection and average σ_{xx} stress on the bottom surface of the deck at 60 seconds into the K5 earthquake scenario are shown in Figures 7-14a and b, respectively. The loading pattern in which the traffic load is applied only on the side span shows up-lift at the middle-span and sagging effect in the vicinity of the pin support whereas applying the traffic load on the entire span or only on the middle-span leads to sagging deflections over middle span and hogging deflections over end (side) spans. The maximum deflection during earthquake scenario K5 occurred when the traffic load was applied only on the middle-span. After the Kobe earthquake (60 seconds into the K5 earthquake scenario), the residual σ_{xx} stresses at the bottom of the deck were within the elastic range (see figure 7-14b).

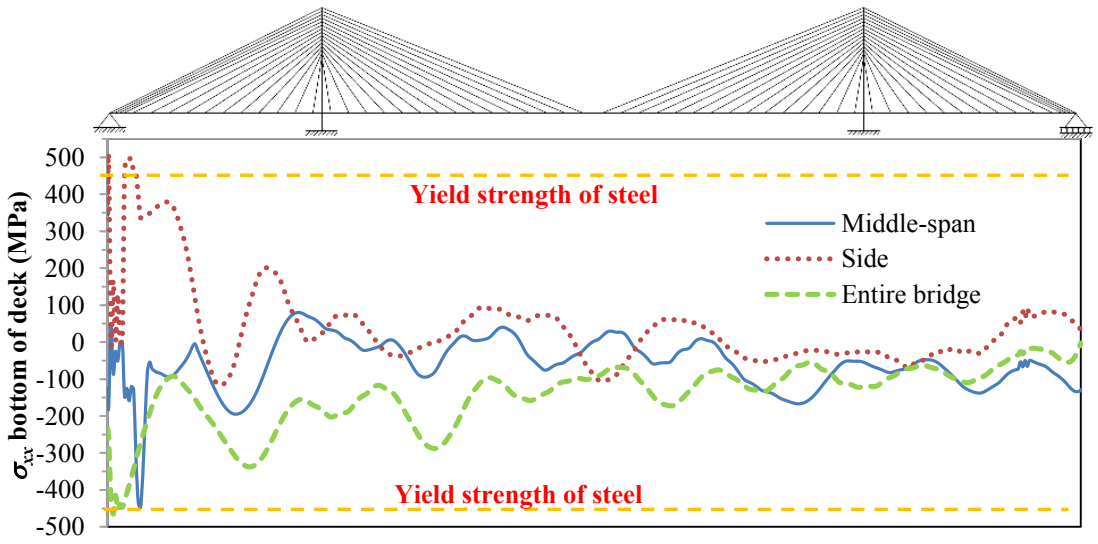

Figure 7-13 σ_{xx} on bottom of the deck around 10 seconds into the K5 earthquake scenario (first element reached the plastic strain).

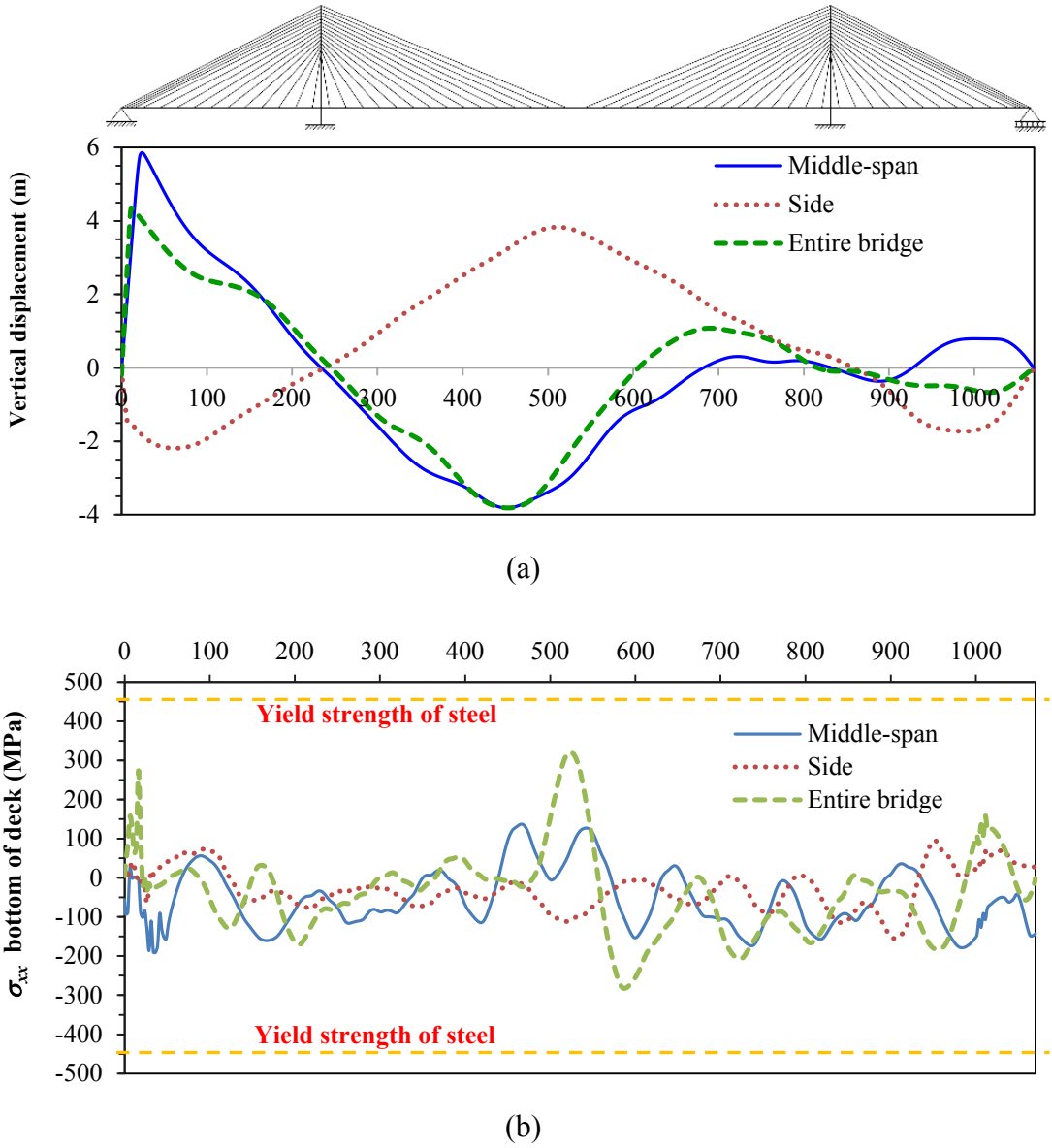

Figure 7-14 Envelop of (a) vertical displacement and (b) σ_{xx} on the bottom surface of the deck at 60 seconds into the K5 earthquake scenario.

Envelop of maximum tensile stresses in the cables expressed as a percentage of cable ultimate strength within earthquake scenario K5 for three different traffic load patterns are shown in Figure 7-15. It is observed that the maximum tensile stresses occur in the short cables (e.g. No. 13, 15, 48 and 50) when the traffic loads are applied on the entire bridge and side spans. In the short cables No. 13, 15, 48 and 50, the tensile stresses have reached the breakage stress of the cables. When the traffic load was applied on the middle-span, cable no.1 reached 90% of the breakage stress. Such a scenario is critical, because cable no.1 is one of the cables that its loss can potentially trigger the zipper type of collapse.

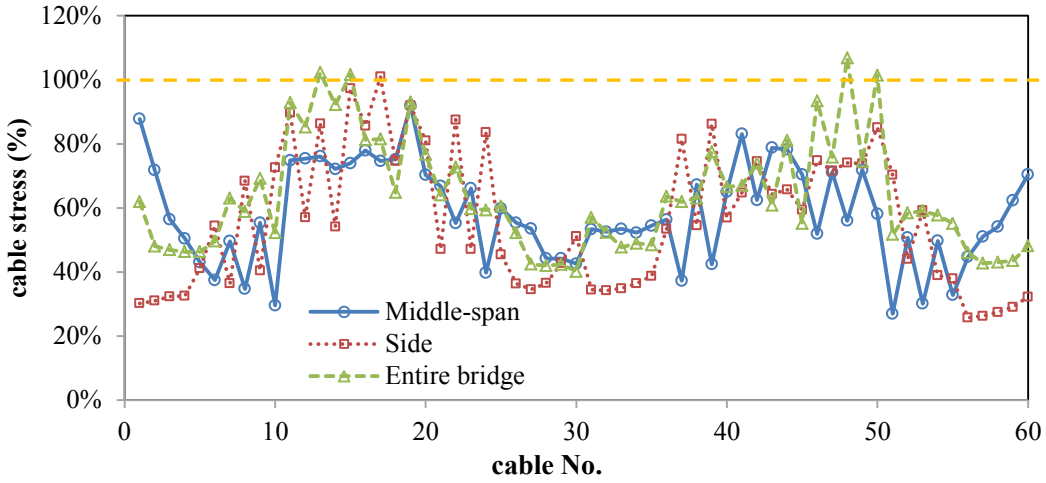

Figure 7-15 Envelop of the maximum tensile stress in the cables.

7.6 Sensitivity analysis

With regard to the variability in strength and stiffness of materials, a sensitivity analysis is carried out to demonstrate the robustness of the FE results and also evaluate influence of the mechanical properties of steel (i.e. yield strength f_y and elastic modulus E) on the potential progressive collapse response of the cable stayed bridge subject to seismic actions. The scenario-K5 (Kobe earthquake applied along the bridge) that led to maximum vertical deflection and maximum stresses in the structural components (i.e. deck and cables) and ±10% variability in the steel modulus of elasticity E and yield strength σ_y are considered in this sensitivity analysis. LS-DYNA software in conjunction with an explicit solver is used in the sensitivity analysis. The sensitivity of average σ_{xx} stress on the bottom surface of the deck (along the deck) at 9.7 seconds into the earthquake (when the maximum stress occurred during the seismic event) with respect to the yield strength f_y and elastic modulus E of the steel during scenario–K5 is shown in Figure 7-16.

In addition, the sensitivity of deflection response (along the deck) and the sensitivity of average σ_{xx} stress component on bottom surface of the deck at 60secdonds (when the Kobe earthquake was converged) with respect to the yield strength and elastic modulus of the are shown in Figure 7-17.

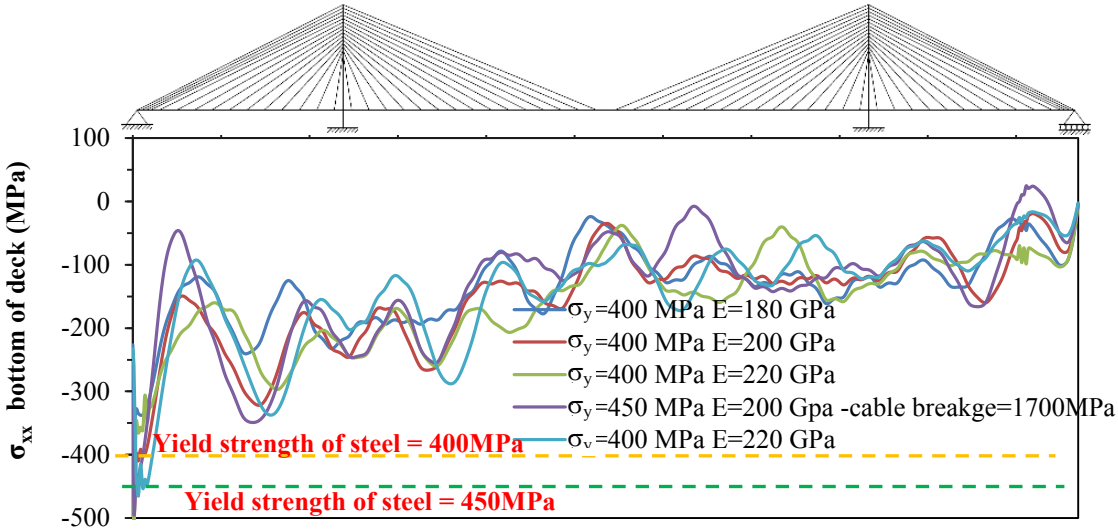

Figure 7-16 σ_{xx} on the bottom of deck at 9.7 seconds into the K5 earthquake scenario.

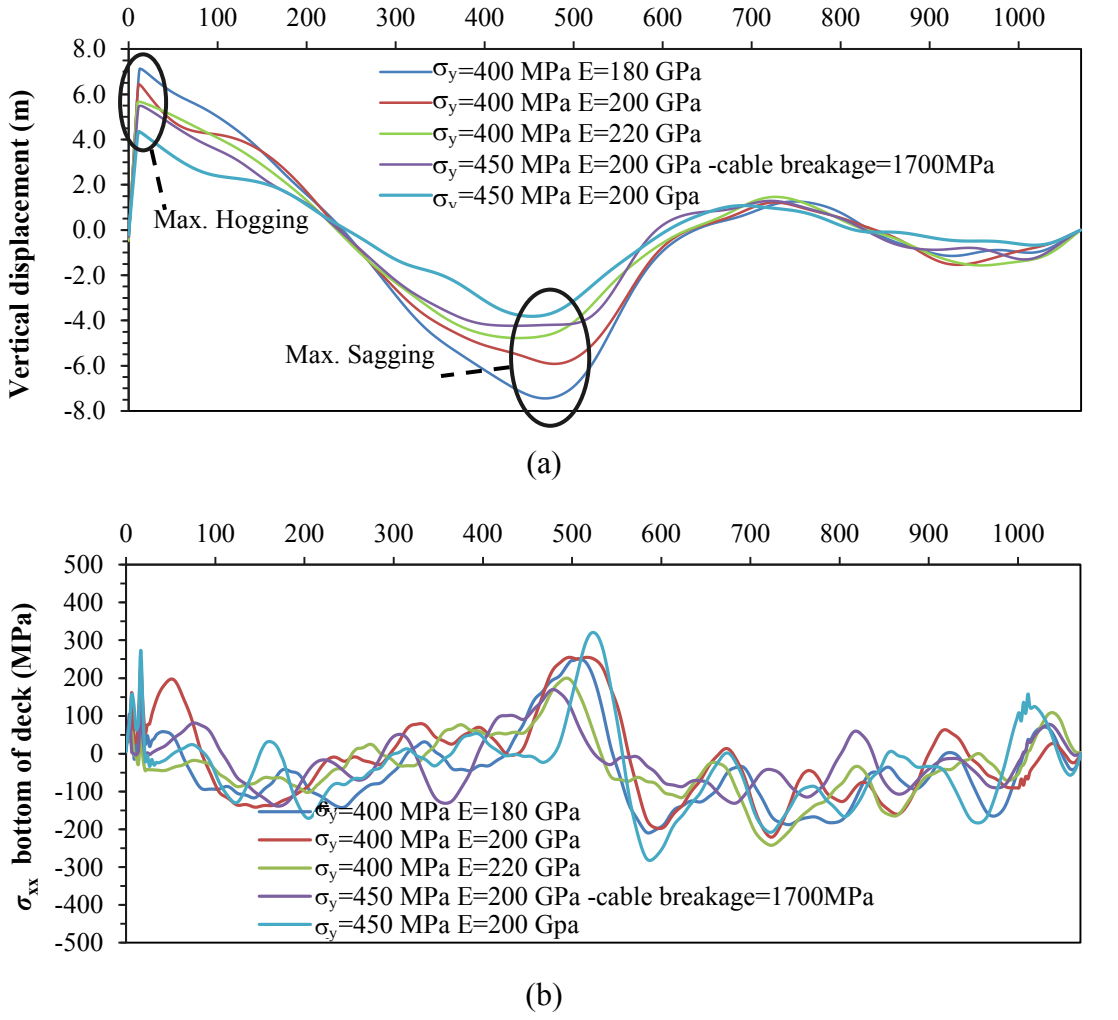

Figure 7-17 (a) Deflected configuration of the deck and (b) σ_{xx} on the bottom surface of the deck at 60 seconds into the K5 earthquake scenario.

It is observable that the σ_{xx} stress on the bottom of the deck can exceed the yield strength of steel at 9.7 seconds into the K5 earthquake scenario. Accordingly, the deck cross sections in the vicinity of the pin support are identified as the most critical sections within along the deck earthquake loading scenarios. Moreover, the vertical deflection, especially maximum hogging around the pin support is quite critical during earthquake loading scenarios.

Moreover, envelop of maximum tensile stresses in the cables expressed as a percentage of cable ultimate strength within scenario K5 is shown in Figure 7-18. It is observed that the maximum tensile stress in the short cables (such as No. 13, 15, 48 and 50) has reached the breakage stress of the cables. In some of the models, the tensile stress in the cables exceeded the cable breakage stress; however, no cable loss occurred. Furthermore, the bridge model did not show any zipper type of progressive collapse during this earthquake loading scenarios.

Finally, Table 7-4 summarises the timing when the first element reached to the plastic strain (ε_p=0.06) and total number of lost elements due to plastic strain failure. With regard to the results shown in Table 7-4, it is seen that the deflected configuration of the deck (locations of maximum sagging and hogging deflection) is sensitive, however, the variation of stress along the deck (locations of maximum) are not sensitive to the yield strength and elastic modulus of steel. This is clearly demonstrative of the robustness as well as adequacy of the results obtained from the FE models.

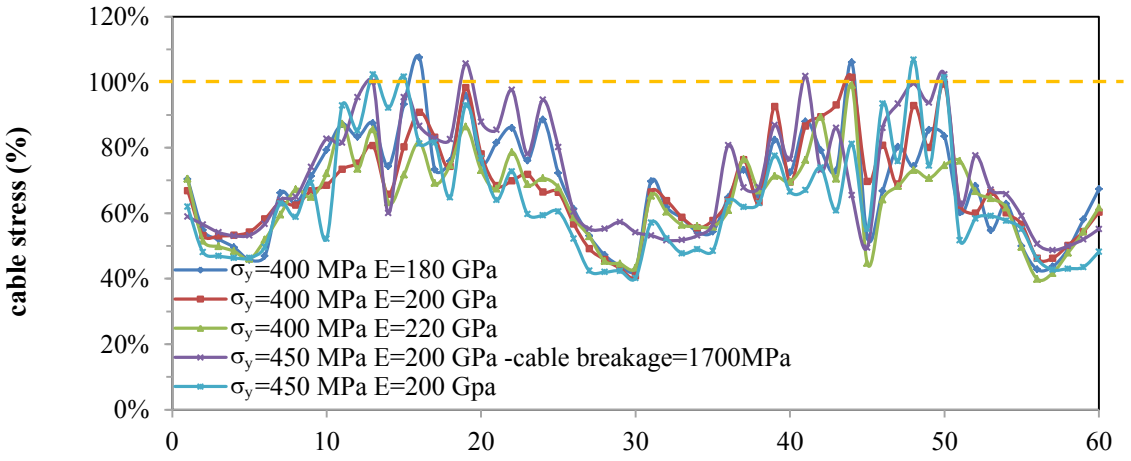

Figure 7-18 Envelop of the maximum tensile stress in the cables

Table 7-4 Summary of sensitivity analysis results.

Scenario name	yield stress (MPa)	young's modules (GPa)	Instant of time when plastic strain occurred	Number of lost elements
σ_y=400 MPa *E*=180 GPa	400	180	33.1 sec	218
σ_y=400 MPa *E*=200 GPa	400	200	31.4 sec	206
σ_y=400 MPa *E*=220 GPa	400	220	30.4 sec	225
σ_y=450 MPa *E*=200 GPa	450	200	31.4 sec	216
σ_y=450 MPa *E*=200 Gpa cable strength= 1700MPa	450	200	38.8 sec	196

7.7 Preparing for experimental work

To verify the numerical analysis, an experimental work was planned and initiated by the candidate for the next phase of this research but was deemed beyond the scope of the current program.

7.7.1 Numerical model

At first, a steel cable stayed bridge model, inspired by Okuwaka Bridge in Japan (JSCE, 2010), was designed according to AS5100 (AS5100.2, 2004). The dimensions of the bridge and geometry of sections as well as the configuration of cables for the bridge considered in this chapter are shown in Figure 7-19.

The full scale bridge is symmetric and has a total span length of 120 m supported by a single 55 m tall tower and 6 pairs of cables spaced (20 m apart) along the deck. Furthermore, all cables are regularly spaced (5 m apart) over the tower. The bridge deck is 25 m wide (4 traffic lanes according to AS5100.2 (2004) and 1.5 m deep and is made of a multi-cell steel box girder as depicted in Figure 7-19b. This bridge deck is restrained by pin support at the far left end and by roller support at the far right end (Figure 7-19a), and there is no direct connection between the deck and the pylons. The fully fixed cross section of tower leg is shown in Figure 7-19c.

The modulus of elasticity, E, and the yield stress of steel, σ_y, as well as the geometrical properties of the deck, including second moment of area, I, and cross sectional area, A,, are given in Table 7-5.

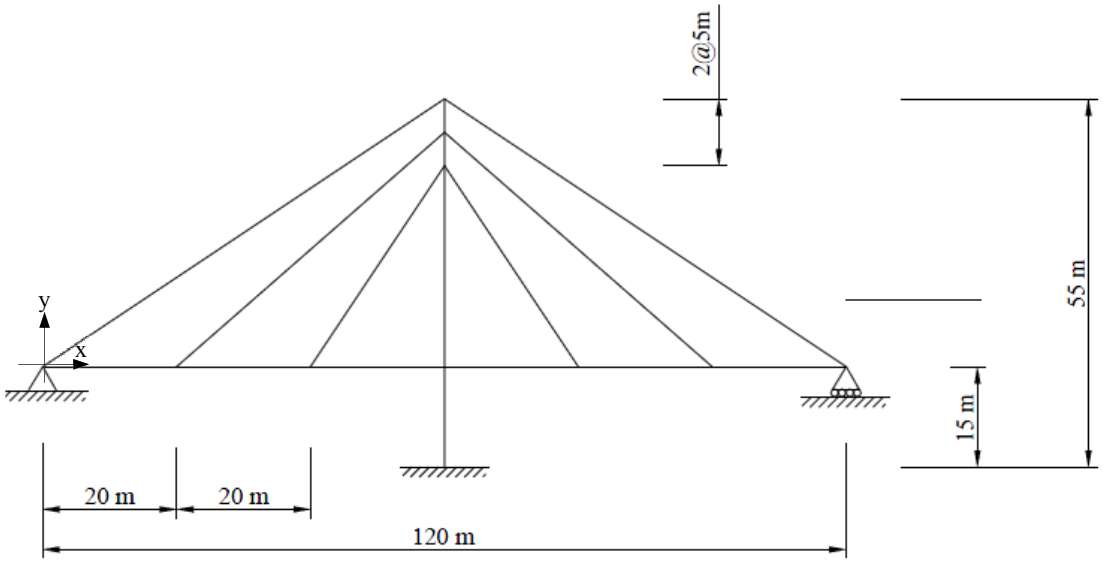

(a) Bridge configuration

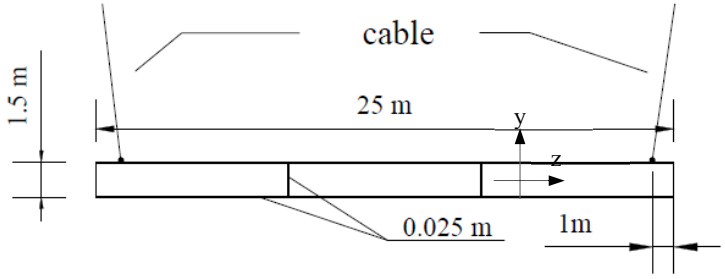

(b) Deck

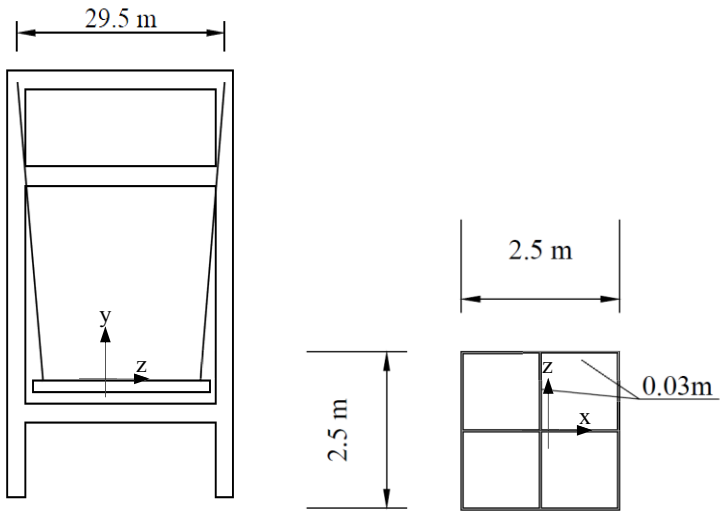

(c) Tower

Figure 7-19 Configuration for numerical model

Table 7-5 Deck properties.

	Numerical model	Geometric scaling factor (λ=1/50)	numerical model *x* scaling factor	Exp. values	difference
Material	Steel			PVC	
Density (kg/m^3)	7850	λ^3		1300	
Modulus of Elasticity (MPa)	2.00E+05	λ	4.00E+03	3.80E+03	-5%
A (m^2)	1.40E+00	λ^2	5.58E-04	5.72E-04	3%
I (m^4)	6.94E-01	λ^4	1.11E-07	1.14E-07	3%
EI (Nm^2)	1.39E+11	λ^5	4.44E+02	4.35E+02	-2%
EA (m^2)	2.79E+11	λ^3	2.23E+06	2.17E+06	-3%
Weight (N)	1.29E+07	λ^3	1.03E+02	1.75E+01	-83%
Mass (kg)	1.31E+06	λ^3	1.05E+01	1.78E+00	-83%

7.7.2 Design for experimental model

In this study, the geometric scaling-factor is set at 1/50. A prototype model should be designed and developed with the properties listed in Table 7-4. According to this list, PVC (Poly Vinyl Chloride) was selected with the modulus of elasticity of 3.8 MPa (about 1/50 of steel material). A simple drawing for the bridge configuration, including cross sectional areas of deck and tower for this bridge model, is shown in Figure 7-20. By comparison, the cross-section of the numerical cross section is somewhat different because of satisfying the factors EA and EI (see Table 7-5). The error ranges are within 10%.

PVC sheets for deck and tower were cut into several pieces and glued together. In the numerical model, the deck is supported by pin- and roller-support at each end. For the experimental model, pin- and roller-support are created by PVC roller installed into a bearing system as shown in Figure 7-21.

For cables, springs (see Figure 7-22) are installed which have 1/50 of the cable stiffness compared with the numerical model. Also, cables are connected by 4 forks and springs see in Figure 7-22.

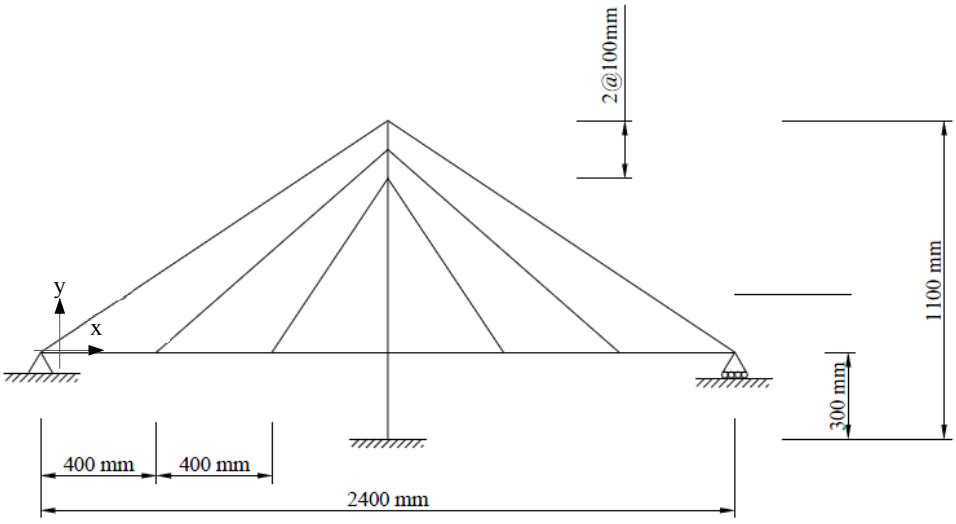

(a) Bridge configuration

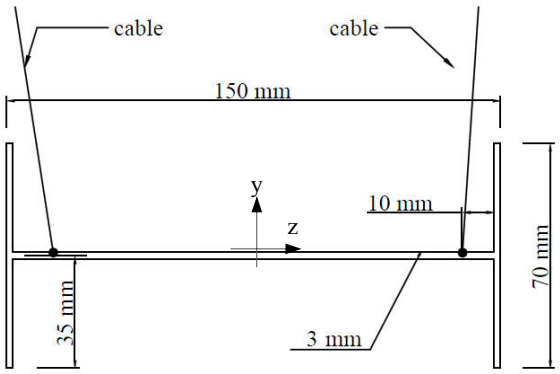

(b) Deck

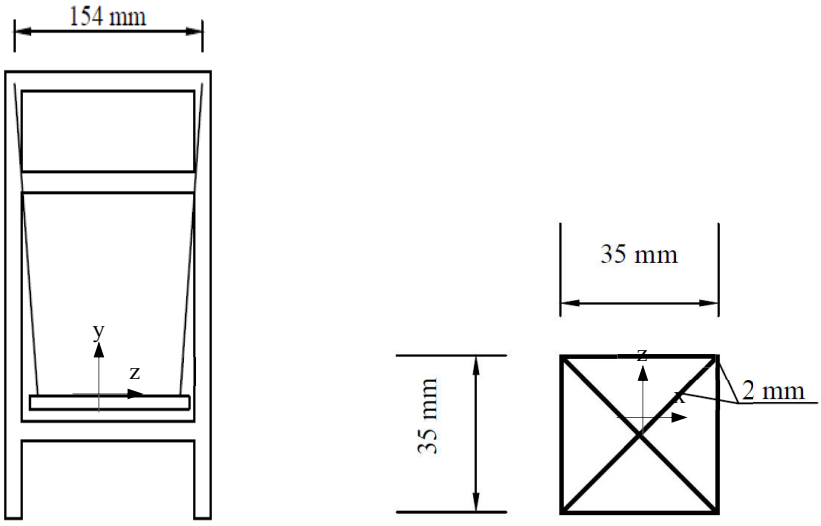

(c) Tower

Figure 7-20 Experimental bridge model (dimensions in mm)

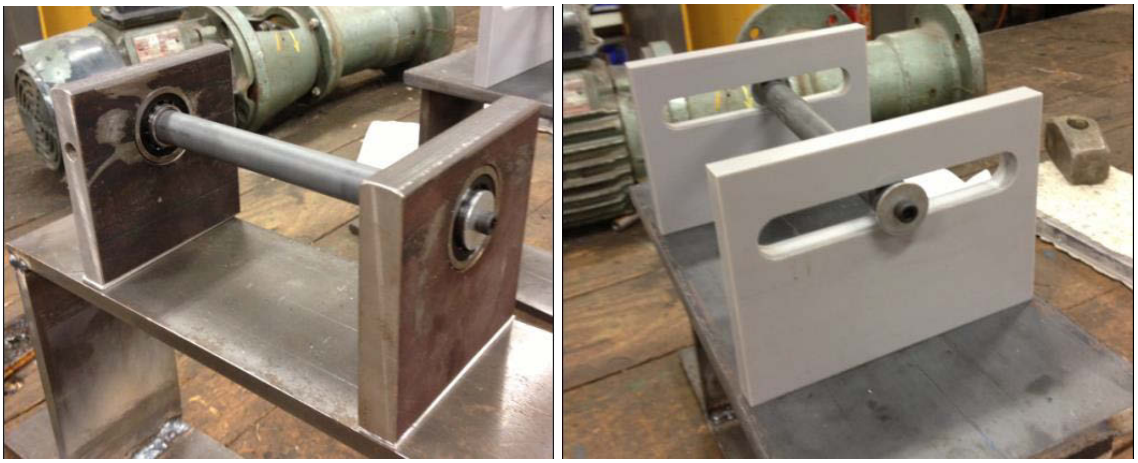

(a) Pin support system (b) Roller support system

Figure 7-21 End support system for experimental prototype

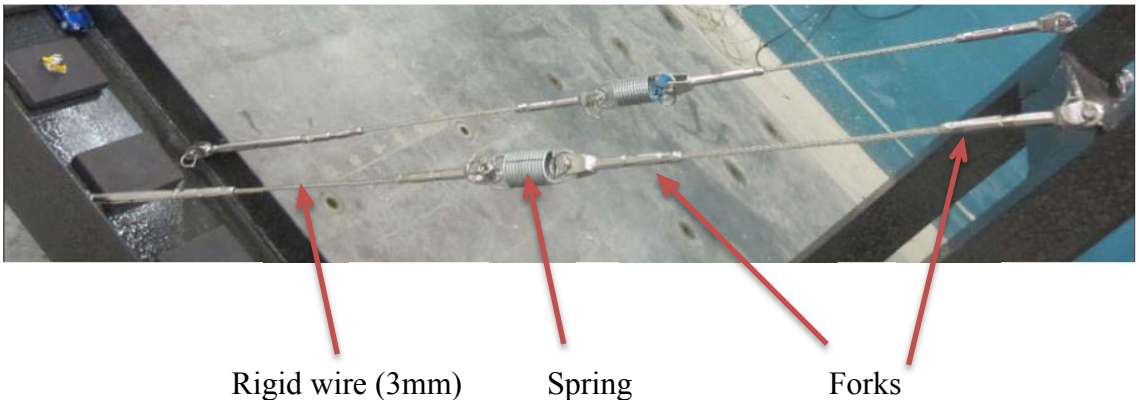

Figure 7-22 Devised mechanism for post-tensioning the cables.

7.7.3 Pre-test

The prototype bridge (see Figure 7-23) was attached to the shake table and the first pre-test was done. Two LVDTs were installed on the top of the tower and left side of the deck, and 11 accelerometers were placed around the deck and tower side. As can be seen clearly, cables look too heavy compared with the other segments. In reality, weight of the cables should be negligible. Thus, in the initial prototype testing, cable vibrations constituted the first natural frequencies which is not supposed to be the case according to the numerical analyses.

7.7.4 Re-modelling

According to this pre-testing, the cable material should be changed in order to satisfy the model properties. Once this is done, the experimental test can continue. The plan is to use 4 different scaled earthquake ground accelerations.

(a) Bridge model on the shake table

(b) LVDT

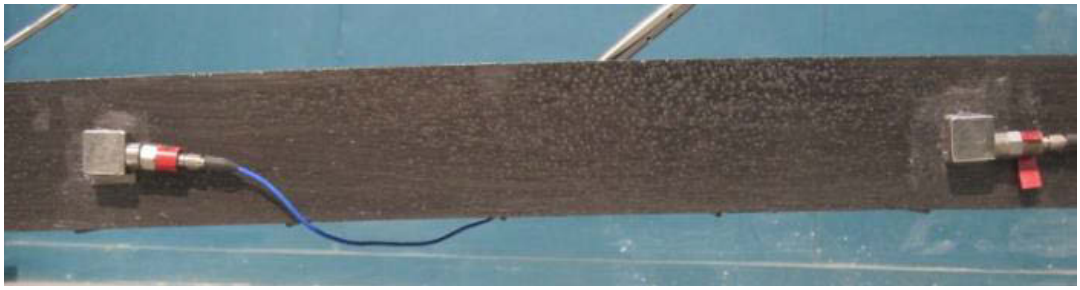

(c) Accelerometers

Figure 7-23 (a) Prototype on the shake table, (b) LVDT and (c) accelerometer

7.8 Concluding remarks

A numerical study of an idealised cable-stayed bridge model subjected to four seismic ground excitations was carried out in this chapter. A comprehensive parametric study was undertaken and the importance of using a representative model under several seismic loadings with non-linear effects was investigated. With regards to the parametric studies in this chapter, the following conclusions can be drawn;

- The earthquake load applied longitudinally (along x-direction) and at 30-degree to this direction created the highest deformation and stresses in the deck. This was particularly the case for Kobe earthquake loading scenarios.

- Implicit analysis carried out using ANSYS software encountered some convergence problem owing to high stress concentration and large deformations. The numerical convergence issue was particularly severe when Kobe earthquake was applied along the bridge deck.

- The stress in the towers remained below the yield strength of steel in all of the considered seismic loading scenarios. In the deck, the sections in the vicinity of the pin support were identified as the most critical sections in terms of stresses induced in the deck during earthquake loading scenarios.

- The short stays adjacent to the towers were found to be the most critical ones in terms of maximum tensile stress induced in the cables during seismic actions. The stress in these short cables exceeded the breakage stress of cables during Kobe earthquake when applied longitudinally or at 30-degrees; however, no cable loss occurred during these earthquake loading scenarios.

- Significant vertical displacement of the deck (hogging) occurred around the pin support by longitudinal earthquake excitation. These large hogging deflections were associated with permanent damage in the deck.

- The bridge model studied in this model was not subjected to zipper-type collapse although the formation of plastic hinges within the deck did occur.

Chapter 8 : Conclusions

8.1 Summary of each chapter

Dynamic responses of a hypothetical cable-stayed bridge under several severe conditions (such as sudden loss of cable, blast loading and seismic loading) were studied in this thesis. Finite element (FE) models of a cable-stayed bridge designed according to Australian standards was developed and analysed statically and dynamically as part of this research. Two commercial FE programs, namely, ANSYS and LS-DYNA, were used.

Chapter 3:

One of the most critical situations for a cable stayed bridge is the sudden loss of cable(s) which can be the cause of potential progressive collapse. As discussed in Chapter 2, some standards, such as PTI, recommend considering any single loss of cable in the design phase by static analysis using a Dynamic Amplification Factor (*DAF*) set at 2. However, due to bridge characteristics (a complex multi degree of freedom system), *DAF*=2 has been questioned and investigated in some research works and concluded that a simplified approach (with *DAF*s set at 2) could be seemingly quite unsafe since some of the *DAF*s could exceed this limit significantly. It is, therefore, recommended to conduct a dynamic analysis for evaluating the response of the bridge subjected to a sudden loss of cable. In this thesis, the *DAF*s associated with different locations, load durations and number of lost cables were investigated along with the effect of damping ratio. Moreover, the relationship between *DAF*s and the potential of progressive collapse were determined. The studies on *DAF*s were done by using a liner 2D model. Therefore, the potential progressive collapse was instead presented by Demand-Capacity Ratio (*DCR*). Based on this new relationship, the most critical cable(s) were determined. The key conclusions were as following:

- The loss of the longest back stays are the most critical ones (the highest *DCR* values were observed for all structural components).
- The *DAF* for the bending moment and axial force at different sections along the deck, towers and cables can take values much higher than two (typically adopted by

different guidelines), however, the *DCR* value is usually less than 100% in most such cases. In other words, material nonlinearity has minor effect on the global progressive collapse response of the bridge due to cable loss, and it is not un-conservative to allow a *DAF* of greater than two as long as *DCR* remains below one.

- The *DAF* values alone, do not provide any information about the progressive collapse response of the cable stayed bridge under study, whereas *DCR* values at different locations of the structure can be used as an indicator of material nonlinearity and formation of plastic hinges.
- Damping ratio has minor impact on the dynamic progressive collapse response of the cable stayed bridges as long as the adopted value of the critical damping ratio is within the acceptable range (less than 2% of critical for the bridge considered in this study).

Chapter 4:

All research related to *DAF*s and *DCR*s were conducted successfully by using the 2D linear-elastic model. However, the author noticed some limitations in the 2D model. Therefore, a detailed 3D non-linear model was also developed and analysed and the accuracy of both 2D and 3D models were verified by comparing the results associated with two different sudden cable loss situations. It was shown that the linear elastic 2D FE models can adequately predict the dynamic response (i.e. deflections and main stresses within the deck, tower and cables) of the bridge subject to cable losses. In 3D model, some material yielding did occur at different locations, although they were found to be localized.

Chapter 5:

It was suspected that unsymmetrical loading pattern in out-of plane with unsymmetrical cable loss could be critical in terms of progressive collapse, since it was anticipated that these unsymmetrical situations could lead to significant local stress concentrations as well as torsional effects. Thus, a parametric study was undertaken and the effect of cable loss scenarios (symmetrical and unsymmetrical) and loading patterns (symmetrical and unsymmetrical) were investigated. In this chapter, one additional deck configuration was introduced; ie, maintaining the original steel box girder and also considering an open orthotropic deck. The stress levels, torsional effects and the

progressive collapse response of the bridge at global and local levels were investigated. According to the research,

- The configuration of the deck has minor influence on the dynamic response of the bridge following loss of one or two cables, while box girders exhibited lower torsional effects.
- The tensile stresses in cables, following symmetrical or unsymmetrical cable loss and loading scenarios remained well below the breakage stress of the cables, and accordingly, for the cable stayed bridge considered in this study, loss of one or even two cables did not trigger a zipper-type progressive collapse.
- The change in shape (geometry) and the reduction in axial stiffness of the stays due to variation of stress levels in the cables were evaluated with respect to Ernst's modulus. The variation of Ernst's modulus in the longest stays was found to be less than 12% and this is demonstrative of the magnitude of geometrical nonlinearities in the cables during progressive collapse assessment of the cable stayed bridges.
- In the analysed bridge, material nonlinearity (yielding of steel) and buckling of steel plates did not occur at global as well as local levels. Accordingly, it was concluded that the zipper-type collapse triggered by formation of plastic hinges is unlikely to happen in the cable stayed bridges that have lost two cables or less.

Chapter 6:

According to above research, it was noted that loss of cable analysis is quite important in design of a cable-stayed bridge. Also, the cause of the loss of cable should be considered. One possible and critical situation would be blast loading. After 911 terrorist attacks, blast loading has been considered an important loading scenario for iconic structures including the bridge structures. Some pertinent studies have been published on highway bridges, as well as cable stayed bridges. Some bridges showed lower durability against blast loadings. For a large scaled bridge, a comprehensive analysis concluded that the piers were the most important components, which means loss of piers would lead to progressive collapse as expected. In this research, the main focus was on the loss of cable(s) due to blast loadings. First of all, the damag created by different amount of explosive materials applied along the bridge deck were determined and concluded that

- More than 4.5 tonnes of TNT equivalent material could lead to loss of one to three cable(s)
- The reason behind loss of cable is not direct damage to the cables but damage to anchorage zone(s).

Accordingly, the global response of the bridge model with cable losses due to blast loading was compared with the responses obtained from applying the simple cable loss analysis. The concussions are as follows:

- The dynamic behaviour of blast load analysis with cable losses can be adequately predicted by simple cable loss analysis, regardless of the number of cables lost.
- The average difference between the results obtained from the blast load analysis and cable loss analysis is around 15% to 25%.

Chapter 7:

Finally, the dynamic responses of the cable-stayed bridge under study subjected to seismic loadings were analysed. The earthquake loading is also one of the most important and potentially extreme loading for the bridge structures, since several bridges have suffered during the past large earthquakes; even some of them completely collapsed. There is a vast amount of research on bridges subjected to seismic loads, especially in Japan. For cable-stayed bridges, end-supports (such as piers, rollers, or pins) were affected by seismic loading significantly and in need of special attention. On the other hand, some researchers have claimed that there is not enough research conducted regarding the general design concepts of the cable-stayed bridges under seismic loadings.

In this research, using a detailed 3D model, the author determined the most critical earthquake type and the direction on each bridge component. It was found that:

- The earthquakes applied longitudinally created the highest deformations and stresses in the deck, especially the Kobe earthquake of 1995.
- For the tower, the stresses remained below the yielding point in any seismic loadings

This analysis (ie, Kobe earthquake applied along the bridge length) was also done using LS-DYNA software to determine the damage mechanism(s). It was observed that:

- Significant vertical displacement (uplift) on the deck can happen around pin support by longitudinal earthquake movement, which created permanent damage.
- The bridge model studied in this analysis did not trigger a zipper-type collapse although the formation of any plastic hinge within the deck did occur.

8.2 Overall Conclusions

In summary, the extreme loading scenarios considered in this thesis cannot be ignored when bridge designers design cable-stayed bridges. For sudden loss of cable scenarios and because a 2D linear model is accurate enough for unsymmetrical loading patterns, and cable loss situations are not significant for symmetrical cases, the linear 2D model can be used. However, *DAF*s =2 are not adequate for many cases, thus, dynamic analysis is strongly recommended. For blast loading analysis, cable loss and damage caused by blast loading can be adequately predicted by simple cable loss analysis. However, a 3D model is more suitable for the blast analysis since symmetrical cable loss is unlikely to happen under blast. Finally, under seismic loadings, eg, a Kobe 1995 type earthquake (known as near field earthquake possessing impulsive accelerations) the loading is more critical when applied along the bridge model. If the bridge engineers would like to capture the bridge damage accurately, the model should be developed in LS-DYNA software. The permanent damage can be detected in this analysis.

8.3 Suggestion for further research

This research has been quite comprehensive and involved a large scale steel cable-stayed bridge. However, a concrete bridge should also be investigated, especially under blast loadings and seismic loadings, since it is anticipated that the concrete bridges will show less resilient than the steel cable-stayed bridges.

Also, an initial experimental work was commenced at University of Technology Sydney with the aim of using the shake table but was deemed outside the scope of the current

study. Although, numerical results presented in this thesis are quite comprehensive and convincing, however, they should be verified by some experimental tests. As discussed in Section 7-5, the prototype should be able to model and capture the dynamic dynamic behaviour of the bridge. To do so, cable elements can be replaced by rigid cable with forks (which were too heavy) to a right wire, which could be smaller wires with more appropriate springs. Then, the dynamic tests can be conducted using a shale table. The model can be tested on the shake table to determine its global responses (tower and deck deflection, the accelerations, etc.) under severe earthquake accelerations. This will be a valuable research.

References

AASHTO 2010. AASHTO LRFD bridge design specifications. Washington, D.C, U.S: American Association of State Highway and Transportation Officials,.

ÅKESSON, B. B. 2008. *Understanding Bridge Collapses,* London, Taylor & Francis/Balkema.

ANSYS® 2009. Help System, Coupled Field Analysis Guide. *In:* ANSYS, I. (ed.) 12.1 ed.: ANSYS® Academic Research.

ANWARUL ISLAM, A. K. M. & YAZDANI, N. 2008. Performance of AASHTO girder bridges under blast loading. *Engineering Structures,* 30**,** 1922-1937.

AOKI, Y., SAMALI, B., SALEH, A. & VALIPOUR, H. 2011. Impact of sudden failure of cables on the dynamic performance of a cable-stayed bridge. *In:* PONNAMPALAM, V., ANCICH, E. & MADRIO, H. (eds.) *AUSTROADS 8th BRIDGE CONFERENCE.* Sydney, Australia.

AOKI, Y., SAMALI, B., SALEH, A. & VALIPOUR, H. 2012a. Assement of Key Response Quantities for Design of a Cable-Stayed Bridge Subjected to Sudden Loss of Cable(s). *In:* SAMALI, B., ATTARD, M. M. & SONG, C. (eds.) *Australasian Conference on The Mechanics of Structures and Matreials, ASMCM 22.* Sydney, Australia: Taylor&Francis Group.

AOKI, Y., VALIPOUR, H. R., SAMALI, B. & SALEH, A. 2012b. A Study on Potential Progressive Collapse Response of Cable-Stayed Bridges. *Advances in Structural Engineering,* 16**,** 18.

ARUP 2010. *Stoncecutters Bridge Hong Kong Design and Construction,* Hong Kong, Ove Arup and Partners Hong Kong Ltd.

AS1170.4 2007. Structural design actions - Earthquake actions in Australia. Sydney, Australia: Australian Standard.

AS4100-1998 1998. Steel structures. Sydney, Australia: Australian Standard.

AS5100.2 2004. Bridge design - Part2:Design load. *Design loads.* Sydney, Australia: Austrarial standard.

AS5100.6 2004. Bridge design - Steel and Composite Construction. *Steel and composite construction.* Sydney, Australia: Australian Standard.

AS/NZS1170.2 2002. AS/NZS 1170.2:2002 : Structural design actions - Wind actions. *Structural design - General requirements and design actions - Part 2: Wind actions.* Sydney, Australia: Australian Standard.

AUSTRALIA, E. M. 2007. Lessons from London and considerations for Australia : London Terrorist Attacks, 7 July 2005 / Attorney-General's Department Emergency Management Australia. Canberra, Australia.

AUTODYNE, A. 2007. ANSYS AUTODYNE Use Manual v11.0. Century Dynamic Inc.

BENSI, M., BHATTACHARYA, B. & M.J.CHAJES 2005. Evaluating the risk of a terrorist attack on a cable-stayed bridge: a probabilistic, structural analysis based approach. Newark, Delaware: University of Delaware.

BRUNEAU, M. 1998. Performance of steel bridges during the 1995 Hyogoken–Nanbu (Kobe, Japan) earthquake—a North American perspective. *Engineering Structures,* 20**,** 1063-1078.

CAI, J.-G., XU, Y.-X., ZHUANG, L.-P., FENG, J. & ZHANG, J. 2012. Comparison of various procedures for progressive collapse analysis of cable-stayed bridges. *Journal of Zhejiang University SCIENCE A*.

CALVI, G. M., SULLIVAN, T. J. & VILLANI, A. 2010. Conceptual Seismic Design of Cable-Stayed Bridges. *Journal of Earthquake Engineering,* 14**,** 1139-1171.

CANADA, T. C. T. 2009. Terrorist Attack Methodology and Tactics Against Bridges and Tunnels: January 2002–December 2008. *In:* BRANCH, S. I. (ed.) *INTELLIGENCE REPORT - ÉVALUATION DE RENSEIGNEMENTS* -. Canada: Transport Canada

CHEN, D. W., AU, F. T. K., THAM, L. G. & LEE, P. K. K. 2000. Determination of initial cable forces in prestressed concrete cable-stayed bridges for given design deck profiles using the force equilibrium method. *Computers & Structures,* 74**,** 1-9.

CHOI, H. & KIM, J. 2011. Progressive Collapse-Resisting Capacity of RC Beam–Column Sub-Assemblage. *Magazine of Concrete Research.*

CLOUGH, R. W. & PENZIEN, J. 1993. *Dynamics of Structures,* New York, McGraw-Hill, Inc.

DENG, R.-B. & JIN, X.-L. 2009. Numerical simulation of bridge damage under blast loads. *W. Trans. on Comp.,* 8**,** 1564-1574.

DEPARTMENT OF DEFENCE, D. & UNIFIED FACILITIES CRITERIA, U. 2002. DoD minimum antiterrorism standards for building. *UFC 4-010-01*. US Army Corps of Engineering, Wasington (DC).

D.COOK, R., MALKUS, D. S., PLESHA, M. E. & WITT, R. J. 2002. Concepts and applications of finite element analysis, University of Wilconsin, JOHN WILEY & SONS,INC.

DOD 2005. UFC 4-023-03. *Design of Structures to Resist Progressive Collapse.* Washington, United States of America: Department of Defence.

DUTTA, A. 2002. Adaptive finite element analysis of structures subjected to transient dynamic loads using time marching scheme. *Computers & Structures,* 80**,** 2313-2319.

DYKE, S. J., CAICEDO, J. M., TURAN, G., BERGMAN, L. & HAGUE, S. 2003. Phase I benchmark control problem for seismic response of cable-stayed bridges. *Journal of Structural Engineering,* 129**,** 857-872.

FUJIKURA, S., BRUNEAU, M. & LOPEZ-GARCIA, D. 2008. Experimental Investigation of Multihazard Resistant Bridge Piers Having Concrete-Filled Steel Tube under Blast Loading. *Journal of Bridge Engineering,* 13**,** 586-594.

FUJINO, Y., KIKKAWA, H., NAMIKAWA, K. & MIZOGUCHI, T. 2005. Seismic retrofit design of long-span bridges on metropolitan expressways in Tokyo. *Transportation Research Record: Journal of the Transportation Research Board,* 11**,** 335-342.

FUJINO, Y. & SIRINGORINGO, D. 2011. Strategies for Structural Health Monitoring of Bridges:Japan's Experience and Practice. *In:* PONNAMPALAM, V., ANCICH, E. & MADRIO, H. (eds.) *AUSTROADS 8th Bridge Conference* Sydney, Australia: Sarasavi Publishers.

GANEV, T., YAMAZAKI, F., ISHIZAKI, H. & KITAZAWA, M. 1998. Response analysis of the Higashi–Kobe Bridge and surrounding soil in the 1995 Hyogoken–Nanbu Earthquake. *Earthquake Engineering & Structural Dynamics,* 27**,** 557-576.

GHALI, E. & KRISHNADEV, M. 2006. Physical and mechanical metallurgy of premature failure of tie rods of a cable-stayed bridge. *Engineering Failure Analysis,* 13**,** 117-126.

GIMSING, N. J. & GEORGAKIS, C. T. 2011. *Cable supported bridges: concept and design*, John Wiley & Sons.

GRAM, M. M., CLARK, A. J., HEGEMIER, G. A. & SEIBLE, F. 2006. Laboratory simulation of blast loading on building and bridge structures. *In:* N. JONES, T. U. O. L., UK AND C.A. BREBBIA, WESSEX INSTITUTE OF TECHNOLOGY, UK (ed.) *Structures Under Shock and Impact IX*

GSA 2003. Progressive Collapse Design Guidelines. *Applied to Concrete Moment-Resisting Frame Buildings.* Tennessee, United States of America: General Services Administration.

HAO, H. & TANG, E. K. C. 2010. Numerical simulation of a cable-stayed bridge response to blast loads, Part II: Damage prediction and FRP strengthening. *Engineering Structures,* 32**,** 3193-3205.

HAO, S. 2010. I-35W Bridge Collapse. *Journal of Bridge Engineering,* 15**,** 608-614.

HAYASHI, H., MARUI, T., TANIGUCHI, N. & KAYANO, S. 2000. Restoration of Hanshin Expressway after Kobe/Awaji Earthquake – challenge of 623 days before opening. *Cement and Concrete Composites,* 22**,** 29-38.

HAYASHIKAWA, T., MATSUI, Y. & KANEKO, T. 2000. Non-linear dynamic behaviour and seismic isolation of steel towers of cable-stayed bridges under great earthquake ground motion. *12th World Conference on Earthquake Engineering.* Auckland, New Sealand.

H.J. Ernst. Der E-Modul von Seilen unter Brucksichtigung des Durchhangers . Der Bauingenieur 40, n.2, 1965. pp.52-55.

HOSHIKUMA, J.-I. Damage of Highway Bridges Due to the Great East Japan Earthquake. Proceedings of The 27th US-Japan Bridge Engineering Workshop, 2011.

HUANG, R. Y., GRIGORIADIS, A. M. & HALPIN, D. W. Simulation of cable-stayed bridges using DISCO. 26th conference on Winter simulation 1994 Orlando, Florida, United States Society for Computer Simulation International, 1130 - 1136

HUANG, Y., WANG, J. & JIN, D. 2011. Performance of a Rigid Frame Arch Bridge under Near-fault Earthquake Ground Motion. *Advanced Materials Research,* 250-253**,** 5.

HUSSAIN, N., FALBE-HANSEN, K. & KITE, S. 2010. *Stonrcutters Bridge Hong Kong Design and Construction,* Kowloon Tong, Hong Kong, Ove Arup and Prtners Hong Kong Ltd.

IMBSEN, R. A. 2007. *AASHTO Guide Specifications for LRFD Seismic Bridge Design* [Online]. Washington, DC, U.S: American Association of State Highway and Transportation Officials.

INFANTI, S., PAPANIKOLAS, P., BENZONI, G. & CASTELLANO, M. Rion-Antirion Bridge: Design and full-scale testing of the seismic protection devices. Proc., 13th World Conf. on Earthquake Engineering, 2004. FIP Industriale Vancouver.

JACINTO, A. C., AMBROSINI, R. D. & DANESI, R. F. 2001. Experimental and computational analysis of plates under air blast loading. *International Journal of Impact Engineering,* 25**,** 927-947.

JANJIC, D., PIRCHER, M. & PIRCHER, H. 2003. Optimization of Cable Tensioning in Cable-Stayed Bridges. *Journal of Bridge Engineering,* 8**,** 131-137.

JENKINS, B. M. & GERSTEN, L. N. 2001. Protecting Public Surface Transportation Against Terrorism and Serious Crime: Continuing Research on Best Security Practices. *In:* FTA (ed.) *MTI Report 01-07.* San Jose, CA: San José State University.

JIA, J. & OU, J. SEISMIC ANALYSES OF LONG-SPAN CABLE-STAYED BRIDGES SUBJECTED TO NEAR-FAULT PULSE-TYPE GROUND MOTIONS. Proceedings of the 14 World Conference on Earthquake Engineering, 2008.

JO, B. W., BYUN, Y. J. & TAE, G. H. 2002. Structural behavior of cable anchorage zones in prestressed concrete cable-stayed bridge. *Canadian Journal of Civil Engineering,* 29**,** 171-180.

JSCE 2010. Steel Cable-Stayed Bridge -Technologies and Its Progress-. *Steel Structures Series 20.* Tokyo, Japan: Japan Society of Civil Engineers.

KAO, C.-S. & KOU, C.-H. 2010. The influence of broken cables on the structural behavior of long-span cable-stayed bridges. *Journal of Marine Science and Technology,* 18**,** 10.

KAWASHIMA, K. 2009. *Seismic Design of Urban Infrastructure (Lecture Note),* Tokyo, Japan, Department of Civil Engineering, Tokyo Institute of Technology.

KAWASHIMA, K., KOSA, K., TAKAHASHI, Y., AKIYAMA, M., NISHIOKA, T., WATANABE, G., KOGA, H. & MATSUZAKI, H. Damages of Bridges during 2011 Great East Japan Earthquake. Proceedings of 43rd Joint Meeting, US-Japan Panel on Wind and Seismic Effects, UJNR, Tsukuba Science City, Japan, 2011.

KHAN, R. A., DATTA, T. K. & AHMAD, S. 2006. Seismic risk analysis of modified fan type cable stayed bridges. *Engineering Structures,* 28**,** 1275-1285.

KIGER, S. A., SALIM, H. A. & IBRAHIM, A. 2010. Bridge Vulnerability Assessment and Mitigation against Explosions. *In:* DESIGN, N. C. F. E. R. (ed.). Columbia: University of Missouri-Columbia.

KIM, J. & KIM, T. 2009. Assessment of progressive collapse-resisting capacity of steel moment frames. *Journal of Constructional Steel Research,* 65**,** 169-179.

KOKOT, S., ANTHOINE, A., NEGRO, P. & SOLOMOS, G. 2012. Static and dynamic analysis of a reinforced concrete flat slab frame building for progressive collapse. *Engineering Structures,* 40**,** 205-217.

KONSTANTAKOPOULOS, T. G., RAFTOYIANNIS, I. G. & MICHALTSOS, G. T. 2012. Suspended bridges subjected to earthquake and moving loads. *Engineering Structures,* 45**,** 223-237.

KOSEKI, J., KODA, M., MATSUO, S., TAKASAKI, H. & FUJIWARA, T. 2012. Damage to railway earth structures and foundations caused by the 2011 off the Pacific Coast of Tohoku Earthquake. *Soils and Foundations*.

KWASNIEWSKI, L. 2010. Nonlinear dynamic simulations of progressive collapse for a multistory building. *Engineering Structures,* 32**,** 1223-1235.

KWON, W. & QIAN, H. 2012. The Tacoma Narrows Bridge Collapse.

LAM, N., MENDIS, P. & NGO, T. 2004. Response Spectrum Solutions for Blast Loading. *Electronic Journal of Structural Engineering, ,* 4**,** 16.

LANGE, D., RÖBEN, C. & USMANI, A. 2012. Tall building collapse mechanisms initiated by fire: Mechanisms and design methodology. *Engineering Structures,* 36**,** 90-103.

LAWVER, D., DADDAZIO, R., VAUGHAN, D. & STANLEY, M. 2003. Response of AISC steel column sections to blast loading. *Americal society of Mechanical Engineers, Pressure Vessels and Piping Division,* 454**,** 10.

LAZAR, B. E., TROITSKY, M. S. & DOUGLASS, M. M. 1972. Load Balancing Analysis of Cable Stayed Bridges. *Journal of the Structural Division,* 92**,** 15.

LEE, C.-H., KIM, S., HAN, K.-H. & LEE, K. 2009. Simplified nonlinear progressive collapse analysis of welded steel moment frames. *Journal of Constructional Steel Research,* 65**,** 1130-1137.

LEE, J. B., ZHENG, Z., KASHFI, S., CHIA, J. & YI, R. 2013. Observation of bus ridership in the aftermath of the 2011 Floods in Southeast Queensland, Australia.

LI, Q. M. & MENG, H. 2002. Pressure-Impulse Diagram for Blast Loads Based on Dimensional Analysis and Single-Degree-of-Freedom Model. *JOURNAL OF ENGINEERING MECHANICS,* 128**,** 6.

LSTC 2007. LS-DYNA KEYWORD USERE'S MANUAL *In:* CORPORATION, L. S. T. (ed.).

MAHONEY, E. E. 2007. *Analyzing the effects of blast loads on bridges using probability, structural analysis, and performance criteria*, ProQuest.

MALÍK, J. 2013. Sudden lateral asymmetry and torsional oscillations in the original Tacoma suspension bridge. *Journal of Sound and Vibration*.

MCCALLEN, D. 2009. The Response of Long-Span Bridges to Low Frequency, Near-Fault Earthquake Ground Motions.

MCCONNELL, J. R. & BROWN, H. 2011. Evaluation of progressive collapse alternate load path analyses in designing for blast resistance of steel columns. *Engineering Structures,* 33**,** 2899-2909.

MEGAWATI, K., HIGASHIHARA, H. & KOKETSU, K. 2001. Derivation of near-source ground motions of the 1995 Kobe (Hyogo-ken Nanbu) earthquake from vibration records of the Akashi Kaikyo Bridge and its implications. *Engineering Structures,* 23**,** 1256-1268.

MEMISOGLU APAYDıN, N. 2010. Earthquake performance assessment and retrofit investigations of two suspension bridges in Istanbul. *Soil Dynamics and Earthquake Engineering,* 30**,** 702-710.

MENDIS, P. & NGO, T. 2003. The bali bombing - investigation on building performance.

MITCHELL, G., TOLNAI, M., GOKANI, V., PICÓN, R., YANG, S., E.KLINGNER, R. & WILLIAMSON, E. B. 2006. Design of Retrofit Vehicular Barriers Using Mechanical Anchors. *In:* RESEARCH, C. F. T. (ed.). Austin TX: The University of Texas at Austin.

MIYACHI, K., NAKAMURA, S. & MANDA, A. 2012. Progressive collapse analysis of steel truss bridges and evaluation of ductility. *Journal of Constructional Steel Research,* 78**,** 192-200.

MOUSTAFA, A. & TAKEWAKI, I. 2010. Deterministic and probabilistic representation of near-field pulse-like ground motion. *Soil Dynamics and Earthquake Engineering,* 30**,** 412-422.

MOZOS, C. M. & APARICIO, A. C. 2010a. Parametric study on the dynamic response of cable stayed bridges to the sudden failure of a stay, Part I: Bending moment acting on the deck. *Engineering Structures,* 32**,** 3288-3300.

MOZOS, C. M. & APARICIO, A. C. 2010b. Parametric study on the dynamic response of cable stayed bridges to the sudden failure of a stay, Part II: Bending moment

acting on the pylons and stress on the stays. *Engineering Structures,* 32**,** 3301-3312.

MOZOS, C. M. & APARICIO, A. C. 2011. Numerical and experimental study on the interaction cable structure during the failure of a stay in a cable stayed bridge. *Engineering Structures,* 33**,** 2330-2341.

MU, Y., ZHANG, Z., CHEN, J. & MIAO, F. Seismic Responses Analysis of a Self-Anchored Cable-Stayed Suspension Bridge. International Conference on Transportation Engineering (ICTE 2009), 2009. ASCE, 1692-1698.

MYLONAKIS, G., SYNGROS, C., GAZETAS, G. & TAZOH, T. 2006. The role of soil in the collapse of 18 piers of Hanshin Expressway in the Kobe earthquake. *Earthquake engineering & structural dynamics,* 35**,** 547-575.

NAKANISHI, H., MATSUO, K. & BLACK, J. 2013. Transportation planning methodologies for post-disaster recovery in regional communities: the East Japan Earthquake and tsunami 2011. *Journal of Transport Geography,* 31**,** 181-191.

NCHRP 2003. NCHRP REPORT 489: Design of Highway Bridges for Extreme Events. *In:* BOARD, T. R. (ed.). Washington, U.S: NATIONAL COOPERATIVE HIGHWAY RESEARCH PROGRAM.

NEGRÃO, J. H. O. & SIMÕES, L. M. C. 1997. Optimization of cable-stayed bridges with three-dimensional modelling. *Computers & Structures,* 64**,** 741-758.

NETHERCOT, D. A., IZZUDDIN, B. A., ELGHAZOULI, A. Y. & VLASSIS, A. G. 2007. Aligning progressive collapse with conventional structural design. 1-21.

NGO, T. & MENDIS, P. Modelling reinforced concrete structures subjected to impulsive loading using the Modified Continuum Lattice Model. The 18th Australasian Conference on the Mechanics of Structures and Materials, 1-3 December 2005 2005 Perth, Australia. Taylor and Francis, 953-959.

NGO, T., MENDIS, P., GUPTA, A. & RAMSAY, J. 2007a. Blast Loading and Blast Effects on Structures–An Overview.

NGO, T., MENDIS, P., HONGWEI, M. & MAK, S. 2005a. High strain rate behaviour of concrete cylinder subjected to uniaxial compressive impact loading. *The 18th Australasian Conference on the Mechanics of Structures and Materials.* Perth, Australia: Taylor and Francis

NGO, T., MENDIS, P. & KRAUTHAMMER, T. 2007b. Behavior of Ultrahigh-Strength Prestressed Concrete Panels Subjected to Blast Loading. *Journal of Structural Engineering,* 133**,** 1582.

NGO, T., NGUYEN, N. & MENDIS, P. An investigation on the effectiveness of blast walls and blast-structure. The 18th Australasian Conference on the Mechanics of Structures and Materials, 1-3 December 2005 2005b Perth, Australia. Taylor and Francis, 961-967.

NI, Y., WANG, J. & LO, L. 2005. Influence of Stabilizing Cables on Seismic Response of a Multispan Cable-Stayed Bridge. *Computer-Aided Civil and Infrastructure Engineering,* 20**,** 142-153.

OKAMOTO, Y. & NAKAMURA, S. 2011. Static and seismic studies on steel/concrete hybrid towers for multi-span cable-stayed bridges. *Journal of Constructional Steel Research,* 67**,** 203-210.

OTSUKA, H., YAMAHIRA, K. & KOMIYA, Y. 2007. Research on seismic safety, retrofit, and design of a steel cable-stayed bridge. *MDCMS 1 1st International Conference on Modern Design, Construction and Maintenance of Structures.* Hanoi, Vietnam, December 2007.

PAIK, J. K. & KIM, B. J. 2008. Progressive collapse analysis of thin-walled box columns. *Thin-Walled Structures,* 46**,** 541-550.

PAZ, M. 2004. *Structural dynamics : theory and computation,* Boston, U.S, Kluwer Academic Publishers.

PLAUT, R. H. 2008. Snap loads and torsional oscillations of the original Tacoma Narrows Bridge. *Journal of Sound and Vibration,* 309**,** 613-636.

POWELL, G. 2005. Progressive Collapse: Case studies Using Nonlinear Analysis. *The 2005 Structures Congress.* New York, New York, United States: American Society of Civil Engineers.

PTI 2007. Recommendations for Stay Cable Design, Testing and Installation. USA: Post-Tensioning Institute.

ROADS, Q. T. A. M. 2012. Queensland Transport and Roads Investment Program 2011-12 to 2014-15.

RUAN, X., SHI, X. & LI, X. Failure Analysis of Tendon Breakout on Bottom Slab of A Pre-Stressed Concrete Box Gird Bridge During Construction. *Engineering Failure Analysis*.

RUIZ-TERAN, A. M. & APARICIO, A. C. 2007. Dynamic amplification factors in cable-stayed structures. *Journal of Sound and Vibration,* 300**,** 197-216.

RUIZ-TERAN, A. M. & APARICIO, A. C. 2009. Response of under-deck cable-stayed bridges to the accidental breakage of stay cables. *Engineering Structures,* 31**,** 1425-1434.

SAADEGHVAZIRI, M. A. & YAZDANI-MOTLAGH, A. R. 2008. Seismic behavior and capacity/demand analyses of three multi-span simply supported bridges. *Engineering Structures,* 30**,** 54-66.

SALEM, H. M., EL-FOULY, A. K. & TAGEL-DIN, H. S. 2011. Toward an economic design of reinforced concrete structures against progressive collapse. *Engineering Structures,* 33**,** 3341-3350.

SEO, K., KURITA, K., MOTOKI, K., MOMII, T., SHIGETA, T. & NIWA, N. Interpretation on Some of Principal Structural Damage During the 1995 Kobe Earthquake. Proceeding of 13th World Conference on Earthquake Engineering, 2004.

SHI, Y., LI, Z.-X. & HAO, H. 2010. A new method for progressive collapse analysis of RC frames under blast loading. *Engineering Structures,* 32**,** 1691-1703.

SHIRATO, M. 2009. PROCEEDINGS OF THE 25th U.S. – JAPAN BRIGDE ENGINEERING WORKSHOP. *In:* P.W.R.I. (ed.). Tsukuba, Japan: CENTER FOR ADVANCED ENGINEERING STRUCTURAL ASSESSMENT AND RESEARCH PUBLIC WORKS RESEARCH INSTITUTE.

SIRINGORINGO, D. M. & FUJINO, Y. 2007. Dynamic characteristics of a curved cable-stayed bridge identified from strong motion records. *Engineering Structures,* 29**,** 2001-2017.

SIRINGORINGO, D. M. & FUJINO, Y. 2008. System identification applied to long-span cable-supported bridges using seismic records. *Earthquake Engineering & Structural Dynamics,* 37**,** 361-386.

SIRINGORINGO, D. M., FUJINO, Y. & NAMIKAWA, K. 2013. Seismic Responses Analyses of the Yokohama-Bay Cable-Stayed Bridge in the 2011 Great East Japan (Tohoku) Earthquake. *Journal of Bridge Engineering*.

SMITH, P. J. 2013. Terrorism in Asia: A Persistent Challenge Sustained by Ideological, Physical, and Criminal Enablers. *Handbook of Asian Criminology.* Springer.

SON, J. & ASTANEH-ASL, A. 2012. Blast Resistance of Steel Orthotropic Bridge Decks. *Journal of Bridge Engineering,* 17**,** 589-598.

SON, J. & LEE, H.-J. 2011. Performance of cable-stayed bridge pylons subjected to blast loading. *Engineering Structures,* 33**,** 1133-1148.

SOUTHWICK, G. J., PETHICK, A. J., THALAYASINGAM, P., VIJAYASEKARAN, V. S. & HOGG, J. J. W. 2002. Australian doctors in Bali: the initial medical response to the Bali bombing. *MEDICAL JOURNAL OF AUSTRALIA,* 177**,** 624-626.

STAROSSEK, U. 2011. Progressive Collapse and Bridge Dynamics. *National Scientific Seminar on Dynamics and Progressive Collapse in Cable-Stayed Bridges.* Hanoi, Vietnam.

STODDART, E. P., BYFIELD, M. P., DAVISON, J. B. & TYAS, A. 2013. Strain rate dependent component based connection modelling for use in non-linear dynamic progressive collapse analysis. *Engineering Structures*.

TABATABAEI, Z. S. & VOLZ, J. S. 2012. A Comparison between Three Different Blast Methods in LS-DYNA : LBE, MM-ALE, Coupling of LBE and MM-ALE. *In:* LSTC (ed.) *12th International LS-DYNA Users Conrefence 2012.* Dearborn, Mishigan USA.

TALEBINEJAD, I., FISCHER, C. & ANSARI, F. 2011. Numerical Evaluation of Vibration-Based Methods for Damage Assessment of Cable-Stayed Bridges. *Computer-Aided Civil and Infrastructure Engineering,* 26**,** 239-251.

TANG, E. K. C. 2009. *Numerical Simulation of a Long Span Bridge Response to Blast Loading.* Masters of Engineering, University of Western Australia.

TANG, E. K. C. & HAO, H. 2010. Numerical simulation of a cable-stayed bridge response to blast loads, Part I: Model development and response calculations. *Engineering Structures,* 32**,** 3180-3192.

TEYSSANDIER, J.-P., COMBAULT, J. & MORAND, P. The Rion-Antirion bridge design and construction. Proceedings of the 12th World Conference on Earthquake Engineering. Auckland, New Zealand, 2000.

TM5-1300 1990. Structure to resist the effects of accidental explosions. Washington, DC, USA: Department of the Army, Navy and Air Force Technical Manual.

TSAI, M.-H. & YOU, Z.-K. 2012. Experimental evaluation of inelastic dynamic amplification factors for progressive collapse analysis under sudden support loss. *Mechanics Research Communications,* 40**,** 56-62.

UNJOH, S., TERAYAMA, T., ADACHI, Y. & HOSHIKUMA, J.-I. 2000. Seismic retrofit of existing highway bridges in Japan. *Cement and Concrete Composites,* 22**,** 1-16.

VLASSIS, A. G., IZZUDDIN, B. A., ELGHAZOULI, A. Y. & NETHERCOT, D. A. 2009. Progressive collapse of multi-storey buildings due to failed floor impact. *Engineering Structures,* 31**,** 1522-1534.

WALTHER, R. 1999. *Cable stayed bridges,* London, Thomas Telford.

WANG, P. H., TSENG, T. C. & YANG, C. G. 1993. Initial shape of cable-stayed bridges. *Computers & Structures,* 46**,** 1095-1106.

WANG, Y. C. 2011. Performance Based Fire Engineering Research of Steel and Composite Structures: a Review of Joint Behaviour. *Advances in Structural Engineering,* 14**,** 613-624.

WEIAB, H., WANG, Z. & FENG, Q. 2011. Seismic Analysis and Design of Minpu Double-Deck Cable-Stayed Bridge. *Procedia Engineering,* 14**,** 1501-1509.

WILLIAMSON, E. B. & WINGET, D. G. 2005. Risk Management and Design of Critical Bridges for Terrorist Attacks. *Journal of Bridge Engineering,* 10**,** 96-106.

WINGET, D. G., PE, M., MARCHAND, K. A. & WILLIAMSON, E. B. 2005. Analysis and design of critical bridges subjected to blast loads.

WOLFF, M. & STAROSSEK, U. 2008. Structural robustness of a cable-stayed bridge *Handling Exceptions in Structural Engineering: Robustezza Strutturale, Scenari Accidentali, Complessità di Progetto.* Roma, Italy.

WOLFF, M. & STAROSSEK, U. 2009. Cable loss and progressive collapse in cable-stayed bridges. *Bridge Structures,* 5**,** 17-28.

WOLFF, M. & STAROSSEK, U. 2010. Cable-loss analyses and collapse behavior of cable-stayed bridges. *IABMAS2010, The Fifth International Conference on Bridge Maintenance, Safety and Management.* Philadelphia, USA.

WRIGHT, A. & FRENCH, M. 2008. The response of carbon fibre composites to blast loading via the Europa CAFV programme. *Journal of Mater Sci,* 43**,** 10.

WU, Q., TAKAHASHI, K. & NAKAMURA, S. 2003. The effect of cable loosening on seismic response of a prestressed concrete cable-stayed bridge. *Journal of Sound and Vibration,* 268**,** 71-84.

YABUNO, M., FUJIWARA, T., SUMI, K., NOSE, T. & SUZUKI, M. 2003. Design of" Tatara Bridge". *IHI engineering review,* 36**,** 40-56.

YANG, C.-Y. & CHEUNG, M. M. S. 2011. Shake Table Test of Cable-Stayed Bridge Subjected to Non-Uniform Excitation. *Procedia Engineering,* 14**,** 931-938.

YANG, D.-C., GE, Y.-J., XIANG, H.-F. & MA, Z. J. 2011. 3D Flutter Analysis of Cable Supported Bridges Including Aeroelastic Effects of Cables. *Advances in Structural Engineering,* 14**,** 1129-1147.

YAZDANI-PARAEI, H., MOHARRAMI, H., MAALEK, S. & HEYDARI, M. 2012. Optimum design of cable-stayed bridges. *Australian Journal of Structural Engineering,* 12**,** 99-118.

ZHANG, M. H., SHARIF, M. S. H. & LU, G. 2007. Impact resistance of high-strength fibre-reinforced concrete. Thomas Telford.

ZHANG, M. H., SHIM, V. P. W., LU, G. & CHEW, C. W. 2005. Resistance of high-strength concrete to projectile impact. *International Journal of Impact Engineering,* 31**,** 825-841.

ZHU, S., LEVINSON, D., LIU, H. X. & HARDER, K. The traffic and behavioral effects of the I-35W Mississippi River bridge collapse. *Transportation Research Part A: Policy and Practice,* In Press, Corrected Proof.

ZOLI, T. & WOODWARD, R. 2005. Design of Long Span Bridges for Cable Loss *IABSE Symposium.* Lisbon, Portugal.